

YALINA Facility
A Sub-Critical Accelerator-Driven System (ADS) for
Nuclear-Energy Research Facility Description and an
Overview of the Research Program (1997-2008)

Nuclear Engineering Division

About Argonne National Laboratory

Argonne is a U.S. Department of Energy laboratory managed by UChicago Argonne, LLC under contract DE-AC02-06CH11357. The Laboratory's main facility is outside Chicago, at 9700 South Cass Avenue, Argonne, Illinois 60439. For information about Argonne, see www.anl.gov.

Availability of This Report

This report is available, at no cost, at <http://www.osti.gov/bridge>. It is also available on paper to the U.S. Department of Energy and its contractors, for a processing fee, from:

U.S. Department of Energy
Office of Scientific and Technical Information
P.O. Box 62
Oak Ridge, TN 37831-0062
phone (865) 576-8401
fax (865) 576-5728
reports@adonis.osti.gov

Disclaimer

This report was prepared as an account of work sponsored by an agency of the United States Government. Neither the United States Government nor any agency thereof, nor UChicago Argonne, LLC, nor any of their employees or officers, makes any warranty, express or implied, or assumes any legal liability or responsibility for the accuracy, completeness, or usefulness of any information, apparatus, product, or process disclosed, or represents that its use would not infringe privately owned rights. Reference herein to any specific commercial product, process, or service by trade name, trademark, manufacturer, or otherwise, does not necessarily constitute or imply its endorsement, recommendation, or favoring by the United States Government or any agency thereof. The views and opinions of document authors expressed herein do not necessarily state or reflect those of the United States Government or any agency thereof, Argonne National Laboratory, or UChicago Argonne, LLC.

**YALINA Facility
A Sub-Critical Accelerator-Driven System (ADS)
for Nuclear-Energy Research Facility Description and an Overview
of the Research Program (1997-2008)**

by
Yousry Gohar and Donald L. Smith
Nuclear Engineering Division, Argonne National Laboratory

January 2010

Work supported by the
Office of Global Nuclear Material Threat Reduction
U.S. Department of Energy
Under Contract DE-AC02-06CH11357

Table of Contents

Abstract-----	3
Preface-----	4
Executive Summary-----	5
I. Introduction-----	7
II. Basic Physics Concepts-----	10
III. Research Objectives-----	21
IV. YALINA Project Chronology-----	23
V. Formal Research Agreements-----	27
VI. General Description of the Facility -----	32
VII. Safety Apparatus and Procedures-----	42
VIII. YALINA Thermal-----	44
IX. YALINA Booster-----	52
X. Experimental Instrumentation-----	57
XI. Measurement Techniques-----	64
XII. YALINA Booster Conversion Project to Low Enrichment Fuel-----	86
XIII. Argonne Modeling Activities and Comparisons with Experiments-----	87
XIV. YALINA Project Principal Achievements-----	100
XV. Future Plans for the YALINA Project-----	101
Acknowledgements-----	102
References and Publications-----	103
Appendices-----	109
Appendix A: Belarusian Scientists-----	109
Appendix B: Foreign Scientists-----	110
Appendix C: Participating Organizations-----	111
Appendix D: YALINA Thermal Benchmark Specifications-----	112
Appendix E: YALINA Booster Benchmark Specifications-----	134

Abstract

The YALINA facility is a zero-power, sub-critical assembly driven by a conventional neutron generator. It was conceived, constructed, and put into operation at the Radiation Physics and Chemistry Problems Institute of the National Academy of Sciences of Belarus located in Minsk-Sosny, Belarus. This facility was conceived for the purpose of investigating the static and dynamic neutronics properties of accelerator driven sub-critical systems, and to serve as a neutron source for investigating the properties of nuclear reactions, in particular transmutation reactions involving minor-actinide nuclei. This report provides a detailed description of this facility and documents the progress of research carried out there during a period of approximately a decade since the facility was conceived and built until the end of 2008. During its history of development and operation to date (1997 – 2008), the YALINA facility has hosted several foreign groups that worked with the resident staff as collaborators. The participation of Argonne National Laboratory in the YALINA research programs commenced in 2005. For obvious reasons, special emphasis is placed in this report on the work at YALINA facility that has involved Argonne's participation. Attention is given here to the experimental program at YALINA facility as well as to analytical investigations aimed at validating codes and computational procedures and at providing a better understanding of the physics and operational behavior of the YALINA facility in particular, and ADS systems in general, during the period 1997 – 2008.

Preface

The YALINA facility is rather unique in that it provides an opportunity to study the characteristics of typical accelerator driven sub-critical systems (ADS) on a very small scale, since the major portion of neutron spectrum at various points in a sub-critical core stimulated by relatively low-energy neutrons (approximately 14 MeV) bears a strong resemblance in shape to spallation neutron sources that are produced in much larger and more costly machines. The YALINA project began in the late 1990's with the commissioning of a neutron generator and construction of an accompanying sub-critical core assembly at the Sosny nuclear laboratory of the National Academy of Sciences of Belarus. Early-on, this facility benefitted from extensive collaborations with foreign scientists from Europe under the auspices of ISTC and IAEA Coordinated Research Programs (CRP). Argonne National Laboratory, representing the United States, began its collaboration with YALINA in 2005 with the launching of an IAEA CRP involving a number of foreign countries as well as Belarus. Argonne has played a fairly minor role in the experimental aspects of the YALINA programs, but it has been a dominant player in the analytical campaign since 2005. In particular, the major goal of Argonne and the U.S. Department of Energy, through the Global Nuclear Threat Reduction Program, has been to help Belarusian scientists to design core configurations for YALINA that utilize LEU uranium rather than HEU for the YALINA booster concept. Migration from 90% ^{235}U enrichment to 36%, and ultimately to 21%, is progressing well. In addition, Argonne has been able to obtain useful experimental data to aid in validating its analytical code suite for ADS applications. In some cases, observed C/E discrepancies stimulated additional measurements at the YALINA facility, based upon suggestions from Argonne that led to success in resolving these discrepancies.

The year 2008 marks the end of roughly a decade of research at YALINA and the beginning of a new round of experimental studies at this facility using predominantly LEU core designs. While there is extensive documentation on the work at YALINA during the past decade from various progress reports, conference contributions, theses, and journal publications, no single document traces the history of this research and provides an overview discussion of the technical issues involved. That was the motivation for undertaking the writing of the present report. No attempt is made here to address every last detail but rather to provide the reader with a rather broad, if sometimes superficial, overview of the evolution of the YALINA project, of the research conducted there, and of the knowledge gained from this work. In certain chapters of this report the emphasis is almost entirely on the work that has involved Argonne. This is appropriate since the objective here is to provide documentation from Argonne's own perspective. An extensive list of references is provided to which the interested reader can refer to learn not only some further details about the work involving Argonne but also about those activities of scientists from other foreign countries working in collaboration with the staff scientists at YALINA during this period.

Executive Summary

The important need to convert nuclear waste generated from nuclear power reactors to smaller volumes with lower chemical and radioactive toxicity by reprocessing and transmuting the long-lived fission products and the minor actinides, in order to obtain public support for utilizing and continuing development of fission nuclear energy, has prompted investigation of the possibility of using sub-critical accelerator driven systems (ADS) for this purpose. The YALINA facility was conceived as a low-cost, zero-power ADS that could prove useful as a surrogate for investigating many of the physical characteristics and potential applications of high-power, full-scale ADS systems that are under design consideration but remain to be built. Such a small-scale facility could serve as a test bed for exploring the properties of a large-scale facility. It is predicated on the fact that the neutron spectra of large-scale facilities with spallation neutron source could be produced on a small scale by clever engineering design and exploitation of the physical properties of neutrons from spontaneous-fission production or nuclear reactions induced by low-energy accelerators.

The YALINA project began with the conversion of a nuclear laboratory that in former times had been used for the development of a small mobile reactor concept at the Institute of Physics and Power Engineering in Sosny, a village located on the outskirts of Minsk, Belarus. This laboratory has well-shielded underground vault areas and the infrastructure needed for supporting such a facility. Furthermore, the staff of this institute possessed the experience needed for its development and operation. The first step in the development process was commissioning a low-energy deuteron accelerator (operating at a maximum potential of 250 kV) for neutron production through the $D(d,n)^3\text{He}$ reaction ($\approx 2.5\text{-MeV}$ neutron energy) and the $T(d,n)^4\text{He}$ reaction ($\approx 14.1\text{-MeV}$ neutron energy) and acquisition of a ^{252}Cf spontaneous-fission point neutron source (Maxwellian spectrum with average energy $\approx 2\text{ MeV}$). This accelerator and its associated beam transport system were placed into operation during the time frame 1997 – 2000. The next step was the design and the construction of a rectangular parallelepiped core assembly with dimensions < 1 meter. The overall dimensions of this assembly, including shielding and reflector, would not exceed 2 meters on any side. Fuel-pin and measurement channels that would allow the maximum possible flexibility in fuel loadings and measurement opportunities were incorporated in the design. Components fabricated from steel, lead, carbon, boron-carbide, and polyethylene were used in the construction of the matrix that would hold the fuel rods. Work on the design and construction details was completed in the 2001 – 2002 time-frame and licensing for full operation of the facility was obtained from the Belarusian government shortly thereafter.

The first core design, designated YALINA Thermal (or YALINA-T for short) involved exclusive use of EK-10 fuel pins (UO_2 10%-enriched in ^{235}U) for the core loading. The intent was to produce a neutron spectrum that was predominately thermal throughout the core except close to the driver neutron source. The neutron source could be located at various positions along the central axis of the core. However, it was realized that this configuration cannot simulate the high energy part of the neutron spectrum of the future ADS. Consequently, the “booster” concept was conceived and put into operation in the time frame 2004 – 2005. In this approach, an extended driver neutron source that would resemble more closely the extended fast-neutron environment associated with spallation was developed by employing concentric layers of fuel pins surrounding the spontaneous fission or accelerator neutron source that contained either 90%- or 36%-enriched uranium, and were placed in a lead matrix surrounding the central axis. This fast zone was surrounded with a layer of natural uranium and boron carbide rods, which allows fast neutrons to migrate to the thermal region beyond while blocking the streaming of thermal neutrons into the fast region. This interface layer was called the “valve” because of its function. An

added advantage of this design is that it provides a fast spectrum in a portion of the assembly for use in studying the transmutation of minor actinide waste through fast-neutron fission. This assembly is called YALINA Booster (or YALINA-B for short).

Extensive measurements of neutron spectra, reactor kinetics, monitor detector system performance, and transmutation rates have been performed during the past decade in both YALINA-T and YALINA-B. This work has been supported by the Belarusian government, several ISTC and IAEA grants, and bi-lateral arrangements with foreign institutes. Numerous foreign collaborators from various countries have worked with the Belarusian YALINA staff on this research. This work has led to numerous reports, conference contributions, and journal articles as well as several student theses.

Argonne National Laboratory first became involved with YALINA around 2005 through the Russian Research Reactor Fuel Return program of DOE. Argonne had two main interests in participating in this work. The first objective was to demonstrate that such a facility could eventually be designed and constructed using LEU fuel. This objective is consistent with the U.S. goal of eventually removing HEU from research facilities located around the world in order to reduce the threat of nuclear proliferation. Work is almost completed to migrate away from HEU in steps from the 90%- and 36%-enrichment fuel-loading of the YALINA Booster configuration to one involving only 21% and 10% enrichment. The second objective was to study the physics of ADS and to refine the ADS computational methods. Excellent progress is being achieved toward fulfilling both objectives.

Argonne intends to continue its collaboration with researchers in Belarus at the YALINA facility. High on the agenda will be to develop new measurement and analytic techniques that can be applied at future ADS facilities, to test new configuration with different LEU fuels, and to perform further transmutation reaction measurements in typical ADS spectra.

I. Introduction

The word “Yalina” means “spruce” in the Belarusian language. This is a reference to the extensive spruce tree forests that cover a portion of Belarus, and to the fact that the Radiation Physics and Chemistry Problems Institute, where the facility YALINA is situated, is located in a forest in Sosny, a small village located in the outskirts of Minsk, the capital city of Belarus, approximately 20 km to the East of the city center. The Institute of Power Engineering Problems (Sosny) is the parent organization of the Radiation Physics and Chemistry Problems Institute. It was created in 1989 when the Institute for Nuclear Power Engineering of the Academy of Sciences was divided into three institutes: 1) The Institute for Power Engineering Problems (IPEP); 2) The Institute for Physical and Chemical Radiation Problems; and 3) The Institute for Radiation-Ecological problems. Together, these three Institutes form the Sosny Scientific and Engineering Complex under the Belarusian Academy of Sciences. At present, Sosny conducts civilian nuclear research experiments at the YALINA sub-critical facility. It houses a thermal sub-critical assembly (YALINA Thermal or YALINA-T) and a booster sub-critical assembly (YALINA Booster or YALINA-B). These are two alternative configurations of the common YALINA structure. YALINA-T runs exclusively on low-enriched uranium ($10\% \text{ }^{235}\text{U}$), i.e., LEU, fuel while the original YALINA-B utilizes highly enriched uranium fuel (36 and 90% ^{235}U) plus low-enriched uranium ($10\% \text{ }^{235}\text{U}$) fuel. IPEP scientists are currently working with the U.S. Department of Energy to convert the HEU region of the YALINA-B core to LEU in stages. Detailed experimental and analytical work is being conducted at each stage to carefully characterize this ADS system and its various core configurations.

It is well established that the global need for safe, economically viable, and reliable nuclear power will continue to grow in the decades ahead for a variety of reasons. First, the available sources of more conventional fossil fuels will dwindle with time and thus become ever more expensive. The steady growth of the world’s population at a rate of roughly 1% per year, coupled with the much more rapid growth in demand for resources, including energy, fueled by rapid economic growth in the developing nations, will stress the traditional energy sources thereby necessitating a wider use of nuclear power. This need is accentuated by the developing realization that emission of carbon dioxide from the burning of fossil fuels appears to be implicated in an observed trend toward global warming.

However, the growth of nuclear power is not without its problems, and it is accompanied by objections from vigorous detractors. The two most significant of these problems to be dealt with are the safe disposition of long-lived nuclear waste from fission power and the risks associated with the proliferation of nuclear technologies and nuclear materials, potentially into the hands of rogue nations or terrorist groups. Such misuse might jeopardize the safety and security of everyone else. It is widely accepted that technological and political solutions can and will be found eventually to deal with these problems if timely and sufficient attention is paid to developing them.

The use of accelerator driven systems, in which sub-critical cores of fissionable material are driven by external neutron sources generated using charged-particle-induced nuclear reactions, is one technological option that is being considered by nuclear scientists and world leaders charged with the responsibility of formulating nuclear energy policy. These sub-critical cores – that by the nature of their geometric design and fuel compositions are inherently sub-critical – are potentially inherently safe to operate. Although they are sub-critical, by operating very close to criticality while driven by an external source, they offer the possibility for energy amplification. That means that the power gained from nuclear fission in these devices will exceed the power required to operate the accelerator in addition to satisfying the additional power consumption needs of the facility. Thus, in principle, ADS systems can be devised to

serve as legitimate energy sources with self-sustaining fuel cycles. ADS systems are also seen as offering the potential to burn unwanted long-lived minor actinide nuclear waste from more conventional reactors thereby offering the possibility of reducing the volume, radioactive toxicity, and heat load associated with long-term storage of nuclear waste materials.

Although the ADS concept is appealing, rather limited practical experience has been acquired for this approach. While a few mock-up experiments have been performed at high-energy accelerator facilities using relatively low-intensity charged-particle beams, no facilities operating at the high currents required for efficient waste transformation or practical energy production have actually been built. Several ADS research facilities that could serve this function, at least for demonstration purposes, are being planned for the future, and design work is in progress. However, eventual deployment of such systems for commercial use in the production of electric power, or for transmuting the waste that has been produced by contemporary nuclear power reactors, lies several decades in the future. Such systems would involve relatively high-power accelerator systems (owing to the need for high currents), high-energy, charged-particle beams to produce copious neutrons by spallation reactions, and externally-driven cores. They would certainly not be zero-power devices. In the absence of solid experimental information to validate computer codes that would be used to design these facilities and establish their operational procedures, rather large design margins would be required to insure safety, thereby adding significantly to their cost and potentially limiting their longevity. However, much can be learned about how such systems would behave from smaller low- or zero-power sub-critical assemblies that could serve to validate the designs of much larger systems. It will be seen in Chapter II why this is the case as a consequence of the underlying physical processes of neutron production and the neutronic characteristics of fissionable cores. This is the role that the YALINA facility was conceived to play. By making use of an existing reactor research facility in Sosny, including subterranean shielded vaults and an intense neutron generator, it has proved to be possible to construct and commission the YALINA facility, and to put it into operation in an active and productive ADS research program at a very modest cost.

The objective of this report is to document the evolution of the YALINA project from its inception somewhat more than a decade ago (1997) to late 2008, to describe the facility and its operation, and to document some important highlights from the research that has been conducted by the YALINA staff and foreign collaborators during this period. There are numerous progress reports, conference contributions, workshop contributions, and journal articles that provided the detailed information upon which this summary report is based. No attempt is made in the text of this report to present and specifically reference all the material from these earlier sources. Instead, the goal will be to provide, in one document, a convenient and coherent overview of the history and achievements of the YALINA research program with particular attention to those aspects in which Argonne National Laboratory has been involved. It should be stressed here once again that in addition to using experimental data from YALINA measurements to validate the computational methods and computer codes, Argonne maintains a strong interest in demonstrating that an ADS facility such as YALINA facility can operate with low-enrichment uranium (LEU) fuel as well as high-enrichment uranium (HEU) fuel.

This report is divided into fifteen chapters and five appendices, including the present Introduction but excluding the Preface, Executive Summary, Acknowledgements, and References and Publications. The chapters in the main body of this report (other than this Introduction) address the following topical areas: Chapter II – relevant physical concepts; Chapter III – research objectives for the YALINA project; Chapter IV – chronology of the YALINA project; Chapter V – formal agreements supporting the work of the YALINA project; Chapter VI – a general description of the YALINA facility; Chapter VII – safety apparatus and procedures at YALINA; Chapter VIII – a description of the YALINA Thermal concept and core design; Chapter IX – a description of the YALINA Booster concept and core design; Chapter X – a

description of the experimental instrumentation at YALINA; Chapter XI – a discussion of the various measurement techniques employed in YALINA research; Chapter XII – a brief discussion of the YALINA-Booster conversion project to LEU fuel; Chapter XIII – a discussion of the Argonne modeling work for YALINA Booster and comparisons to available experimental data; XIV – a brief list of the principal achievements of the YALINA project during the past decade; and Chapter XV – a brief description of future plans for YALINA for 2009 and beyond. The five appendices included in this report address specific topics in greater detail.

II. Basic Physics Concepts

This chapter discusses several basic physics issues that pertain to distinct aspects of the YALINA facility. These are: A) the concept of accelerator-driven sub-critical nuclear reactors; B) the interaction of energetic particles (protons or neutrons) with heavy-element nuclei; C) the production of neutrons by low-energy deuteron bombardment of deuterium and tritium targets; D) nuclear fission processes of actinide materials; and E) the transmutation of fission-product and minor-actinide nuclear waste products in ADS systems. While sealed spontaneous-fission neutron sources such as ^{252}Cf or (α ,n) sources such as Pu-Be or Am-Be are used in some experiments at integral facilities as starter sources or auxiliary sources for certain geometric mapping measurements, they will not be discussed in this chapter because they are not considered to be key components of any proposed ADS systems nor of the YALINA facility either.

A. Accelerator-driven Sub-critical Nuclear Reactors

Since the late 1930's it has been known that certain heavy nuclei fission readily when bombarded with neutrons, and release a great deal of energy since the two product nuclei (fission at modest incident energies is almost entirely binary fission) are more tightly bound than the original heavy target. Typically, the amount of energy released is about 200 MeV per fission event. It is manifested in the kinetic energy of approximately 2.5 prompt neutrons (a statistical average called "nu-bar" that varies somewhat from isotope to isotope and with the incident energy of the neutrons that induce fission), the recoil energy of the fission fragments, and excitation energy of the fission-product nuclei. These fissionable nuclei, generally called actinides, range from $Z = 89$ (actinium) upwards to the heaviest known element at $Z = 103$ (lawrencium). The most common known fissionable materials in nuclear technology are called major actinides. These include mainly certain isotopes of uranium and plutonium. The major actinides are so designated because they are the basic fuels and/or fertile materials of the most considered nuclear fuel cycles. However, it is only fair to also include thorium in this category because there is a less common nuclear fuel cycle which is being considered quite seriously in some countries (e.g., India) that involves this element as well. The so-called minor actinides include isotopes of neptunium, americium, curium, berkelium, and californium. These materials are not considered to be primary fuels but are generally byproducts of the operation of nuclear reactors. In particular, these materials are produced in nuclear reactors in most cases by transmutation reactions involving mainly neutron capture followed by a variety of decay processes. All other actinide elements play essentially no practical role in nuclear fission energy technologies.

Fissionable actinide isotopes can be divided into two broad categories. One category involves those nuclei that fission with thermal neutrons as well as higher energy neutrons. The second category (excluding minor contributions from fission that can occur at sub-threshold energies at specific resonances) involves isotopes that fission primarily with fast neutrons (usually called threshold-fissionable isotopes). The principle actinide isotopes that fission with thermal neutrons are: ^{233}U (associated with the thorium fuel cycle), ^{235}U , and ^{239}Pu . In once-through fuel cycles, fuel rods containing primary fissionable materials are removed from the reactor after their contribution to the total reactivity declines below the design point for the reactor, and they are then either stored or buried as radioactive waste. In this mode, any residual fuel that remains in the fuel rods, or that is produced by operation of the reactor, e.g., plutonium, is usually lost to future use. In the case of recycling, the fuel rods are chemically processed. Usable fuel is recovered and the rest is disposed of as waste. In the waste stream the longest lived radioactive isotopes are usually the minor actinides. For this reason, there is a strong motivation to reduce the volume of unusable minor-actinide isotopes from the residual waste stream for disposal to

reduce the heat and radio-toxicity load on the waste burial sites. One scheme being considered for doing this is to “burn” or “transmute” as many of these minor actinides as possible in reactors designed specifically for this purpose. While thermal reactors can transmute some actinide materials, critical fast reactors or other nuclear devices operating with harder (more energetic) neutron spectra have been determined to be much more efficient for this purpose.

Accelerator-driven sub-critical systems (ADS) are manifestations of one particular scheme promoted for the transmutation of unwanted nuclear waste. The basic principle is as follows. An assembly of fissionable material (called the core in reactor terminology) is sub-critical if the amount of material present, coupled with its physical arrangement and complement of supplementary materials such as those that comprise the fuel lattice structure, moderators, reflectors, fuel-rod cladding, etc., is insufficient to achieve a sustained fission reaction chain. In reactor language, this is signified by $k_{\text{eff}} < 1$. In fact, such sub-critical cores are designed so that in no conceivable scenario can k_{eff} actually approach 1 (i.e., criticality) no matter what the situation (flooding, core meltdown, structural failure, etc.). This assures that these facilities are inherently safe, at least from the perspective of criticality. The parameter k_{eff} is basically defined as the excess of neutrons present in the fissionable material within the reactor core. If $k_{\text{eff}} = 1$, the number of neutrons introduced from fission is perfectly balanced by the number of neutrons removed by nuclear reactions in the core plus those that escape the system. If an external neutron source is introduced (e.g., a spontaneous-fission neutron source such as ^{252}Cf or an accelerator neutron source), then fissions will occur in the sub-critical assembly at some sustained and determinable rate. However, once the external source is removed, the neutron inventory from fission in the core will die away relatively quickly. By contrast, a critical reactor does not rely on an external neutron source other than to serve as a “starter” of the chain reaction. Critical reactor cores are designed to have a small amount of excess reactivity ($k_{\text{eff}} > 1$) that can be controlled and kept right at criticality during operation by the insertion of rods with a material such as cadmium or a boron compound that is capable of “soaking” up excess neutrons due to large neutron capture cross sections in certain energy regions (e.g., at specific resonances or thermal energy). So, a delicate balance is maintained during the operation of critical reactors by the position and number of these control rods introduced into the core in such a way that $k_{\text{eff}} = 1$. Delayed neutrons, i.e., those neutrons emitted from highly excited neutron-unstable states of fission products, and not from fission itself, play an important role in assuring reactor controllability. The reason for this is that the time scale for prompt fission is so short that it is virtually impossible to effectively control criticality by any physical means, e.g., inserting or withdrawing control rods. However, the time scale for delayed neutron emission is sufficiently long, on average, that control by physical methods is quite feasible. A great deal is known about the properties of critical reactors as a consequence of research spanning more than 60 years, as well as from the operation of many research and power generating reactors around the world. However, much less is known from experimental experience about the properties of sub-critical reactors driven by external neutron sources.

The way a sub-critical assembly responds in operation is governed by its inherent design and the geometry and spectrum of the external neutron source used to “drive” the assembly. In principle, a spontaneous-fission neutron source, the most commonly one used being ^{252}Cf , can be used as a driver. This, of course, has been investigated in YALINA. The “clean” neutron spectrum from a point source of this material is approximately Maxwellian in shape with an average energy of ≈ 2 MeV. However, the available “power” (essentially the neutron flux) from these radioactive sources is very limited. This directly limits the power level attainable in the sub-critical facility. Furthermore Californium sources are, for all intents and purposes, steady-state neutron sources that do not permit convenient investigation of the dynamic response of the sub-critical core to switching the external source “on” or “off”. For this reason, accelerator neutron sources are considered to be the only possible practical approach to implementing the sub-critical reactor concept.

The ADS concept has also been promoted as a potential energy source as well as a means for transmuting radioactive waste. It has been argued that an ADS device designed to operate very close to but just below criticality (k_{eff} slightly less than unity) can act as an energy amplifier. That is, the amount of energy required to operate the accelerator and other components of the facility is less than the fission power produced by the driven system. However, this idea was more in favor a decade ago than it is today because it has long been known that it is also possible to accomplish this same objective using suitably designed critical reactors with technologies that are much more fully developed than those for ADS, and with proven records of excellent reliability. Nevertheless, there is some merit in considering the ADS concept as an energy producing approach, and it is generally acknowledged that it would be imprudent to fail to investigate its properties and to consider the possibility of constructing one or more demonstration facilities to test the concept on a realistic size scale. Such facilities exist conceptually on drawing boards, but none have yet been built or put into operation. ADS facilities operating at power levels sufficient to transmute meaningful quantities of nuclear waste, or to produce significant levels of net power for an energy grid, would be expensive to construct and operate and would require further development of accelerator technology. Therefore, there is a strong motivation to build much smaller, zero-power ADS facilities that would explore many aspects of the behavior of much larger ADS systems at dramatically lower cost, and would also test the predictive power of computational procedures that could be used for full-scale ADS systems. This approach is not unlike the widespread use of zero-power critical facilities to test design concepts for higher-power critical reactors. It is with these considerations in mind that the YALINA facility in Minsk (Sosny), Belarus, came into being.

B. Neutron Production from Nucleon Bombardment of Heavy Nuclei

The amount of energy that it takes to separate a nucleon from any particular isotope varies widely with the incident particle type and nuclear structure of the isotope in question. However, as a rule of thumb, that amount of energy is on the order of or less than 10 MeV to remove a single neutron. This is the so-called neutron separation energy for a single neutron. For present purposes, we are concerned only with the energy introduced by the bombardment of materials by either high-energy protons or neutrons.

A great deal is known theoretically about the process of proton-induced emission of neutrons from bombarded heavy nuclei. Furthermore, spectra of neutrons produced by these processes, commonly known as spallation neutrons, have been measured over a wide energy range to test these theories. First, it should be noted that heavy nuclei are to be preferred to light or even medium weight nuclei as spallation targets. The reason for this is that the binding energy per nucleon tends to decrease with increasing mass number, so it takes less incident energy to release a single nucleon. Another consideration is that certain heavier-mass nuclei such as tantalum or tungsten have the ability to withstand high temperatures that result from the heating produced by recoil energy of the bombarded or scattered particles or by ionization induced by incident charged particles. Lead, bismuth, and mercury in liquid form, can also be good absorbers and transfer media for this heat as well as serving as sources of spallation neutrons. Uranium has sometimes been used as a high-Z target material in such investigations.

In the case of conceptual ADS designs for full-scale systems, the approach is to use accelerators that can generate high-current proton beams with energies of 1 GeV or even higher. Targets of heavy elements designed to handle high-power beam loads would be bombarded with protons to produce copious neutrons which, in turn, would act as the driving force of the ADS reactor core. How are neutrons actually produced when high energy protons (or neutrons for that matter as a consequence of secondary emission processes) interact with high-Z materials? Of course, the incident nucleon can lead to emission of one or a few very high energy secondary neutrons by a direct collision process (billiard-ball effect).

However, it is more likely that an incident high-energy nucleon will simply heat up the target nucleus and initiate a nucleon-meson cascade within the nucleus. In this process the super-heated target isotope boils off successive neutrons, sequentially forming intermediate lighter-mass residual isotopes as the system cools toward an equilibrium state, first through a cascade process, then through pre-equilibrium emission, and finally through the evaporation process. The pre-equilibrium and evaporation neutrons tend to be much lower in energy than the primary incident nucleon. So, while the neutron spectrum has a very high energy component in spallation sources, most of the neutrons emitted have considerably lower energies on average. Thus, the higher the beam energy and power, the more neutrons that are emitted, and these neutrons tend to be emitted with energy spectra characteristic of the effective temperature of the excited emitting nuclei. So, the choice of a high-energy particle beam for conceptual large scale ADS devices is based in the desire to produce as many neutrons as possible rather than on having very high-energy neutrons present in the system. Furthermore, the effective core-driver spectra in conceptual ADS systems would be considerably lower in energy than the fundamental spallation spectrum due to down-scattering of the emitted neutrons by the target assembly and within the general environment of the core of the ADS system itself.

If a target of heavy isotopes is bombarded with 14-MeV neutrons, the dominant reaction channels, other than compound elastic scattering, are inelastic scattering and $(n,2n)$ reactions. As it is the case for bombardment with much higher-energy nucleons, the neutron emission mechanism includes pre-compound and evaporation steps. Relative to the spallation sources, the few neutrons with very high energies are missing. In summary, the emission-neutron spectra one observes in the energy range 1–4 MeV are very similar in shape for the case of 14-MeV neutron bombardment and the spallation sources. This is clearly evident from Fig. II.1. It is for this reason that the combination of a sub-critical core driven by an external 14-MeV generator, as is the case for YALINA facility, can be very effective in studying the likely behavior of much larger facilities that would actually be driven by external spallation neutrons involving much higher incident nucleon beams. As already mentioned, when the incident nucleon energy is high, the main difference in the emitted neutron spectrum from the 14-MeV incident nucleon case is the presence of a small component of very higher-energy neutrons and a larger number of neutrons emitted per incident neutron. In Fig. II.1 it is demonstrated that number of neutrons emitted per incident 650-MeV proton the factor is approximately 13.8 times the number emitted for 14.1-MeV incident neutrons. These neutron-emission spectra can be calculated with reasonable accuracy using contemporary theoretical codes, with the understanding that different models are used to address different incident energy domains. At very high incident energies, the individual structures of the target nuclei are of much less concern than in the case of incident particles in the range of a few tens of MeV or lower energy where detailed target nucleus structure effects are very influential.

Actually, if the target assembly and core are quite massive, as they will be for all but the smallest integral configurations, the very high energy neutrons emitted from spallation sources will in turn lead to emission of additional lower-energy neutrons in much the same way as the primary incident nucleons. This will largely deplete the primary spallation spectrum of high energy neutrons bringing the effective driver spectrum produced from a spallation target even closer to one resembling that produced by 14.1-MeV neutrons from a D-T neutron generator.

C. Neutrons from Deuteron Bombardment of Deuterium and Tritium

So-called neutron generators are relatively small accelerators (a few meters in length at most including the ion source) that operate with relatively high currents of relatively low-energy deuterons incident on targets that contain either gaseous deuterium or tritium or that contain these isotopes of hydrogen absorbed within a metallic matrix (usually titanium metal). The deuterons are accelerated to

energies ranging from about 100 to a few hundred keV maximum. In order to obtain optimal yield in such machines, some excess primary charged-particle energy is required to overcome Coulomb losses experienced by the beam either in penetrating the entrance window to a gas target cell or in traversing the metal matrix containing the absorbed deuterium or tritium. The design and operating characteristics of the particular accelerator used to drive the YALINA facility are described in detail in Chapter VI.

Two distinct nuclear reactions are employed in neutron generators. The first reaction is the $D(d,n)^3\text{He}$ with a Q-value of +3.27 MeV. For typical neutron generators, this leads to production of neutrons with energies around 2.5 MeV. The second reaction is $T(d,n)^4\text{He}$ with a Q-value of +17.50 MeV. This leads to production of neutrons with energies typically around 14.1 MeV. Although neither reaction is a threshold reaction in the conventional sense, there is a threshold effect for both reactions due to Coulomb suppression of the reaction cross section at low incident-deuteron energies. The $D(d,n)^3\text{He}$ reaction is the less favorable of the two mentioned here as a driver for a low-power ADS system for two reasons. First, the neutron energy is relatively low (2.5 MeV). Second, the cross section is considerably lower than the $T(d,n)^4\text{He}$ reaction at comparable energies in the region below a few hundred keV owing to the presence of a strong resonance in the d+T reaction just above threshold. Thus, for a neutron generator the yield of fast neutrons from d+T is typically two orders of magnitude larger than for d+D. However, the d+D reaction is frequently used to test equipment and to make certain exploratory measurements at nuclear facilities such as YALINA because tritium ($T = {}^3\text{H}$) is radioactive (12.32 year half life) and difficult to handle safely as a target material whereas deuterium ($D = {}^2\text{H}$) is stable and very easy to handle. Both reactions have been used in YALINA experiments, as is apparent in subsequent chapters of this report.

D. Neutron Fission Reactions

Much has been learned and written about nuclear fission since its discovery 70 years ago. Here we will focus only on a few properties of neutron-induced fission reactions and indicate where the sources of evaluated numerical data can be found for use in the calculations that have been carried out in support of the YALINA project.

As indicated in Chapter I, nuclear fission is the principle energy source in contemporary controlled nuclear-energy systems. As mentioned, each fission event typically yields on the order of 200 MeV of energy. While nuclear fusion can also generate vast amounts of energy through the $D(d,n)^3\text{He}$ and $T(d,n)^4\text{He}$ reactions, as well as certain other reactions involving light nuclei, exploitation of this energy source has occurred mainly in the laboratory or in nuclear weapons. The development of controlled fusion power sources for peaceful uses is in progress, but practical implementation of that form of nuclear energy is likely to be many decades in the future.

As mentioned earlier, fissionable isotopes fall into two categories: those that fission with thermal neutrons as well as fast neutrons (e.g., ${}^{235}\text{U}$ and ${}^{239}\text{Pu}$) and those that fission mainly with fast neutrons (e.g., ${}^{238}\text{U}$ and ${}^{237}\text{Np}$). Fig. II.2 is a plot of the evaluated neutron-fission cross section for ${}^{235}\text{U}$ while Fig. II.3 is that for ${}^{238}\text{U}$ fission. Fission cross sections for other actinide materials exhibit similar qualitative behavior although the numerical details will differ significantly from one isotope to the next. For all practical purposes, it is observed that a single fission event will generate two energetic recoiling fission-product nuclei emission plus an average of approximately 2.5 neutrons (ν -bar). Again, the finer details depend on the target isotope and incident energy of the neutron.

Actinides that exhibit strong fission cross sections at thermal energies do so because there is a strong bound-state, s-wave resonance very close to the neutron separation energy for the composite

system of incident neutron plus the target. Both thermally fissionable and threshold-fissionable isotopes exhibit resonant structure in the energy region beginning at around 1 eV and persisting into the high-keV energy range. Accurate knowledge of the fission cross sections for all materials encountered in the YALINA experiments is essential in order to be able to calculate what is observed and thereby understand the operating characteristics of not only YALINA but ADS systems in general. Libraries of evaluated cross sections from diverse sources have been produced, and these can be obtained from various nuclear data repositories in the United States, Europe, Russia, and Asia. In the United States, the main source of this information is the National Nuclear Data Center (NNDC) at Brookhaven National Laboratory (www.nndc.bnl.gov). The most recent official U.S. nuclear data library is ENDF/B-VII.0. The plots shown in Figs. II.2 and II.3 were generated from this database. In addition to knowing the fission cross sections, knowledge of the prompt and delayed fission-neutron yields (ν -bar prompt or delayed) is also essential to accurately calculate the neutron inventory in an ADS system. As mentioned earlier, knowledge of delayed neutron yields is critical to understanding how a critical reactor facility can be controlled. It also plays a significant role in the behavior of sub-critical ADS systems. These data can also be obtained from the data centers such as the NNDC.

All these data can be used in various forms, depending on the codes that will be utilized for analysis purposes. Deterministic codes generally use group-cross section libraries whereas Monte Carlo system simulation codes generally use point cross section libraries. These specially processed and formatted libraries are based on the same fundamental information. There are differences – some minor and some major – between the numerical values for corresponding quantities in the libraries with different origins, reflecting varying degrees of uncertainty in the knowledge of these physical quantities. It is important to perform system calculations using nuclear data libraries from various origins since there can be significant differences in cross sections for various reaction processes including fission. This is especially true for reactions and energy regions where experimental data are limited (e.g., several of the minor actinides), and where strong reliance is made on nuclear theory to estimate some of the cross sections which are found in these libraries. By comparing computed results obtained using different libraries it is possible to estimate the uncertainty associated with the analytical results. Examples of this are seen in Chapter XIII.

It is important to avoid giving the wrong impression concerning the contemporary status of fission cross section data. In fact, the cross sections for those fission reactions that dominate the neutronics of ADS systems such as YALINA (i.e., the major-actinide cross sections) tend to be quite well known over most of the energy range of interest. Therefore, it is important to note that the YALINA experiments are not intended to yield data to improve these cross sections but rather to test computational procedures. Furthermore, differences in the fission cross sections for the major actinides from different global libraries tend to be rather modest. Therefore, computations using the different libraries are intended primarily to check on the sensitivity of results to these small differences (usually of rather little consequence) and to build confidence in the computational procedures that utilize these libraries. Where the differences are significant, e.g., for certain minor actinides, then data from integral measurements such as those carried out at YALINA can make important contributions toward improving knowledge of these cross sections. These cross sections can influence transmutation calculations in a major way, but the impact is generally far less on system neutronics and on calculations of neutron spectra at various locations in the ADS core.

E. Transmutation of Nuclear Waste

For all practical purposes, the transmutation of nuclear waste is dominated by fission and capture cross sections for the actinides and on neutron capture for the fission products. In a broad sense, the desired transmutation of light water reactor (LWR) nuclear waste to shorter-lived species can be

accomplished best in a fast-neutron spectrum where fission of the minor actinide nuclei tends to prevail relative to capture. This is in contrast to the situation encountered in thermal neutron spectra where capture is dominant (except for thermally fission actinides such as ^{235}U). Fission transmutes long-lived minor actinides to shorter-lived fission products while neutron capture tends to breeds more minor actinide isotopes of higher mass number than the target materials. Several of these are exceedingly long-lived. Neutron fission is discussed in Section II.D so the focus in this section is on the neutron capture process which is important for transmuting fission product nuclei. In order to gain an understanding of the issues involved in transmutation, it is useful to give two examples of radiative neutron capture cross sections. While $^{238}\text{U}(n,\gamma)$ produces valuable ^{239}Pu fuel indirectly from the decay of ^{239}U , capture in certain other actinides can generate troublesome long-lived minor actinides. $^{129}\text{I}(n,\gamma)$ is an example of capture transmutation of a long-lived fission product (^{129}I with a 1.57×10^7 year half life) to the much shorter-lived ^{129}I (with a 12.36 hour half life).

Unlike neutron fission, capture cross sections cannot be classified into two distinct categories. All capture cross sections tend to have similar characteristics: a $1/v$ shape at low energies, resonance structure in the eV to high-keV region, and a smooth and generally decreasing cross section in the MeV energy range. However, the similarities are deceptive because the effectiveness of the capture reaction on transmutation is very strongly dependent on the neutron spectrum, on the actual behavior in the $1/v$ region, on the detailed resonance structure, and to some extent on the cross section in the fast region. Capture cross sections tend to be known the best at thermal energy and in the $1/v$ region above thermal, less well known in the resonance region, and generally rather poorly known in the fast region where the cross section tends to become quite small. There is no fundamental theory that can explain the details of the resonance structure (spins, strengths, and widths of the resonances). Therefore, unless there are detailed measurements of resonance properties, the cross section will be rather poorly known there as well. The combination of often poorly known fission cross sections for many minor actinide nuclei and frequently poorly known radioactive capture cross sections for some important fission products results in a state of considerable uncertainty in the area of transmutation science and technology. Experiments such as those that have been performed or planned at the YALINA facility and other ADS and reactor facilities will be very valuable in sorting out the scientific issues of nuclear waste transmutation.

F. Other Relevant Nuclear Data Issues

Neutron elastic and inelastic scattering and neutron emitting reaction cross sections such as $(n,2n)$, $(n,3n)$, or (n,xn) have a significant influence on the neutronics characteristics of a nuclear facility because they impact heavily on neutron transport through materials.

Elastic scattering involves collisions in which no energy is imparted to the target nucleus other than recoil (kinetic) energy. Elastic scattering neither adds nor subtracts from the neutron inventory in the core. However, scattering does change the direction of a propagating neutron (neutron transport), and elastic scattering processes therefore play an important role in how reflectors affect the reactivity of a fissionable core. Also, in spite of the term “elastic”, neutrons that undergo elastic collisions do lose energy because of the kinetic energy transfer to the target that is required to conserve momentum. Collisions with heavy nuclei result in less loss of energy for the neutrons while those with light nuclei impart more energy to the recoiling target. Also, the larger the scattering angle, the greater the energy loss experienced by the scattered neutron. In the case of scattering from hydrogen, kinematic considerations prevent scattering in the laboratory system beyond 90 degrees. At very low energies, and for moderate- to heavier-mass target nuclei, elastic scattering is quasi-isotropic. However, at higher energies scattering tends to be forward peaked. Elastic scattering cross sections and angular distributions available from data libraries used for transport calculations are reasonably well known for most of the common materials found in reactor

assemblies (both critical and sub-critical). Heavy use has been made of nuclear-model calculations in generating these cross sections, but these are mainly based on spherical and deformed optical models whose parameters have been validated by comparisons with elastic scattering experimental data obtained from experiments involving both elemental and isotopic samples.

Inelastic scattering also does not alter the neutron inventory in the core. While this process leaves the target nucleus in an excited state, it does not change the chemical (Z) or isotopic (A) nature of the target. Any single scattering event leaves the target in a specific discrete excited quantum state. The evaluated data files usually provide cross sections and angular distributions corresponding to several of the lowest lying excited states of common materials based, once again, based on experimental data and nuclear modeling. However, at elevated excitations these states may be sufficiently close in excitation energy that they cannot be easily distinguished. Under these conditions both experiments and calculations usually involve continuum approximations. Inelastic scattering angular distributions are far more isotropic, in general, than elastic scattering distributions. Inelastic scattering cross sections are considerably less well-known than elastic cross sections, although a considerable body of experimental data on inelastic scattering exists as well as a general understanding of the physics mechanisms that underpin the nuclear models.

Reaction cross sections such as $(n,2n)$, $(n,3n)$, and (n,xn) , where “ x ” could signify a charged particle such as a proton or alpha particle, also can have an influence on neutron transport, but to a lesser extent than elastic and inelastic neutron scattering. In the case of $(n,2n)$ and $(n,3n)$ reactions, neutrons are added to the core inventory whereas (n,xn) reactions, when “ x ” is a charged particle, do not alter the neutron inventory. While considerable data exist for certain materials for the angle integrated cross sections, especially for the $(n,2n)$ reaction, very little experimental information is available for neutron emission angular distributions since these involve three or more particles in the exit channel (including the reaction product) nuclei thus leading to continuum neutron spectra. Therefore, neutron-emission information in evaluated libraries is almost always based on nuclear modeling that has been validated to the extent possible by comparisons with available neutron-emission experimental data.

..... *Figures for Chapter II begin on the following page*

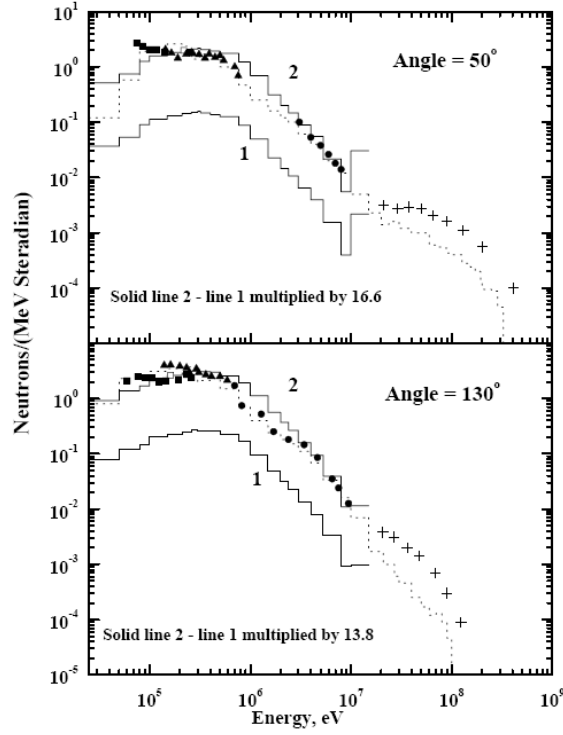


Figure II.1: Comparison of experimental and calculated energy spectra of leakage neutrons at angles 50° and 130° from uranium targets bombarded with 750-MeV protons and 14.1-MeV neutrons from a D-T neutron generator, respectively. The histograms represent results of calculations with the computer code LAHET while the points are experimental data. The normalization factor for histogram-2 is per one incident 750-MeV proton while that for histogram-1 is per one incident neutron with energy 14.1 MeV. The difference in the scale of these curves is approximately a factor of 13.8 over the energy range 1 to 10 MeV, but it is evident that the shapes are very similar at energies below 10 MeV.

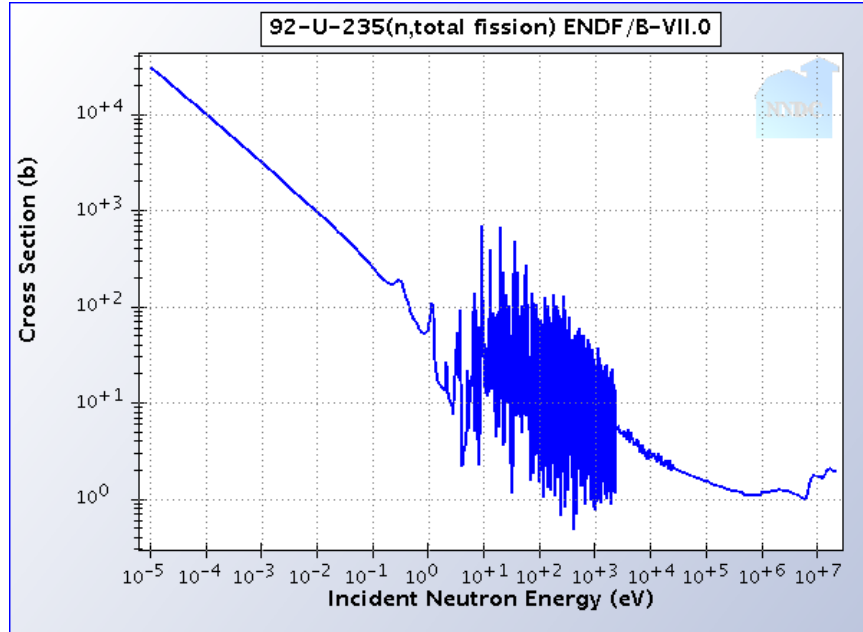


Figure II.2: ^{235}U total neutron fission cross section from ENDF/B-VII.0.

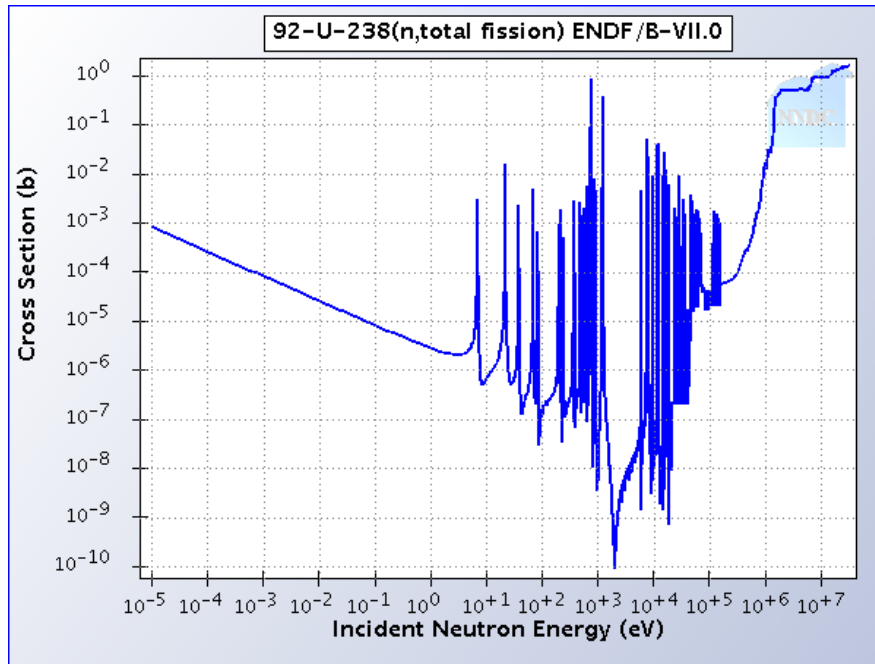


Figure II.3: ^{238}U total neutron fission cross section from ENDF/B-VII.0.

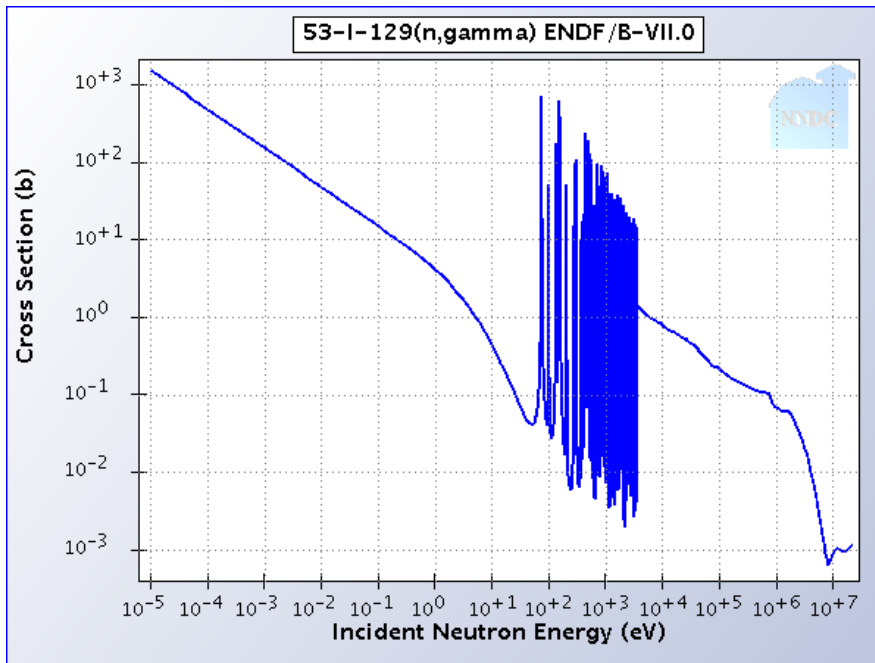


Figure II.4: ^{129}I neutron radiative-capture cross section from ENDF/B-VII.0.

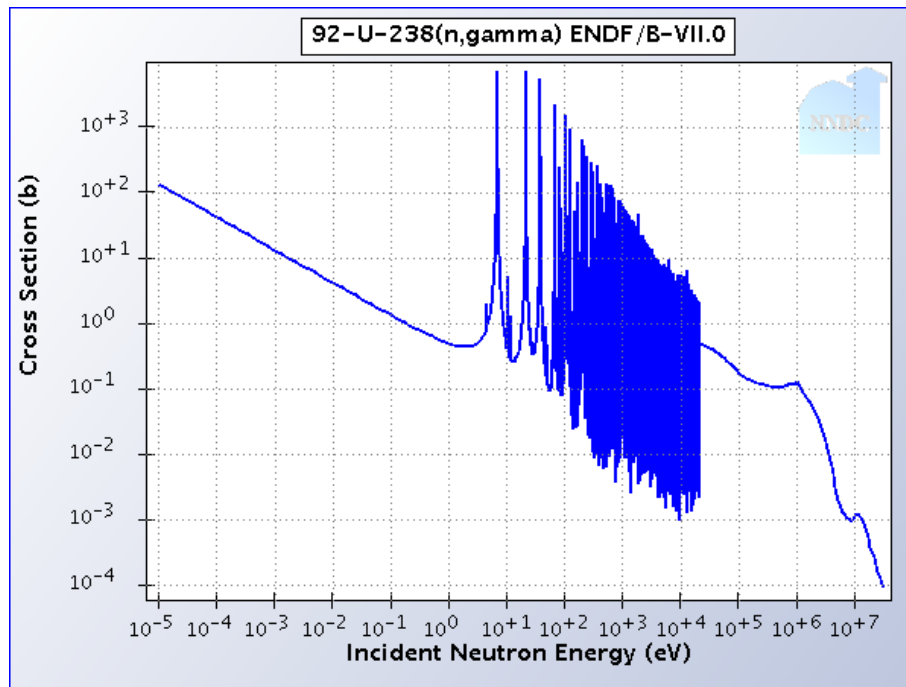


Figure II.5: ^{238}U neutron radiative-capture cross section from ENDF/B-VII.0.

III. Research Objectives

The United States became involved in research at the YALINA facility in a significant way in 2005 with the beginning of direct participation by scientists from the Nuclear Engineering Division, Argonne National Laboratory. This Chapter describes the principal motivations for this activity on the part of Argonne. The United States has three main objectives for this collaborative effort. The first is to validate its computational methods for ADS systems using actual experimental data. YALINA is a valuable test bed for furthering this objective since it is an ADS facility that has actually been built and is not just in the conceptual or design phase. Furthermore, its operation can be sustained for an extended period of time with considerable flexibility and at a relatively low operating cost. The second objective is to demonstrate that the YALINA facility can conduct a viable research program in ADS and waste transmutation physics using core configurations fueled with LEU. If so, this would provide a well-justified basis for eventual removal of HEU materials from the facility with a considerable reduction of security risk. The third objective is to establish a friendly and productive collaboration with Belarusian scientists involving shared research in an area of mutual interest.

Considering the first objective, Argonne uses its analytical code suite and computational experience to model the YALINA experiments that involve various chosen core configurations. Examples of these are the thermal configuration (YALINA-T) and the “booster” configuration (YALINA-B) described in this report. In so doing, Argonne is able to generate its own analytical results, obtained using various computational methods and evaluated nuclear databases, and to compare them with corresponding results obtained by Belarusian scientists and researchers from institutes in other countries who are also involved in this collaboration. These computational results are then validated by consideration of data acquired at YALINA in order to select the most appropriate computational tools, nuclear databases, and analytical procedures for future ADS applications. This information is also valuable for further investigation of various nuclear-waste transmutation options. The framework for collaboration with both Belarus and other nations involved in the YALINA research is provided by the IAEA, largely through the coordinated research program mechanism (CRP).

The second objective, as also mentioned briefly in the Introduction, involves encouraging the eventual migration of ADS research at YALINA from use of HEU to core configurations involving only LEU, is closely coupled to the U.S. Department of Energy National Nuclear Security Agency Global Threat Reduction Initiative long-term objective of removing HEU with Russian assistance from FSU countries in Eastern Europe and Asia, thereby reducing the risk of nuclear proliferation and nuclear terrorism that might occur as a consequence of HEU divergence from nuclear facilities. Argonne is using its analytical tools and procedures, validated by in-house computational exercises over many years as well as by comparisons with computed results obtained from collaborating countries and with experimental data, to suggest suitable YALINA core configurations that would contain only LEU for use in future experimental work at this facility.

The third objective is a relatively intangible one, namely building constructive relationships. This goal is likely to be achieved if the collaborative scientific activities involving the United States and Belarus are carried out by scientists from both countries by working together. Furthermore, it is important that the respective national nuclear energy programs as well as the personal careers of individual scientists benefit from sharing the fruits of this work. The experience of the past several years since Argonne has been involved with YALINA suggests that this objective, however intangible it may be, is indeed being achieved quite successfully.

In order to insure success in the pursuit of these objectives, Argonne scientists frequently travel to Belarus for discussions with their Belarusian counterparts concerning the details of ongoing research and for experiment planning sessions. Argonne scientists have also become involved directly in some of these measurements, and they are assisting YALINA facility staff in acquiring experimental hardware and software, in developing analytical tools, in preparing joint publications dealing with experimental and computational results that are presented at workshops and conferences, in working out the details of core designs aimed at achieving successful operation of the facility solely with LEU, and finally in planning future research campaigns in the areas of ADS and waste transmutation physics as well as facility monitoring and diagnostics methodologies.

IV. YALINA Project Chronology

YALINA operates today as a viable and productive research facility, and it is expected to continue to do so for several more years. The year 2008 did mark a turning point in the sense that the transformation from operation with both LEU and HEU to operation entirely with LEU is now well underway. Future work will emphasize research with LEU cores. This chapter traces the evolution of the YALINA sub-critical facility from its origins in 1997 to late 2008 compiled from information available in a collection of progress reports, theses, journal publications, and other types of available written communications. This chronology is presented in the form of short bullets that are intended to provide the reader with a brief insight into some the steps that have brought the YALINA facility along from its inception to the present day. Since the objective is to provide the reader with an overview of the evolution of the YALINA project, no attempt is made here to insure that every possible step along the way is included in this chronology or to provide precise milestone dates. In fact, it has proved to be rather difficult to determine exactly which tasks and achievements could be attributed to any particular year since many of the progress reports, conference contributions, and other documentation available for preparation of the present report refer to past work as well as future plans along with discussions of ongoing work, frequently without a clear distinction between them. Also, several of these documents are not dated explicitly. While the distinction between various tasks and achievements from year-to-year is somewhat blurred, the general impression of the evolution of YALINA research over the past decade that this chapter provides is believed to be fairly realistic.

Further details on the individual aspects of this work can be found in other chapters of this report or in the documents listed in References and Publications. No mention is made here of specific publications, status reports, conference attendance, etc., since these appear by date in Reference and Publications at the end of the report. Furthermore, owing to repetition many of the details mentioned here are discussed in several of these listed documents

1997

- Installation and testing of neutron generator NG-12-1 was begun.
- An ISTC grant for development of an ADS sub-critical facility (YALINA) was sought.

1998

- Neutron generator NG-12-1 was commissioned.
- A deuterium target for $D(d,n)^3\text{He}$ neutron source measurements was installed.
- Neutron flux measurements were performed for the neutron generator.
- Radiation doses in vault rooms nearest to neutron generator were measured.
- Thermal neutron fluxes were measured in a paraffin and graphite moderator near the target.
- An irradiation of a lead target surrounded by moderator material was performed.
- Plans were made to convert the NG-12-1 accelerator so that would operate in pulsed mode.
- ISTC grant (#B-070-98) for the YALINA facility was approved on 1 September 1998.
- A detailed technical schedule for ISTC Project #B-070-98 was prepared.
- Construction of the uranium-polyethylene assembly (the original YALINA) was completed.
- Monte Carlo calculations of k_{eff} and neutron spectra were performed for YALINA.
- Planning the selection of nuclear radiation detectors for the YALINA facility was completed.
- Discussions were held on partnerships with foreign institutes concerning YALINA research.

1999

- Modifications were made to the high-voltage supply unit of the NG-12-1 neutron generator.
- A pneumatic sample transport system was installed and tested.
- Testing of the MCNP-4A Monte Carlo code was performed.
- Neutron transport code validation studies were carried out.
- Calculations were done of the YALINA physical characteristics with a thermal neutron spectrum.
- Preliminary simulation studies of YALINA with a fast-neutron spectrum were performed.
- Transmutation rates for ^{129}I and ^{237}Np and others were calculated for several neutron fields.
- Procedures for performing neutron measurements at YALINA were established.
- A detailed facility safety analysis was performed.
- Detailed calculations of sub-critical core reactivity worth for various configurations were done.
- A licensing application to create a sub-critical assembly with two configurations was submitted.
- Design and analytical collaborations with scientists from several foreign countries began.
- The selection of materials to be used in transmutation studies was completed.

2000

- The selection of fuel element loading combinations for YALINA-T was completed.
- The first fuel loading of YALINA-T was accomplished.
- The license to service and operate YALINA-T was received.
- Issues associated with acquiring a Ti-T target from Ukraine were still being addressed.
- Samples of the ^{129}I , ^{237}Np , and ^{243}Am isotopes were ordered from suppliers in Russia.
- Inter-comparisons were made between Monte Carlo criticality calculations by the collaborators.

2001

- Operation of YALINA-T with $\text{D(d,n)}^3\text{He}$ and ^{252}Cf external neutron sources drivers was tested.
- Neutron flux levels for both driver modes with a loading of 280 fuel rods were established.
- Further work on preparing the experimental areas for the YALINA project was completed.
- Measurements were made of neutron flux spatial distributions and reaction rates in YALINA-T.
- Work on testing the noise method to measure the sub-criticality level for YALINA-T was begun.
- Measurements of both k_{eff} and k_{source} were performed in static and pulsed modes at YALINA-T.
- The first (n,γ) transmutation measurements for ^{129}I , ^{237}Np , and ^{243}Am samples were completed.
- Comparisons between calculated and measured isotope transmutation rates were performed.
- Computer simulations of YALINA-T operation with a $\text{T(d,n)}^4\text{He}$ external source were performed.
- Acquisition of a Ti-T target from Ukraine was still pending due to customs problems.

2002

- Measurements to determine the spatial kinetics of YALINA-T by various means were continued.
- Measurements of sub-criticality parameters for YALINA-T by various means continued.
- Further measurements to map the YALINA-T spectrum continued using active and foil dosimetry.
- Further measurements to determine (n,γ) transmutation rates in YALINA-T were undertaken.
- Fission reaction rates and spectral indices were measured in the experimental channels.

- A Ti-T target was finally obtained, installed, tested, and put into operation.
- An application for extension of the original ISTC project for YALINA was prepared.

2003

- Mapping of the YALINA-T core spectrum using the T(d,n) ^4He source was undertaken.
- Reactivity changes due to removal of specific rods were determined.
- Sub-criticality parameters for YALINA-T were measured with the T(d,n) ^4He source.
- Extensive Monte Carlo modeling studies were performed for comparison with experiments.
- Comparisons were made of results calculated using various neutron data libraries.
- The application for extension of the original ISTC project for YALINA was approved.

2004

- Experimental measurements of criticality parameters by various methods were performed.
- Monte Carlo studies of the anticipated behavior of the booster concept were carried out.
- The design of the YALINA Booster (YALINA-B) core was completed.
- Construction of the YALINA-B core assembly was completed.
- The YALINA-B assembly was installed.
- Initial experimental tests of the YALINA Booster concept were carried out.
- Measurements confirmed unidirectional neutron connection between booster and thermal zones.
- A program for YALINA-B research was established.
- A proposal for a new IAEA CRP on coupling of an external neutron source to a core was prepared.

2005

- The IAEA CRP was launched with participants from many countries (including the U.S.).
- Lead organization assignments for each topical area of the CRP were established.
- Radial and axial neutron flux distributions and spectral indices were measured for YALINA-B.
- The effects of the B₄C “valve” zone in YALINA-B were measured without uranium fuel.
- Reactivity worth measurements for fuel pins and control rods were determined for YALINA-B.
- The reactivity effect of the lead target was determined.
- A determination of the prompt neutron lifetime in various regions of YALINA-B was performed.
- The effect of borated-polyethylene shielding on the assembly sub-criticality level was determined.
- A research collaboration of the YALINA scientists with Argonne National Laboratory began.
- The planning of a “roadmap” for eventual migration of YALINA-B from HEU to LEU began.
- Possible ways to reduce the drop in performance from HEU to LEU fuel were explored.
- Initial measurements with LEU fuel in YALINA-B were performed.

2006

- Transition from the YALINA-T to YALINA-B core was completed.
- Extensive measurements of sub-criticality parameters were performed using various methods.
- Comparisons were made of the characteristics of YALINA-B and YALINA-T system responses.
- Axial flux distribution measurements were made with ^3He (n,p), $^{235,238}\text{U}$ (n,f), and ^{197}Au (n, γ).
- Spectral-index determinations were made using $^{235,238}\text{U}$ (n,f) data.

- Radial distribution measurements were made with $^{197}\text{Au}(n,\gamma)$.
- The applicability of pulsed neutron sources for controlling sub-critical systems was studied.
- Studied the correlation between k_{eff} and quantity of fissile material and neutron source position.
- Optimal procedures for fitting neutron flux decay curves were investigated.

2007

- Detailed specifications for YALINA-T and YALINA-B were documented.
- New instrumentation and data acquisition software were obtained and installed.
- Detailed models for analysis code inputs were prepared by Argonne for YALINA-B.
- Variations due to use of different evaluated nuclear data libraries were investigated by Argonne.
- Argonne calculated k_{eff} , k_{source} , and β using various codes.
- Argonne calculated reaction rate per source particle vs. position using $^3\text{He}(n,p)$ and $^{235}\text{U}(n,f)$.
- Neutron spectrum calculations were performed by Argonne.

2008

- A report on recent Argonne analytical work on YALINA-B was completed (ANL-NE-08/13).
- A paper on Argonne's analytical work was presented at PHYSOR-2008 in Interlaken, Switzerland.
- Confirmation of the performance of newly deployed equipment and software was in progress.
- Sub-criticality parameter measurements by various procedures were being wrapped up.
- Spectrum, flux, and reaction-rate calculations were done for $\text{D}(d,n)^3\text{He}$ and $\text{T}(d,n)^4\text{He}$ sources.
- Extensive analyses to validate experimental and analytical procedures were being performed.
- 90% enriched fuel was being replaced with 36% fuel and a new core configuration was being tested.
- Analysis related to the replacement of 36% fuel with 21% fuel was in progress.

V. Formal Research Agreements

The YALINA project was developed and research has been carried out during the past ten years within the framework of several research agreements that have provided or are providing essential funding for the project as well as opportunities for collaboration with foreign investigators. Synopses of these formal agreements are presented in this section.

ISTC Project #B-070-98

Title of the project:

Experimental and Theoretical Research of the Peculiarities of Transmutation of Long-lived Fission Products and Minor Actinides in a Sub-critical Assembly Driven by a Neutron Generator

Initial date of the project: 1 September 1998

Project duration: 72 months (1998 – 2004)

Contracting institute: National Academy of Sciences of Belarus

Participating institute: The Power Engineering Problems Institute

Project manager: Dr. Anna Kiyavitskaya

Scientific leader: Dr. Serguej Chigrinov

Official foreign collaborators:

M. Hron (Czech Republic), I. Slesarev (France), C. Broeders (Germany), G. Cherardi (Italy), H. Klippel (the Netherlands), A. Kochetkov (Russia), E. Gonzalez-Romero (Spain), and W. Gudowski (Sweden)

Representatives from other organizations involved:

Y. Kadi (CERN), A. Stanculescu (IAEA), and G. Kulikov (ISTC)

Overview of the intent of the program:

The research carried out under the terms of this agreement was designed to study the neutronics of accelerator driven systems (ADS), to measure transmutation rates of fission product (FP) and minor actinide (MA) nuclei, to investigate the spatial kinetics of sub-critical systems driven with an external neutron source, to test experimental methods for estimation of the sub-criticality level, to measure neutron spectra, and to investigate the dynamic characteristics of sub-critical systems driven with a pulsed-neutron generator as an external source. The information to be gained from such a research program was considered to be of great importance for the design of future ADS facilities and for validating the results of computational procedures to be used in the development of such devices. At the time that this collaboration was initiated, there was intense interest in ADS systems, particularly in Europe. This interest was stimulated by strong involvement on the part of influential European scientists such as Carlo Rubbia,

and by some experimental studies performed at CERN. Interest in the U.S. was never quite as intense as that found in Europe, but there was nevertheless a mild interest on this continent in the possibility of producing inherently safe subcritical fission reactors that could be used for waste transmutation and, possibly, for energy production.

Major tasks and achievements in this project at YALINA:

- Preparations were completed in the facility control room, accelerator vault, and sub-critical assembly vault areas.
- The neutron generator NG-12-1 was placed into operation for use as a neutron source capable of operating in both d+D and d+T modes, using deuteron beams and both deuterium and tritium bearing targets.
- A ^{252}Cf spontaneous neutron source was also put into service as an alternative neutron source to the neutron generator source for certain measurements.
- The design, construction, assembly, and start-up procedures for the uranium-polyethylene sub-critical assembly of YALINA (YALINA-T) were completed.
- The procedures for loading of the fissile materials and general safety monitoring procedures for operating this facility were developed, as required to obtain approval for licensing of this facility by the government of Belarus.
- Extensive Monte Carlo calculations of the neutronics characteristics of the assembly were performed as a requirement to satisfy Belarusian government regulations.
- Comparisons of calculated results obtained using various nuclear data libraries were performed.
- Experimental procedures for the irradiation of samples, spectrum unfolding, and measurement of the multiplication factor for the sub-critical system were developed and tested.
- Distributions of reaction rates and spectral indices were measured in the radial and axial experimental channels of the assembly by means of various activation techniques.
- Measurements were made on the dependence of neutron flux density on the type and position of the external neutron source at the sub-critical level $k_{\text{eff}} = 0.977$ (the limit is $k_{\text{eff}} \leq 0.98$ for all conceivable variations of external factors as well as the inherent design of the facility).
- Results were obtained from some measurements using the external neutron generator in pulsed mode to determine k_{eff} for this system.
- Preliminary measurements were made of transmutation rates of ^{129}I , ^{237}Np , and ^{243}Am in the thermal spectrum of YALINA-T.
- Reports were given at various scientific conferences by YALINA staff members as well as foreign collaborators on the results from work carried out at this facility.
- Widespread recognition by European collaborators as well as the IAEA of the uniqueness of the YALINA experiment, and the capability of this facility to support ADS research was achieved.
- Widespread encouragement was elicited from external advisors for an extension of the ISTC project beyond the original three-year contractual period.

IAEA Coordinated Research Programme #132006

Title of the project:

Analytical and Experimental Benchmark Analyses of Accelerator Driven Systems (ADS)

Initial date of the project: 1 October 2005

Project duration: 60 months (2005 – 2010)

Contracting institute: Joint Institute of Power and Nuclear Research “Sosny” (Belarus)

Chief investigator: Anna Kiyavitskaya

Field of research:

Calculation of Benchmark Neutronics of a Booster (Cascade) Assembly Driven by External Neutron Sources

Participating countries:

Argentina, Belarus, Belgium, Brazil, China, France, Germany, Hungary, Italy, Japan, Netherlands, Pakistan, Poland, Russia, Spain, Sweden, Ukraine, and United States (principally Argonne National Laboratory)

Overview of the intent of the CRP:

The objective statement of this CRP given below is provided in the following IAEA Website:

<http://www.iaea.org/inisnkm/nkm/aws/fnss/crp/crp7.html>

“Several countries with nuclear programs are considering ADS systems as a method to implement nuclear waste transmutation in the scope of their nuclear waste management strategies. The proposed CRP will advance the MS efforts toward designing a demonstration facility by providing the information exchange and collaborative research framework needed to ensure that the tools to perform detailed ADS calculations, namely from the high energy proton beam down to thermal neutron energies, are available. The specific objective of the proposed CRP is to improve the present understanding of the coupling of ADS spallation sources with multiplicative sub-critical nuclear systems. In the previous IAEA-CRP on ‘Use of Th-based Fuel Cycle in ADS to Incinerate Pu and to Reduce Long-lived Waste Toxicities’, reactor physics benchmark calculations on ADS with fixed external neutron sources have been performed. Comparison of the results of this CRP shows that large discrepancies exist both related to the use of different methods and data. By including comparisons with integral experiments, the proposed CRP will contribute to the clarification of these discrepancies and validate also those results for which satisfactory agreement was reached in the previous CRP. The proposed CRP will address all major physics phenomena of the spallation source and its coupling to the sub-critical system. Integrated calculation schemes will be used by the participants to perform computational and experimental benchmark analyses.”

United States involvement in the CRP:

The principle objectives of the United States in its involvement with this CRP are the following: 1) to participate in experiments to obtain high quality data at the YALINA facility; 2) to test its computational procedures through comparisons of calculated and measured results; 3) to demonstrate that the YALINA facility (and other ADS systems as well) can operate successfully with a core loading limited to low-enrichment uranium (LEU); and 4) to maintain contact with and thereby benefit from the research carried out by the foreign participants in this CRP, including Belarus. The U.S. institute involved

in this CRP is Argonne National Laboratory, a U.S. Department of Energy facility located in DuPage County in suburban Chicago, Illinois.

ISTC Project #B1341

Title of the Project:

Analytical and Experimental Evaluating (of) the Possibility of Creation of (a) Universal Volume Source of Neutrons in the Sub-critical Booster Assembly with Low Enriched Uranium Fuel Driven by the Neutron Generator

Initial date of the project: 6 June 2006

Project duration: 30 months (2005 – 2008)

Contracting institute: National Academy of Sciences of Belarus

Participating institutes: Joint Institute of Energy and Nuclear Research (Sosny)

Project manager: Dr. Anna Kiyavitskaya

Scientific leader: Dr. Anna Kiyavitskaya

Official foreign collaborators:

Argonne National Laboratory (U.S.A.), Royal Institute of Technology (Sweden), Forschungszentrum Karlsruhe (Germany), and Ministerio de Ciencia y Tecnologia (Spain).

Representatives from other organizations involved:

None mentioned.

Overview of the intent of the program:

The following description was extracted directly from a contemporary document that describes the establishment of this ISTC project:

“The policy of minimization and elimination (of) the use of highly enriched uranium (HEU) in commerce has been an important part of international non-proliferation activities for many years. Significant progress has been accomplished in converting research reactor fuel from HEU to low enriched uranium (LEU) fuel. About forty research reactors have been already converted to LEU fuel all over the world. Belarus and U.S. experts are working jointly to evaluate the possibility of converting the high enriched fuel zones (36 and 90% enrichment) of Belarus sub-critical assembly (YALINA Booster or YALINA-B) to use low enriched uranium ($\leq 21\%$ enrichment). Therefore the main objective of the ISTC Project is to study the possibility of converting the high-enriched fuel zones (90 and 36% enrichment) of booster (cascade) sub-critical assembly YALINA-B for use of low enriched uranium without penalizing its functionality. The secondary objective is to perform theoretical and experimental investigations of neutronics of accelerator driven systems (ADS) at (a) sub-critical facility YALINA-B, at different sub-criticality levels, in (a) wide range of core configurations

and compositions of the assembly constituent elements (HEU and LEU nuclear fuel, structure materials, thermal neutrons absorbers, reflectors, shielding etc.).”

“The basic aspects of the accelerator driven systems with (the) application of high energy proton beams for spallation neutrons production due to the interaction of high-energy particles with heavy nuclei targets (W, Pb, Bi, Th and U) are recently widely discussed in scientific publications all over the world. This approach is used for the development of Accelerator Driven Transmutation Technology (ADTT) proposed by Los Alamos National Laboratory. A typical ADS consists of (a) high-energy proton accelerator, neutron producing target and blanket (sub-critical assembly for neutron and energy production). However, the experimental research in this field is rather scarce because the experiments with application of up-to-date high-energy accelerators (LAMPF, AGS, ISR, JINR...) are time consuming, difficult and expensive. The experiments with application of accelerators with high beam currents are planned only for the future. In this connection the ADS experiments with application of low energy accelerators, in particular D-D or D-T mode neutron generators of high intensity may be of great importance. Such experiments can give valuable information about the transmutation reaction rates of minor actinides (MA) and long-lived fission products (LLFP) in different neutron spectra, the cross sections for different reactions, kinetics parameters of coupled systems etc. The program of experimental research at the YALINA-B facility covers the investigation of fast and thermal neutron fields behavior in different zones, kinetic parameters of the system, the effect of one-directional neutron coupling between the fast and thermal zones, spatial distribution of neutron flux density, time dependence of neutron flux density by different neutron pulse durations, transmutation reaction rates on minor actinides and long lived fission products nuclei, etc. Validation of the existing experimental methods and techniques is being carried out along with their further development for the use in other ADS experiments. The results being obtained will improve the ADS design capabilities and reduce the cost. The computer simulation of the YALINA-B neutronics is being performed with applications of the Monte-Carlo method. Validation of computational methods and nuclear data libraries is being accomplished. Detailed analysis of the experimentally measured and calculated results as well as inter-comparison is part of this activity.”

Major tasks and achievements in this project:

Belarusian and U.S. specialists have joined their efforts to evaluate the consequences of converting the HEU fuel zones (^{235}U enrichment = 36% and 90%) of the booster sub-critical assembly YALINA Booster (YALINA-B) to LEU. Effort has been expended to find possible ways of reducing the drop in performance due to the lowering ^{235}U enrichment, as suggested in the main objective of the ISTC Project. This investigation has been comprised of two phases: the first phase involves replacing 90% enriched uranium fuel with 36% enriched UO_2 . The second phase involves replacing 36% enriched UO_2 with 21% enriched UO_2 . The first phase of this investigation consisted of performing experimental and analytical studies to define the sub-critical performance with the original HEU configuration and the modified configuration without the 90% enriched uranium metal fuels has been completed. A new design concept with the 21% enriched UO_2 was established leading to a new configuration in the fast zone with the objective of optimizing the system so as to keep the same performance achieved previously. A new operating license was applied for to perform experiments with the new core design. The second phase of the project involves performing experiments to confirm the sub-critical assembly performance with the 21% enriched UO_2 loaded in the core. This work was progressing as of late 2008 and experimental results are being compared with corresponding analytical calculations.

VI. General Description of the Facility

The YALINA facility is located at the Institute of Physical and Chemical Radiation Problems of the Belarus National Academy of Science in Sosny, in a small village situated on the outskirts of Minsk, Belarus. This facility was developed in the late 1990's in an area of the laboratory formerly devoted earlier to other reactor physics experiments. This chapter offers a general description of the vault area, ion source, accelerator, beam transport system, sub-critical assembly and support/transport platform, target monitoring systems, control and safety systems, and remote experimental areas.

A. Layout of the Facility

The YALINA facility is entirely underground and occupies several shielded vaults dedicated respectively to the control room, accelerator and beam transport system, the sub-critical core assembly, a beam monitoring area, and additional areas for counting irradiated samples, etc. Fig. VI.1 is a schematic diagram of the general layout of this facility.

While this underground facility is entirely enclosed with earth and concrete shielding, and certain individual vaults are separated by fixed concrete walls, additional separate vault areas have been created using stackable shielding that be removed or repositioned in order to facilitate access to the various elements of the facility. Access to high radiation areas is controlled by gates, and mazes are used to block line-of-sight viewing of these areas from non- or low-radiation areas during facility operation.

Two vault areas specifically devoted to the accelerator plus beam transport system and the sub-critical assembly are shown schematically in Fig. VI.2.

B. Accelerator and Beam Transport System

The accelerator used to drive the YALINA sub-critical assembly is shown in Fig. VI.3. This accelerator belongs to a class of machines known as neutron generators. They are among the most common type of accelerators found in low-energy nuclear physics laboratories around the world. This particular accelerator bears the name NG-12-1, and it had been in use for other purposes prior to installing it as an integral component of the YALINA facility. NG-12-1 is of the Cockcroft-Walton type that has no moving parts and generates a terminal voltage of up to 250 kV by means of an electronic voltage multiplication and rectifier network. The beam-transport system and target are maintained at ground potential. Cockcroft Walton accelerators can be built to accommodate quite high beam currents owing the robust charging capabilities offered by the Cockcroft-Walton voltage multiplying principle. This particular accelerator can deliver in excess of 10 mA of current at 250 kV, translating to more than 2.5 kW of potential beam power on target.

The ion source is of the duoplasmitron type, and it is capable of producing a current up to several hundreds of milliamperes. Duoplasmitron sources are characterized by high gas efficiency and a high content of atomic ions. In order to obtain a purely atomic beam of deuterons, a system for ion separation by an electromagnet is used in the terminal of the NG-12-1 accelerator. This accelerator can be operated in both steady-state and pulsed modes. An electronic beam-chopper is used to generate pulsed beams. This enables the generation of neutron pulses with duration 0.5 – 100 microseconds and repetition rates from 1 Hz to 10 kHz. The ability to generate pulsed beams of deuterons (and hence a source of pulsed

neutrons) is very important for certain experiments that are conducted at YALINA, as we shall see in later chapters of this report.

A photograph of the accelerator facility appearing in Fig. VI.3 indicates the ion source, the high-voltage deck, the beam transport system, and the target assembly. Notice in this photograph that the entire accelerator is shown to be situated in a single vault location. In fact, the stackable vault wall separating the target assembly from the rest of the accelerator (as shown schematically in Fig. VI.2) had been removed for servicing at the time this photograph was recorded. Not clearly shown in this photograph are the various pumps used to maintain a high vacuum in the accelerator and beam-transport system. Four NORD-200 absorption magnetic-discharge pumps are used for this purpose. Since mechanical pumps are not employed, there is no concern for the troublesome buildup of oil films inside the beam transport lines or on the target assemblies that is often associated with older-type mechanical vacuum pumping systems.

On the whole, the beam transport system at this facility is a relatively simple when compared with more complex accelerator beam-transport systems commonly found at larger accelerator facilities. The beam transport line is relatively short (a few meters) so the ion optics system needed to direct and focus the deuteron beam is not particularly critical. Steering electrodes, magnetic quadrupole lenses and a bending magnet are used to create a beam spot on target of about 2-3 cm in diameter, as shown in Fig. VI.4. In this photograph, the beam spot is seen glowing with a bluish/white light as a consequence of the interaction of the beam impinging on a vacuum sealing quartz “dummy” target placed at the end of the beam transport tube. This beam viewing technique enables the beam to be carefully aligned with respect to the YALINA sub-critical core assembly. Careful alignment of the charged-particle beam transport system is extremely important to achieve in order to avoid misinterpretation of the core neutron-intensity scan data and inappropriate modeling of the system for neutronics calculations. The final short section of the beam transport system can be oscillated, without breaking the vacuum, in order to better distribute the beam power deposited in the target (for cooling purposes) and for more uniform depletion of the deuterium or tritium target materials (in order to extend the usable target lifetimes). Target oscillation thus significantly enhances the neutron output that can be obtained from each target, integrated over its effective lifetime, leading to major operating cost reductions. The motor used to achieve this oscillatory motion is also shown in Fig. VI.4.

C. Neutron Producing Targets

As discussed in Chapter II, Section C, two deuteron-induced fusion nuclear reactions, $D(d,n)^3\text{He}$ and $T(d,n)^4\text{He}$, can be used to produce neutrons with a low-energy, high-current neutron generator. With the NG-12-1 accelerator facility, $\approx 2.5\text{-MeV}$ neutrons are generated using deuterium (D) targets and $\approx 14.1\text{-MeV}$ neutrons are obtained with tritium (T) targets. This can be compared with the Maxwellian spectrum from ^{252}Cf spontaneous fission with $\approx 2\text{ MeV}$ average energy. Furthermore, with the NG-12-1 accelerator two different types of targets assemblies can be used, irrespective of the type of neutron producing reaction.

One such arrangement is a low-current target assembly which consists basically of a disk that contains a thin titanium film of approximately 2 mg/cm^2 sprayed onto an oxygen-free copper base (see Fig. VI.5). This titanium film is saturated with either deuterium (D/Ti) or tritium (T/Ti) at atom-ratio levels of ≈ 1.5 . When deuterium is used for the target material in this configuration the total neutron yield is $\approx 2 - 3 \times 10^{10}$ neutrons/second. This low-current target can be oscillated at 560 rpm to facilitate cooling (as mentioned above) and the beam current is limited to 1-2 mA.

For higher-current operations (up to 12 mA) and production of intense 14-MeV neutron fields, a more sophisticated and massive rotating target assembly can be used (also shown in Fig. VI.5). Once again this target rotates at 560 rpm, and oscillates at a rate of 2 cycles per minute, both of these motions facilitate cooling and insure uniform beam exposure to the entire surface of the target. With this arrangement, neutron yields of $\approx 1.5 - 2 \times 10^{12}$ neutrons/second can be achieved from a fresh target. The high-current target assembly is one of the most sophisticated and costly components of the accelerator facility. These target units need to be periodically recharged with tritium by foreign companies (e.g., in Russia or Ukraine) to compensate for the depletion (burn-up) of tritium target material. The typical service life of this target is about 50 hours of continuous operation at full beam power.

Both the low-current and high-current targets are water-cooled to further aid in beam heat removal, with water flow rates on the order of 0.9 m/cm^3 per hour and water temperatures no higher than 15 degree Centigrade.

The possibility of measuring the absolute neutron fluence from the source when using the $T(d,n)^4\text{He}$ reaction by detecting the associated alpha particles is provided at the YALINA facility. This standard technique is illustrated schematically in Fig. VI.6.

C. Sub-critical Assembly

The heart of the YALINA facility is the zero-power sub-critical core assembly. It is a rectangular parallelepiped that is 40-cm wide by 40-cm long by 57-cm high. This unit is mounted on a rigid support table and positioning mechanism that enables the sub-critical core to be carefully positioned with respect to the external neutron source. This arrangement is shown in Figs. VI.7 and VI.8.

The sub-critical assembly itself has been designed to enable a wide range of core fuel pin loadings to be accommodated, as befits a research facility. Two of these configurations, known as YALINA-T and YALINA-B, are discussed in detail in Chapters VIII and IX, respectively. In its most basic configuration, which is essentially YALINA-T, the core of the assembly consists mainly of polyethylene blocks with a maximum of 280 separate channels into which fuel rods can be inserted. Several variations to this arrangement are possible, as described in later chapters. The fuel pin lattice, as seen from one end, is basically a square with 2.0-cm pitch (spacing between fuel rod channels). The central part of the sub-critical assembly accommodates a neutron producing lead target approximately 8 cm by 8 cm in transverse cross section and 60-cm long. The core is surrounded by a 40-cm thick high-purity graphite reflector and a 1.5-mm thick cadmium layer. There are four channels, each 55 mm in diameter, for locating the detectors used by the neutron flux monitoring system at the boundaries of the core. In addition, there are three experimental channels, each 25 mm in diameter, positioned at radii of 5, 10, and 16 cm from the central axis of the core. These are used for placing samples of various types or for positioning a Cf-source inside the core. Finally, there are two radial channels and one axial channel, each 25 mm in diameter, located in the graphite reflector. Figs. VI.8 and VI.9 are photographs that show the exterior of the assembly and its relationship to the beam tube of the accelerator. The various components are described in greater detail in Chapters VIII and IX as well as in Appendices D and E.

D. Facility Control and Monitoring Apparatus

All operational aspects of YALINA, other than physical movement of some of the apparatus, as required for alignment, etc., are controlled remotely from a single central control room that is well shielded from the high-radiation areas. This includes control of the ion source, accelerator high voltage deck, beam transport system, target-rotation mechanism, vacuum-pump control system, and water-

circulation system. Various conventional radiation detectors are used for monitoring and safety purposes at the YALINA facility, as discussed in more detail in Chapter X.

..... Figures for Chapter VI begin on the following page

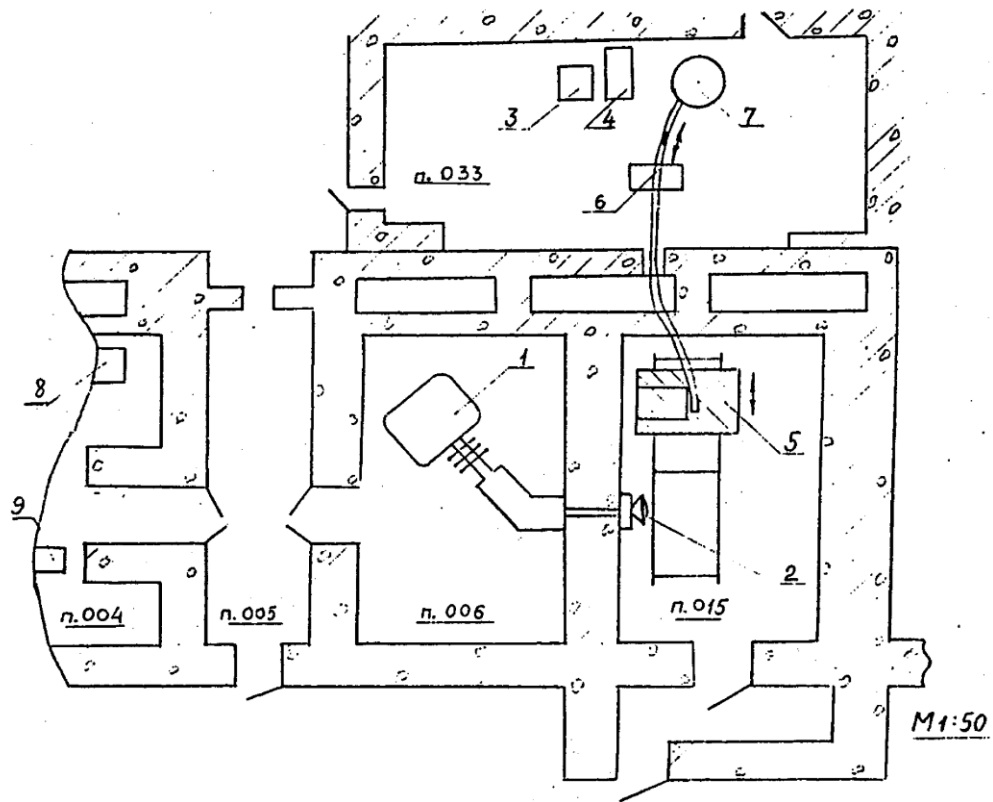


Figure VI.1: Underground vault layout of the YALINA facility.

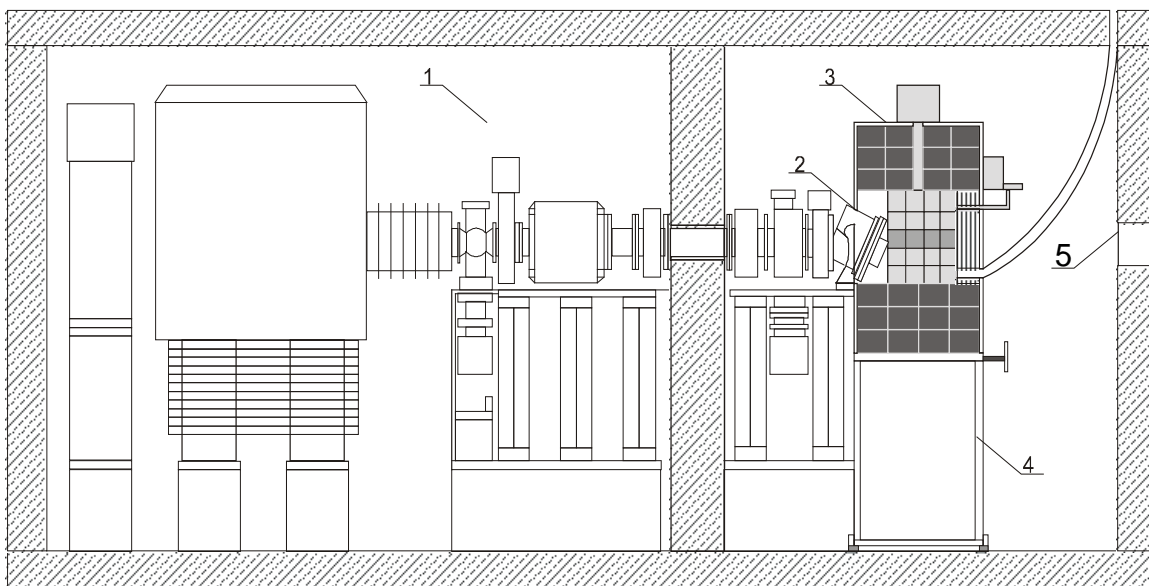


Figure VI.2: Schematic diagram of the accelerator and beam transport system (located in the left vault) and the sub-critical assembly (located in the right vault). Key: 1 – beam transport system; 2 – one of two different types of neutron producing target used in this facility; 3 – sub-critical assembly; 4 – sub-critical assembly mounting and positioning platform; 5 – port for monitoring neutrons from the target by detectors located in a third vault (not shown).

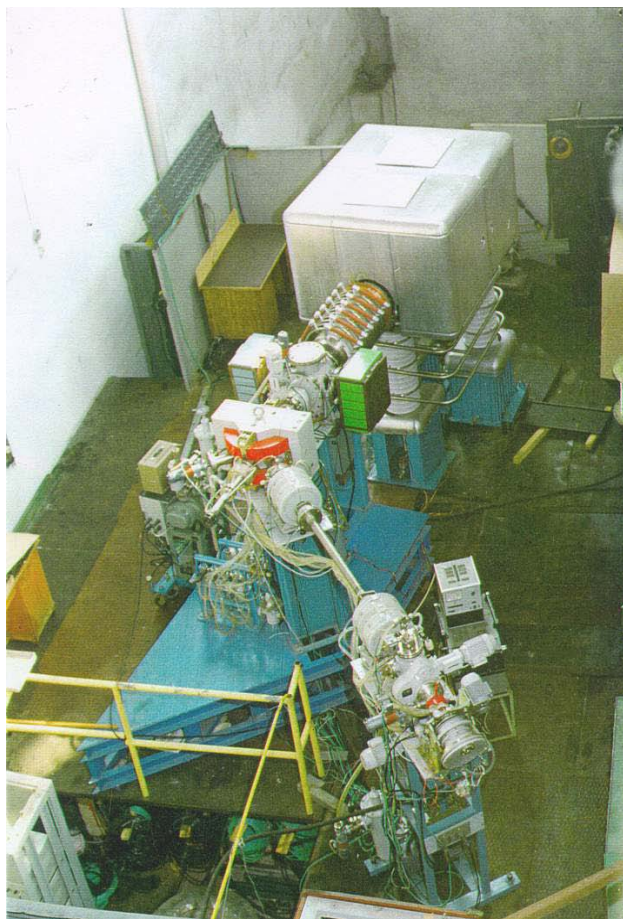


Figure VI.3: View from above of the entire NG-12-1 Neutron Generator Facility

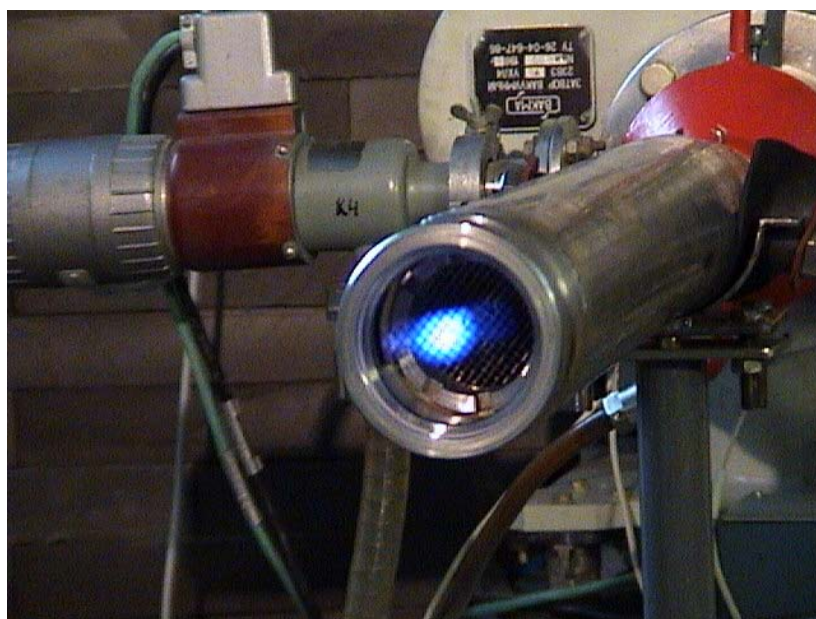


Figure VI.4: Deuteron beam profile at the end of the NG-12-1 accelerator beam transport system viewed using a quartz “dummy” target as a beam stop. Notice the target oscillating motor on the left side.

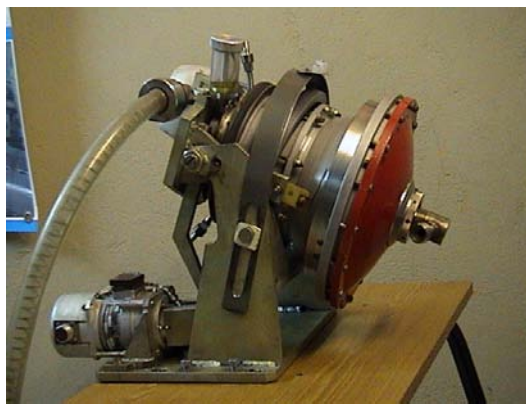


Figure VI.5: Low-current (left) and high-current (right) targets used in the NG-12-1 accelerator.

Absolute monitoring of the neutron flux

- Detection of the charged particles emitted backward by Si detector located at 0.8m of the target
- efficiency $\epsilon = 10^{-7}$ reliable because simply geometrical (no beam optics).

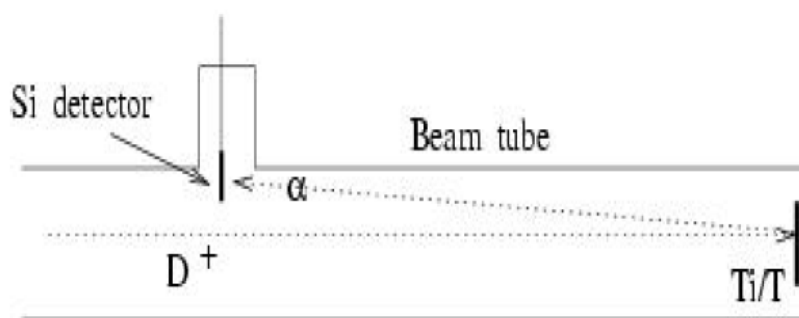


Figure VI.6: Absolute measurement of the source neutron fluence from the $T(d,n)^4\text{He}$ reaction using the associated-particle detection technique.

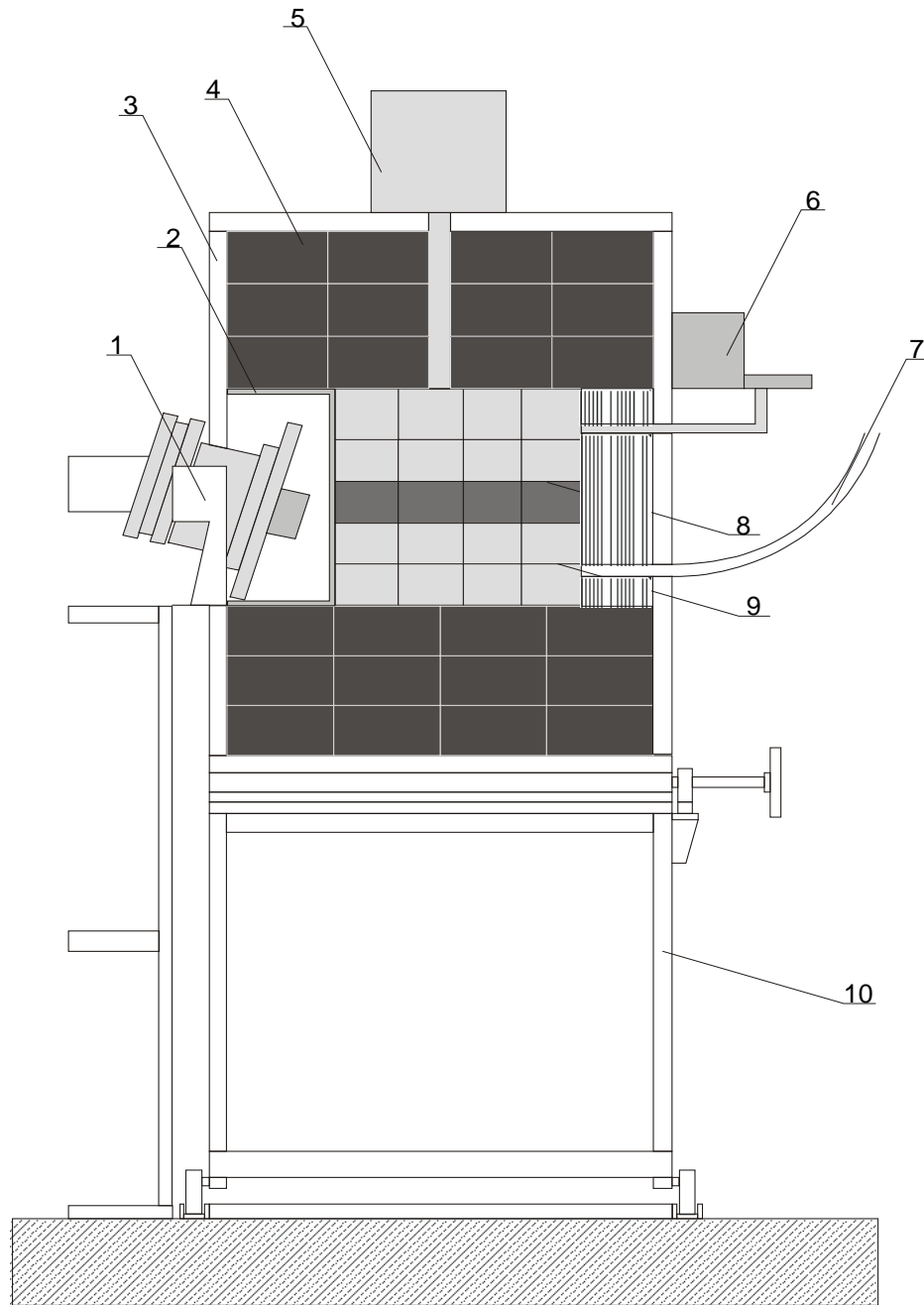


Figure VI.7: Schematic diagram of the YALINA sub-critical assembly. Key: 1 – target unit; 2 – shielding screen; 3 – cadmium screen; 4 – reactor-type graphite reflector; 5 – protective container of the starter Pu-Be neutron source; 6 – control rod mechanism; 7 – rabbit sample-transport system tubing; 8 – lead target; 9 – assembly core; 10 – movable platform.

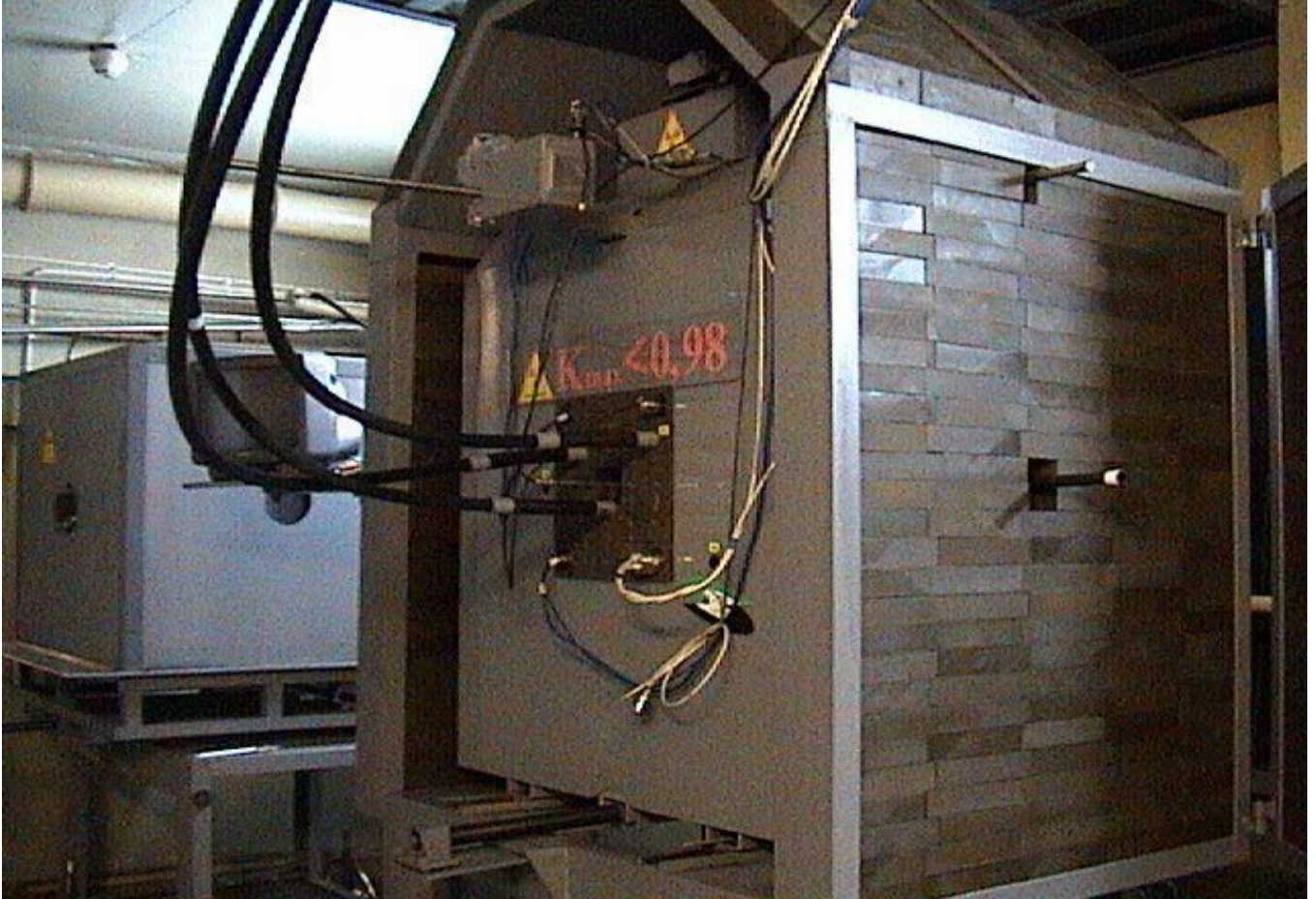


Figure VI.8: Perspective view of the YALINA-T facility as seen from front and one side.



Figure VI.9: Side view of the YALINA assembly moved to one side in order to reveal the beam tube and small target assembly.

VII. Safety Apparatus and Procedures

First and foremost, the basic design and material composition of the sub-critical assembly is such that the neutron multiplication factor remains less than unity (sub-critical) at all times and under all possible variations of external factors such as temperature, pressure, etc., including the hypothetical event of complete flooding of the vault room. The facility design value is $k_{\text{eff}} \leq 0.98$, as is clearly indicated by labeling on the front exterior of the core assembly (see Fig. VII.1). A backup mechanism that allows for the quick insertion of three B₄C rods into the core insures that YALINA will never go critical. Although rarely – if ever used – this mechanism does provide ultimate backup safety assurance in the event of unforeseen extraordinary circumstances that might lead the assembly to approach criticality.

In addition to ensuring criticality safety through the abovementioned basic design considerations, a variety of additional vital-support physical, electrical, and radiation safety features have been incorporated into the design and operation of the facility. There are physical safety-control mechanisms, such as interlocks, in place to minimize the possibility of radiation exposure accidents. Radiation dosimetry monitoring systems are in operation whenever the beam is on the neutron-producing target. An alarm system is in place to signal the possible occurrence of radiation excursions. Additional physical protection and security alarm systems are in place to avert unauthorized entry into radiation and high-voltage areas during operation of the facility. Fire extinguishing apparatus is available throughout the facility. Emergency backup-electrical systems are provided in case of power loss. An emergency water-supply system is available to avert damage to equipment or a compromise of the target vacuum seal due to target overheating. A communications system between the control room and various facility vault areas is in place. A rabbit system is available to facilitate the movement of the starter neutron source and experimental samples into the vault containing the sub-critical assembly.

Finally, and most important, a variety of operational procedures approved by the government of Belarus and laboratory safety personnel are followed rigorously by YALINA staff as well as by visiting researchers. Individuals are trained in the safety systems of YALINA as well as these procedures. They must become familiar with the operation of all facility safety equipment before they are allowed to work in this area. As mentioned above, $k_{\text{max}} < 0.98$ is a guiding spirit of operations at the YALINA facility, and a large sign to that effect is attached to end of the sub-critical core assembly (see Fig. VII.1).

..... *The single figure for Chapter VII appears on the following page*

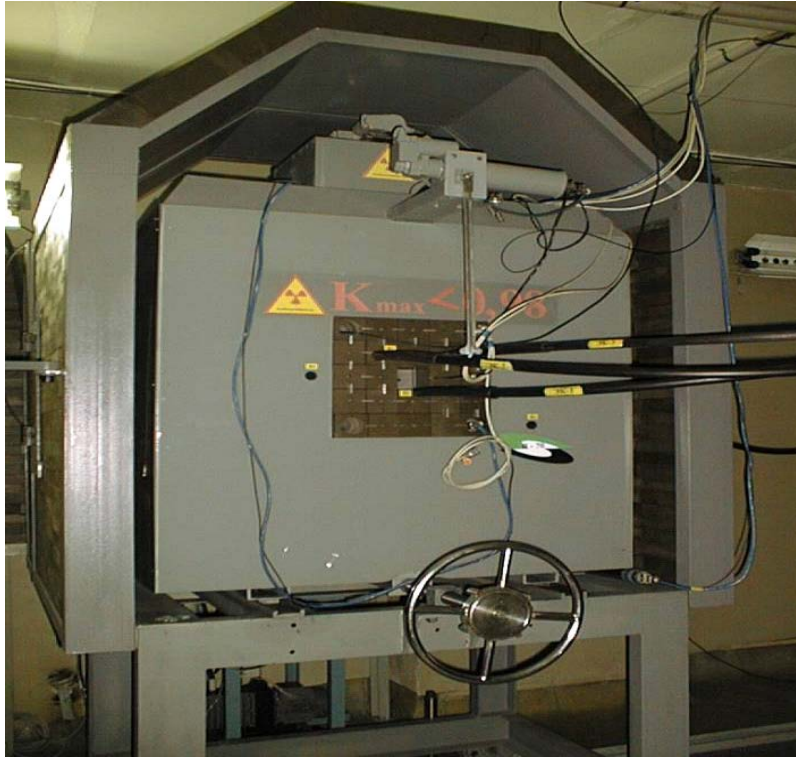


Figure VII.1: YALINA sub-critical core assembly (end view opposite from accelerator-beam target).

VIII. YALINA Thermal

The original core configuration that was assembled for YALINA was essentially YALINA Thermal (or YALINA-T for short) as described in this chapter. It is a zero-power sub-critical assembly driven by a high-intensity neutron generator. The core is a rectangular parallelepiped 40.0-cm wide, 40.0-cm long, and 57.0-cm high. It is assembled from polyethylene blocks with channels to place the fuel pins. The core has a square lattice with 2.0-cm pitch. The central part of the sub-critical assembly is a neutron producing lead target with dimensions 7.8 cm by 7.8 cm and total length of 57.6 cm formed from 12 blocks that can be slipped into a square cross-section cavity, with 8.0 cm by 8.0 cm dimensions, centered on the axis. When the deuteron beam is used for generating neutrons, a part of this hole is occupied by the beam tube. There are four channels that are 55 mm in diameter for accommodating neutron flux monitoring detectors at the boundaries of the core and three experimental channels with diameter of 25 mm located at radii of 5, 10, and 16 cm from the central axis of the assembly. These are used for placing various types of samples or a ^{252}Cf spontaneous fission neutron source inside the core. The core itself is surrounded by a high-purity graphite reflector 40.0 cm thick and a 1.5-mm thick cadmium layer. There are two axial experimental channels and one radial experimental channel with diameter of 25 mm located in the graphite reflector. The fuel rods that are loaded into the core consist of UO_2 dispersed in a matrix of magnesium oxide. The ^{235}U enrichment of the EK-10 uranium fuel rods (UO_2) equals 10%. Fig. VIII.1 is a 3-D cutaway diagram of YALINA-T that shows its major components.

Fig. VIII.2 is a more detailed end view of the polyethylene matrix that shows and identifies the various channels for the fuel pins and measurement equipment. Various fuel loading configurations are possible with this facility. However, the array is designed so that $k_{\text{eff}} < 0.98$ always for a fully loaded core, even in the case of the worst possible internal or external accident scenario (e.g., structural failure of the fuel matrix or flooding of the assembly and its surroundings with water). The reference fuel loading configurations for the inter-comparison of measured and calculated results between various participants on research collaborations involving YALINA Thermal correspond to 216, 245, and 280 EK-10 fuel rods with corresponding total masses of ^{235}U equal to 1.67, 1.89, and 2.16 kg, respectively. For complete technical details on the YALINA Thermal assembly, refer to Appendix D (YALINA Thermal Benchmark Specifications).

In Fig. VIII.2, one notices that the central area of the core near the axis, which is also the axis of the accelerator beam and external neutron producing target, consists of lead. This region measures 8-cm wide, 8-cm high, and 60-cm long. A side view of this arrangement is shown in Fig. VIII.3. The role of the lead component is to shift the neutron spectrum from that of the primary neutron source to one more comparable to a spallation neutron source, as discussed in Chapter II.

As would be expected, the neutron flux intensity is not uniform throughout the core. Fig. VIII.4 shows flux intensity profiles determined at several axial positions and three radial positions within the core region.

Although the design objective was to produce a predominantly thermal neutron spectrum in the core, the actual spectrum is not purely thermal since the external driver neutron sources – whether from the $\text{D(d,n)}^3\text{He}$, $\text{T(d,n)}^4\text{He}$, or ^{252}Cf spontaneous-fission sources – all have essentially fast-neutron spectra. Consequently, one would expect to find primary neutrons in the few-MeV (up to 14 MeV for the tritium target source) and down-scattered neutrons from there on down in energy to the thermal range at all positions within the core. Of course, the relative intensities of these various components will vary sharply with the specific location within the core. The fast component would be its strongest

in regions close to the target and to the lead scattering material. Fig. VIII.5 shows geometrically averaged spectra corresponding to three radial distances from the central axis. Indeed, the thermal component is dominant, but the fast component is also quite significant. What is interesting to note is that the neutron fluence in the spectrum is relatively flat from about 0.2 eV up to nearly 100 keV, a dynamic range of more than five orders of magnitude. The spectral variations at different positions within the core provide the option of performing measurements that are sensitive to spectral differences, and thus the opportunity to learn more about the behavior of sub-critical assemblies than would be possible if the spectrum were uniform throughout. An important category of experiments that can benefit from this versatility is the determination of transmutation rates for minor actinides and fission products (see Chapter II). This is crucial from the point of view of assessing the viability of ADS systems for future use in the transmutation of nuclear waste.

An additional feature of YALINA-T that adds to its versatility as a research facility is the option of performing measurements with a variety of fuel loading configurations and numbers of fuel pins up to the design maximum of 280. This possibility is evident from Fig. VIII.2. Actually, there are 317 fuel pin channels in the YALINA Thermal assembly, as can be seen from Fig. VIII.6, but not all of them are used. Fig. VIII.6 shows the YALINA core fuel pin arrangement for the design maximum loading of 280 fuel pins. By varying the number of fuel pins in the loading, the possibility of investigating the performance of YALINA Thermal at various levels of sub-criticality (various values of k_{eff}) is afforded. Fig. VIII.7 shows both measured and calculated values of k_{eff} as a function of the number of fuel pins in the core. By considering the presence or absence of individual fuel pins, it is possible to determine their reactivity worth, i.e., their individual contributions to the overall core reactivity.

..... Figures for Chapter VIII begin on the following page

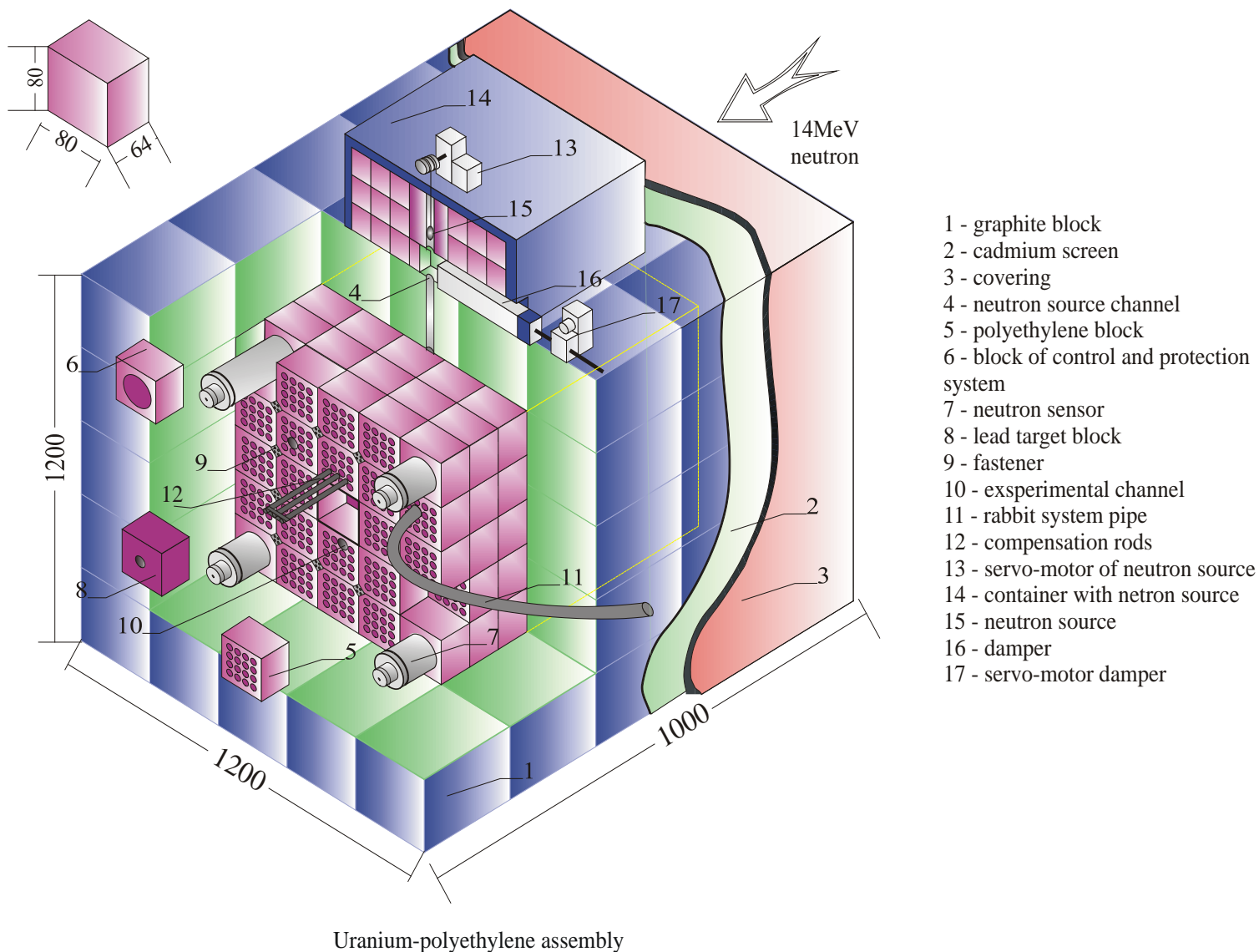
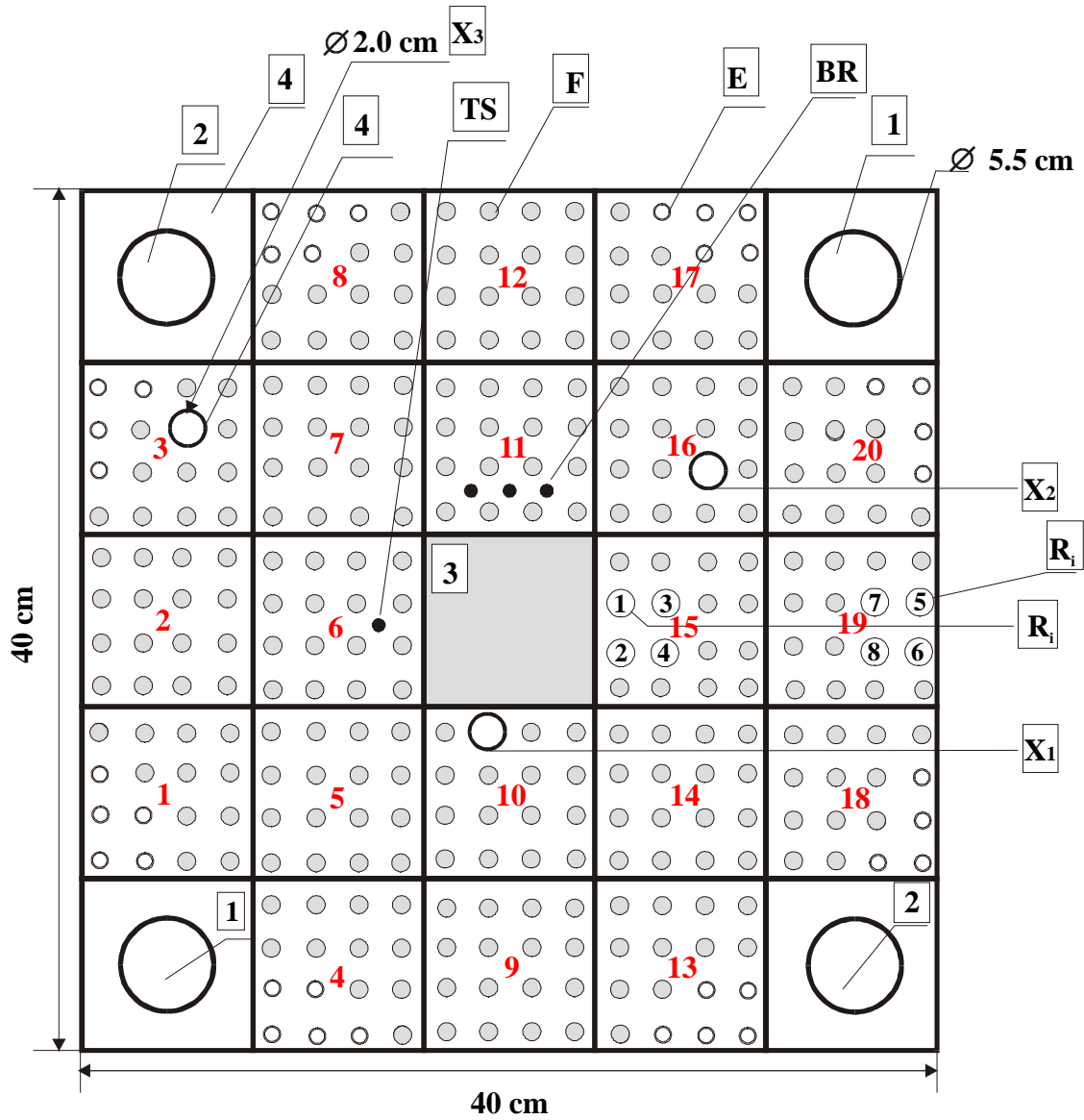


Figure VIII.1: Cutaway 3-D view of YALINA Thermal sub-critical core assembly. Dimensions are in mm.



1	Detector SNM-11	X _i	Experimental channel
2	Detector KNK-56	R _i	Central and peripheral fuel rods removed for reactivity change calculations
3	Lead	TS	Temperature sensor
4	Polyethylene	BR	B ₄ C rods
F	Channel with a fuel rod		
E	Empty channel (filled with air)		

Figure VIII.2: Cross-section view of the core in the YALINA Thermal sub-critical assembly.

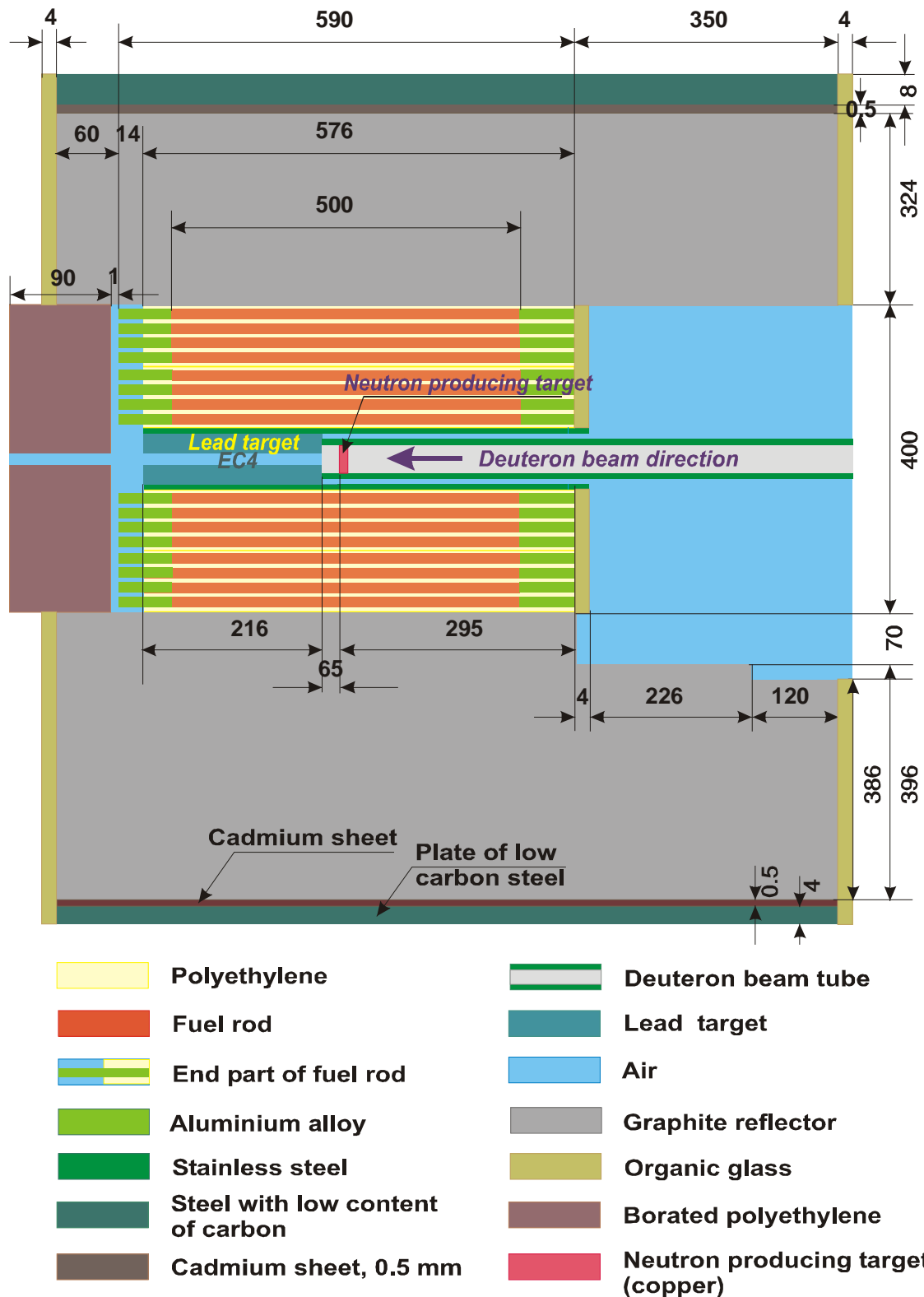


Figure VIII.3: The sub-critical assembly of YALINA Thermal. Key: 1 – target unit; 2 – shielding screen; 3 – cadmium screen; 4 – reactor type graphite reflector; 5 – protective container of starter Pu-Be neutron source; 6 – compensation rod mechanism; 7 – rabbit system pipeline; 8 – lead target, 9 – the core of the assembly; 10 – movable platform. Dimensions are in mm.

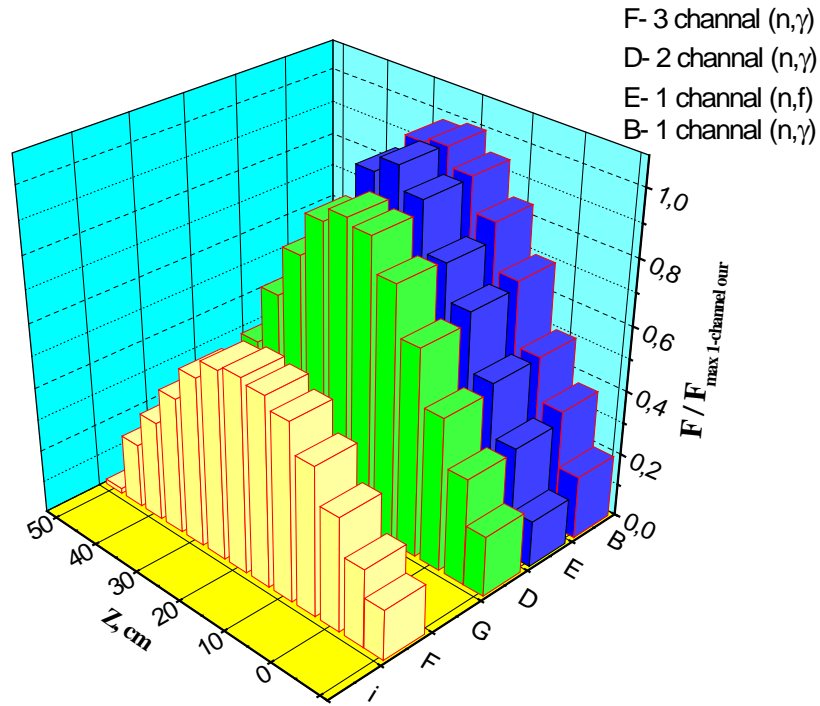


Figure VIII.4: Neutron flux distribution in the experimental channels of the uranium-polyethylene assembly YALINA Thermal driven by a ^{252}Cf spontaneous-fission neutron source.

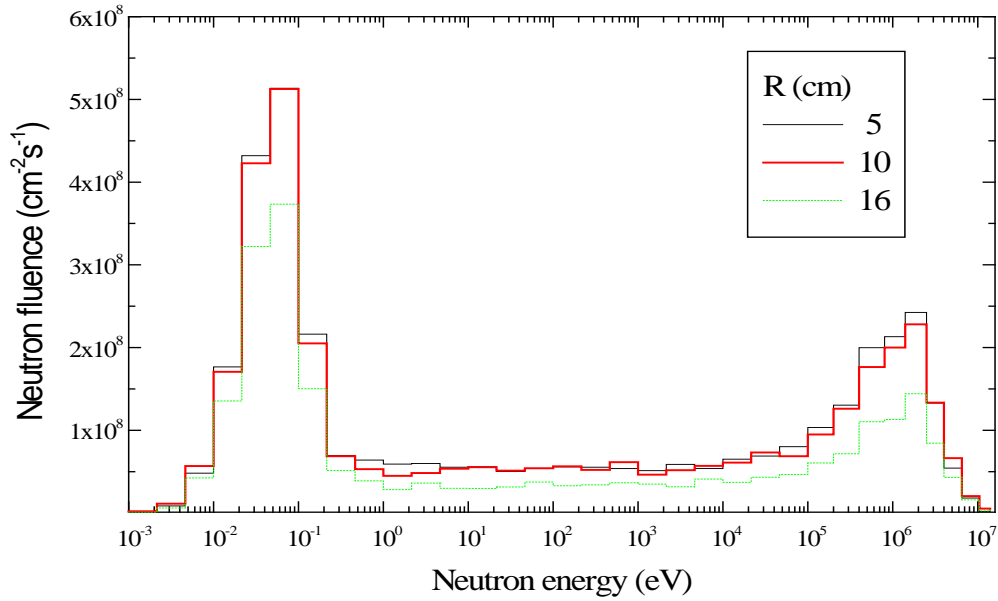


Figure VIII.5: Calculated neutron spectra for YALINA Thermal averaged over sample volumes in the experimental channels of the sub-critical assembly when driven by the neutron generator with the $\text{T(d,n)}^4\text{He}$ source. For normalization purposes, it is assumed that neutron source intensity equals to 10^{12} n/s.

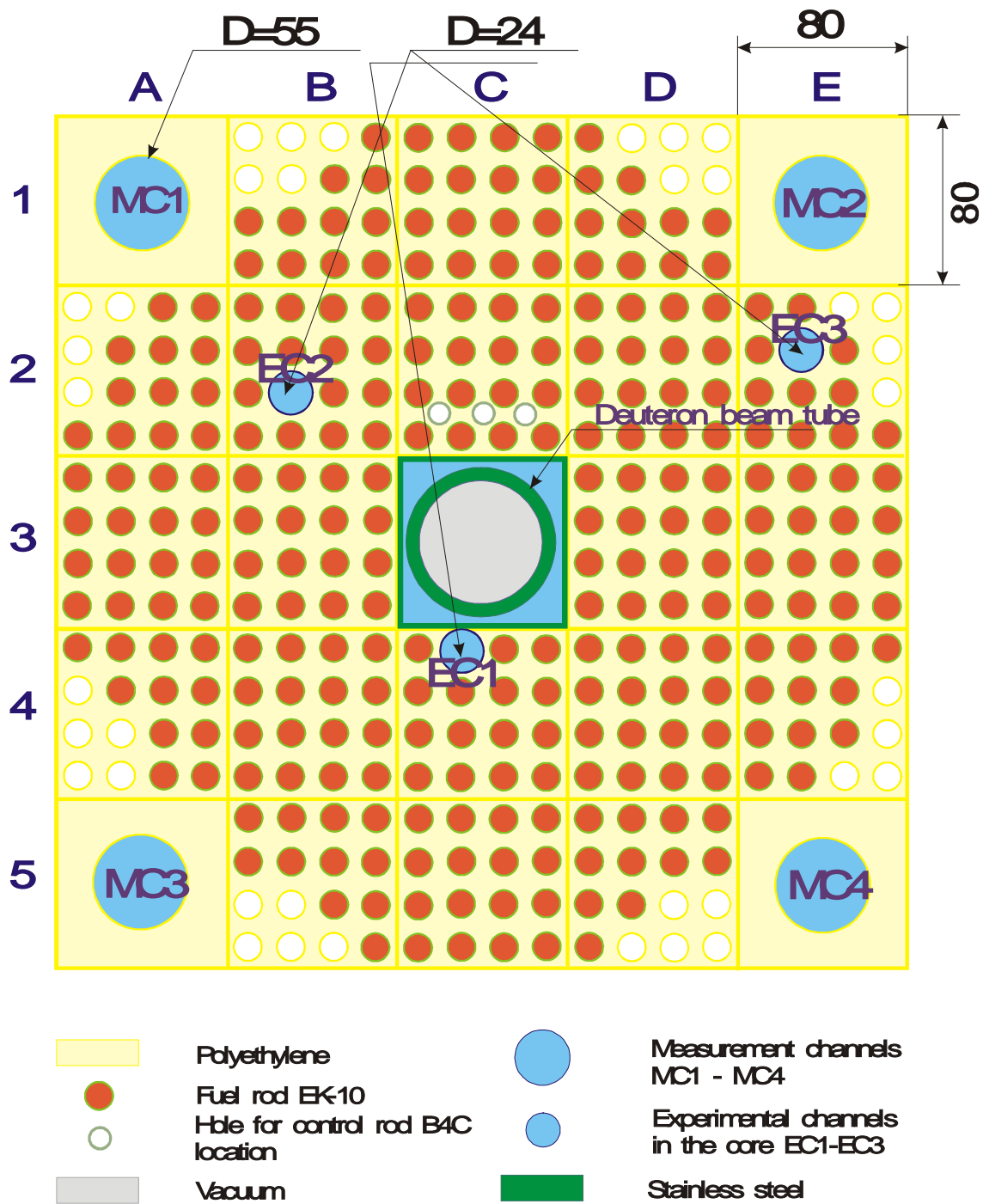


Figure VIII.6: X-Y cross-section of YALINA-T core with 280 EK-10 fuel rods ($-295 \text{ mm} < Z < -10 \text{ mm}$).

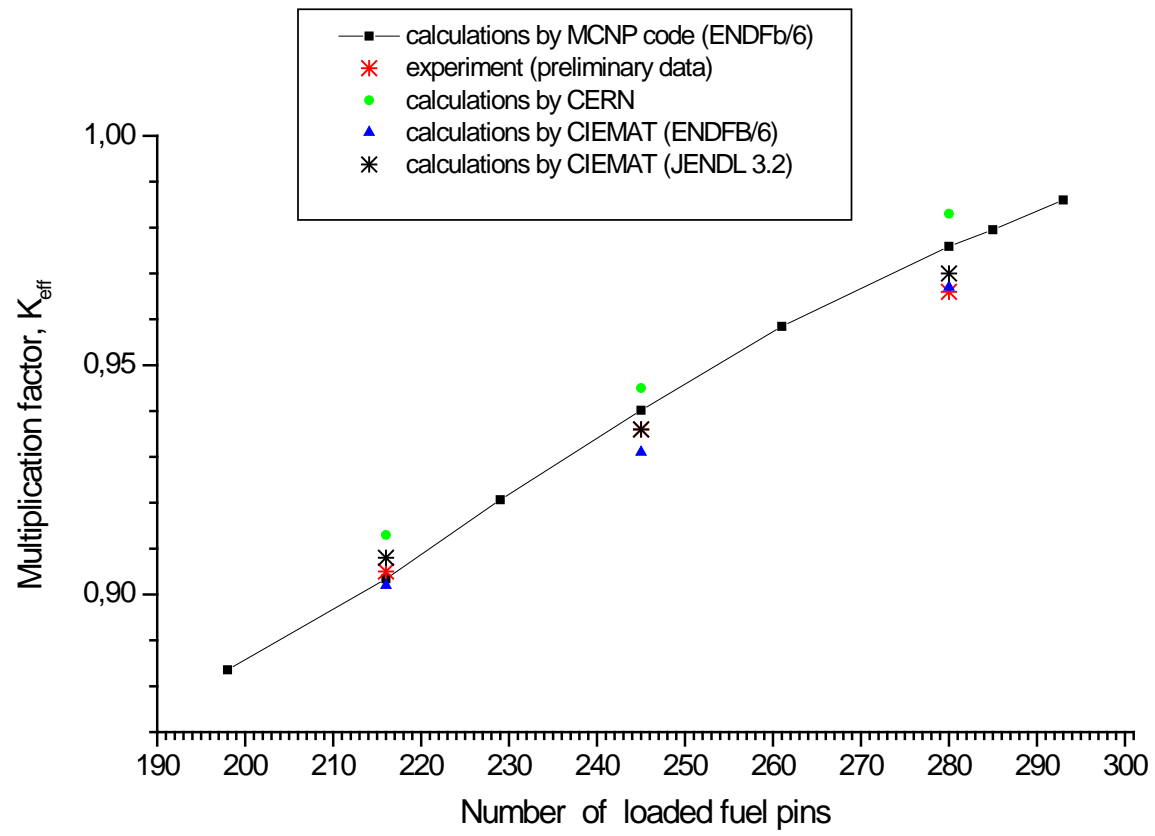


Figure VIII.7: Dependence of neutron multiplication factor k_{eff} versus number of fuel pins in the loading.

IX. YALINA Booster

In a full-scale ADS system the external neutron source would be produced by high-energy protons (several hundred MeV or even higher) incident on a high-Z target material such as tungsten, lead, or mercury. A spallation-neutron spectrum would be produced, and that would be modified by elastic and inelastic scattering in the target material to generate the equivalent of an extended boil-off neutron spectrum that would then couple to a core containing fissionable material. As has been described in preceding chapters, the YALINA facility was constructed with the aim of approximating such a coupled system of external source with sub-critical core, but on a much smaller scale. In YALINA, external neutrons are produced either by a ^{252}Cf spontaneous-fission point source or an accelerator source produced by low-energy deuterons incident on targets of deuterium or tritium via the $\text{D(d,n)}^3\text{He}$ or $\text{T(d,n)}^4\text{He}$ reactions, respectively. These primary accelerator sources are also basically point sources. Although a lead block is present in a portion of the central axis of YALINA thermal, the spatial extent and the neutron spectrum of the external driver source is still rather limited for simulating the spallation neutron source. Since investigations of the coupling of the external neutron source to the core of fissionable material are essential for the development of ADS technology, a means for generating an external neutron driver source that would more closely resemble that of a spallation neutron driven system had to be sought to broaden the possibilities for relevant research at the YALINA ADS test facility. The solution chosen was to design an extended source system using the concept of a cascade booster. The basic concept and layout of the YALINA Cascade Booster (or YALINA-B for convenience) is discussed in this chapter.

In the booster configuration, the assembly is divided into three regions. The first region – that closest to the primary neutron source – is actually called the booster region. In this region an extended source of fast neutrons with a spectrum and time profile resembling that of a spallation source is generated. The second region is best described as a “gate” or “valve”. It allows fast neutrons to propagate from the booster region to the core region beyond but prevents low-energy neutrons from migrating back into the booster region from the core. Finally, the third region is a thermal core region rather like YALINA Thermal. These three regions are shown schematically in Figs. IX.1 and IX.2, and they are described in general terms below. A photograph of the front end of YALINA-B is shown in Fig. IX.3. Detailed dimensions and materials compositions for the components of YALINA-B are provided in Appendix E.

The booster region itself is actually divided into two distinct sectors. The first sector – the one closest to the axis of YALINA-B – consists of lead having a square lattice of holes drilled with pitch equal to 1.14 cm. Fuel rods of metallic uranium enriched to 90% in ^{235}U are inserted into these holes. Of course, at the very center of the assembly, along the axis, there is a cavity to allow for insertion of the accelerator beam tube and target. The second sector envelops the first one on four sides, and it also consists of lead with a square lattice of holes having a pitch equal to 1.6 cm. Fuel rods consisting of UO_2 with uranium enriched to 36% in ^{235}U are inserted into these holes.

The next region – the intermediate (or “valve”) region – is 3-cm thick. It surrounds the booster region on four sides. Here, a layer of holes is drilled into the lead with a pitch of 1.6 cm, and rods consisting of either natural uranium (0.7% ^{235}U) or B_4C are inserted into these holes. This region serves as an absorber of thermal neutrons, but it is relatively permeable to fast neutrons due to the small effective capture cross section for higher-energy neutrons.

The third and final region – and the largest one geometrically – is the thermal region. It envelops the inner regions on four sides and consists of polyethylene that contains a square matrix of

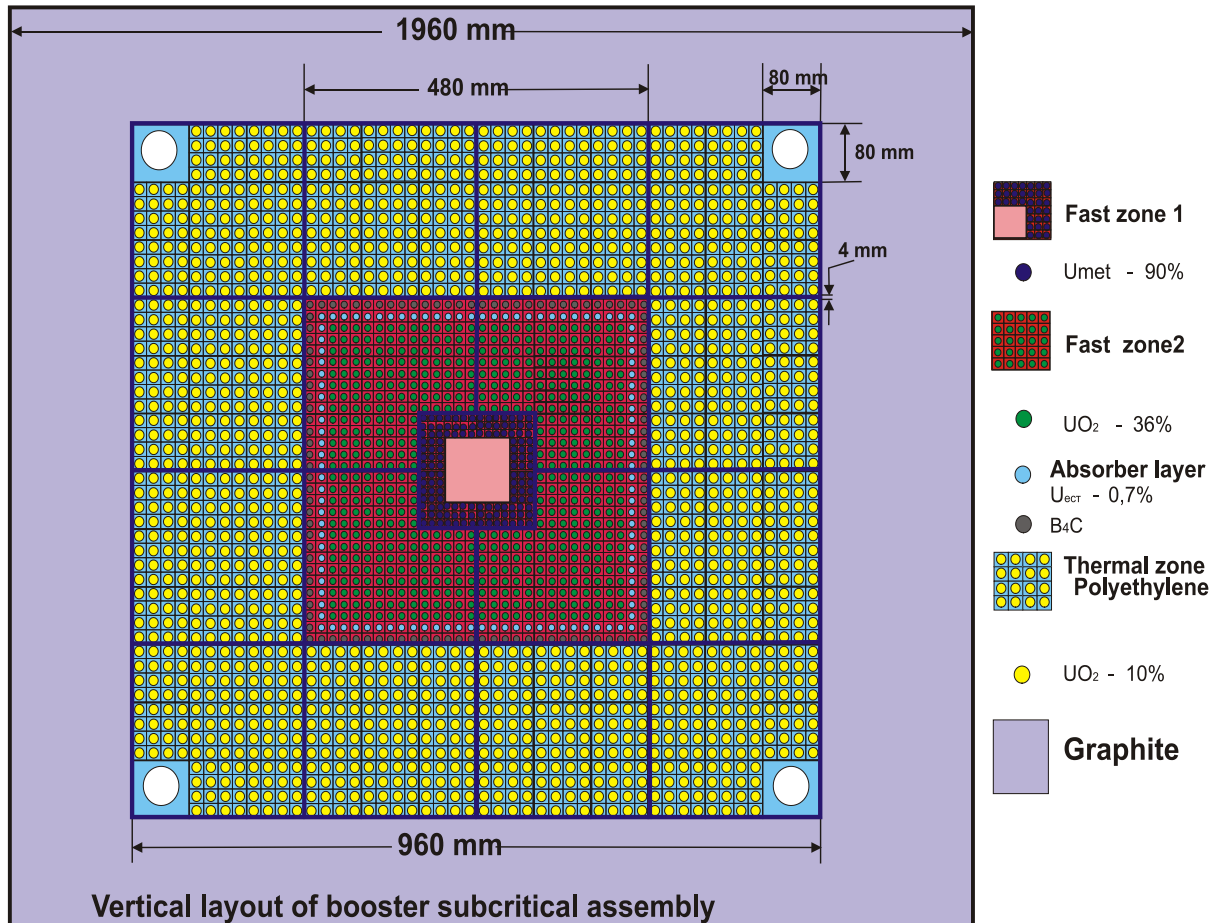
holes drilled with a 2-cm pitch. Into these holes are inserted fuel rods of UO_2 having uranium enriched to 10% in ^{235}U . In most respects, the geometrical arrangement, composition, and fuel loading in this region is identical to that found in the YALINA-T core.

The booster region has k_{eff} equal to 0.67 while the thermal region has k_{eff} equal to 0.95. The k_{eff} for the combined core assembly in YALINA-B (consisting of all three abovementioned regions) is – as is the case for YALINA Thermal – no greater than 0.98. By insuring that both regions (fast and thermal) of the YALINA Booster core are independently sub-critical, maintenance of criticality safety of the facility during operation is assured.

The consequence of this design is that YALINA-B effectively consists of a sub-critical extended-volume neutron source driving a thermal assembly in a manner that more closely resembles what would be expected for a full-scale ADS system that would be driven by a high energy proton beam and extended spallation neutron source such as, for example, the SAD facility that is being developed in Dubna, Russia. This is evident from the neutron-spectrum and time-distribution comparisons shown in the plots of Fig. IX.4.

The final observation that will be made in this chapter is that by having two distinct regions of the core with two very different neutron spectra – one with fast neutrons that resembles a partially moderated spallation source and the other with predominantly thermal neutrons – the possibility of performing a wide variety of transmutation measurements on samples of minor actinides and fission products is afforded, thereby enabling important objectives of ADS research to be pursued at the YALINA facility. As was pointed out earlier in this report, the two main objectives of the YALINA research project are to study transmutation of waste products from fission nuclear power and the static and dynamic properties of an ADS system that consists of a sub-critical core of fissionable material coupled to an external accelerator neutron source.

..... Figures for Chapter IX begin on the following page



$K_{eff} = 0.975 - 0.98$

Booster zone ($K_{eff} = 0.67$):

dimension, cm = 48 x 48 x 50
 Umet. is enriched to 90% in ²³⁵U
 UO₂ is enriched to 36% in ²³⁵U
 neutron flux density with energy:
 $E_n > 0,1 \text{ MeV}, 10^9 \text{ n/(cm}^2 \text{ s)}$
 moderator = Pb

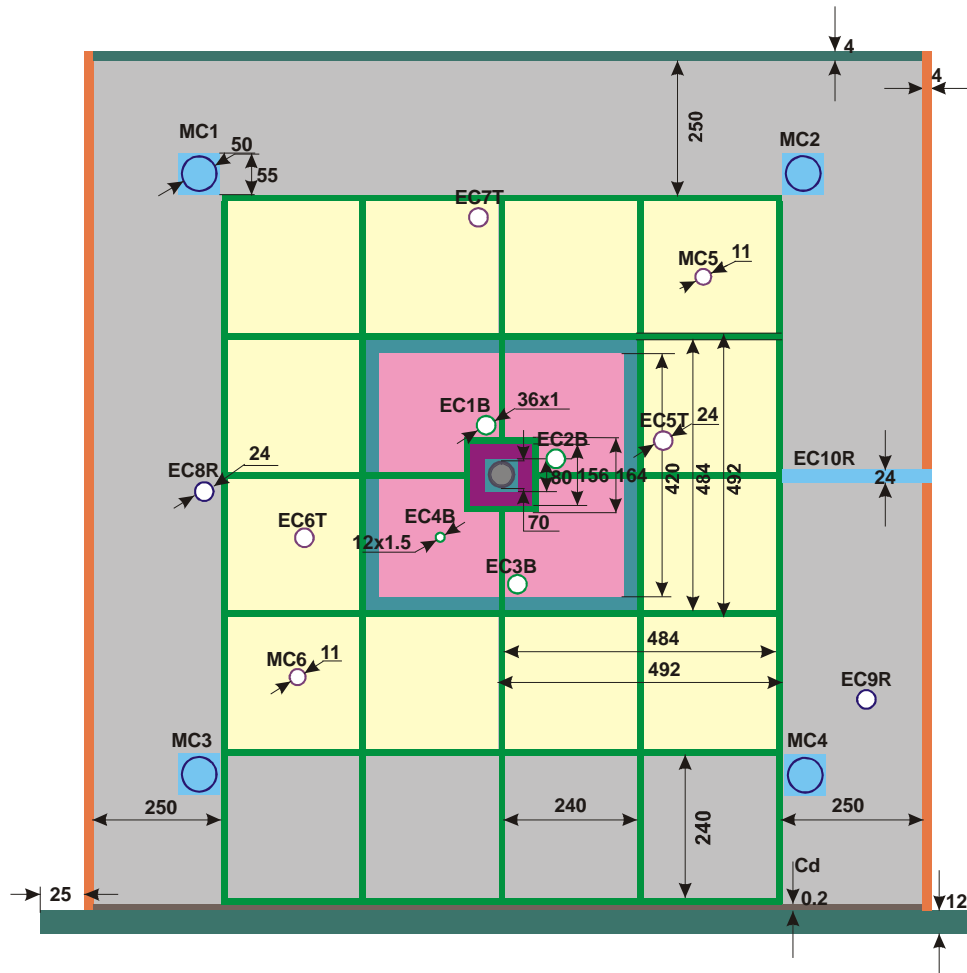
Intermediate zone:











thickness, cm = 3
 material Umet (natural uranium) + B₄C
 moderator = Pb
Uranium load (kg) - 5 – 0.23; U-8 - 31.8

Thermal zone ($K_{eff} = 0.95$):

thickness, cm = 24
 fuel : UO₂ is enriched to 10% in ²³⁵U
 moderator = polyethylene
 reflector = graphite
 Thermal neutron flux density:
³H –target $10^9 \text{ n/(cm}^2 \text{ s)}$
 multiplication factor = 50

Figure IX.1: Schematic diagram of the YALINA-B core.



	Umet. of 90% enrichment		UO2 of 36% enrichment
	Thermal neutron absorber Umet.(nat)+B4C		Thermal zone
	Air		Organic glass
	Graphite reflector		Cd layer
	Stainless steel frame		Mild (low carbon) steel

EC1B - EC4B - experimental channels in booster zone

EC5T - EC7T - experimental channels in thermal zone

EC8R - EC10R - experimental channels in reflector

MC1 - MC4 - measurement channels in reflector for
neutron flux monitoring

MC5 – MC6 - experimental channels in the thermal zone for neutron flux monitoring

At the back side of the assembly, the experimental channels do not penetrate the
borated-polyethylene or the organic glass.

EC8R (-52, -3.2), EC9R (60, -35.6), EC11RT New (- 4.2, Reflector and Poly, diameter 1 cm)

Figure IX.2: Materials composition map of YALINA-B core with dimensions in mm.

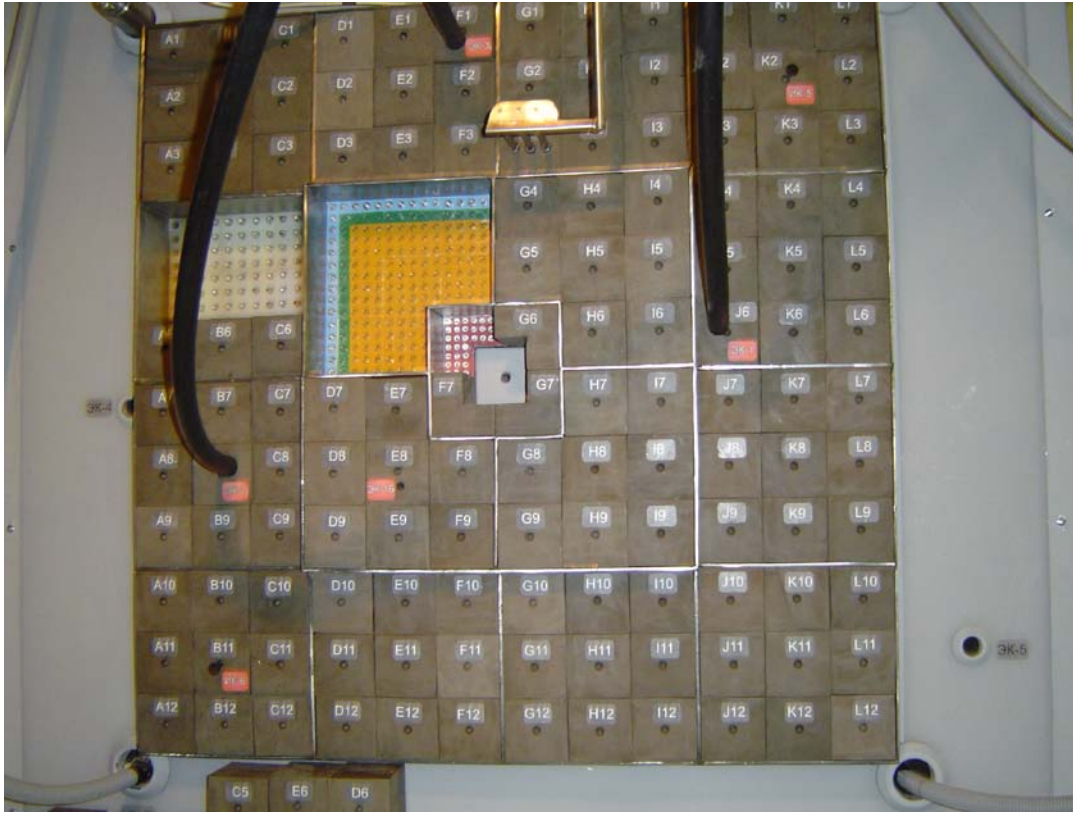


Figure IX.3: YALINA-B core assembly showing the different zones.

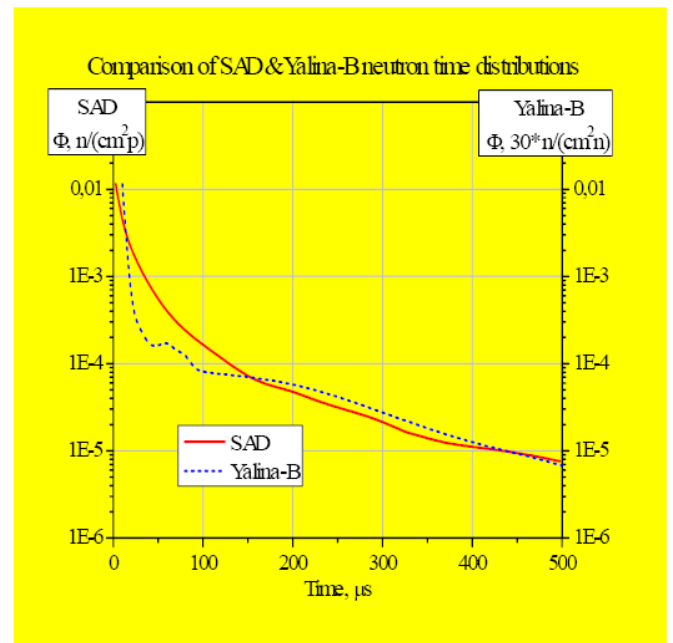
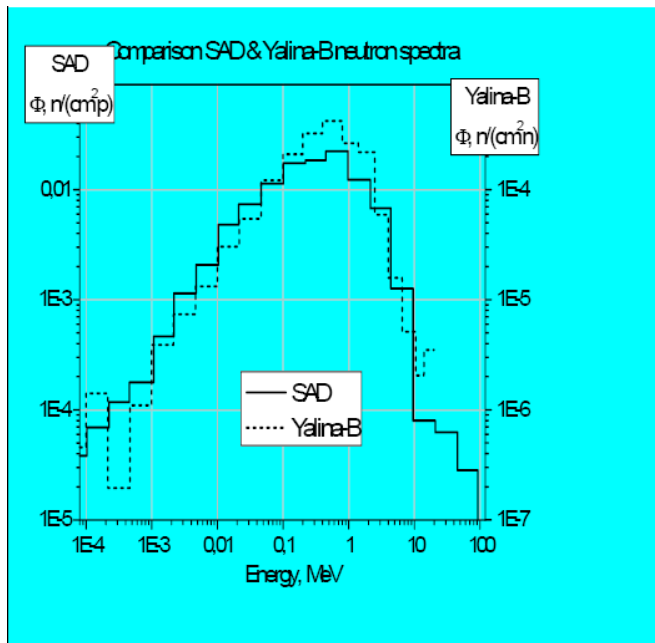


Figure IX.4: Comparison of the calculated neutron spectrum and time distribution for YALINA-B in the booster region with the corresponding results for the SAD spallation-driven ADS facility in Dubna, Russia.

X. Experimental Instrumentation

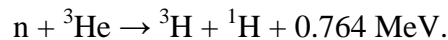
The instruments used for monitoring the performance of YALINA and for acquiring and recording experimental data that characterize the static and dynamic properties of this ADS facility are considered in this chapter. The basic characteristics and capabilities of the various types of detectors used for radiation measurements, as well as the data acquisition and analysis apparatus available at the YALINA facility, are described. The roles that these resources play at this laboratory are emphasized rather than actually cataloguing specific pieces of equipment.

A. Radiation Detectors

At YALINA Facility, several types of neutron and gamma radiation detectors are employed for facility monitoring and for acquiring experimental data. Among these are ^3He -gas detectors, thin-film fission chambers, mica solid-track detectors, thin-film breakdown counters, HPGe photon detectors for remote gamma-ray counting of irradiated samples, and BF_3 counters. Descriptions of intrinsic features of each class of detectors and the manner in which they are used at YALINA facility are provided in the following sub-sections of this report.

^3He -gas proportional counters

Helium-3 is a most important isotope used in instrumentation for neutron detection. It has a high absorption cross section for thermal neutrons and it is used as a converter gas in neutron detectors. The neutron is converted and made detectable through the nuclear reaction



The charged particles tritium ($T = {}^3\text{H}$) and proton ($p = {}^1\text{H}$) are then detected by creating an ionization-charge cloud in the stopping gas of a proportional counter or a Geiger-Müller tube. The cross section for this nuclear reaction process is very well known since it is one of the fundamental neutron cross-section standards. Most commercial ^3He -gas detectors of the type used at the YALINA facility are proportional counters with pressurized ^3He as the filler gas. Pressurization is required to insure that the charged particles will give up all their kinetic energy to ionization in the chamber before reaching the charge collection electrode. A brief review of the main features of these types of detectors is in order.

A proportional counter is a type of gaseous ionization chamber that works on the same principle as the Geiger-Müller counter but uses a lower operating voltage so that the ionization charge produced is proportional to the energy deposited rather than an energy-independent yield of ions associated with a charge multiplying cascade followed by a complete breakdown (avalanche) throughout the volume of the detector (Townsend Discharge). The ionizing particles (in this case tritium or proton recoils), if they have sufficient energy, liberate electrons from the atomic orbitals of the gas atoms leaving an electron and positively-charged atom commonly known as an ion pair. As the charged particle travels through the chamber it leaves a trail of ion pairs along its trajectory. The electrons created in this process drift toward a readout electrode, known as the anode, under the influence of an applied electric field. At the same time, the positive ions drift towards the cathode at much lower speed. In practical devices, the drift times are measured in microseconds and milliseconds, respectively, so these detectors produce relatively long pulses and thus are not capable of very high counting rates. A proportional counter differs from a simple ionization chamber in that the operating voltage is sufficiently high that the drifting electrons gain enough energy over a mean free path to create further ion pairs when they

collide with other neutral atoms of the gas. The electrons created in these new events also drift toward the readout electrode and can create further ion pairs themselves. In this manner, a cascade of ion pairs can be created. If the operating voltage is chosen carefully, each avalanche process occurs independently of other avalanches which derive from the same initial ionizing event. Therefore, even though the total number of electrons liberated can increase exponentially with distance, the total amount of charge created remains proportional to the amount of charge liberated in the original event. By measuring the total charge produced between the electrodes, one can ascertain the total kinetic energy of the particles since the number of ion pairs created by the incident ionizing charged particle is proportional to its energy. The geometry of the electrodes and the voltages on them are chosen such that in most of the volume of the counter the electric field strength is not enough to produce an avalanche. The electrons just drift until they get close to the anode, where a strong field allows avalanche multiplication to occur. In this way each electron is multiplied by approximately the same factor (up to about a million) independent of the distance it has covered in the low-field 'drift region'. This process of charge amplification improves the signal-to-noise ratio of the detector. It also reduces the amount of amplification required from external electronics. The proportionality between the energy of the charged particle travelling through the chamber and the total charge created makes proportional counters useful for charged-particle spectroscopy. However, the energy resolution of a proportional counter is limited because both the initial ionization event and the subsequent 'multiplication' event are subject to statistical fluctuations.

As indicated above, proportional counters are widely available commercially. Those used at YALINA facility have been chosen to fit into the experimental channels, and they find their most common application at this facility in scanning the neutron yield at various positions within the sub-critical assembly during steady-state operation of the accelerator, or for measurements of the neutron-yield decay versus time following a neutron pulse from the accelerator as required to determine the criticality parameter k_{eff} for the sub-critical assembly by various methods to be described in Chapter XI.

Fission-chamber detectors

Fission chambers are also gas-filled detectors operating at voltages in the proportional region, as described for ^3He -gas proportional counters. Therefore, the details of charged collection discussed above are not repeated here. Fission chambers can be either "home-made" or obtained commercially. The latter is the case for those used at the YALINA facility. The electrode geometry can vary widely depending on the design of the detector. Basically, one electrode is usually held at ground potential while the other voltage is held at an elevated potential (either positive or negative) with respect to ground. One electrode is coated with a thin film of fissionable material while the second is pure metal. The fissionable layer has to be very thin so that most of the fission fragments will penetrate that layer with essentially full energy to produce ionization in the filler gas of the chamber. Consequently, fission detectors have very low efficiency. A variety of specific filler gases, or combinations of gasses, are used in these chambers. Pure argon or methane, or combinations of these two gases, are quite commonly employed.

The most common fissionable materials used in fission detectors for routine neutron field measurements such as at the YALINA facility are: ^{235}U (enriched), ^{238}U (depleted in ^{235}U), or natural uranium. In some cases ^{237}Np is used, but rarely in commercial detectors. Chambers that contain predominantly ^{235}U are effective for detecting thermal neutrons whereas those with ^{238}U (or possibly ^{237}Np) are mainly sensitive to fast neutrons. The mechanism of neutron fission has been described in Chapter II, Section D, so it will not be repeated here. The ionization charge produced by the recoiling fission fragments is collected at an electrode, integrated and amplified to generate a detectable pulse

that records the fission event. Coupling from electrode to the preamplifier is generally capacitive so that there is no sensitivity to the particular potential at which the electrode is held. Since the energy released in fission generally far exceeds the energy of the incident neutrons, the pulse sizes corresponding to individual fission events are essentially independent of the neutron energy. This is especially true for a reactor core such as YALINA facility where the neutrons have either thermal energies or, at most, energies up to a few MeV.

At YALINA, fission detectors are used for multiple purposes. An important one is spectral indexing. This amounts to measuring the ratio of thermal neutrons to fast neutrons. This can be accomplished using two detectors, one with thermally-fissionable and one with fast-neutron fissionable active materials, as described above. Single detector probes containing multiple foils, each with distinct materials, can also be used to speed up the measurement process and reduce systematic errors due to drifting conditions (e.g., varying neutron output from the driver source) and geometric reproducibility uncertainties. Carefully calibrated fission detectors (containing very well known masses of fissionable material) can also be used to make absolute measurements of neutron fluence. Measurements of all these described types have been performed at YALINA during the course of its operation for the past decade.

Solid-state track detectors

A solid-state nuclear track detector or SSNTD (also known as an etched track detector or a dielectric track detector, DTD) is a sample of a solid material (photographic emulsion, crystal, glass, plastic, or, as in the case of YALINA, mica) exposed to nuclear radiation (neutrons or charged particles, and occasionally also gamma rays), that is etched and then examined microscopically. In YALINA, these detectors have been used solely for neutron detection. The tracks of nuclear particles are etched faster than the bulk material and the sizes and shapes of these tracks yield information about the mass, charge, energy and direction of motion of the particles. The main advantages over other radiation detectors are the detailed information available on individual particles, the persistence of the tracks allowing measurements to be made over long periods of time, and the simple, cheap, and robust construction of the detector.

The basic mechanism of solid state nuclear track detection is that charged particles damage the detector within nanometers along the track in such a way that the track can be etched many times faster than the undamaged material. In the case of neutron detection, the charged particles that damage the matrix material are the recoiling target nuclei. The etching is performed in a strong caustic solution (usually sodium hydroxide) at elevated temperatures and takes several hours. The process enlarges the damage to conical pits of micrometer dimensions that can be observed with a microscope. For a given type of particle, the length of the track gives the energy of the particle. The charge can be determined from the etch rate of the track compared to that of the bulk. If the particles enter the surface at normal incidence, the pits are circular; otherwise the nature of the elliptical shape and orientation of the elliptical pit mouth indicate the direction of incidence.

Use of these detectors is limited only to measurements under steady-state conditions since there is no time sensitivity to the response. Furthermore, information about the neutron field can only be deduced at a later time after chemically processing the individual track detectors followed by scanning under a microscope. However, when used in remote geometries, they allow a high homogeneity of the tracks and, thus, high reliability in the track identification. These detectors have been used in the YALINA project to map the relative neutron flux at various points in the core experimental channels with the both the $D(d,n)^3\text{He}$ reaction and ^{252}Cf spontaneous fission used as the sources of external neutrons.

Thin-film breakdown counters

Thin-film breakdown counters (TFBC) are metal-oxide-silicon capacitors intended for detection of heavy ions and, in particular, fission fragments. The operating principle of the TFBC is based on the phenomenon of electric breakdown in a metal-oxide-silicon structure caused by an ion passing through a thin silicon dioxide layer. The breakdowns are non-shorting since they lead to vaporization of a small part of the electrode area and leave no conducting path between the electrodes. The main features of the TFBCs are: the threshold properties, i.e., the insensitivity to light charged particles, neutrons and γ -radiation, real-time operating and good timing properties, ease of operation (no high voltage is required, no gases, large output signals, which makes preamplifiers unnecessary), low cost, compact design, and long-term stability under heavy radiation conditions. TFBCs have been developed into mature nuclear instruments that are useful in a number of applications such as nuclear cross section measurements, particle beam monitoring, neutron dosimetry, and studies of the performance of nuclear reactors such as YALINA.

In a typical application, a primary particle induces nuclear reactions in a sample (referred to as the radiator). This in turn acts as a source of strongly ionizing secondary particles (e.g., fission fragments) that are detected by one or several TFBCs. There are two possibilities for the mutual positioning of the TFBC and the radiator, namely in remote geometry or sandwich geometry. Remote geometry implies that the TFBC and the radiator are separated by a distance which is comparable to or larger than the dimensions of the detector sensitive area. In many cases it is possible to choose a radiator-detector distance and a bias voltage that allow detection of all fragments entering the sensitive area of the TFBC. In this case, the detection efficiency as a function of the bias voltage reaches a plateau and the efficiency is then defined solely by the available solid angle. The simplicity of the detection efficiency determination is an attractive feature of the remote geometry. On the other hand, this design is not suitable in applications involving low event rates or detector space limitations. In the sandwich geometry, the sensitive surface of the TFBC and the surface of the radiator are situated parallel to each other at a distance that is small in comparison with the dimensions of the detector sensitive area. The fragments can travel this distance in air without significant energy loss so evacuation to vacuum conditions is not necessary in such a setup. This makes the sandwich design more practical than the remote one. A more significant advantage of the sandwich geometry is that it offers the maximum possible sensitivity of the detector to the primary beams. For this reason, the sandwich design is used in applications involving low-intensity beams.

TFBCs are being used at YALINA for neutron measurements in the energy region 30 keV – 15 MeV, i.e., the fast neutron region, especially for spectrum unfolding applications where various fission reactions involving ^{232}Th , ^{234}U , ^{235}U , ^{236}U , ^{238}U , ^{237}Np , ^{239}Pu , ^{240}Pu , and ^{241}Pu as targets, each fissionable material having its own response characteristics, serve to provide valuable information for use in spectral unfolding analyses.

Germanium photon detectors

Germanium detectors are mostly used for photon spectroscopy in nuclear physics. While silicon detectors cannot be thicker than a few millimeters, germanium can have a depleted, sensitive thickness of centimeters, and therefore can be used as a total absorption detector for gamma rays up to few MeV. These detectors are also called High Purity Germanium detectors (HPGe) or Hyperpure Germanium detectors. Before current purification techniques were refined, germanium crystals could not be produced with purity sufficient to enable their use as spectroscopy detectors. Impurities in the crystals trapped electrons and holes, ruining the performance of the detectors. Therefore, germanium crystals were doped with lithium ions, i.e., Ge(Li), in order to produce an intrinsic region in which the electrons

and holes would be able to reach the contacts and produce a signal. When germanium detectors were first developed, only very small crystals were available. Low efficiency was the result, and germanium detector efficiency is still often quoted in relative terms to a standard NaI detector. Crystal growth techniques have improved, allowing detectors to be manufactured that are as large as or larger than commonly available NaI crystals. Such very large detectors are generally very costly and they are not found among the complement of instruments at the YALINA facility. Present-day HPGe detectors commonly still use lithium diffusion to make an n^+ ohmic contact and boron (B) implantation to make a p^+ contact. Coaxial detectors with a central n^+ contact are referred to as n-type detectors, while p-type detectors have a p^+ central contact. The thickness of these contacts represents a dead layer around the surface of the crystal within which energy depositions do not result in detector signals. Typical dead layer thickness are several-hundred micrometers for a Li-diffusion layer and a few tenths of a micrometer for a B-implantation layer.

The major drawback of Germanium detectors is that they must be cooled to liquid nitrogen temperatures during operation to produce spectroscopic data. At higher temperatures, the electrons can easily cross the band gap in the crystal and reach the conduction band, where they are free to respond to the electric field. The system therefore produces too much electrical noise to be useful as a spectrometer. Cooling to liquid nitrogen temperatures, i.e., to 77.36 deg Kelvin, reduces thermal excitations of valence electrons so that only a gamma-ray interaction can give an electron the energy necessary to cross the band gap and reach the conduction band. Cooling with liquid nitrogen is inconvenient, as the detector requires hours to cool down to operating temperature before it can be used, and cannot be allowed to warm up during use. Ge(Li) crystals can never be allowed to warm up as the lithium would drift out of the crystal ruining the detector. HPGe detectors can be allowed to warm up to room temperature when not in use.

At the YALINA facility HPGe detectors are used to measure gamma-ray yields from samples of various materials activated by neutrons in the core during operation. A wide range of samples and nuclear reactions can be used to provide spectral sensitivity over a wide range of energies. Typically, this experimental information is used to adjust (or refine) spectrum shapes based on system modeling. The practice of neutron dosimetry in reactors is highly developed, and the staff at the YALINA facility is well versed in applying these techniques.

B. Data Taking Apparatus and Procedures

Several categories of nuclear data acquisition instrumentation are represented in the equipment complement at the YALINA facility. One category is “preamplifiers” that act to shape and impedance-matching of the raw pulses obtained from active detectors to the recording electronics. Note that this would not apply for nuclear track detectors since they are totally passive. A second category is “amplifiers” that both shape and amplify the signals from preamplifiers so that they can be further processed in the data recording sequence. Normally there is a one-to-one relationship between a single nuclear event and the signals produced and amplified by the electronics. Thus, such equipment can be rightly referred to as nuclear “counting” equipment. This one-to-one relationship is extremely important for quantitative nuclear measurements such as nuclear process yields and, ultimately cross sections, that are directly proportional to the counts of measured nuclear radiation. An additional category of electronics is devoted to “time measurements”, i.e., recording the precise time of the occurrence of a nuclear event. Such measurements can be made with time precisions ranging from sub-nanosecond to several milliseconds, depending on the physical processes and nature of the measurement involved. Time information can be recorded electronically by a variety of means, e.g., time-to-amplitude converters. Data pertaining to time and amplitude (pulse height) of recorded nuclear events need to be stored for later processing. This can be done with single-channel or multi-channel

pulse-height analyzers (that through time-to-amplitude converters can also record timing information) or, more commonly today by small computers (PCs) that are appropriately interfaced to the nuclear electronics. Software required to store and manipulate information from nuclear measurements must also be provided for computer-based data taking apparatus to be useful. At YALINA, commercially developed software, e.g., the GENIE system, used in conjunction with PCs, is widely employed for data recording and analysis purposes.

Most of the instrumentation and software used for nuclear measurements and data recording at YALINA is commercial. During the past decade of operation of this facility there have been numerous upgrades of the electronics hardware, computer systems, and computer software, reflecting both changes in the technologies as well as availability of financial support needed to acquire these resources. Funding to facilitate these upgrades has been acquired from a variety of sources including grants through the ISTC and IAEA CRPs (see Chapter V) as well as support from individual foreign countries. Argonne has played a role in assisting the YALINA staff to acquire some of this instrumentation and in helping them to put it into effective operation. These steps in improving the instrumentation capabilities at YALINA have led to more flexible measurement opportunities, a greater volume of data, better accuracy for the measurements, and more sophisticated and reliable data analysis. Good quality as well as an extensive quantity of data is essential to provide increasingly sophisticated data analysis codes with the information needed for their validation and effective use.

..... The single figure for Chapter X appears on the following page



Fig. X.1: A typical modern High Purity Germanium detector (disconnected from liquid nitrogen dewar)

XI. Measurement Techniques

This chapter describes various experimental methods employed to acquire data on the operating characteristics and performance of both YALINA Thermal and YALINA Booster. The focus is on techniques in general, and not on specific measurement campaigns that have been undertaken during the past ten years. Over this time period, these various techniques have been applied at YALINA for many different core configurations, external neutron sources, fuel loadings, etc., far too numerous to document in detail in this report. In fact, many of these procedures are used at other nuclear facilities and could be used at full-scale ADS systems as well. Actually, due to high radiation levels that will be encountered in large-scale facilities certain measurements that can be made at zero-power facilities such as YALINA are not possible in large-scale machines due to swamping of the active detectors by very high pulse rates. The YALINA project therefore provides a test bed for exploring the feasibility of such measurements at ADS facilities. The detectors and associated instrumentation used in these measurements are described in Chapter X so these experimental details are not discussed in this chapter.

In the broadest sense, the measurement techniques can be divided into two categories: static and dynamic. Other categorizations could be used, e.g., active and passive, but static and dynamic seems most appropriate in the present context.

By “static”, it is meant those measurements that are performed while the YALINA facility is operating in a steady-state mode. That is, every attempt is made to keep the flux levels constant with time at each position in the core during the period of the measurement. For the most part, this is accomplished by keeping the external driver source of neutrons at a steady level. This is quite simple to do when a radioactive neutron source such as ^{252}Cf spontaneous fission is used. However, accelerators and beam targets being what they are, it is much more challenging to maintain steady-state conditions when the external neutron source is accelerator-based. Nevertheless, it is precisely under these circumstances that future large-scale ADS facilities would be expected to operate, so developing procedures to maintain near steady-state conditions is essential for the development and study of ADS technologies. Furthermore, depending on the type of detector used, it is possible in certain situations to correct the experimental data for fluctuations in the external driver source.

By “dynamic”, it is meant those measurements that are performed under circumstances where the YALINA facility is subject to a sudden change in operating conditions. There are various possibilities for introducing sudden changes that can be envisioned. For example, a fuel rod could be removed or a control rod inserted. However, for the most part investigations of the dynamic response properties of YALINA, or any ADS facility, will require sudden changes to be made in the beam level of the external driver neutron source. In Chapter VI it was noted that the neutron generator used as an external driver for YALINA can be pulsed, with various pulse widths and repetition rates available (within the ranges specified in that chapter). One of the most important features of YALINA to be investigated is the criticality parameter, better known as k_{eff} . The only way that this can be measured for a sub-critical facility such as YALINA is by observing the dynamic behavior in response to changes in the external driver source.

Most of the properties that can be measured in an ADS system such as YALINA can also be calculated using modern simulation codes and computational resources, either based on Monte Carlo simulation or on deterministic models. Very detailed and explicit models of the target assembly and core, including precise geometries and comprehensive materials compositions, can (and should) be included in these models. In fact, more can be calculated than can be measured. Consequently,

measurements tend to serve the purpose of benchmarking computational exercises rather than the other way around. The benchmarking experiments play a vital role in validating these data as well as the simulation codes and computer models of the ADS system. The calculations depend on extensive nuclear data, and the existing evaluated nuclear data files are often incomplete and vary a great deal in quality from isotope to isotope. Experimental results can be used either in a qualitative manner, to validate the models by comparing calculated and measured results, or they can be used to actually improve quantitative knowledge of the system parameters and computational results through the application of rigorous mathematical data-adjustment algorithms. This complicated interplay between measurement and modeling will be mentioned further in Chapters XII and XIII. It suffices here to say that measurement and modeling are synergistic in the roles they play in gaining an understanding of ADS systems in general and YALINA specifically. The knowledge that can be acquired by the combination of measurement and modeling exceeds what can be learned by either approach alone. Even when measured and modeling results are discrepant (they disagree significantly) knowledge is gained because when such discrepancies are uncovered this usually leads to a search for their origin. Ultimately, improved measurements and/or modeling exercises are carried out that eventually reduce the discrepancies to well within what would reasonably be expected from the current status of nuclear data and measurement or computational uncertainties. This approach has been invoked frequently by the Argonne analysis group as a consequence of working in close collaboration with Belarusian experimental collaborators at YALINA.

A. Static Measurements

Static measurements can be further categorized according to those that involve neutron spatial, flux level, and energy profile measurements at various accessible locations in the core, and those intended to determine reaction rates, including transmutation rates for fissionable materials as well as certain fission products. In a large-scale, high-flux facility, one would also be concerned with the measurement of materials damage effects. However, since YALINA is a relatively low-flux, zero-power facility, such measurements are not feasible at this facility.

Measurements of relative spatial flux levels in the core

By relative spatial flux levels it is meant ratios of flux levels at various points in the assembly to a selected reference point, but not absolute measurements. Referring to Chapter X, scans of relative spatial flux levels in the core can be made using active counters such as ^3He -gas proportional counters, active fission chambers, or thin-film breakdown counters. As noted in Chapters VIII and IX as well as Appendix D and E, these detectors can be inserted in the experimental channels included in the core designs for YALINA Thermal and YALINA Booster and even be moved incrementally by remote control without a need for human access to the assembly during measurements. Each of these detector options has its own advantages and disadvantages, as discussed in Chapter X. ^3He -gas proportional counters have relatively high efficiency for low-energy neutrons, leading to decent count rates and shorter measurement times (thus less demands on maintaining beam stability). With a $1/v$ response, these detectors react predominantly to thermal neutrons and thus are well suited for relative flux profile measurements in YALINA Thermal or in the thermal sector of YALINA Booster where the predominant component of the neutron spectrum is comprised of thermal neutrons. By using thin sleeves of Cd surrounding these detectors it is possible to eliminate the influence of thermal neutrons and measure the higher-energy neutron component as well. This is one of the oldest (and crudest) types of spectral indexing measurements used at reactor facilities. Nevertheless, it is effective and, as mentioned earlier in this chapter, the responses of these detectors with and without Cd shielding can be modeled in computations. Fig. XI.1 shows a typical scan of the YALINA-T core with a ^3He detector. Figure XI.2 shows a corresponding scan in the radial direction when a ^{252}Cf source is placed at the

center of the core. Fig. X.3 shows how the flux profile depends strongly on the location of the driving neutron source.

Fission chambers have much lower efficiency than ^3He -detectors. However, by varying the choice of fissionable material, it is possible to have detectors with notably different neutron-energy responses. This is evident from the discussions in Chapter II. Materials commonly used in fission chambers for this purpose are ^{235}U (responsive to both thermal and fast neutrons) and ^{238}U , ^{232}Th , or ^{237}Np which are responsive mainly to fast neutrons. There are other possibilities as well, as mentioned briefly in Chapter X. These more sophisticated measurements can provide much more informative data about the neutron spectra at various locations in the assembly than can be obtained from cadmium-shielded detector measurements alone. Furthermore, if the detectors are well calibrated regarding their geometric construction and quantity of fissionable material, it is also possible to obtain reasonably accurate measurements of absolute neutron flux as long as the count rates are sufficiently modest that individual fission events can be recorded without interference from preceding or following events. Figure XI.4 shows results from a core profile measured using a ^{232}Th fission detector.

Measurements of absolute neutron flux levels in the core

It is mentioned above that absolute flux levels at various positions in the assembly can be measured using well-calibrated fission detectors. These measurements rely to a large degree on knowledge of the mass and isotopic composition of fissionable material, and on knowledge of the fission cross sections. A variety of assay methods are employed to measure the number of fissionable atoms present in a detector. None of these involve actually weighing the material because the amount of material involved is too small to be weighed directly for the reasons discussed in Chapter X. These determinations require rather sophisticated assaying techniques, but in the final analysis most determinations are made from ratio measurements to standardized fission detectors. Several corrections are required to the raw spectral data recorded by fission chambers in order for them to be used as absolute fluence monitors. These include extrapolations to low pulse heights, fission fragment absorption corrections, etc. In the final analysis, absolute measurements with accuracies in the few percent range are possible on a routine basis using fission chambers provided that the neutron spectrum is reasonably well known (more about that below).

Various passive techniques can also be used for measuring absolute flux levels. One possibility involves use of solid-state track detectors. Since use of these detectors involves removal of the detectors from the core and chemical and optical processing, as described in Chapter X, data are not obtained in real time. However, if done carefully by experienced researchers it is possible to make relatively accurate measurements of neutron fluence (integrated flux) since individual tracks due to neutron-reaction events can be counted. Other neutron dosimetry techniques that involve the measurement of neutron-induced radioactivity in various irradiated sample materials can also be used for absolute fluence (time integrated flux) determination. As is the case for fission measurements, knowledge of the neutron spectrum as well as detailed properties of the radioactive decay (half lives, branching ratios, etc.) is required for such absolute measurements. Again, these measurements are made off-line using calibrated gamma-ray, alpha-particle, or beta-particle detectors, following removal of the dosimeter materials from the core. As mentioned above, Cd covers for the sample materials can shift the spectrum response to higher energies thereby providing additional information for use in measurements of neutron fluence. Fig. XI.5 shows some typical measurements in YALINA-T using the $^{129}\text{I}(n,\gamma)^{130}\text{I}$ reaction.

Measurements of neutron spectra in the core

Complete direct measurements of neutron spectra are quite difficult and possible only under certain circumstances. In particular, measurements from near-point pulsed neutron sources by time-of-flight techniques have been made for fast-neutron spectra. Such measurements are generally not possible in an integral facility such as YALINA. Instead, dosimetry measurements involving various materials and reactions (both threshold and non-threshold) are used to acquire response data that can then be used to adjust (that is effectively unfold) the calculated spectra such that optimal agreement between calculation and experiment is achieved. These measurements are both tedious and very demanding of accurate nuclear data. Furthermore, they tend to suffer from a fundamental problem, namely, a lack of suitable threshold response dosimeters for energies in the keV to few-hundred-keV energy range. Nevertheless, recent improvements in the knowledge of reaction cross sections, coupled with very sophisticated models of integral nuclear facilities such as YALINA, is leading to the possibility for obtaining a much better knowledge of neutron spectra in these facilities than was possible a few decades ago. These experimental and computational methods of neutron dosimetry are being applied routinely in the YALINA research program. Table XI.1 lists the reaction set used for neutron spectrum adjustment (unfolding) when the $T(d,n)^4\text{He}$ neutron source reaction is employed and neutron energies up to 15 MeV can be expected.

Measurements of radioactive waste transmutation

The physics of actinide and fission product waste transmutation is discussed in Chapter II. Transmutation involving neutron capture is best accomplished in thermal-neutron spectra whereas transmutation of minor actinide waste through fission processes is accomplished best in fast-neutron spectra. YALINA Thermal and YALINA Booster (taken together) offer possibilities for transmutation measurements to be performed using both types of spectra. Conceptually, the measurement of transmutation rates is straightforward. One begins with samples of the material one wants to transmute and irradiates these sample in a known neutron spectrum with a known flux level for a well-determined time (in other words, for a known neutron dose or fluence). One then removes the sample and measures the amount of product material generated relative to the original material composition of the sample. In practice, such measurements are usually extremely difficult. Here is why this is the case. First, it is frequently difficult to prepare pure and well characterized samples of the materials one wishes to transmute because they are often highly radioactive and chemically unstable. Second, it can be extremely difficult to measure the yield of transmuted material after irradiation, even with the aid of chemical processing, because of high levels of radiation background that mask the signal from the transmuted material. Also, chemical processing separates only species with different atomic number (distinct elements) but cannot separate different isotopes of the same element. Finally, many of the transmutation cross sections are poorly known. In some cases they are based almost entirely on estimates from nuclear modeling. The latter estimates may have some validity in the fast neutron region where cross sections tend to be smooth and nuclear models can be validated by comparisons with more extensive data corresponding to neighboring nuclei. However, in the resonance region such tricks don't work. There is no substitute for detailed knowledge of the spins, widths, and strengths of individual resonances, and these can be determined only from detailed experiments. An active field of research is the measurement of the resonance properties for individual target isotopes that play a role in waste transmutation. Such work is being carried out at such facilities as the Los Alamos National Laboratory LANSCE or the CERN N-TOF facility. Eventually, the combination of such microscopic measurements and integral yield measurements at facilities such as YALINA will help to improve our knowledge of waste-transmutation rates for individual isotopes that play a role in the nuclear fuel cycle. Much work clearly remains to be done.

B. Dynamic Measurements

While static measurements, as described in the preceding section, can yield a great deal of information about the characteristics of ADS systems such as YALINA, it is necessary to turn to dynamic measurements to learn how to operate these facilities safely. These measurements are more complicated and indirect than the static measurements described in the preceding section. To understand the techniques requires understanding some of the basic principles of fission-reactor kinetics and knowledge of the meaning of some key parameters related to criticality. To deduce these parameters experimentally requires a combination of measurements and calculations as well as resorting to some simplifying assumptions about the kinetics of nuclear reactors and topology of the core. A review of these issues is necessary in order to truly understand the different experimental procedures.

Of greatest concern regarding the safe operation of any nuclear energy facility that involves fission is the matter of criticality. A qualitative description of criticality appears in Chapter II. From a system modeling point of view, the criticality parameter, commonly called k_{eff} , is defined as the ratio of the number of neutrons in the $(n+1)$ -th generation as compared to the n -th generation. This can be calculated either by Monte Carlo simulation or deterministic analyses for complex assemblies. If $k_{\text{eff}} < 1$, the system is said to be sub-critical. If it is exactly equal to 1, it is said to be critical. If $k_{\text{eff}} > 1$, the system is said to be super-critical. That k_{eff} could be greater than unity at all stems from the fact that fission of actinide materials by a single neutron can produce more than one neutron per fission (see Chapter II). In fact, approximately 2.5 prompt neutrons (on average), as well a tiny additional fraction ($< 1\%$) of delayed neutrons resulting from the decay of highly excited neutron-emitting unstable fission products, result from a single fission event. Fission-power nuclear reactors almost always operate in the steady-state critical mode ($k_{\text{eff}} = 1$) where the number of neutrons generated is precisely balanced in real time by the number that are absorbed or escape the assembly. Since a precise balance between neutrons generated and neutrons absorbed is required to maintain this steady operating mode (precise criticality), some control mechanism is obviously required to prevent super-criticality (a runaway situation that can lead to an accident). The prompt neutrons are emitted so rapidly, in fact simultaneous with fission itself on a time scale on the order of 10^{-20} seconds, that control would be impossible if the assembly were prompt critical, i.e., achieved criticality on the basis of prompt neutrons alone. Needless to say, fission nuclear weapons are super-critical devices based on the presence of prompt fission neutrons alone. However, the delayed neutrons are emitted over a very long time period when compared to prompt neutrons. Therefore, they provide the only means for controlling a nuclear reactor. Reactors are thus designed to be sub-critical to prompt neutrons and can achieve the critical state only as a consequence of allowing just the right number of total neutrons, i.e. prompt neutrons plus delayed neutrons, to be present in the assembly (referred to in the nuclear engineering community as “prompt sub-critical, delayed critical”).

Fission reactions and subsequent neutron escape happen very quickly, as mentioned above. Most neutrons emitted by fission events are prompt: they are emitted essentially instantaneously. Once emitted, the average neutron lifetime (τ) in a typical core is on the order of a millisecond. This is much longer than the 10^{-21} seconds mentioned above because the neutrons emitted in fission “bounce” around the core through scattering collisions with core materials until either they produce another fission, are captured, or eventually escape. However, a millisecond is still a very short time from the perspective of a chain reaction. So if the neutron inventory growth factor is as small as 0.01, then in one second the reactor power will vary by a factor of $(1+0.01)^{1000}$, or more than ten thousand. Fortunately, the effective neutron lifetime is much longer than the average lifetime of a single neutron in the core. About 0.65% of the neutrons produced by ^{235}U fission (and about 0.75% of the neutrons produced by ^{239}Pu fission) are not generated immediately but rather are emitted by radioactive decay of fission products, with an

average lifetime of about 15 seconds. These delayed neutrons increase the effective average lifetime of neutrons in the core, to nearly 0.1 seconds, so that a core with neutron inventory growth factor of 0.01 would increase in one second by only a factor of $(1+0.01)^{10}$, or about 1.1 -- a 10% increase. This is a controllable rate of change. Consequently, most nuclear reactors can be safely operated in the prompt sub-critical, delayed-critical condition. The prompt neutrons alone are not sufficient to sustain a chain reaction, but the delayed neutrons make up the small difference required to keep the chain reaction going. This has implications on how reactors are controlled: when a small amount of control rod material is slid into or out of the reactor core, the power level changes at first very rapidly due to prompt sub-critical multiplication or depletion and then more gradually, following an exponential growth or decay curve of the delayed critical reaction. Further increases in reactor power can be performed at any desired rate simply by pulling out a sufficient length of control rod -- but decreases are limited in speed, because even if the reactor is taken deeply sub-critical, the delayed neutrons are produced by ordinary radioactive decay of fission products and that decay cannot be hastened.

Measurement of the criticality point for a reactor capable of going critical is quite easy. The first such measurement was performed in December 1942 on CP-1 in Chicago by Enrico Fermi and his scientific collaborators. Our concern here is with the dynamics of ADS systems, and YALINA in particular. ADS facilities are designed to be inherently sub-critical for ALL neutrons (prompt and delayed), even under extreme conditions that might be encountered in a worst-case accident. That is they can never achieve $k_{\text{eff}} = 1$, even considering the total inventory of neutrons consisting of prompt plus delayed components. This is accomplished by the design considerations of geometry, quantity of fuel, and fuel composition (basically, the choice of ^{235}U enrichment is the predominating consideration for most sub-critical ADS facilities including YALINA). In this sense, sub-critical ADS facilities are inherently safe, at least from a criticality standpoint.

For any particular sub-critical assembly design, k_{eff} can be calculated using either Monte Carlo or deterministic simulation codes (see Chapter XIII). However, the measurement of k_{eff} for sub-critical assemblies is quite difficult and not at all straightforward. The further from criticality for a particular system, the less precise the experimental determinations become for k_{eff} since some of the approximations to be described below represent more severe departures from reality than would be the case closer to unity. As is pointed out below, all currently used measurement techniques for determining k_{eff} and related reactor kinetics parameters are based on certain simplifying assumptions concerning the neutronics of the core. Fortunately, these assumptions turn out to be rather good in the case of YALINA. Still, some methods have proved to be more reliable than others, and the gaining of this knowledge has been an important consequence of the research program at YALINA. Brief descriptions of the various methods that have been used in criticality-parameter measurements for YALINA are given below, but first we need to examine the origins of the equations upon which these methods are based and to define some of the important parameters. The study of the distribution in energy, space, and time of neutron density at various locations in a fission reactor assembly is called reactor kinetics. This defines precisely the term that has already been used loosely in preceding paragraphs of this chapter. It is a complicated analytical discipline which we will oversimplify in this presentation to a sufficient extent so it is possible to more easily understand the dynamic measurement procedures carried out at the YALINA facility.

Elementary reactor kinetics

The distribution of neutrons in a reactor obeys the neutron transport equation. This equation is a form of the well-known Boltzmann transport equation, and in that respect it treats neutrons as a fluid, i.e., the working fluid of a nuclear reactor. However, unlike conventional fluids, there is no conservation principle in play. Neutrons are created and released in the assembly and they are also

removed or disappear from the assembly, both owing to a variety of physical processes. The physics of nuclear fission has several quirks that affect the design and behavior of nuclear reactors; we will not delve into a discussion of all these details here although some are mentioned.

In a nuclear reactor, the neutron population at any instant is a function of the rate of neutron production (due to fission and neutron multiplication reactions) and the rate of neutron losses (via non-fission absorption mechanisms and leakage from the system). The neutron life-cycle balance equation, which includes six separate factors, the product of which is equal to the ratio of the number of neutrons in any generation to that of the previous one. This parameter is called the effective multiplication factor (k); it is also referred to as k_{eff} . The factors included in this factor are: fast non-leakage factor; resonance escape probability; thermal non-leakage factor; thermal fuel-utilization factor; reproduction factor; and fast-fission factor. As mentioned above, $k = (\text{neutrons produced in one generation}) / (\text{neutrons produced in the previous generation})$; when the reactor is critical, $k = 1$, when the reactor is sub-critical, $k < 1$, and when the reactor is supercritical, $k > 1$. Reactivity is an expression of the departure from criticality. The parameter $\delta k = (k - 1)/k$ is a dimensionless quantity that measures reactivity. As mentioned above, when the reactor is critical, $\delta k = 0$; when the reactor is sub-critical, $\delta k < 0$; and when the reactor is supercritical, $\delta k > 0$. Reactivity is frequently represented by the lowercase Greek letter rho (ρ). We can express the formula relating k (or k_{eff}) and ρ as

$$\rho = (k_{\text{eff}} - 1) / k_{\text{eff}} \quad (\text{XI.1})$$

A variety of approaches to simplifying the transport equation can be applied. The most useful one for present purposes is based on the point-reactor model with a separation of space and time variables. If we write 'N' for the number of free neutrons in a reactor core and 'τ' for the average lifetime of each neutron (before it either escapes from the core or is absorbed by a nucleus), then according to this approximation the neutron density versus time in a nuclear reactor can be described, if the delayed neutrons are neglected, to a remarkable degree of accuracy, at least over a limited time ranges, by the following simple differential equation

$$dN / dt \approx \alpha N / \tau \quad (\text{XI.2})$$

Here, α is a constant of proportionality and dN / dt is the rate of change of the neutron count in the core. This type of differential equation describes exponential growth or exponential decay, depending on the sign of the constant α , which is just the expected number of neutrons after one average neutron lifetime has elapsed:

$$\alpha = P_{\text{impact}} P_{\text{fission}} \nu_{\text{bar}} - P_{\text{absorb}} - P_{\text{escape}} \quad (\text{XI.3})$$

Here, P_{impact} is the probability that a particular neutron will strike a fuel nucleus, P_{fission} is the probability that the neutron, having struck the fuel, will cause that nucleus to undergo fission, P_{absorb} is the probability that it will be absorbed by something other than fuel, and P_{escape} is the probability that it will "escape" by leaving the core altogether. Here, ν_{bar} (nu-bar) is the number of neutrons produced, on average, by a fission event – it is a fundamental physics quantity with values between 2 and 3 for both ^{235}U and ^{239}Pu as well as all other fissionable actinide isotopes. Values of nu-bar are available in evaluated nuclear data libraries as a function of energy for most fissionable isotopes. It should be noted in passing that the neutron energy dependence of nu-bar is rather weak but still non-negligible insofar as careful analyses of criticality are concerned. As suggested, the parameter α can be either negative (for sub-critical assemblies) or zero (for critical assemblies) or positive for supercritical assemblies. In all our discussions related to YALINA, $\alpha < 0$. Furthermore, we can write

$$\alpha = (\rho - \beta_{\text{eff}}) / \Lambda \quad (\text{XI.4})$$

Here, Λ represents the neutron reproduction time or mean neutron generation time and β_{eff} is the effective fraction of delayed neutrons, i.e., that fraction of delayed neutrons weighted with their probability to induce a new fission in the chain reaction. More generally, β , the precursor yield fraction, is defined as

$$\beta = (\text{number of precursor atoms}) / (\text{number of prompt neutrons} + \text{number of precursor atoms}) \quad (\text{XI.5})$$

Characteristic values of β , a fundamental physics quantity, exist for each fissionable isotope. Since in a reactor or sub-critical assembly there may be several isotopes involved, and the delayed neutrons have various energies, β_{eff} has to be calculated from basic evaluated nuclear data. These data are derived from measurements that are made quite separately from those associated with reactor kinetics and, as is the case for cross sections, β values used in calculating β_{eff} are available from evaluated nuclear data libraries.

Although the physical origin of prompt and delayed neutrons is quite different, all other factors being equal these neutrons behave in the same manner in a reactor. The main difference is that at their birth prompt neutrons exhibit a spectrum that is approximated reasonably well by continuous Maxwellian distributions with average energies of about 2 MeV whereas delayed neutrons are emitted from discrete excited states of fission product nuclei. On the average, delayed neutrons at birth have lower energies (about 0.5 MeV on average) than prompt fission neutrons. This is of relatively little consequence in thermal reactors where most of the neutrons are eventually moderated to energies far below the source energies, but in fast (neutron-spectrum) reactors the probabilities to induce new fissions for prompt and delayed neutrons can be considerably different on the average. This, of course, affects the computed value of β_{eff} as can be surmised from the preceding discussion.

Eq. (XI.2) applies when there is no external neutron source and all neutrons are generated internally within the core. This is not the case for an externally driven system such as YALINA. Therefore, this equation needs to be modified as follows when there is an external source of neutrons with a rate of production R_{ext} :

$$dN / dt \approx \alpha N / \tau + R_{\text{ext}} \quad (\text{XI.6})$$

In equilibrium, the rate of change of neutrons in the core is zero, i.e., $dN / dt = 0$. Thus,

$$N \approx \tau R_{\text{ext}} / (-\alpha) \quad (\text{XI.7})$$

For a sub-critical core, $\alpha < 0$ so equilibrium with a positive number of neutrons in the core is achieved. Furthermore, as α approaches zero for a sub-critical core that, nevertheless, is quite close to criticality, N can become a very large number. The number of fissions taking place in the core is proportional to N under equilibrium conditions, and thus the power (heat) generated by the facility can be made arbitrarily large, in principle, provided that R_{ext} is large (a high power, high energy external beam and spallation neutrons) leading to the notion that a driven sub-critical facility can be used as an energy source near criticality. This, of course, is not the case for YALINA since R_{ext} is quite modest, and the design limit of $k_{\text{eff}} < 0.98$ insures that this facility will never operate close to criticality. Although the chain reaction is not self-sustaining, it acts as a multiplier that increases the equilibrium number of neutrons in the core. So, this sub-critical multiplication effect can be used in two ways: as a probe of

how close a core is to criticality and as a way to generate fission power without the risks associated with a critical mass.

Techniques for measuring the criticality parameters of sub-critical assemblies

A number of different methods have been used to determine the criticality (kinetic) parameters of various configurations of YALINA. In this section six of these methods are described. Two others – the Gozani Method and the Reciprocal Count Method – are not described.

It is possible to describe the following methods used to determine the criticality parameters in the YALINA assemblies in terms of the formulas given in the preceding section.

The PNS Slope-Fitting Method

This method uses the neutron generator in the pulsed neutron source (PNS) mode (with relatively short pulses on the order of a few microseconds) as the external driver neutron source. The measurements are generally performed using ^3He proportional counters (with and without Cd screening) to measure the relative neutron flux in the core as a function of time following the pulses. However, fission detectors have also been used for this purpose at YALINA. There is no need to calibrate these detectors, either for absolute efficiency or neutron energy sensitivity. Only the time between the start of the short pulse and the time when the count occurs (dwell time) is recorded. The pulse-repetition rate needs to be much longer than the pulse width. Measurements of this type have been made in both YALINA Thermal and YALINA Booster. In order to obtain sufficient raw data for this method, these data must be accumulated as a function of time for very many individual pulses (a dwell-time history). When this is done one observes count rates like those shown in Figs. XI.6 and XI.7.

One observes from these plots that a portion of each curve is linear on a semi-log plot of counts vs. dwell time, as one would expect from Eq. (XI.2). Since the relative number of events due to delayed neutrons is rather small, this region is dominated by prompt neutrons. From the slope of this curve, one deduces the parameter α in Equation (XI.2). Given β_{eff} and Λ , both of which are determined by other means (usually by calculation), one deduces the reactivity ρ through Equation (XI.4) and, ultimately, k_{eff} through Equation (XI.1). If the statistical uncertainty of the dwell-time data is small, and one limits the analysis to the log-linear region, one can obtain reasonably reliable results by this method. To improve the quality of the fit, experimenters sometimes fit broader ranges of the curve using a function that is a sum of exponentials, but this is just a refinement of the basic method.

The Sjöstrand or PNS Area Method

This approach makes use of the fact that the decay of the prompt neutron flux occurs on a much shorter time scale than the neutrons from the delayed precursors. One can thus examine a time range which is sufficiently short that the delayed component can be treated as essentially constant. The basic characteristic of the time curves, as shown in Figs. XI.6 and XI.7 as well as in Eq. XI.8 below, is that there is a growth in counts for a short time after time zero as the neutrons from the external source migrate through the core producing chain reaction fissions. Onset of the decay then occurs but it is dominated by the decay of prompt fission neutrons in the core. At long times, all the prompt fission neutrons have essentially disappeared and the count is dominated by the delayed neutrons. Therefore, one can envision calculating the relative number of prompt and delayed events in the spectrum by decomposing the counts into two components and calculating the respective areas (and hence the

number of events) associated with prompt (A_p) and delayed (A_d) neutrons. This decomposition is shown in Fig. XI.8

It can be shown that the following formula applies:

$$\rho / \beta_{\text{eff}} = - A_p / A_d \quad (\text{XI.8})$$

Thus, given β_{eff} one can deduce the reactivity ρ and, ultimately, k_{eff} from Eq. (XI.1). In practice, the prompt-area component is obtained by trapezoidal numerical integration and the delayed neutron area is obtained by averaging the values from the last several milliseconds where the curve has clearly flattened out. The actual data analysis details for doing this are a bit more involved than the preceding sentence would suggest in order to be sure that one takes appropriate measures to separate the contributions from the two distinct physical origins when doing the summing of counts in the two regions. It is clear that both the PNS Slope Method and Area Method can be applied to the same sets of experimental data. The ratio $\rho / \beta_{\text{eff}}$ is expressed in terms of the units “dollars” or “\$” in the United States.

Source-Jerk Method

As the title suggests, the source-jerk method of measuring reactivity involves operating a sub-critical reactor in the steady state at a certain flux level, n_0 , and suddenly removing the neutron source (in the case of YALINA this would involve turning off or blocking the accelerator beam from reaching the neutron-producing target). The system will make a prompt jump to a lower flux level, n_1 . It will not remain at this point but rather will decay further according to the collective decay rates of the various delayed-neutron precursor groups. This process is illustrated by the experimental count-rate data measured at YALINA, as shown in Fig. XI.9.

It can be shown following some algebra that the reactivity in dollars (\$) can be expressed as

$$(\rho / \beta_{\text{eff}}) = (n_1 - n_0) / n_1 . \quad (\text{XI.8})$$

As mentioned above, β_{eff} is a calculated quantity so one can deduce ρ from Eq. (XI.8) and, ultimately, k_{eff} , from Eq. (XI.1). While this approach seems very simple in principle, in practice the determination of n_1 and n_0 involves some detailed analysis that takes into consideration the decay half lives of the delayed-neutron precursors as well as the explicit fitting of experimental data, as shown in Fig. XI.9. The reason for this being the case is that both n_1 and n_0 must correspond to the exact time of the “source jerk” while the data needed for analysis, by necessity, span time intervals both prior to and after this event.

The Rossi- α , Pulsed Rossi- α , and Feynman- α Methods

These three methods have the following features in common: First, all they are all used to deduce α , which is just the expected number of neutrons after one average neutron lifetime has elapsed, as indicated in Eq. (XI.3). Second, these methods involve, in one manner or other, observing the departure from statistically expected count rates that result from the presence of fission neutrons. Recall from Eq. (XI.4) that there is a simple relationship between reactivity ρ and α , β_{eff} , and Λ . Both β_{eff} and Λ are calculated quantities so determination of α yields ρ and this ultimately enables k_{eff} to be determined through Eq. (XI.1).

The Rossi- α and Pulsed Rossi- α methods are quite similar, differing only in the fact that the second approach is based on data acquired using a pulsed neutron source. Due to the presence of fission chain reactions in the multiplying medium (the sub-critical core in the case of YALINA), some of the detected neutrons may be correlated in time to each other. This happens because more than one neutron is emitted simultaneously from each fission event. In such cases it is possible that these two neutrons will be detected very close in time. It can be shown that the probability to detect one more neutron after the first neutron decreases exponentially in time with the prompt neutron decay constant α . The experimental technique involves plotting the experimentally derived probability function and extracting α from fitting the appropriate analytical function for this distribution to the data. This procedure is indicated schematically in Fig. XI.10.

The Feynman- α method, sometimes referred to as the noise analysis method, is also based on the departure of counting rates in a nuclear reactor from statistical expectations, i.e., in this case observed departures from Poisson statistics, owing to the presence of fissile materials. If $\langle c \rangle$ represents the average number of measured counts in a detector from many such counts made for a given time interval ΔT , and $\sigma(c)^2$ is the corresponding standard deviation of the series of such counts for this time interval, then the ratio can be expressed by

$$[\sigma(c)^2 / \langle c \rangle]_{\Delta T} = 1 + Y(\Delta T) , \quad (\text{XI.9})$$

where Y is the deviation from the expected value for this ratio that would have been unity if Poisson statistics had applied. It has been shown that Y can not only be determined as a function of the measurement time ΔT , but can also be expressed analytically in a rather complicated formula that contains α . Therefore, α can be deduced by measuring counts for many different time intervals and fitting the appropriate formula to these data.

The first three approaches have their own individual drawbacks due to consequences of the particular approximations that are made in deriving the formulas used for the analyses: The PNS Area Method tends to underestimate the criticality but yields low statistical errors. The PNS Slope Method is difficult to apply in practice but seems to give reliable results, especially closer to criticality. The Source-Jerk method tends to overestimate the criticality and it also involves large uncertainties due to the low level of the neutron fluence in the domain where the parameter n_0 needs to be determined. Comparisons of some results obtained by these three methods are shown in Fig. XI.11.

The last three methods are rather indirect and, as a result, are subject to a number of uncertainties (statistical and otherwise) in the associated data analysis procedures that are difficult to estimate in the context of the YALINA experiments when compared with the more direct PNS Slope, PNS Area, and Source-Jerk Methods. Nevertheless, these three additional approaches, when applied, have been found to yield results which are usually reasonably consistent with those obtained by the more widely used techniques. However, one general observation from a number of measurements of each type is that more reliable experimental criticality parameter values could be obtained from data taken at locations interior to the core rather than near the periphery where edge effects appear to influence the kinetic behavior and lead to conditions that depart from those assumed in deriving the kinetic equations that are used for analyses of the data. This, of course, is not a very surprising result. It should be noted that the farther from criticality, the more divergent the results from measurements of the kinetic parameters by various methods tend to be. Again, this is a consequence of the very restrictive assumptions that are made in deriving those forms of the kinetic equations that are amenable to applications in analyzing experimental data that are obtained by the various described methods.

Measurement of time dependence of the neutron flux

In addition to enabling measurement of the usual reactor kinetic parameters, the availability of a pulsed neutron source facilitates measurements of the time dependence of the neutron flux at various locations in the core in response to a single neutron pulse Fig. XI.12 is an example of such response curves as measured for the YALINA Booster configuration of the core.

..... Tables and figures for Chapter XI begin on the following page

Table XI.1: A neutron-dosimetry reaction set used at the YALINA facility for unfolding the fast-neutron portion of the spectrum when the $T(d,n)^4\text{He}$ reaction is used as the external neutron source.

$^{47}\text{Ti}(n,p)^{47}\text{Sc}$	$^{111}\text{Cd}(n,n')^{111}\text{Cd} \text{ (Eeff} = 0.25 \text{ MeV)}$
$^{55}\text{Mn}(n,\alpha)^{52}\text{V} \text{ (Eeff=0.64MeV)}$	$^{204}\text{Pb}(n,n')^{204\text{m}}\text{Pb} \text{ (Eeff=0.90 MeV)}$
$^{115}\text{In}(n,n')^{115\text{m}}\text{In} \text{ (Eeff=0.34 MeV)}$	$^{90}\text{Zr}(n,p)^{64}\text{Cu} \text{ (Eeff=2.0 MeV)}$
$^{58}\text{Ni}(n,p)^{58}\text{Co} \text{ (Eeff=2.7 MeV)}$	$^{59}\text{Co}(n,p)^{59}\text{Fe} \text{ (Eeff=2.8 MeV)}$
$^{65}\text{Cu}(n,p)^{65}\text{Ni} \text{ (Eeff=3.5 MeV)}$	$^{27}\text{Al}(n,p)^{27}\text{Mg} \text{ (Eeff} = 4.5 \text{ MeV)}$
$^{24}\text{Mg}(n,p)^{24}\text{Na} \text{ (Eeff=4.93MeV)}$	$^{48}\text{Ti}(n,p)^{48}\text{Sc} \text{ (Eeff=5.0 MeV)}$
$^{56}\text{Fe}(n,p)^{56}\text{Mn} \text{ (Eeff} = 6.60 \text{ MeV)}$	$^{59}\text{Co}(n,\alpha)^{56}\text{Mn} \text{ (Eeff=7.10 MeV)}$
$^{27}\text{Al}(n,\alpha)^{24}\text{Na} \text{ (Eeff} = 7.45 \text{ MeV)}$	

Table XI.2: Some nuclear-waste isotopes selected for irradiation in YALINA Thermal.

Sample	σ, barn (therm)	mass, g	ϵ, detection efficiency of the detector	S_{imp}, est. number of detected pulses
Sr-90	0.9 ± 0.5 0.014 ± 0.0024	0.00002	0.017	$2.6 \bullet 10^1$
Tc-99	20 ± 1 22.9 ± 1.3	0.16	0.032	$1.7 \bullet 10^6$
Sn-126	0.297	0.0952	0.016	$9.5 \bullet 10^5$
I-129	27 ± 2.2	1.53	0.026	$5.8 \bullet 10^9$
Cs-135	8.7 ± 0.5	2.3	0.021	$1.7 \bullet 10^7$
Cs-137	0.11 ± 0.033 0.25 ± 0.02	0.000031	0.015	$9.5 \bullet 10^2$
Np-237	$\sigma_c = 169 \pm 3$ $\sigma_f = 0.0019 \pm 0.003$	0.382	0.018	$2.9 \bullet 10^9$ & $1.5 \bullet 10^{10}$
Am-241	$\sigma_c = 832 \pm 20$ $\sigma_f = 3.15$	0.00079	0.018	$2.5 \bullet 10^7$ & $9.8 \bullet 10^7$
Am-243	$\sigma_c = 79.3 \pm 1.8$ $\sigma_f = 0.2 \pm 0.11$	0.0136	0.023	$1.4 \bullet 10^8$ & $4.8 \bullet 10^8$

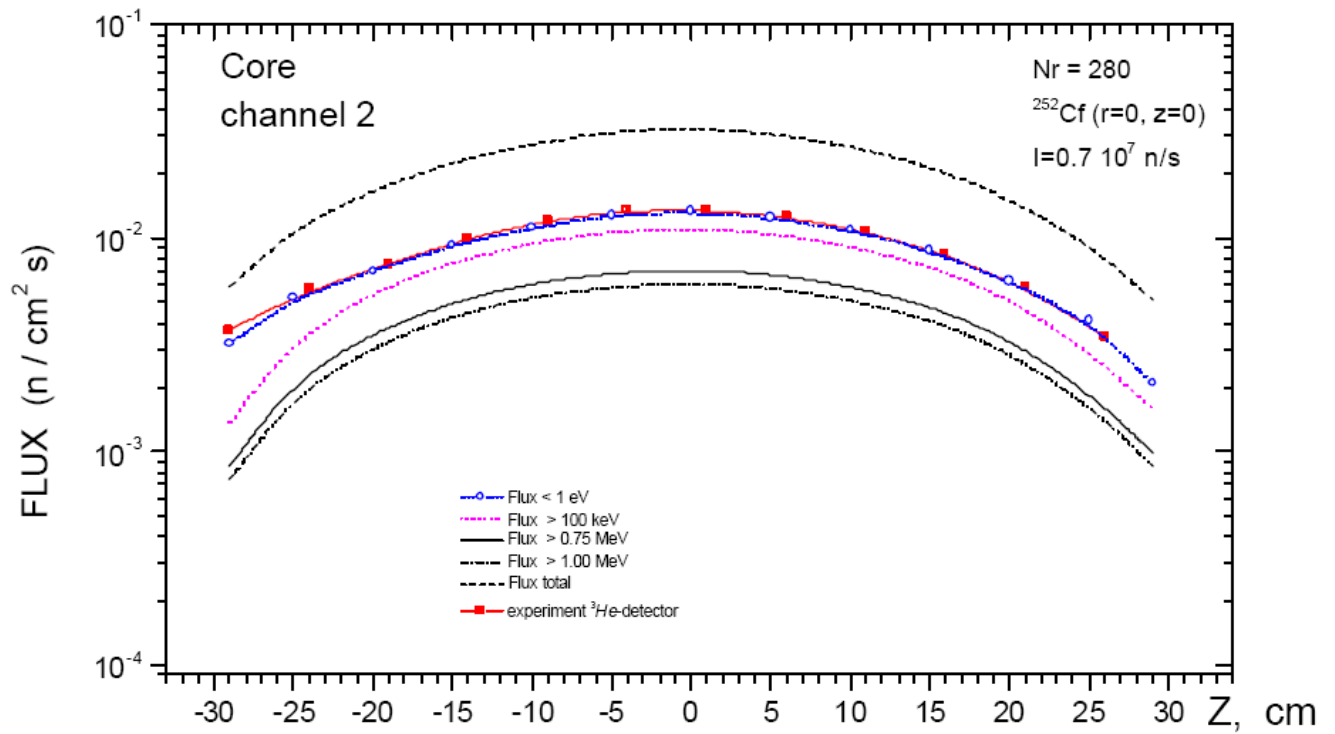


Figure XI.1: YALINA axial core scan data from a ^3He -detector compared with calculations.

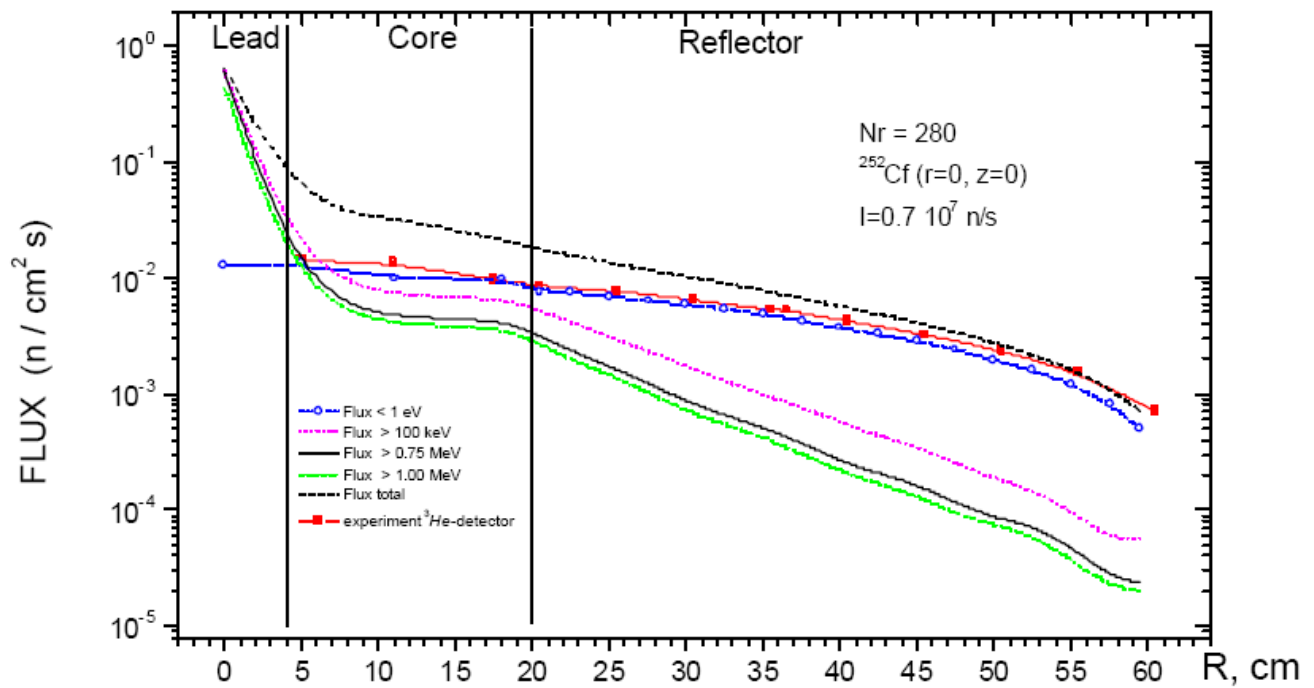


Figure XI.2: YALINA radial core profiles measured with a ^3He -detector and compared with calculations (a ^{252}Cf source was located at the core center for this exercise).

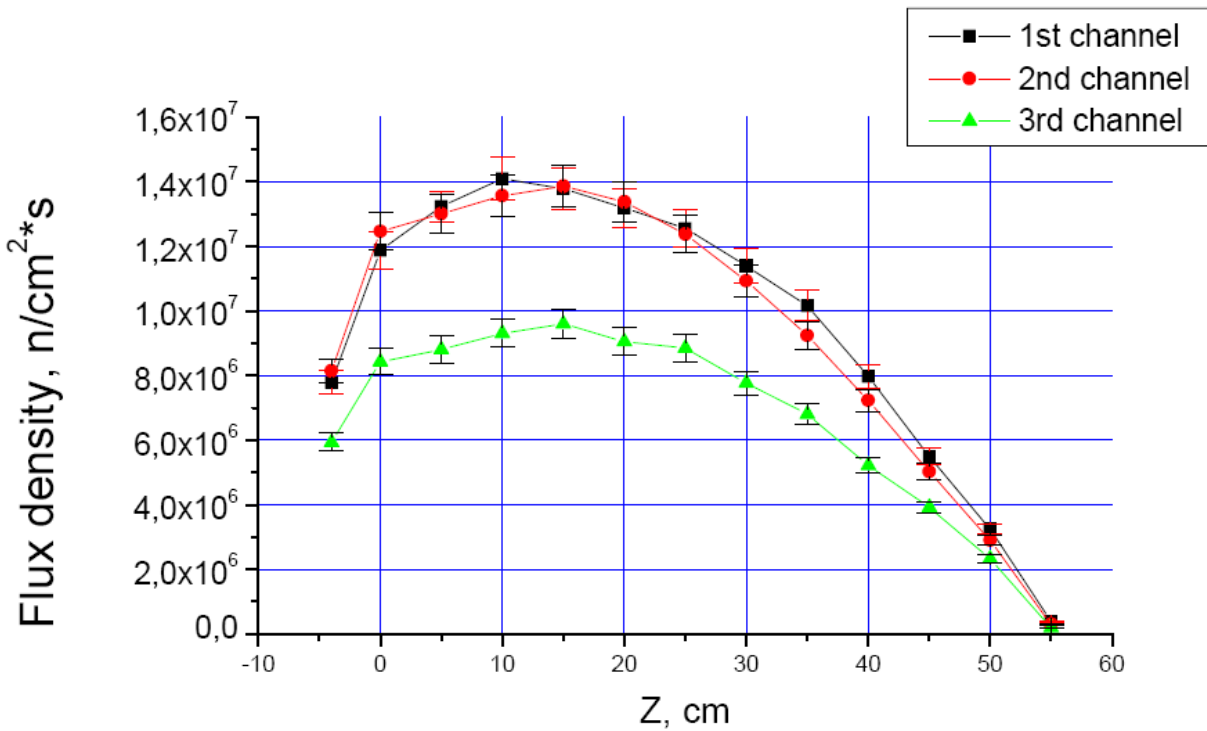
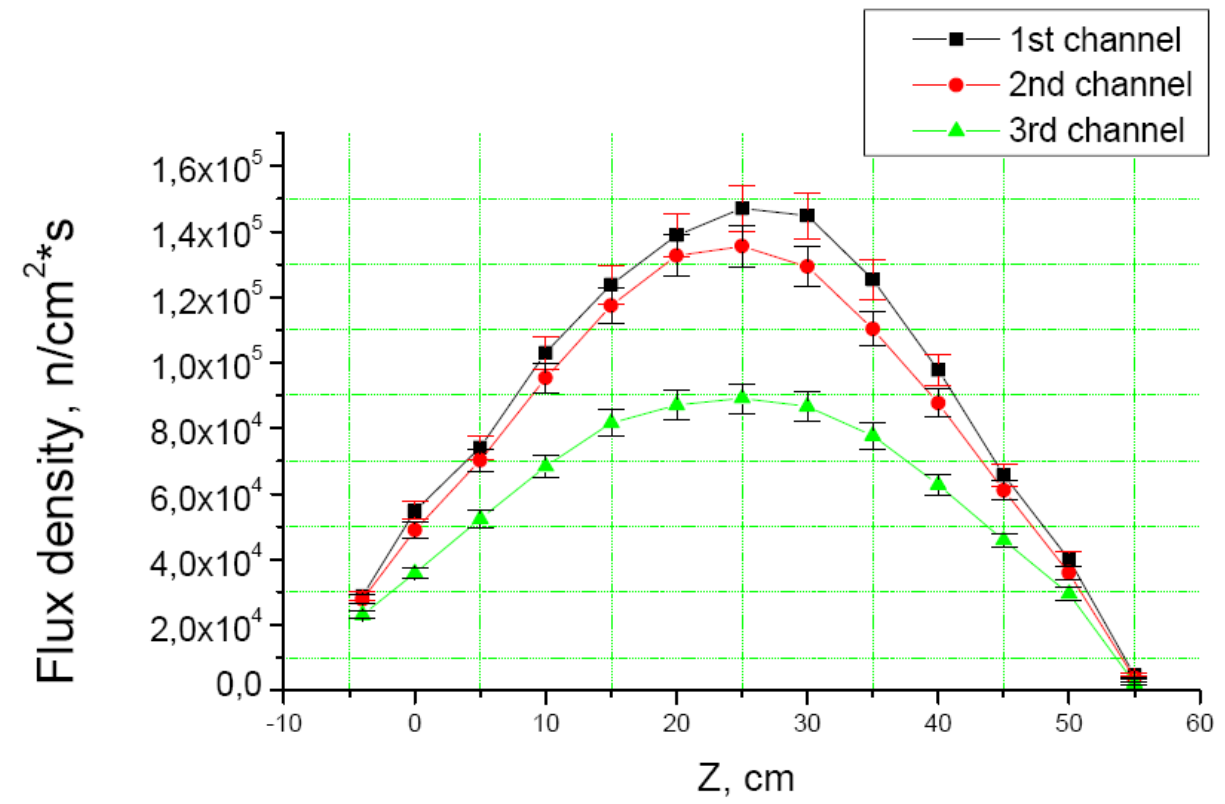


Figure XI.3: Comparison of calculated flux profiles obtained with a ^{252}Cf source placed at the center of the assembly (above) and with the neutron-generator target situated at the end of the assembly (below).

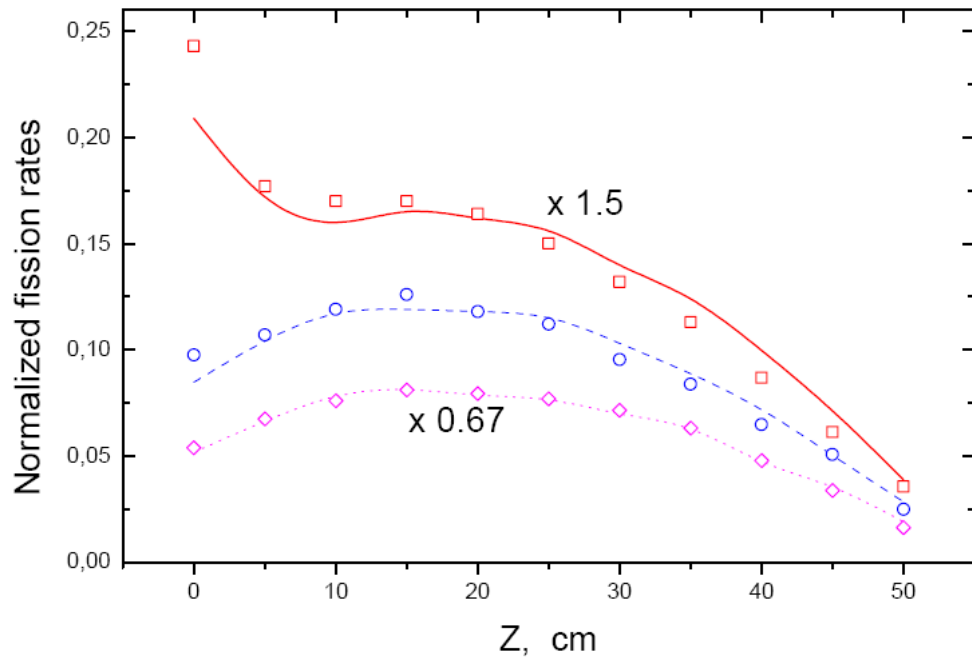


Figure XI.4: ^{232}Th fission-rate axial distributions in YALINA-T for three different measurement channels when driven by neutrons from the $\text{D(d,n)}^3\text{He}$ reaction. The symbols are data points and the curves are calculated using code MCNP.

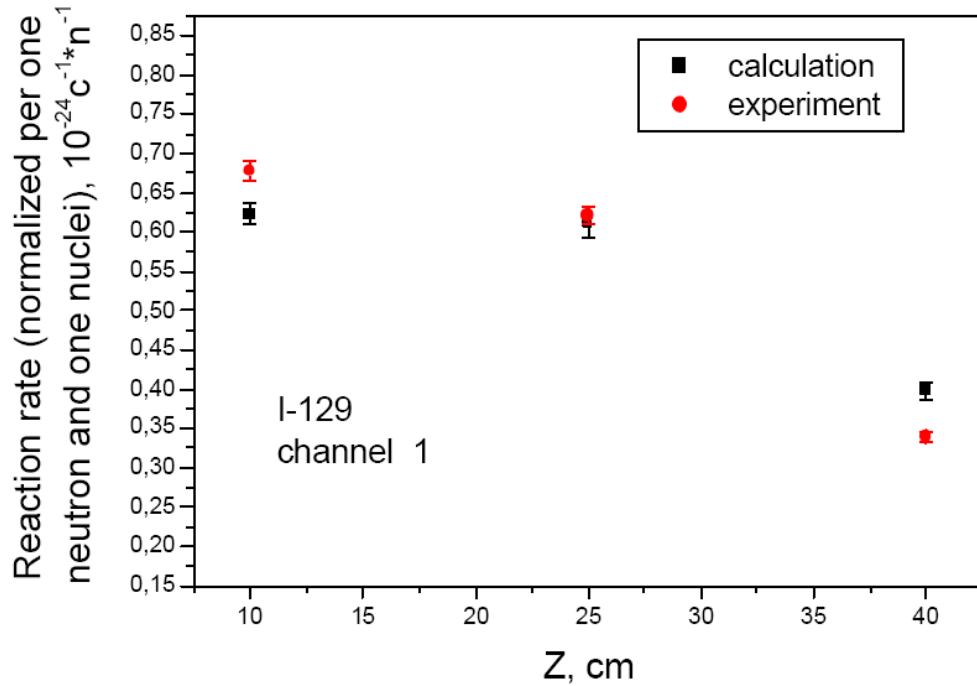


Figure XI.5: Axial distribution of the $^{129}\text{I}(\text{n},\gamma)^{130}\text{In}$ reaction yields in the YALINA-T core.

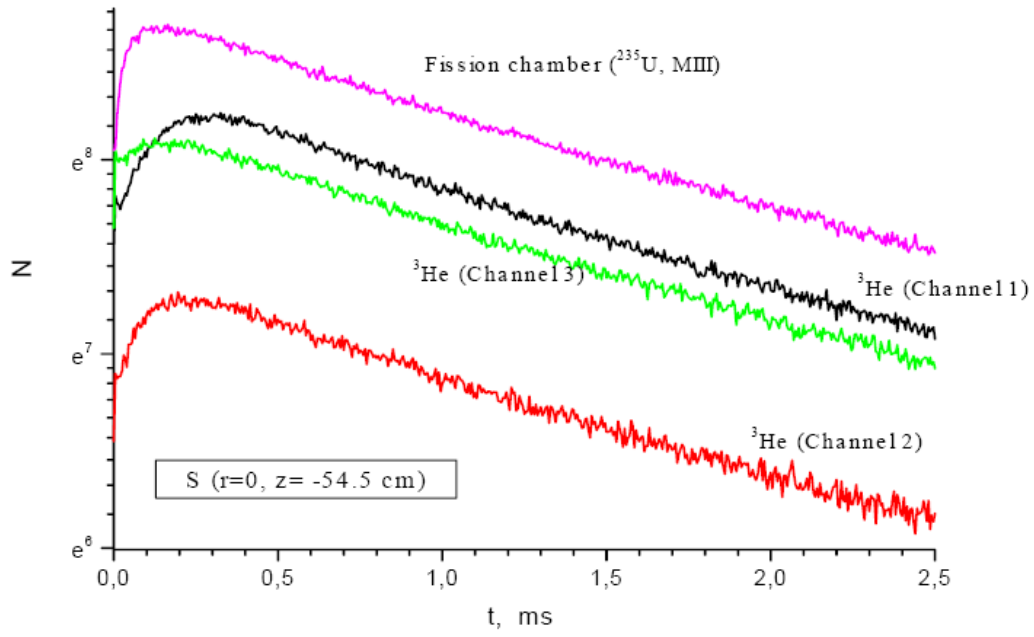


Figure XI.6: Time spectra of neutron events recorded with ^3He proportional counters and a fission chamber in the experimental channels of the YALINA Booster core.

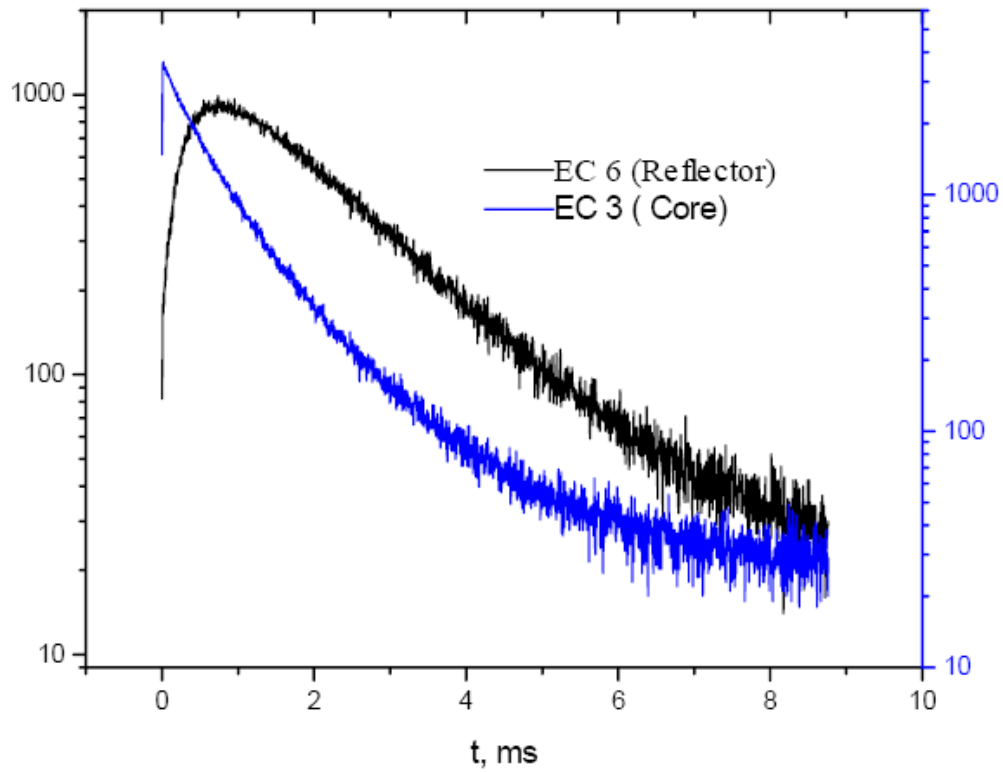


Figure XI.7: Time spectra of neutron events recorded with ^3He proportional counters in an experimental channel of the YALINA Booster core and in the reflector.

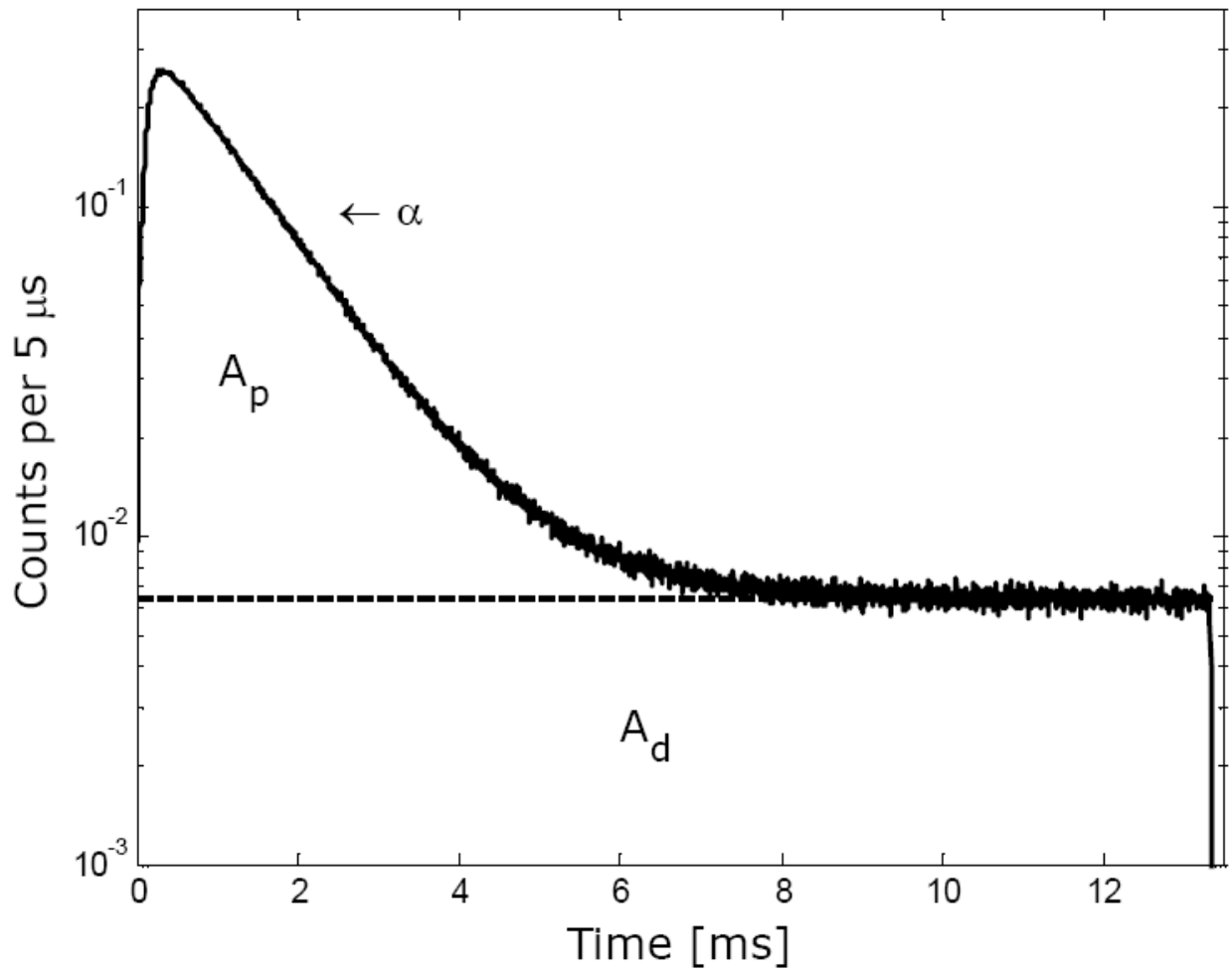


Figure XI.8: Prompt and delayed neutron areas (A_p and A_d , respectively) used in the Area Method are shown along with the origin of the parameter α .

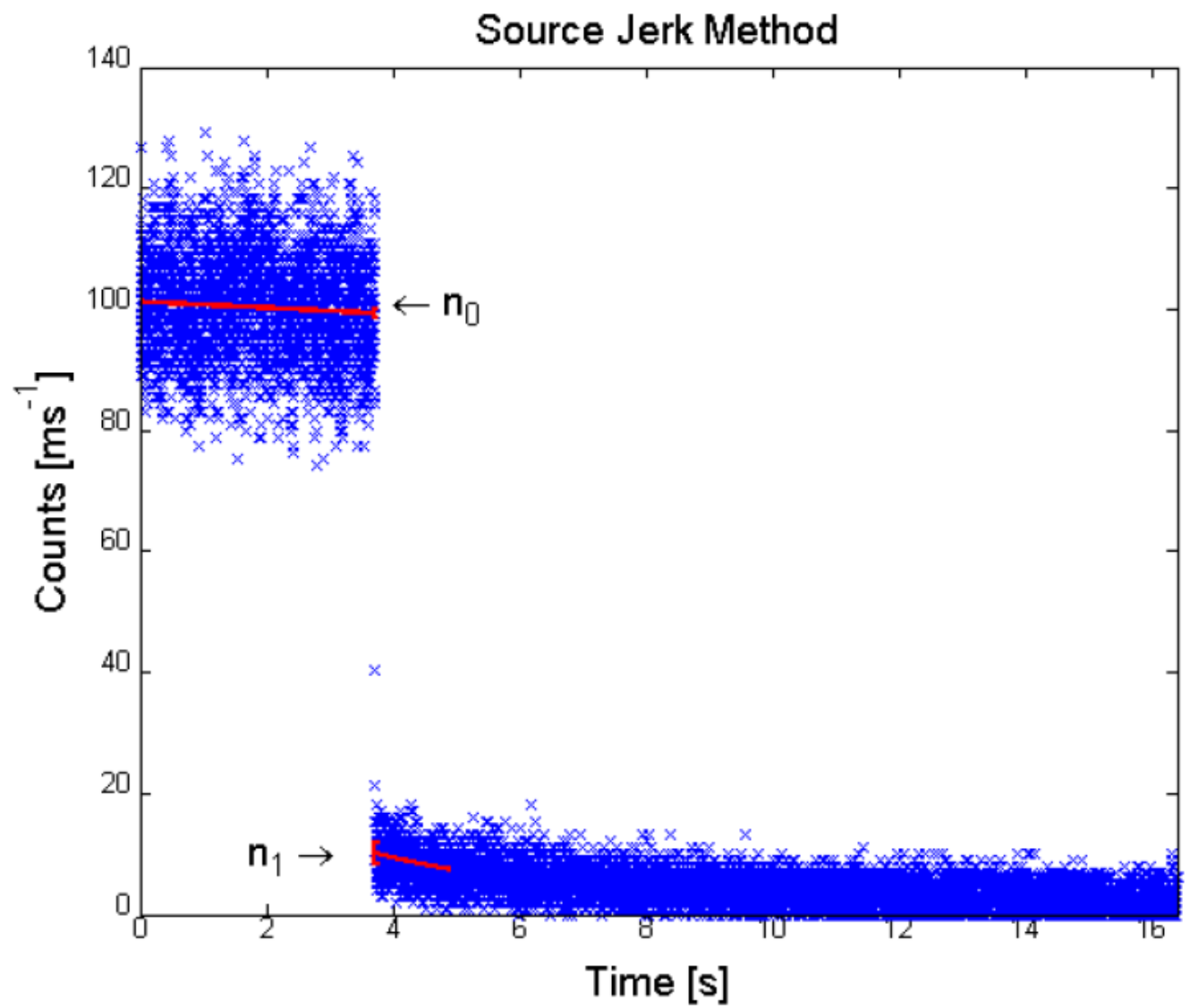


Figure XI.9: Experimental transient core response data obtained at the YALINA facility using the Source-Jerk method for measuring sub-critical reactivity.

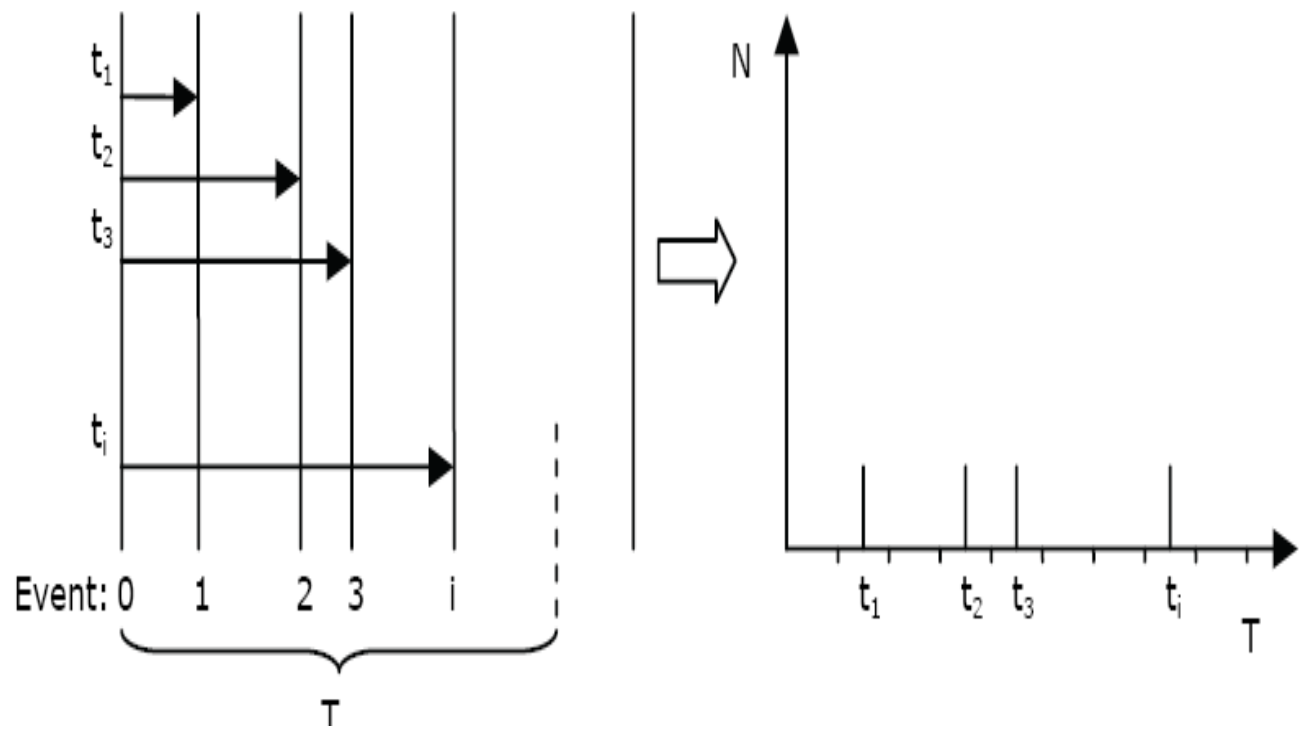


Figure XI.10: Schematic diagram illustrating the manner in which a Rossi- α histogram is generated. The vertical lines indicate occurrence of a neutron event on the indicated time scale.

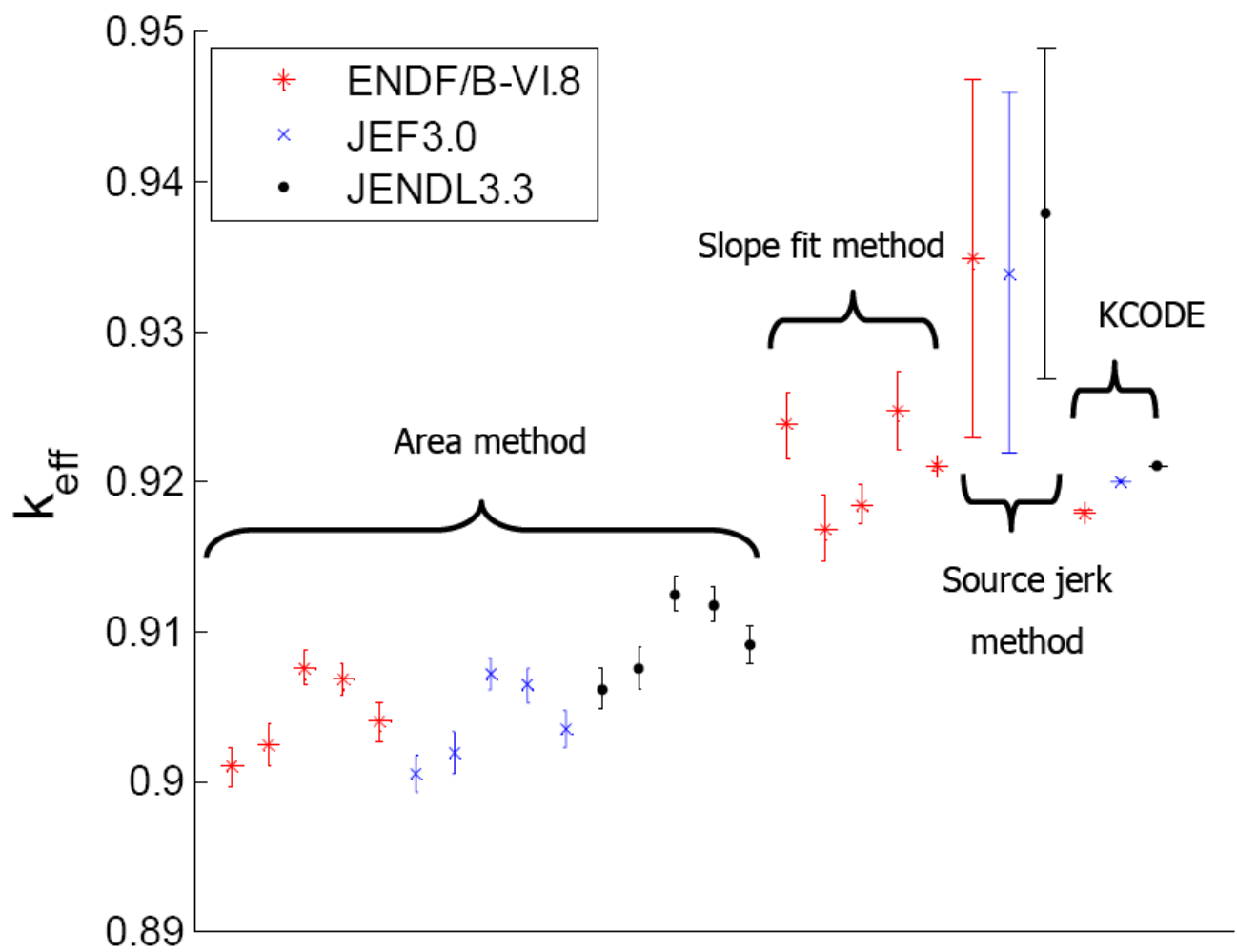


Figure XI.11: A comparison of k_{eff} determinations involving three different experimental methods and three distinct nuclear data libraries for the computations.

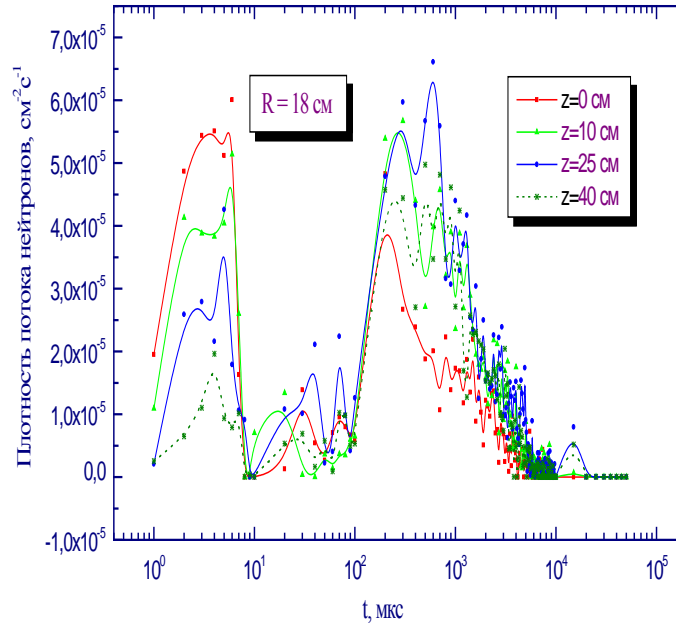
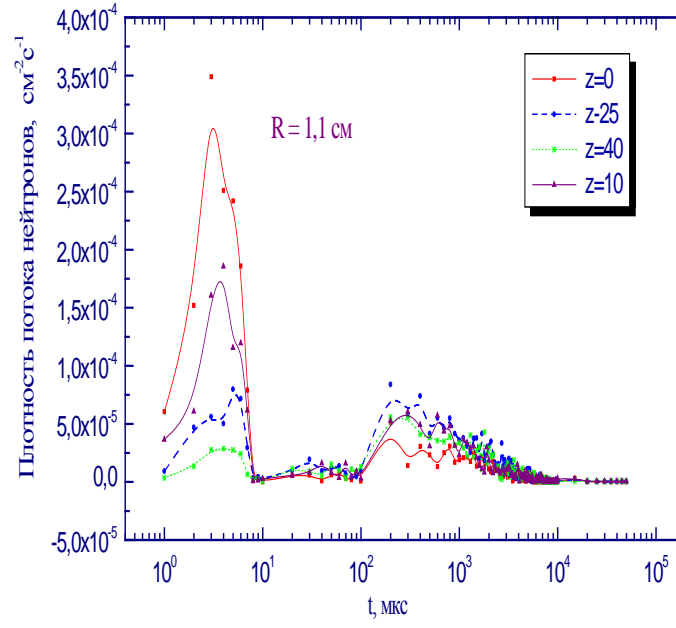


Figure XI.12: Time evolution of the neutron flux after a neutron-generator pulse ($\mu_1=\tau_s$) for different R and Z in YALINA Booster. (DT) $R = 0.0 \text{ cm}$; $Z = -29.5 \text{ cm}$.

XII. YALINA Booster Conversion Project to Low Enrichment Fuel

As mentioned in earlier chapters, an important goal of the research at the YALINA facility has been to explore technically practical means for eventually reducing the enrichment of fissionable fuel employed in the YALINA Booster (YALINA-B) configuration from components with 36% enrichment and 90% enrichment to 21% enrichment without serious determinant to the efficiency and attainable neutron flux levels during operation of the facility, and various aspects of this work are discussed elsewhere in this report. There is no need to repeat these details, but a brief summary of the intentions is worthwhile as a prelude to the next chapter which deals with modeling activities. Measurements and modeling research at the YALINA facility are progressing hand-in hand at YALINA. This is a cautious approach that insures that the maximum amount of information possible about ADS systems can be garnered from this effort. No stone should be left “untuned” in seeking a viable combination of design parameters for such a reduced-enrichment facility. The figures and discussions in the present report do not refer to these advanced design and modeling efforts since most of this work is occurring beyond the cut-off date of 2008 applicable to the present report. The details of an progress on this work of conversion to low enrichment, and the consequences, will be documented in future reports.

In very general terms, the approach that that is being taken is as follows. The first step is to replace the 90%-enriched fuel with 36%-enriched fuel and perform a detailed characterization of this new configuration through both experiments and modeling, as described in Chapter XIII. Preliminary analysis of the kinetic parameters anticipated when the 36%-enriched fuel is replaced with 21%-enriched fuel will also be carried out at this time, followed by removal of the 36%-enriched fuel and its replacement with 21%-enriched fuel. Presumably alternative geometric core configurations will be considered to boost k_{eff} within the confines allowed by the YALINA geometry. It is obvious from basic physics considerations that reducing the fuel enrichment while maintaining an identical geometry for the core loading will likely reduce the reactivity of the core. However, through a clever re-design of the core it should be possible to provide some compensation for this anticipated loss.

Whether operating capabilities comparable to those provided by the original, and well researched, YALINA-B facility, that includes both 90-% and 36%-enriched fuel, can be obtained by clever engineering design remains to be determined from future research. Clearly any core that includes only 21%-enriched fuel in the booster module will be noticeably different from the original design, but it may provide a facility that can still be used for very productive ADS research while, at the same time, satisfying the very real political need to reduce the threat of diversion of enriched fissionable material that could potentially be used for weapons applications by rogue states or terrorist organizations. If so, this will result in a very favorable tradeoff, and one that has been demonstrated repeatedly in the past in the successful conversion of critical research reactors, i.e., by the Argonne RERTR project that has been ongoing for a number of years.

XIII. Argonne Modeling Activities and Comparisons with Experiments

A detailed catalogue of all the analytical and measurement campaigns carried out in the YALINA project during the past decade would lie beyond the scope of the present report. This past work includes the contributions of scientists from many different countries as well as of the Belarusian staff at the YALINA facility. Preceding chapters of this report, in particular Chapters VI through XI, offer glimpses into the various types of experiments and calculations that have been performed at this facility during the time frame 1997 – 2008. The objective in this chapter is to provide an overview of the specific activities carried out by investigators from Argonne National Laboratory during the past several years. Keep in mind that the main objective of Argonne's involvement with this project is to examine the possibilities and consequences (vis-à-vis the mission of the YALINA project) of shifting from HEU to LEU fuel-loading configurations for the booster region of the YALINA core. As stated in the preceding chapter, this migration procedure involves pursuing the following steps for reconfiguring the booster section of YALINA-B: [90%-enriched uranium metal fuel] → [36% enriched UO_2 fuel] → [21% enriched UO_2 fuel]. The thermal region, as has always been the case for both YALINA-T and YALINA-B, has 10% enriched UO_2 fuel material (EK-10 fuel-type pins) and this will continue to be the case. However, before tackling this mission of HEU to LEU migration, it was deemed important to model accurately the original YALINA Booster configuration with 90%-enriched and 36%-enriched ^{235}U in the fuel loading configurations in the booster region (see Chapter IX and Appendix E). This need to compare modeling results with the experimental data acquired at YALINA, in order to refine the models for predicting YALINA Booster performance with HEU and LEU fuel, has evolved into an important objective for the Argonne program, i.e., testing and validating computational resources for accelerator driven systems.

Argonne's focus on measurements and modeling for the YALINA Booster aspect of the YALINA facility is consistent with the fact that Argonne became involved with the YALINA project in 2005. At this year, the emphasis of Sosny work focused on studying the booster configuration as a means to more closely simulate large-scale ADS facilities driven by spallation neutrons. Argonne's modeling and comparisons with experimental data were ongoing as of the end of 2008, so this report clearly does not constitute the closing chapter of this research activity. As will be discussed briefly in Chapter XIV, Argonne intends to continue its collaboration with YALINA researchers for several more years.

Argonne is using sophisticated contemporary system modeling techniques and computer codes for its analytical studies. The utilized system models take fine geometric details of the YALINA core into consideration, with no homogenization, as well as detailed specifications of materials, in performing its calculations for YALINA Booster. This is evident from Appendix E of this report dealing with benchmark specifications for YALINA-B. The Monte Carlo codes used at Argonne include MCNP/MCNPX, MCB, and MONK. These codes are widely used for benchmarking, nuclear system analyses, and nuclear reactor licensing in the U.S., the U.K., and elsewhere around the world. Table XIII.1 offers a comparison of the salient features of the MCNP and MONK code systems. The deterministic code package ERANOS/ECCO/VARIANT has also been used in some of the calculations mentioned in this section. This analyses activity currently incorporates several well-validated nuclear databases (e.g., ENDF/B-VI.0, -VI.6, -VI.8, JEF-2.2, JEFF-3.1, and JENDL-2) in these calculations. These nuclear libraries have been processed as required to satisfy the data input needs of the individual utilized codes. For example, the Monte Carlo codes generally employ continuous-energy processed libraries, although MONK can also use multi-group libraries. As specified in both Appendices D and E, 172-group processed libraries are used exclusively for those cases requiring multi-group input data, e.g., for deterministic calculations. Each of these codes and nuclear databases has its unique strengths

and limitations but, collectively, use of this assembly of diverse computational resources offers the opportunity to gain considerable confidence in the comparisons of system modeling and corresponding experimental results for the YALINA Booster. In particular, comparisons of calculated results for the same quantity – using identical system models but different codes and nuclear databases – can provide an estimate of the uncertainties associated with system modeling that must be considered when comparing these results with experimental data.

The ability to compute nuclear transmutation rates associated with fission and capture (burnup) is extremely important in assessing the performance of ADS systems since nuclear waste transmutation is an essential role that these nuclear systems are expected to fulfill. As indicated in Table XIII.1, both Monte Carlo code systems, MCNP and MONK, can perform such burnup calculations through inclusion of either an intrinsic routine (MONK) or an add-on routine (CINDER90 for MCNP) found in these codes.

Two core configurations have been used for the YALINA Booster, as described in Appendix E. One involves 902 pins in the thermal zone and the second involves 1141 fuel pins in this region. The neutron producing target is the low-current assembly described in Chapter VI rather than the high-current assembly. The analyses include calculation of the multiplication factor and the main neutronics parameters, such as the effective delayed neutron fraction (β_{eff}), the prompt neutron lifetime (l_p), and neutron generation time (Λ). As indicated in Appendix E, no geometrical approximations have been made (other than ignoring the details of individual samples and detectors in some instances). Furthermore, account is taken of all the materials in the assembly, including minor isotopes and impurities, to the extent allowed by the nuclear data libraries. The ENDF/B library used with MCNP contains all the materials needed with two minor exceptions: ^{207}Pb nuclear data are used for ^{204}Pb and ^{138}Ba data are employed for natural Ba in order to allow for limitations of this data library. The impact of these substitutions is expected to be very small. Table XIII.2 gives the material approximations that have been assumed in the various MONK simulations.

The results of the Monte Carlo calculations of the multiplication factor and the main neutronics parameters for the two YALINA Booster configurations mentioned above are given in Table XIII.3 for the case of 1141 EK-10 fuel pins in the thermal zone and Table XIII.4 for the arrangement of 902 EK-10 fuel pins in the thermal zone. The differences between comparable calculated results obtained with different codes and nuclear databases provide a good understanding of the limitations in contemporary system modeling of the YALINA Booster attributable to these sources. These differences are generally relatively modest, but they do provide a measure of the impact of certain approximations and limitations inherent to the diverse computational schemes and nuclear databases.

Comparisons of the Monte Carlo calculated results with corresponding recent experimental values for YALINA Booster show reasonable agreement as can be seen from some examples given in Table XIII.5. As a specific example, the k_{eff} value of 0.97972 (see Table XIII.3) obtained with MCNP and ENDF/B-VI.6 in the case of 1141 EK-10 fuel pins for the ^{252}Cf spontaneous-fission neutron source differs by only 220 pcm from the recent experimental measurements. This is a factor-10 improvement over an earlier published result for this same configuration. Similar results have been observed for deterministic model calculations using ERANOS as exemplified by Table XIII.6.

Extensive calculations of neutron fluence profiles in the experimental channels of YALINA Booster have also been performed. Two examples of comparisons between the MCNPX and MONK results are shown in Figs. XIII.1 and XIII.2. The agreement between these calculated results is very good, but no comparisons with experimental data are provided in these plots. Typical neutron spectra obtained from MCNPX and MONK calculations are shown in Figs. XIII.3 and XIII.4. The agreement

is again reasonably good except in regions of very low fluence. Again, there is no experimental information provided to compare with these results.

Reaction rates for $^3\text{He}(n,p)$, $^{113}\text{In}(n,g)$, $^{115}\text{In}(n,g)$, $^{197}\text{Au}(n,g)$ and $^{55}\text{Mn}(n,g)$ have been calculated for various positions in the experimental channels. The cross sections for these processes are plotted in Fig. XIII.5. Examples of calculated reaction rates and their uncertainties are shown in Table XIII.7.

..... Tables and figures for Chapter XIII begin on the following page

Table XIII.1: Comparison of MCNP and MONK Monte Carlo system simulation codes.

- MONK can only transport neutrons; MCNP can transport neutrons, electrons, and photons; MCNPX can transport over 34 different types of particles at energies lower and higher than 20 MeV.
- MCNP/MCNPX is designed for parallel platforms in distributed memory systems (PVM and MPI) or in shared memory systems (OPENMP); MONK runs only on single processor.
- MONK can perform burnup calculations; the burnup capability has been embedded in MCNPX by integrating CINDER90 computer code package. In both cases, the burnup is limited to a fission neutron source and it is not applicable to an accelerator driven system.
- MONK can efficiently describe complicated geometries by the Woodcock tracking capability referred to as hole geometry.
- MONK takes advantage of the neutron superhistory variance reduction technique. MCNP/MCNPX takes advantage of the space/energy/time weight window variance reduction technique.
- MONK can calculate the external source neutron multiplication factor (k_{src}) for a subcritical assembly. The calculation of k_{src} for a subcritical core in MCNP/MCNPX is possible only by processing the neutron weight summary table or by tallying the secondary neutrons.
- MCNP/MCNPX can solve time dependent transport problems.
- MCNP/MCNPX can calculate the prompt multiplication factor for a critical core by suppressing the generation of delayed neutrons.
- MONK can define a material mixture as a composition of the previously defined materials.
- MONK allows the utilization of symbolic parameters and math expressions.
- MCNP/MCNPX can superimpose an arbitrary mesh to the geometrical model for tallying and variance reduction purposes.
- For three dimensional visualizations, MONK has VISTA-RAY graphical packages while MCNP/MCNPX requires external software packages.

Table XIII.2: Material approximations assumed for the MONK calculations

Missing nuclides (indicated in amaranth) and material approximations in MONK9a

Library	Isotope
BINGO JEF-2.2	⁷⁵ As; ²⁰⁹ Bi; ²⁰⁴ Pb; ⁶⁶ Zn; ⁶⁷ Zn; ⁶⁸ Zn; ⁷⁰ Zn Ba modeled as ¹³⁰ Ba, ¹³² Ba, ¹³⁴ Ba, ¹³⁵ Ba, ¹³⁶ Ba, ¹³⁷ Ba and ¹³⁸ Ba ⁶³ Cu and ⁶⁵ Cu modeled as Cu ²⁰⁶ Pb, ²⁰⁷ Pb and ²⁰⁸ Pb modeled as Pb Sb modeled as ¹²¹ Sb and ¹²³ Sb ²⁸ Si, ²⁹ Si and ³⁰ Si modeled as Si
DICE JEF-2.2	S(α,β) graphite; ⁷⁵As; ²⁰⁴Pb Ba modeled as ¹³⁰ Ba, ¹³² Ba, ¹³⁴ Ba, ¹³⁵ Ba, ¹³⁶ Ba, ¹³⁷ Ba and ¹³⁸ Ba ⁶³ Cu and ⁶⁵ Cu modeled as Cu ²⁰⁶ Pb, ²⁰⁷ Pb and ²⁰⁸ Pb modeled as Pb Sb modeled as ¹²¹ Sb and ¹²³ Sb ²⁸ Si, ²⁹ Si and ³⁰ Si modeled as Si
DICE ENDF/B-VI	S(α,β) graphite; ⁷⁵As; ²⁰⁴Pb Ba modeled as ¹³⁰ Ba, ¹³² Ba, ¹³⁴ Ba, ¹³⁵ Ba, ¹³⁶ Ba, ¹³⁷ Ba and ¹³⁸ Ba Sb modeled as ¹²¹ Sb and ¹²³ Sb ²⁸ Si, ²⁹ Si and ³⁰ Si modeled as Si
WIMS JEF-2.2	C always modeled by C in graphite H always modeled by H in water ⁷⁵ As; ²⁰⁹ Bi; ²⁰⁴ Pb; Sb ⁵⁰ Cr, ⁵² Cr, ⁵³ Cr and ⁵⁴ Cr modeled as Cr ⁶³ Cu and ⁶⁵ Cu modeled as Cu ⁵⁴ Fe, ⁵⁶ Fe, ⁵⁷ Fe and ⁵⁸ Fe modeled as Fe ⁵⁸ Ni, ⁶⁰ Ni, ⁶¹ Ni, ⁶² Ni and ⁶⁴ Ni modeled as Ni ²⁰⁶ Pb, ²⁰⁷ Pb and ²⁰⁸ Pb modeled as Pb S modeled as ³² S, ³³ S, ³⁴ S and ³⁶ S ²⁸ Si, ²⁹ Si and ³⁰ Si modeled as Si

Missing nuclides in MCNPX2.6b, MCNP5, MCNP4c3

Library	Isotope
ENDF/B-VI	²⁰⁴ Pb
ENDF/B-VI	Ba modeled as ¹³⁸ Ba

Missing data in MCB with JEF-2.2

Library	Data
JEF-2.2	Update of all S(α,β) scattering functions to 2002 data
JEF-2.2	Ba modeled as ¹³⁸ Ba

Table XIII.3: k_{eff} , β , l_p , and Λ values for the YALINA Booster configuration with 1141 EK-10 fuel rods.*

Code	Library	Fission neutron source	D-D & fission neutron sources	D-T & fission neutron sources	β [pcm]	l_p [μ s]	Λ [μ s]
MCNPX2.6 β	ENDF/B-VI.6	0.97972 \pm 4	-	-	760 \pm 8	-	-
MCNPX2.6 β	ENDF/B-VI.6	0.97956 \pm 9	0.98883 ^f 0.98690 ^g	0.99148 ^f 0.99145 ^g	749 \pm 16	54 \pm 2 ^b 72 ^c	56 \pm 2 ^b 73 ^c
MCNPX2.6 β	JEFF-3.1	0.98008 \pm 9	-	-	728 \pm 12	-	-
MCNP5	ENDF/B-VI.6	0.98016 \pm 9	-	-	766 \pm 18	-	-
MCNP4c3	ENDF/B-VI.6	0.98004 \pm 7	-	-	747 \pm 15 752 \pm 2 ^a	-	-
MCNP4c3	ENDF/B-VI.0	0.98097 \pm 8	-	-	765 \pm 16 755 \pm 2 ^a	-	-
MCB2 β	JEF-2.2	0.98318 \pm 9	0.98856	0.99291	699 \pm 17	60 \pm 2	61 \pm 2
MONK9a	BINGO JEF-2.2	0.9836 \pm 20	0.9898 \pm 20 ^g	0.9932 \pm 20 ^g	-	-	-
MONK9a	DICE JEF-2.2	0.9824 \pm 20	0.9891 \pm 20 ^g	0.9931 \pm 20 ^g	-	-	-
MONK9a	DICE ENDF/B-VI.0	0.9773 \pm 10	0.9861 \pm 20 ^g	0.9906 \pm 20 ^g	-	48 \pm 5	49 \pm 5
MONK9a	WIMS JEF-2.2	0.9844 \pm 20	0.9912 \pm 10 ^g 0.9926 \pm 20 ^d	0.9910 \pm 10 ^g 0.9930 \pm 20 ^d	-	-	-

Table I legend

a	One run method.
b	Boron concentration equal to 1e-7 atoms/b-cm ² .
c	MCNPX 1/v tally.
d	Source geometry unit.
e	Unified source specification.
f	Using the weights summary table
g	Using the secondary neutrons F4 tally

- Errors shown are statistical.

Table XIII.4: k_{eff} , β , l_p , and Λ values for the YALINA Booster configuration with 902 EK-10 fuel rods.*

Code	Library	Fission neutron source	D-D & fission neutron sources	D-T & fission neutron sources	β [pcm]	l_p [μ s]	Λ [μ s]
MCNPX2.6 β	ENDF/B-6.6	0.92881 \pm 4	-	-	765 \pm 8	-	-
MCNPX2.6 β	ENDF/B-6.6	0.92880 \pm 8	0.95635 ^f 0.95625 ^g	0.97118 ^f 0.97117 ^g	754 \pm 18	54 \pm 2 ^b 74 ^c	58 \pm 2 ^b 80 ^c
MCNPX2.6 β	JEFF-3.1	0.92862 \pm 9	-	-	739 \pm 12	-	-
MCNP5	ENDF/B-6.6	0.92913 \pm 8	-	-	761 \pm 17	-	-
MCNP4c3	ENDF-6.6	0.92918 \pm 9	-	-	764 \pm 12 762 \pm 2 ^a	-	-
MCNP4c3	ENDF/B-6.0	0.93014 \pm 9	-	-	775 \pm 12 763 \pm 2 ^a	-	-
MCB2 β	JEF-2.2	0.93271 \pm 8	0.96061	0.97477	705 \pm 16	59 \pm 2 ^d	63 \pm 2 ^d
MONK9a	BINGO JEF-2.2	0.93350 \pm 20	0.96000 \pm 30 ^g	0.97350 \pm 20 ^g	-	-	-
MONK9a	DICE JEF-2.2	0.93250 \pm 20	0.95980 \pm 30 ^g	0.97350 \pm 20 ^g	-	-	-
MONK9a	DICE ENDF/B-6.0	0.92710 \pm 20	0.95600 \pm 30 ^g	0.97060 \pm 20 ^g	-	49 \pm 5 ^d	53 \pm 5 ^d
MONK9a	WIMS JEF-2.2	0.93460 \pm 20	0.96280 \pm 20 ^g 0.96910 \pm 20 ^d	0.96290 \pm 20 ^g 0.97180 \pm 20 ^d	-	-	-

Table II legend

A	One run method.
B	Boron concentration equal to 1e-7 atoms/b-cm ² .
C	MCNPX 1/v tally.
D	Source geometry unit.
E	Unified source specification.
F	Using the weights summary table
G	Using the secondary neutrons F4 tally

* Errors shown are statistical.

Table XIII.5: Some comparisons of Monte Carlo calculated and experimental results for YALINA-B.

***Preliminary Comparison with the Experimental Results
YALINA Booster with 1141 EK-10 fuel pin loading***

Channel	$\rho/\beta_{\text{eff}} (\$)$	β_{eff}	K_{eff} Exp.	ΔK_{eff} (Exp. – Cal.)	
				MONK	MCNPX
EC1	-3.3627 ± 0.0077	0.00747	0.9755 ± 0.0022	-0.0019	-0.0034
		0.00728	0.9761 ± 0.0022	-0.0013	-0.0028
		0.00695	0.9772 ± 0.0022	-0.0002	-0.0017
EC2	-3.4088 ± 0.0069	0.00747	0.9752 ± 0.0020	-0.0022	-0.0037
		0.00728	0.9758 ± 0.0020	-0.0016	-0.0031
		0.00695	0.9769 ± 0.0020	-0.0005	-0.0020
EC3	-3.5198 ± 0.0081	0.00747	0.9744 ± 0.0022	-0.0030	-0.0045
		0.00728	0.9750 ± 0.0022	-0.0024	-0.0039
		0.00695	0.9761 ± 0.0022	-0.0013	-0.0028

Table XIII.6: Some calculated results for YALINA-B obtained using the deterministic code ERANOS

ERANOS Deterministic Model Results

Nuclear Data	K_{eff}	$K_s(\text{D-D n's})$	K_s
172 groups JEF2.2	0.97747	0.98588	0.99082
172 groups JEF3.1	0.97352	0.98291	0.99054
172 groups ENDF/B-6	0.97277	0.98289	0.99032

Table XIII.7: Calculated neutron capture reaction rates for several materials as obtained for both configurations of the thermal region of YALINA Booster (1141 EK-10 pins and 902 EK-10 pins) are shown in the top table. The lower table gives the uncertainties in these calculated results (in percent).

	1141		902	
	DD	DT	DD	DT
¹⁹⁷ Au	0.00838	0.011099	0.002509	0.004987
In	0.00877	0.01454	0.004626	0.006641
⁵⁵ Mn	0.000416	0.000771	0.000153	0.000282

	1141		902	
	DD	DT	DD	DT
¹⁹⁷ Au	9.73	11.66	8.09	6.62
In	8.18	9.07	9.78	8.61
⁵⁵ Mn	8.06	10.65	7.40	7.39

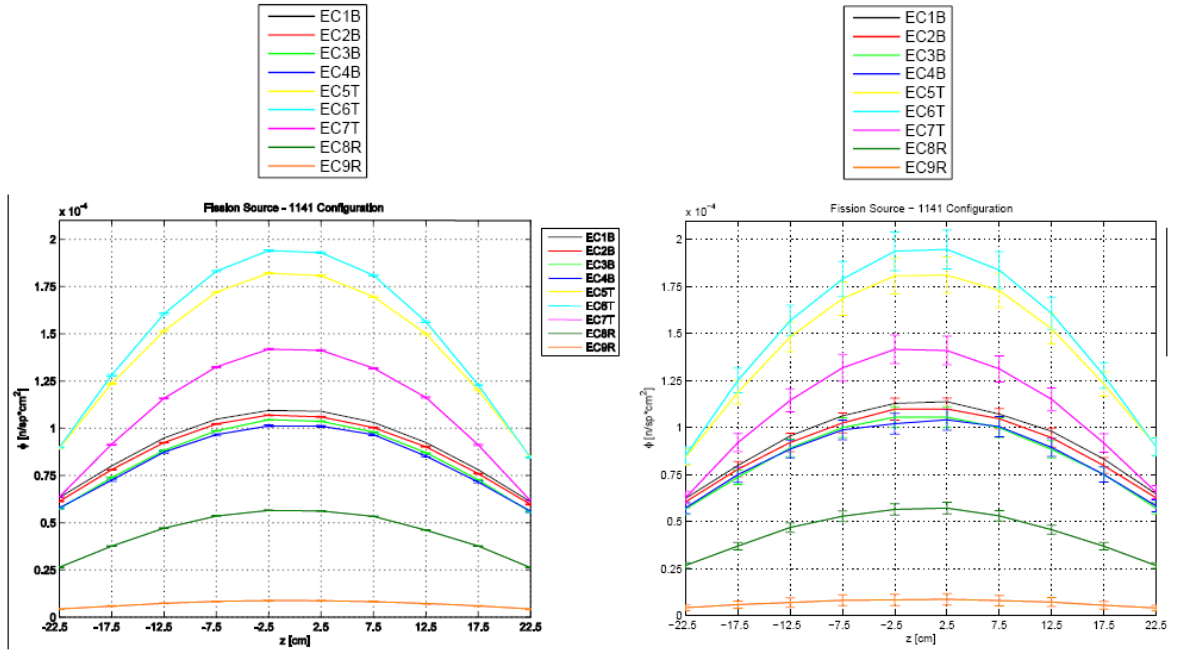


Figure XIII.1: Axial neutron flux distribution in the experimental channels for the fission neutron source calculated by MCNPX (left) and MONK (right). The values are averaged over an experimental channel length of 5 cm.

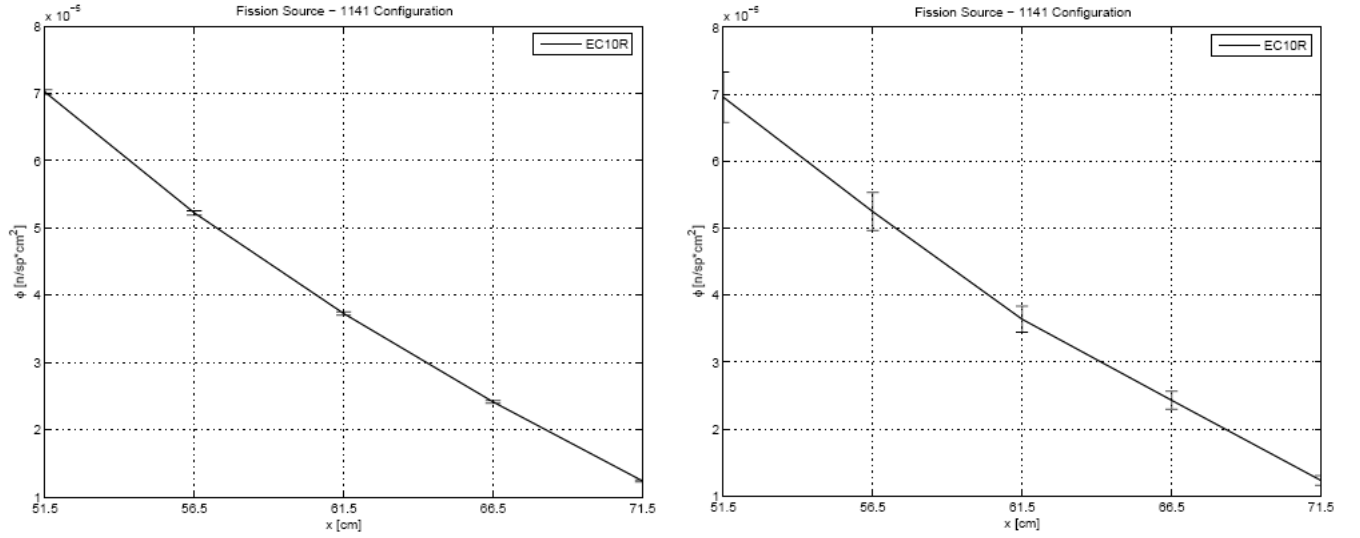


Figure XIII.2: Radial neutron flux profile in the experimental channel EC10R for the fission neutron source calculated by MCNPX (left) and MONK (right). The values are averaged over an experimental channel length of 5 cm.

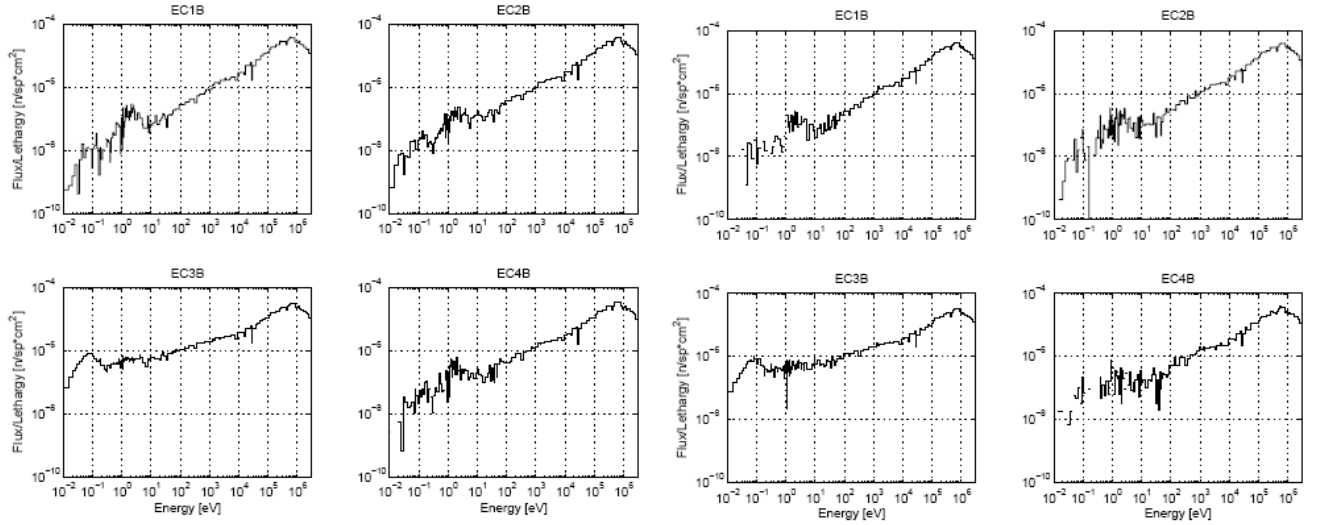


Figure XIII.3: Neutron spectrum of YALINA-B with 1141 EK-10 fuel rods in the experimental channels of the fast zone for the fission neutron source calculated by MCNPX (left) and MONK (right) using 172 neutron-energy-group structure. The spectra were calculated at the center of the active fuel length and over 10 cm experimental channel length.

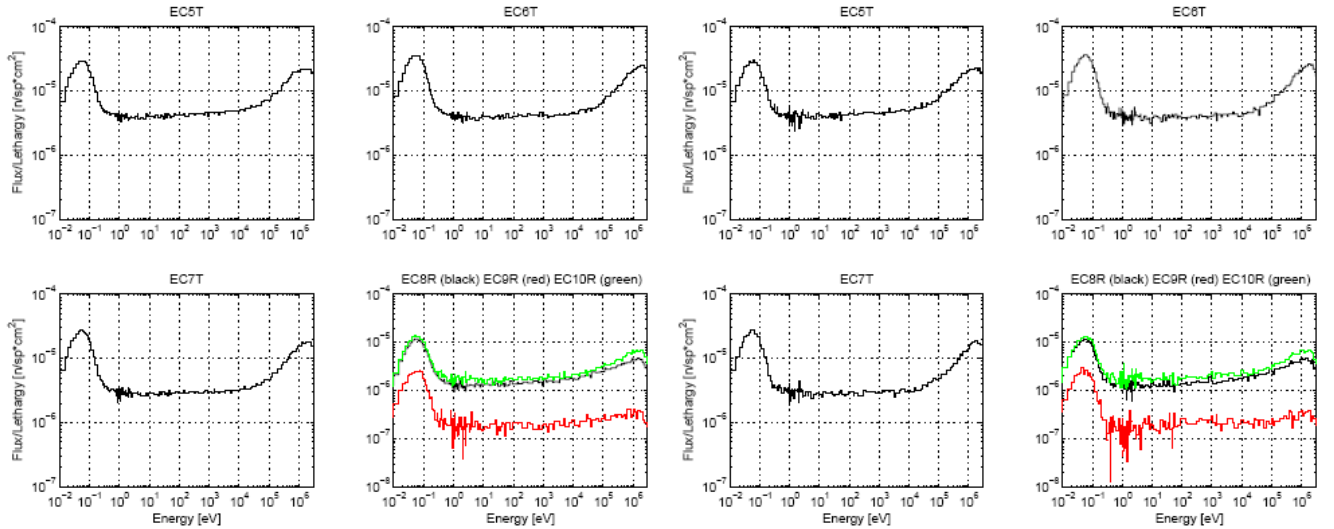


Figure XIII.4: Neutron spectrum of the YALINA Booster with 1141 EK-10 fuel rods in the experimental channels of the thermal and reflector zones for the fission neutron source calculated by MCNPX (left) and MONK (right) using the 172 neutron-energy-group structure. The spectra were calculated at the center of the active fuel length and over 10 cm experimental channel length for EC5T, EC6T, and EC7T, and 5 cm experimental channel length for EC10R.

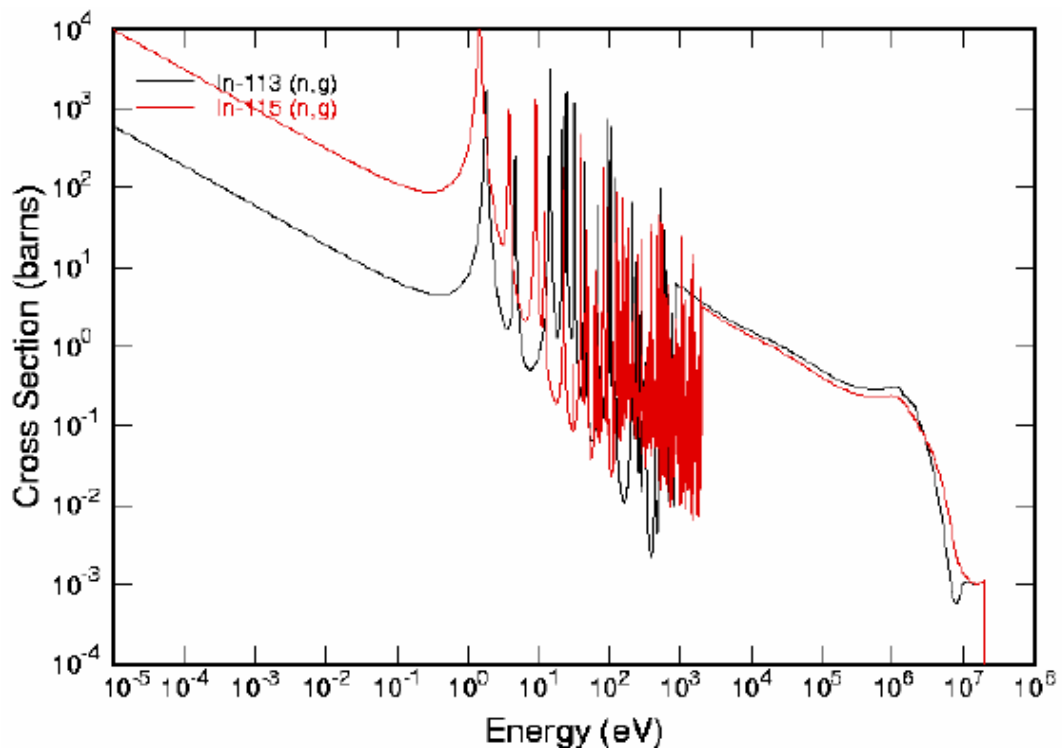
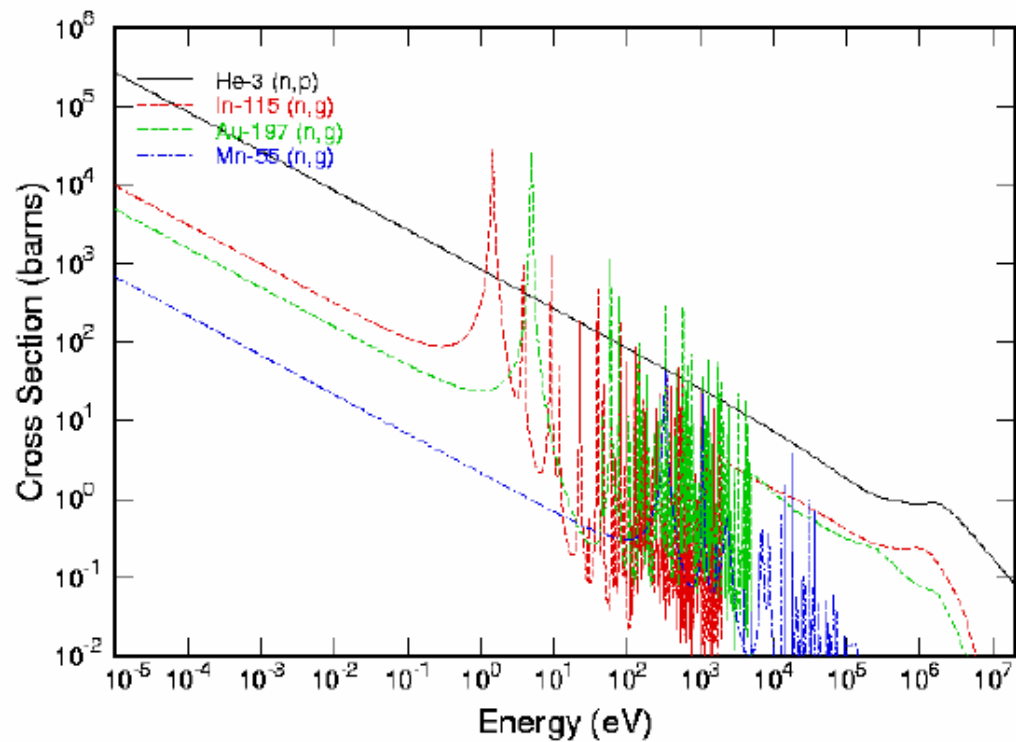


Figure XIII.5: Plots of cross sections taken from JEFF-3.0 and used for reaction-rate calculations.

XIV. YALINA Project Principal Achievements

This short Chapter lists in bullet form what appear, in the opinion of the present authors, to be some of the major achievements of the YALINA project during the past decade.

- Successfully designed and constructed what has proved to be an extremely flexible and productive nuclear reactor research facility at a very low cost.
- Successfully operated this facility for more than a decade and continues to maintain the potential for productive research studies in the future.
- Demonstrated that a sub-critical ADS facility can be used to transmute nuclear waste through both neutron-capture and neutron-fission reactions.
- Measured transmutation reaction rates for several well-known nuclear waste products in spectra generated in an ADS core.
- Developed and tested methods and experimental instrumentation for successfully monitoring the operation of an ADS facility.
- Provided an extensive body of good quality experimental data concerning the coupling of both fission- and accelerator-based external neutron sources to a sub-critical core that can be used for the validation of contemporary computational methods and resources (codes and nuclear databases).
- Demonstrated that the “booster” concept is a very useful approach for simulating, on a small scale, the extended spallation-neutron sources that will be employed in future large-scale ADS facilities.
- Successfully demonstrated the “valve” or “gate” concept that allows fast neutrons to migrate from the booster region to the thermal core but prevents thermal neutrons from migrating into the booster region.
- Established and maintained an extensive network of beneficial research collaborations involving scientists from many different countries.
- Spawned extensive computational analysis projects aimed at gaining a solid understanding of the kinetics of ADS reactor cores.
- Provided an established, working facility that can be used for experimental investigation of ADS design concepts that incorporate use of LEU fuel as opposed to HEU materials in the core.

XIV. Future Plans for the YALINA Project

The research program for YALINA going forward into this new decade will focus on migration of the original YALINA Booster core from the uranium enrichment configuration (90% + 36% + 10%) to an eventual enrichment combination of (21% + 10%), as indicated in Chapter XII. This is to be accomplished in stages, with extensive modeling and measurement campaigns performed at each stage. The process had already begun in 2008.

Analyses will be carried out using the most recent nuclear data libraries available, e.g., ENDF/B-VII.0 and JENDL-3.3, with forms of these libraries have been processed in a manner suitable for the simulation code suite used for this work and validated against the usual benchmarks.

Other measurement activities beyond the standard kinetics measurements described in this report that will be pursued during the next few years should include additional nuclear-waste isotope transmutation studies in ADS neutron spectra as well as refinements of spectrum adjustment (unfolding) calculations to allow a better comparison of calculated and measured spectral results.

Since YALINA is a zero-power facility, access to the core and samples following a run is a fairly quick and routine process. However, for full-scale, high-power ADS facilities this will not be the case. Access to the core may be severely restricted for some time after shutdown due to residual radioactivity from their operation at high fluence levels. Consequently, it will be of interest to explore possible radiation monitoring techniques that can be accomplished remotely. One such potential approach involves exploiting the liquid dosimetry concept first proposed in the mid 1990's by Smith et al. and demonstrated at the Fusion Neutron Source facility (FNS) at the JAEA laboratory in Tokai, Japan. In this approach, various salt compounds containing isotopes that can be activated with various resulting half lives, cross sections, and neutron-spectrum response characteristics are dissolved in water. The solution is circulated in sealed tubes at a constant flow rate to various parts of the system (in this case the accelerator target and the YALINA core) during operation, and the induced gamma-ray activity is measured in real time at an external location. Information about the neutron fluence and spectra at various locations can be deduced from this measured information.

Acknowledgments

The tables and figures, as well as some of the textual material appearing in this report, were either scanned or extracted electronically from the many documents listed below in the section “References and Publications” without referring to them specifically (for convenience and to maintain readability of this report). The authors are therefore very much indebted to the authors of these documents, and hereby gratefully acknowledge their collective contributions without which preparation of the present report would have been impossible. Additional information used in this report was also downloaded from a large number of documents freely available to the public on the Internet, e.g., from Wikipedia. These sources provided useful descriptions of physical concepts, experimental methods, and properties of various types of detectors. Finally, the authors are indebted to the YALINA staff for their kindness and patience when showing him their facility, explaining its operation, and answering his many questions during a very interesting and productive visit to Sosny in October 2007.

References and Publications

Reports, conference proceedings, journal publications, memoranda, and other technical documents that are relevant to the YALINA facility research program, and that have been authored by YALINA staff and/or collaborators working in the YALINA research program or very closely related programs, are included here. They are ordered by date and then alphabetically by lead author within a particular year. This is not a reference list in the usual sense and, as such, explicit citations to these documents do not appear in the text of this report.

1996

[**Chi+1996**] S.E. Chigrinov et al., “Experimental Research of the Transmutation of Long-lived Fission Products and Minor-Actinides in a Sub-critical Assembly Driven by a Neutron Generator,” Proc. ADTTA '96 – Conf. – Kalmar, Sweden, p. 737-744, 1996.

[**Nau+1996**] V.A. Naumov et al., “Code KRATER for Calculation of Neutron Physical Characteristics of Thermal Nuclear Reactors,” Preprint of NAS of Belarus IPEP-14, p. 39, Minsk, Belarus, 1996 (in Russian).

1997

[**Sal+1997**] M. Salvatores et al., “MUSE-1: A First Experiment at MASURCA to Validate Physics of Sub-critical Multiplying Systems Relevant to ADS,” IAEA Technical Document No. 985, Vienna, Austria, pp. 430-436, 1997.

1998

[**Bou+1998**] S.F. Boulyga et al., “Neutron Generator NG-12-1 as a Basic Installation to Perform Researches at Neutron Center of the National Academy of Sciences of Belarus,” Preprint IRPCP-21, Minsk, Belarus, p. 36, 1998 (in Russian).

[**Kie1998**] A.I. Kievitskaia, “Experimental and Theoretical Research on Transmutation of Long-Lived Fission Products and Minor Actinides in a Sub-critical Assembly Driven by a Neutron Generator,” Evaluation Form for Annual Reports of ISTC Projects: Project #B-070-98, 1 September 1998.

1999

[**Chi+1999-1**] S. Chigrinov et al., “The Research on Accelerator Driven Systems in National Academy of Sciences of Belarus,” Proceedings of the IAEA Advisory Group Meeting on National Programs on ADS, Taejeon, Republic of Korea, 1-4 November, 1999.

[**Chi+1999-2**] S.E. Chigrinov et al., “A Sub-critical Facility for Research on Transmutation of Long-Lived Fission Products and Minor Actinides,” Int. “Marburg-Dubna” Workshop on Modeling of Electronuclear Method of Energy Production and Studies of Transmutation of Radioactive Wastes Using the JINR Synchrophasotron-Nuclotron Complex, Dubna, Russia, October 26-29, 1999.

[Chi+1999-3] S.E. Chigrinov et al., “Transmutation of I-129, Np-237, Pu-239, and Am-241 Irradiated in a Target-Moderator System with Relativistic Protons,” Int. “Marburg-Dubna” Workshop on Modeling of Electronuclear Method of Energy Production and Studies of Transmutation of Radioactive Wastes Using the JINR Synchrophasotron-Nuclotron Complex, Dubna, Russia, October 26-29, 1999.

[Chi+1999-4] S.E. Chigrinov et al., “A Sub-critical Facility for Research on Transmutation of Long-Lived Fission Products,” Int. “Marburg-Dubna” Workshop on Modeling of Electronuclear Method of Energy Production and Studies of Transmutation of Radioactive Wastes Using the JINR Synchrophasotron-Nuclotron Complex, Dubna, Russia, October 26-29, 1999.

[Chi+1999-5] S. Chigrinov et al., “Setting of Operation Loading of a Uranium-Polyethylene Sub-critical Assembly Driven by a Neutron Generator,” Report No. 64, RPCPI, p. 54, 1999.

[KC1999] Anna Kievitskaia and Serguei E. Chigrinov, “Experimental and Theoretical Research on Transmutation of Long-Lived Fission Products and Minor Actinides in a Sub-critical Assembly Driven by a Neutron Generator,” Annual Report of the ISTC Project #B-070-98, 14 September 1999.

[Kie+1999] A.I. Kievitskaia et al., “Experimental and Theoretical Research on Transmutation of Long-Lived Fission Products and Minor Actinides in a Sub-critical Assembly Driven by a Neutron Generator,” The 3rd International Conf. on Accelerator Driven Transmutation Technologies and Applications, ADTTA’99, Prague, Czech Republic, 7-11 June, 1999.

[Kri+1999] M.I. Krivopustov et al., “A Lead-Uranium Target with Hard Neutron Spectrum for Transmutation Research,” Int. “Marburg-Dubna” Workshop on Modeling of Electronuclear Method of Energy Production and Studies of Transmutation of Radioactive Wastes Using the JINR Synchrophasotron-Nuclotron Complex, Dubna, Russia, October 26-29, 1999.

[Kul1999] B.A. Kulakov et al., “Neutron Yield in Collisions of Relativistic Ions with Heavy Targets, Transmutation of Radioactive Isotopes,” Proc. of the 14th Intern. Seminar on High Energy Physics Problems, Relativistic Nuclear Physics and Quantum Chromodynamics, Dubna, Russia, August 17-22, 1999.

[Och+1999] M. Ochs et al., “Transmutation of I-129 and Np-237 Using Spallation Neutrons Produced by 1.5-, 3.7-, and 7.4-GeV Protons,” Preprint No. E1-99-1, JINR, Dubna, Russia, p. 28, 1999.

[Ser+1999] I.G. Serafimovitch et al., “A Small-Scale Setup for Research of Some Aspects of Accelerator Driven Transmutation Technologies,” The 3rd International Conf. on Accelerator Driven Transmutation Technologies and Applications, ADTTA’99, Prague, Czech Republic, 7-11 June, 1999.

2000

[Chi+2000] S. Chigrinov et al., “Experimental and Theoretical Research on Transmutation of Long-Lived Fission Products and Minor Actinides in a Uranium-Polyethylene Sub-critical Assembly Driven by a Neutron Generator,” 5th Int. Symposium and Exhibition on Environmental Contamination in Central and Eastern Europe, Prague, Czech Republic, 11-14 September, 2000.

[CR2000] S. Chigrinov and I. Rakhno, “IAEA Benchmark 3.2: Experimental Research of Neutronics of a Sub-critical Uranium-Polyethelene Assembly Driven with a Neutron Generator (The Yalina Experiment),” Technical Report, Radiation Physics and Chemistry Problems Institute, National Academy of Sciences, Minsk, Belarus, 2000.

[**KC2000**] Anna Kiyavitskaya and Serguej Chigrinov, “Experimental and Theoretical Research on Transmutation of Long-lived Fission Products and Minor Actinides in a Sub-critical Assembly Driven by a Neutron Generator,” Annual Report of ISTC Project #B-070-98 (Second Year), October 2000.

2001

[**Bar+2001**] V.S. Barashenkov et al., “Fast Sub-critical Assembly with MOX Fuel for Research on Nuclear Waste Transmutation,” *Journal of Vesti of NAS of Belarus, Ser. Physical – Technical Sciences* **3**, pp. 150-153, 2001 (in Russian).

[**Chi+2001-1**] S.E. Chigrinov et al., “Experimental Investigations on Neutronics of the Accelerator-Driven Transmutation Technologies at the Sub-critical Facility YALINA,” ANA/ADTTA, Reno, Nevada, 11-15 November 2001.

[**Chi+2001-2**] S.E. Chigrinov et al., “The Sub-critical Facility YALINA to Investigate the Peculiarities of Accelerator Driven Transmutation Technologies,” ANA/ADTTA, Reno, Nevada, 11-15 November 2001.

[**Chi+2001-3**] S.E. Chigrinov et al., “Experimental Investigations on Neutronics of the Accelerator Driven Transmutation Technologies at the Sub-critical Facility YALINA,” ARWIF Workshop, Chester, Great Britain, 22-25 October 2001.

[**KC2001**] Serguej Chigrinov and Anna Kiyavitskaya, “Experimental and Theoretical Research on Transmutation of Long-lived Fission Products and Minor Actinides in a Sub-critical Assembly Driven by a Neutron Generator,” Annual Report of ISTC Project #B-070-98 (Third Year), December 2001.

[**Kis2001**] G.V. Kiselev, “Options for Improvement Characteristics of Nuclear/Electric Installations,” Institute of Theoretical and Experimental Physics RF State Research and Engineering Center (GNTTs RF – ITEF), *Atomnaya Energiya (Atomic Energy)* **91**, No. 1, pp. 54-63, 2001.

[**Wan+2001**] J.S. Wan et al., “Transmutation of I-129 and Np-237 Using Spallation Neutrons Produced by 1.5-, 3.7-, and 7.4-GeV Protons,” Special Issue on Accelerator Driven Systems, H.S. Plendl, Ed., *Nuclear Instr. and Methods in Physics Research* **A463**, pp. 634-652, 2001.

2002

[**Chi+2002**] S. Chigrinov et al., “The Research on Accelerator Driven Systems at the NAS of Belarus,” Report IAEA-TM-25032, TWG-FR/108.-49, Vienna, Austria, 2002.

[**Mar+2002**] B.A. Martsinkevich et al., “Unfolding of Fast-neutron Spectra in Wide Energy Range (Up to 200 MeV) at Sub-critical Uranium-Lead Assembly of Electronuclear System (Energy Plus Transmutation),” Preprint P-2002-65, p. 20, Dubna, Russia, 2002.

2003

[**Dah2003**] M. Dahlfors, “Sensitivity to Nuclear Data and Neutron Source Type in Calculations of Transmutation Capabilities of the Energy Amplifier Demonstration Facility,” Licentiate Thesis, Department of Radiation Sciences, Uppsala, Sweden, May 2003.

[**KK2003**] V.F. Kolesov and V. Kh. Khorujnzhii, “Kinetics of Non-periodical Cascade Boosters in Terms of Their Speed and Safety,” *Atomnaya Energiya (Atomic Energy)* **94**, No. 2, pp. 99-109, 2003.

[**Sta2003**] Alexander Stanculescu, “International Status of Accelerator-Driven Systems for Advanced Nuclear Fuel Cycles,” Proceedings of the 14th Annual Conference of the Indian Nuclear Society: Fuel Cycle Technologies – Closing the Fuel Cycle, INSAC-2003, Indira Ghandi Centre for Atomic Research, Kalpakkam, India, 17-19 December 2003.

2004

[**Chi+2004-1**] S.E. Chigrinov et al., “The Research on Accelerator-Driven Systems at the National Academy of Sciences of Belarus,” Review of National Programmes on Fast Reactors and Accelerator-Driven Systems (ADS), Technical Working Group on Fast Reactors (TWG-FR), Vienna, Austria, 10-14 May 2004.

[**Chi+2004-2**] S.E. Chigrinov et al., “Booster Sub-critical Assembly Controlled by a Neutron Generator,” OIEYaI Preprint #14, Integrated Institute of Power Engineering and Nuclear Studies at Sosny, National Academy of Sciences, Minsk, Belarus, 2004 (in Russian).

[**Chi+2004-3**] S.E. Chigrinov et al., “Nuclear Facilities of the National Academy of Sciences of Belarus on the Basis of Highly Enriched Uranium,” The RERTR-2004 International Meeting on Reduced Enrichment for Research and Test Reactors, Vienna International Centre, Vienna, Austria, 7-12 November 2004.

2005

[**Bur+2005**] V.V. Burnos et al., “Features of Neutron Profile Formation in Systems Consisting of a Neutron-Generator Target and a Moderator Irradiated with High-Energy Particles,” Preprint OIEYaI-20, Integrated Institute of Power Engineering and Nuclear Research (OIEYaI), Minsk-Sosny, Belarus, 2005.

[**Chi+2005-1**] S. Chigrinov et al., “Booster (Cascade) Sub-critical Assembly,” 3rd SAD/YALINA Steering Committee Meeting, Dubna, Russia, 27-28 June, 2005.

[**Chi+2005-2**] S. Chigrinov et al., “Experimental and Theoretical Research on Transmutation of Long-lived Fission Products and Minor Actinides in a Sub-critical Assembly Driven by a Neutron Generator,” 2nd ECATS Feasibility Study Meeting, Brussels, Belgium, 20-21 April 2005.

[**Chi+2005-3**] S. Chigrinov et al., “Experimental and Theoretical Investigation of Transmutation of Long-lived Fission Products and Minor Actinides in a Sub-critical Assembly Driven by a Neutron Generator,” 26th Quarter Report, ISTC Project B-070-98, Minsk, Belarus (2005).

[**Kiy+2005**] H. Kiyavitskaya et al., “Experimental Investigations on the Sub-critical Assemblies of Joint Institute for Power and Nuclear Research – Sosny, National Academy of Sciences of Belarus, Workshop on Use of Low-enriched Uranium in Accelerator Driven Sub-critical Assemblies, Vienna, Austria, 10-12 October 2005.

[**Per2005**] Carl-Magnus Persson, “Reactivity Determination and Monte Carlo Simulation of the Sub-critical Reactor Experiment – YALINA,” Master of Science Thesis, Department of Nuclear and Reactor Physics, Royal Institute of Technology, Stockholm, Sweden, 2005.

[Per+2005-1] Carl-Magnus Persson et al., “Analysis of Reactivity Determination Methods in the Sub-critical Experiment Yalina,” *Nucl. Instr. and Methods in Phys. Research A* **544**, pp. 374-383, 2005.

[Per+2005-2] C.-M. Persson et al., “Comparison of Neutron Kinetic Parameters of the Sub-critical ADS Experiments Yalina and Yalina Booster,” 12th International Conference on Emerging Nuclear Energy Systems (ICENES’2005), Brussels, Belgium, August 21-26, on CD-ROM, SCK-CEN, Mol, Belgium, 2005.

2006

[Bur+2006] V.V. Burnos et al., “YALINA Sub-critical Test Bed for Neutron Generation and Experimental Studies in the Area of ADS Technology,” Preprint OIEYaI-24, Integrated Institute of Power Engineering and Nuclear Research (OIEYaI) – Sosny, Minsk-Sosny, Belarus, 2006.

[IAEA2006-1] IAEA Working Material: Research Coordinated Meeting of the Coordinated Research Project on “Analytical and Experimental Benchmark Analyses of Accelerator Driven Systems,” IAEA-RC-1003.1, December 5-9, 2005, TWG-FR/127, Vienna, Austria, 2006.

[IAEA2006-2] IAEA Working Material, Workshop Meeting of the Coordinated Research Project on “Low Enriched Uranium Fuel Utilization in Accelerator Driven Sub-critical Assembly Systems,” Vienna, Austria, November 6-9, 2006.

2007

[Bou+2007-1] V. Bournos et al., “YALINA Booster Benchmark Specifications for the IAEA Coordinated Research Projects on Analytical and Experimental Benchmark Analysis on Accelerator-Driven Systems and Low-Enriched Uranium Fuel Utilization in Accelerator Driven Sub-critical Assembly Systems,” IAEA CRP Document, 2007.

[Bou+2007-2] V. Bournos et al., “YALINA Thermal Benchmark Specifications for the IAEA Coordinated Research Projects on Analytical and Experimental Benchmark Analysis on Accelerator-Driven Systems and Low-enriched Uranium Fuel Utilization in Accelerator Driven Sub-critical Assembly Systems,” IAEA CRP Document, 2007.

[Bur+2007-3] V.V. Burnos et al., “Study of Applicability of the Pulse-Neutron Generator Method for Controlling Variation of Reactivity of Deeply Sub-critical Systems Controlled by Accelerators (ADS) Based on the Booster Sub-critical Assembly of YALINA Sub-critical Test Bed,” Preprint OIEYaI-28, Integrated Institute of Power Engineering and Nuclear Research (OIEYaI) – Minsk-Sosny, Belarus, 2007.

[Goh+2007] Y. Gohar et al., “YALINA Analyses”, Presentation at the Technical YALINA Booster Meeting with YALINA staff, Minsk, Belarus, October 24-26, 2007.

[Kiy+2007] H. Kiyavitskaya et al., “Analytical and Experimental Benchmark Analysis on Accelerator Driven Systems and Low Enriched Uranium Fuel Utilization in Accelerator Driven Sub-critical Assembly Systems,” Report on Contract No. BC:5380.170.3505.D02030231.ADS20074129113389/R1, JIPNR-SOSNY, October 2007.

[**Per2007-1**] Carl-Magnus Persson, “Reactivity Assessment in Sub-critical Systems,” Licentiate Thesis in Physics, Stockholm, Sweden, 2007.

[**Per2007-2**] C.-M. Persson et al., “Neutron Kinetic Characterisation of the Sub-critical ADS Experiment YALINA Booster”, submitted for publication in *Annals of Nuclear Energy*, March 2007.

2008

[**TG2008**] Alberto Talamo and Yousry Gohar, “Monte Carlo Modeling and Analyses of YALINA Booster Sub-critical Assembly – Part I: Analytical Models and Main Neutronics Parameters,” Report ANL-NE-08/13, Argonne National Laboratory, March 2008.

[**Tal+2008**] Alberto Talamo et al., “Monte Carlo Analyses of the Source Multiplication Factor of the YALINA Booster Facility,” PHYSOR-2008: International Conference on the Physics of Nuclear Reactors – Nuclear Power: A Sustainable Resource, Casino-Kursall Conference Center, Interlaken, Switzerland, 14-19 September 2008.

Appendix A

Belarusian Scientists

A list of Belarusian scientists who have been involved with the YALINA project at one point or another since its inception in 1997 is provided in this appendix. The leader of this project during most of these years is indicated separately.

YALINA Project Manager:

Anna I. Kiyavitskaya

Scientific Investigators:

Alexander A. Adamovich

Victor V. Bournos

V.S. Burtsev

Serguej Chigrinov

A. Fokov

Yurij G. Fokov

Oleg I. Jaroshevich

Anatolij M. Khilmanovich

Mikhail K. Kievec

Tamara N. Korbut

Sergei V. Korneev

Alla V. Koulikovskaya

Boris A. Martsinkevich

Sergei E. Mazanik

Igor L. Rakhno

Christina C. Routkovskaia

Ivan G. Serafimovich

Natalia V. Voropaj

O.I. Yaroshevich

Igor V. Zhouk

Appendix B

Foreign Scientists

A list of foreign (non-Belarusian) scientists (including the United States) who have been involved with the YALINA project at one point or another since its inception in 1997 is provided in this appendix.

H. Ait Abderrahim (SCK-CEN, Mol, Belgium)
Alexandra Åhlander (RIT, Stockholm, Sweden)
C.H.M. Broeders (FZK, Karlsruhe, Germany)
Igor Bolshinsky (NNSA, DOE, Washington, DC, United States of America)
V.S. Butsev (JINR, Dubna, Russia)
Yousry Gohar (ANL, Argonne, IL, United States of America)
E. Gonzales-Romero (CIEMAT, Madrid, Spain)
W. Gudowski (RIT, Stockholm, Sweden)
Y. Kadi (CERN, Geneva, Switzerland)
G. Kessler (FZK, Karlsruhe, Germany)
E. Kiefhaber (FZK, Karlsruhe, Germany)
A. Kolros (Czech Technical University, Prague, Czech Republic)
Filip Kondev (ANL, Argonne, IL, United States of America)
G. Kulikov (ISTC, Moscow, Russia)
Carl-Magnus Persson (RIT, Stockholm, Sweden)
Per Seltborg (RIT, Stockholm, Sweden)
Alexander Stanculescu (IAEA, Vienna, Austria)
Thomas Stummer (Vienna University of Technology, Vienna, Austria)
Hiroshi Takahashi (BNL, Upton, NY, United States of America)
Alberto Talamo (ANL, Argonne, IL, United States of America)
M. Tesinsky (Czech Technical University, Prague, Czech Republic)

Appendix C

Participating Organizations

A list of Belarusian and foreign organizations (including the United States) that have been involved with the YALINA project at one point or another since its inception in 1997 is provided in this appendix.

Belarusian Organizations:

- Joint Institute for Power and Nuclear Research (formerly known as The Radiation Physics and Chemistry Problems Institute), National Academy of Sciences of Belarus, Minsk-Sosny
- Institute of Physics, National Academy of Sciences, Minsk-Sosny.

Foreign Organizations (including the United States):

- Belgian Nuclear Reactor Research Center (SCK-CEN), Mol, Belgium.
- Department of Nuclear and Reactor Physics, Royal Institute of Technology, Stockholm, Sweden.
- Institute for Reactor Safety, Forschungszentrum Karlsruhe, Karlsruhe, Germany.
- Vienna University of Technology, Vienna, Austria.
- Nuclear Engineering Division, Argonne National Laboratory, Argonne, IL, United States of America.
- International Science and Technology Center, Moscow, Russia
- Department of Nuclear Energy, International Atomic Energy Agency, Vienna, Austria.
- Joint Institute for Nuclear Research, Dubna, Russia.
- Department of Nuclear Reactors, Faculty of Nuclear Sciences and Physical Engineering, Czech Technical University, Prague, Czech Republic.

Appendix D

YALINA Thermal Benchmark Specifications

The basic design concept and operating procedures of the YALINA Thermal (YALINA-T) sub-critical assembly are discussed in general terms in Chapter VIII so they will not be repeated here. This appendix is devoted to documenting the essential information needed to provide the input for Monte Carlo and deterministic codes used to simulate the performance of this facility, and to establish an orderly procedure for inter-comparing results from various laboratories participating in the IAEA CRP that began in 2005, including Argonne National Laboratory (see Chapter V). This is clearly very important, otherwise meaningful comparisons cannot be made between the results that are generated using different computational methods and nuclear databases, and that are produced by various institutes. It is also a requirement in order to be able to perform meaningful comparisons of these calculations with experimental data. The material presented here includes the exact layout of three thermal core configurations commonly considered in these calculations, including precise dimensions, material compositions, and suggested analytical tasks. The content of this appendix consists of a major portion of a 2007 report listed in the References and Publications section of the present report. The material presented in this appendix is edited from the original document to conform to the format and style of the present report. Also, some of the introductory information in the earlier report has been omitted to avoid redundancy with the main body of the present report.

The sub-critical assembly consists of uranium-dioxide nuclear fuel rods and polyethylene moderator material. It is surrounded by a graphite reflector in the radial direction. These fuel rods are arranged horizontally. The front side of the assembly opposite to the beam entrance is covered by borated polyethylene. The back side of the assembly, where the deuteron beam tube enters, is covered by an organic glass sheet. There are three axial experimental channels (parallel to the fuel rods) in the fuel zone (EC1, EC2, and EC3), one axial experimental channel (EC4) in the target zone, two axial experimental channels (EC5, EC6) in the reflector, and one radial experimental channel (EC7) in the reflector zone at the fuel mid-plane. The experimental channels are shown in Fig. D.1 and further details are provided in Table D.1.

Three different fuel loadings were selected for defining the YALINA Thermal benchmark. These loadings have 216, 245 and 280 EK-10 fuel rods, respectively, and the corresponding ^{235}U masses were 1.67, 1.89, and 2.16 kg, respectively. These fuel loading configurations are shown in Figs. D.2, D.3, and D.4. The recommended benchmark calculations chosen for inter-comparisons between various participating institutes in the IAEA CRP for each configuration were specified as follows (taken directly from the original report, except that the indicated table and figure numbers refer to the present report):

Recommended Benchmark Calculations

1. Axial distribution of the following reaction rates:
 - a. $^3\text{He}(n,p)$ reaction rate in EC1, EC2, and EC3 experimental channels, normalized to one external source neutron and one ^3He atom. The reaction values are calculated using the average neutron flux, $\phi(E)$, in the cylindrical cells specified in Figure D.11 from $z = -250$ mm to $z = 250$ mm in steps of 50 mm. The detector is not modeled in the calculation.
 - b. $^{235}\text{U}(n,f)$ reaction rate in EC1, EC2, and EC3 experimental channels, normalized to one external source neutron and one ^{235}U atom. In all the channels, the reaction rate values are

calculated using the average neutron flux, $\phi(E)$ in the cylindrical cells specified in Figure D.11, from $z = -250$ mm to $z = 250$ mm in steps of 50 mm. The ^{235}U material is not modeled in the calculation.

- c. $^{115}\text{In}(n,\gamma)$ reaction rate in EC2 experimental channel, normalized to one external source neutron and one ^{115}In atom. Values are to be calculated in the ^{115}In samples located from $z = -242$ mm to $z = 208$ mm in steps of 50 mm. The ^{115}In samples are to be simulated together with their polyethylene holder, as shown in Figure D.13, without loading any other isotopes in the holder.
2. Radial distribution of the $^{115}\text{In}(n,\gamma)$ reaction rate in the EC7 radial experimental channel for the radial distances of 200, 250, 300, 350, 400, 450, 500, 550 and 600 mm. All reaction rate values are normalized to one source neutron and one ^{115}In atom. The samples are simulated together with their polyethylene holder, as described in Figure D.13.
3. $^{197}\text{Au}(n,\gamma)$ and $^{55}\text{Mn}(n,\gamma)$ reaction rates in EC2 experimental channel, normalized to one external source neutron and one isotope atom. The samples are to be simulated together with its sample holder, as done in the task 1-C. The isotope loading distribution is shown in Figure D.12. The calculation has to be performed with the holder containing only ^{197}Au or ^{55}Mn .
4. The neutron energy spectra in the EC1, EC2, EC3, EC5, and EC6 experimental channels are calculated at $z=0$ in 172 energy groups structure given in Table D.2. The integral of the neutron spectrum should equal unity.
$$\int \phi(E)dE = 1.$$
5. The neutron flux is calculated as function of time after a neutron pulse insertion. The pulse duration is 5 μs of D-D or D-T neutrons at $z=0$. The neutron flux calculations are performed for a period of 20 ms with two different detectors:
 - a. $^3\text{He}(n,p)$ detector in the EC2 and EC5 experimental channels without modeling the detector in the calculation. The results should be normalized to the maximum value in EC2 experimental channel.
 - b. $^{235}\text{U}(n,f)$ detector in the EC1 experimental channels without modeling the detector in the calculation. The results should be normalized to the maximum value in EC1B experimental channel. The calculations are to be done with 10 μs time bin from 0 to 1 ms and with 100 μs time bin from 1 ms to 20 ms.
6. Kinetic parameters for the three configurations:
 - a. Effective multiplication factor, k_{eff} .
 - b. Source multiplication factor, k_s .
 - c. Mean neutron generation time, Λ .
 - d. Prompt neutron lifetime, l_p , and mean neutron lifetime, l .
 - e. Effective delayed neutron fraction, β_{eff} .

In addition, the participants in the inter-comparison exercises were requested to define the computer code(s), nuclear data libraries, etc., that were used. The following information was also requested:

1. Author(s) of the solutions with affiliation.
2. Name and version of the code used with bibliographic references.
3. Name of the nuclear data library(ies) that have been used with a description of preprocessing or changes made.
4. Description of any geometrical model approximations.

5. Description of the computational methods used for calculating the kinetic parameters k_s , Λ , l_p , l and β_{eff} .
6. Statistical error bars for the Monte Carlo results.

The participants were also requested to use a standardized Excel spreadsheet for reporting their results to facilitate the compilation and comparison of the results.

YALINA Thermal Assembly Design

The sub-critical assembly of the YALINA Thermal facility is made of rectangular parallelepiped sections, as shown in Fig. D.1. The central axis of the assembly is aligned horizontally. The neutron producing target can be situated along the central axis at different distances from the assembly center. A general view of the assembly is shown in Fig. D.6.

Lead Target

An X-Y cross section of the assembly is shown in Fig. D.1. There is a hole with side dimensions of 80×80 mm in the assembly center within a stainless steel frame. A lead zone consisting of 12 blocks in the axial direction, each with x-y dimensions of 78×78 mm and total target length of 576 mm can fit inside the hole. When the deuteron beam is used for generating neutrons, a part of the hole is occupied by the beam tube, as shown in Figs. D.9 and D.10.

Core Assembly

The core consists of 20 polyethylene subassemblies, and the length of the assembly is 576 mm. Each assembly consists of twelve blocks arranged axially. The block dimensions are 80×80×48 mm. The polyethylene material density is 0.923 g/cm³. Each subassembly has 16 holes for loading 16 EK-10 fuel rods. The holes are arranged in a square lattice with 20-mm spacing, as shown in Fig. D.7. The 20-mm lattice dimension is the optimum configuration for neutron multiplication using the EK-10 fuel with polyethylene moderator in a square lattice. The EK-10 fuel rod details are shown in Fig. D.8. The outer diameter of the EK-10 fuel-rod cladding is 10 mm and the inner diameter is 7 mm. The active fuel length is 500 mm and the average amount of ²³⁵U is 7.73 g per rod. The total rod length is 590 mm.

The three experimental channels, EC1, EC2, and EC3 are embedded in the fuel zone. The experimental channel EC4 is located inside the lead-target zone. The fuel zone is surrounded in the radial direction by a graphite reflector. The reflector dimensions are shown in Figs. D.1, D.9, and D.10. There are two axial experimental channels, EC5 and EC6 and one radial experimental channel, EC7 in the graphite reflector. Borated polyethylene blocks are used on the front section of the fuel zone and organic glass sheet is used on the backside of the assembly and the front section of the graphite reflector, as shown in Figs. D.9 and D.10.

In the fuel zone, and close to the target boundary, it is possible to insert three small B₄C rods as is shown in Figs. D.1 to D.5. During the operation these rods are not inserted and, consequently, the holes are filled with air. The diameter of each hole is 11 mm with duraluminum liner. The liner thickness is 0.5 mm. The main parameters of the YALINA-Thermal sub-critical assembly are given in Table D.3.

Geometrical Cross Sections

Simplified X-Z and Y-Z cross sections views are provided in Figs. D.9 and D.10 to help in understanding and generating the calculation models. The detailed material compositions are given in Table D.4.

The Deuteron-Beam Tube

The design details of the deuteron beam tube are shown in Fig. D.14. The material composition is given Table D.4.

Detectors

The experimental measurements used three detectors: a ^3He -detector and two different ^{235}U fission chambers. The detectors are described briefly here. However, their modeling in the calculations can be left out in order to avoid unnecessary difficulties.

The ^3He -detector

The ^3He detector is fabricated by CANBERRA and its model number is 05NHI/IK. The filling gas consists of 8 bar ^3He and 2 bar Kr. The gas-chamber length and diameter are 10 and 9 mm, respectively. The wall thickness of the gas chamber is 0.5 mm and it is made of Ni (73%) and Cu (27%) alloy.

The ^{235}U fission chambers

Two types of ^{235}U fission chambers are used for the experimental measurements, denoted as KHT-5 and KHT-31. They have different sizes and sensitivity. The main parameters of these detectors are given in Table D.5.

..... Tables and figures for Appendix D begin on the following page

Table D.1: List of the experimental channels

Experimental Channels in YALINA-T			
Name	Location	Orientation	Diameter, mm
EC1	Core	Axial	24
EC2	Core	Axial	24
EC3	Core	Axial	24
EC4	Target hole	Axial	11
EC5	Reflector	Axial	24
EC6	Reflector	Axial	24
EC7	Reflector	Radial	24
MC1	Core	Axial	55
MC2	Core	Axial	55
MC3	Core	Axial	55
MC4	Core	Axial	55

Table D.2: Upper boundaries for the 172 neutron-energy groups

Gr.	En. [MeV]	Gr.	En. [MeV]	Gr.	En. [MeV]	Gr.	En. [MeV]
1	1.96403E+01	44	1.50344E-02	87	8.31529E-06	130	9.10000E-07
2	1.73325E+01	45	1.11378E-02	88	7.52398E-06	131	8.60000E-07
3	1.49182E+01	46	9.11882E-03	89	6.16012E-06	132	8.50000E-07
4	1.38403E+01	47	7.46586E-03	90	5.34643E-06	133	7.90000E-07
5	1.16183E+01	48	5.53084E-03	91	5.04348E-06	134	7.80000E-07
6	1.00000E+01	49	5.00451E-03	92	4.12925E-06	135	7.05000E-07
7	8.18731E+00	50	3.52662E-03	93	4.00000E-06	136	6.25000E-07
8	6.70320E+00	51	3.35463E-03	94	3.38075E-06	137	5.40000E-07
9	6.06531E+00	52	2.24867E-03	95	3.30000E-06	138	5.00000E-07
10	5.48812E+00	53	2.03468E-03	96	2.76792E-06	139	4.85000E-07
11	4.49329E+00	54	1.50733E-03	97	2.72000E-06	140	4.33000E-07
12	3.67879E+00	55	1.43382E-03	98	2.60000E-06	141	4.00000E-07
13	3.01194E+00	56	1.23410E-03	99	2.55000E-06	142	3.91000E-07
14	2.46597E+00	57	1.01039E-03	100	2.36000E-06	143	3.50000E-07
15	2.23130E+00	58	9.14242E-04	101	2.13000E-06	144	3.20000E-07
16	2.01897E+00	59	7.48518E-04	102	2.10000E-06	145	3.14500E-07
17	1.65299E+00	60	6.77287E-04	103	2.02000E-06	146	3.00000E-07
18	1.35335E+00	61	4.53999E-04	104	1.93000E-06	147	2.80000E-07
19	1.22456E+00	62	3.71703E-04	105	1.84000E-06	148	2.48000E-07
20	1.10803E+00	63	3.04325E-04	106	1.75500E-06	149	2.20000E-07
21	1.00259E+00	64	2.03995E-04	107	1.67000E-06	150	1.89000E-07
22	9.07180E-01	65	1.48625E-04	108	1.59000E-06	151	1.80000E-07
23	8.20850E-01	66	1.36742E-04	109	1.50000E-06	152	1.60000E-07
24	6.08101E-01	67	9.16609E-05	110	1.47500E-06	153	1.40000E-07
25	5.50232E-01	68	7.56736E-05	111	1.44000E-06	154	1.34000E-07
26	4.97871E-01	69	6.79041E-05	112	1.37000E-06	155	1.15000E-07
27	4.50492E-01	70	5.55951E-05	113	1.33750E-06	156	1.00000E-07
28	4.07622E-01	71	5.15780E-05	114	1.30000E-06	157	9.50000E-08
29	3.01974E-01	72	4.82516E-05	115	1.23500E-06	158	8.00000E-08
30	2.73237E-01	73	4.55174E-05	116	1.17000E-06	159	7.70000E-08
31	2.47235E-01	74	4.01690E-05	117	1.15000E-06	160	6.70000E-08
32	1.83156E-01	75	3.72665E-05	118	1.12300E-06	161	5.80000E-08
33	1.22773E-01	76	3.37202E-05	119	1.11000E-06	162	5.00000E-08
34	1.11090E-01	77	3.05113E-05	120	1.09700E-06	163	4.20000E-08
35	8.22975E-02	78	2.76077E-05	121	1.07100E-06	164	3.50000E-08
36	6.73795E-02	79	2.49805E-05	122	1.04500E-06	165	3.00000E-08
37	5.51656E-02	80	2.26033E-05	123	1.03500E-06	166	2.50000E-08
38	4.08677E-02	81	1.94548E-05	124	1.02000E-06	167	2.00000E-08
39	3.69786E-02	82	1.59283E-05	125	9.96000E-07	168	1.50000E-08
40	2.92830E-02	83	1.37096E-05	126	9.86000E-07	169	1.00000E-08
41	2.73945E-02	84	1.12245E-05	127	9.72000E-07	170	6.90000E-09
42	2.47875E-02	85	9.90556E-06	128	9.50000E-07	171	5.00000E-09
43	1.66156E-02	86	9.18981E-06	129	9.30000E-07	172	3.00000E-09

Table D.3: Main parameters of the YALINA Thermal assembly.

Target Zone	
Material	Pb
Dimensions [mm]	78×78×645
Density [g/cm ³]	11.34
Fuel Zone	
Moderator block dimensions [mm]	80×80×576
Maximum number of fuel rods per block	16
Fuel rod pitch [mm]	20
Fuel material	UO ₂ + MgO
Fuel material density [g/cm ³]	5.042
Fuel enrichment	10%
Fuel material isotopic content, weight fractions:	
- ²³⁵ U	0.079691
- ²³⁸ U	0.728557
- ¹⁶ O	0.142022
- Mg	0.049730
Clad outer diameter [mm]	10
Cladding thickness [mm]	1.5
Cladding material	Aluminum alloy
Moderator	Polyethylene
Moderator density [g/cm ³]	0.923
Hole diameter [mm]	11
Number of experimental channels	4 (EC1 to EC4)
Experimental channels (EC1 to EC3) diameter [mm]	24
Experimental channel EC4 diameter [mm]	11
Graphite Radial Reflector	
Density [g/cm ³]	1.67
Thickness [mm]	310, 400, 526
Reflector Experimental channels	
Number of experimental channels:	3
- Axial channels	EC5, EC6
- axial channel diameter [mm]	24
- Radial channel	EC7
- radial channel diameter [mm]	24
Organic glass sheet	
Organic glass density [g/cm ³]	1.19
Organic glass thickness [mm]	4
Axial Shielding	
Material	Borated polyethylene
Density [g/cm ³]	0.983

Table D.4: YALINA Thermal material compositions.

Material	Composition	Weight fraction
Polyethylene density: 0.923 g/cm ³	C	0.85714000
	¹ H	0.14286000
Air density: 0.00129 g/cm ³	¹⁴ N	0.78850000
	¹⁶ O	0.21150000
Stainless steel alloy 12X18H10T density: 7.9 g/cm ³	C	0.00082000
	⁵⁰ Cr	0.00783052
	⁵² Cr	0.15685511
	⁵³ Cr	0.01812647
	⁵⁴ Cr	0.00458790
	⁵⁸ Ni	0.07842230
	⁶⁰ Ni	0.03124467
	⁶¹ Ni	0.00138111
	⁶² Ni	0.00446982
	⁶⁴ Ni	0.00118210
	Ti	0.00512500
	²⁸ Si	0.00029860
	²⁹ Si	0.00001570
	³⁰ Si	0.00001080
	⁵⁵ Mn	0.00800000
	S	0.00066300
	³¹ P	0.00086300
	⁶³ Cu	0.00132890
	⁶⁵ Cu	0.00061110
	⁵⁴ Fe	0.03763000
	⁵⁶ Fe	0.61196000
	⁵⁷ Fe	0.01439000
	⁵⁸ Fe	0.00193000
	²⁷ Al	0.00038800
	⁷⁵ As	0.00045400
	Ca	0.00012500
	Mg	0.00001300
	Mo	0.00157500
	²⁰⁴ Pb	0.00007063
	²⁰⁶ Pb	0.00121582
	²⁰⁷ Pb	0.00112093
	²⁰⁸ Pb	0.00267062
	Sb	0.00367500
	Zn	0.00094100
Lead (target) density: 11.34 g/cm ³	²⁰⁴ Pb	0.01390573
	²⁰⁶ Pb	0.23937727
	²⁰⁷ Pb	0.22069516
	²⁰⁸ Pb	0.52580513
	⁵⁴ Fe	0.00000035
	⁵⁶ Fe	0.00000570
	⁵⁷ Fe	0.00000013
	⁵⁸ Fe	0.00000002

	¹⁰⁷ Ag	0.00000337
	¹⁰⁹ Ag	0.00000313
	²⁰⁹ Bi	0.00010640
	Ca	0.00000410
	⁶³ Cu	0.00000432
	⁶⁵ Cu	0.00000198
	Mg	0.00000290
	²³ Na	0.00001740
	Sb	0.00006440
	Zn	0.00000250
Low carbon steel (alloy Fe360-B) density: 7.8 g/cm ³	C	0.00140000
	⁵⁰ Cr	0.0000418
	⁵² Cr	0.0008380
	⁵³ Cr	0.0000968
	⁵⁴ Cr	0.0000245
	⁵⁸ Ni	0.0000672
	⁶⁰ Ni	0.0000268
	⁶¹ Ni	0.0000012
	⁶² Ni	0.0000038
	⁶⁴ Ni	0.0000010
	²⁸ Si	0.0004594
	²⁹ Si	0.0000241
	³⁰ Si	0.0000165
	⁵⁵ Mn	0.0040000
	S	0.0001000
	³¹ P	0.0001000
	⁶³ Cu	0.0000685
	⁶⁵ Cu	0.0000315
	⁵⁴ Fe	0.0560858
	⁵⁶ Fe	0.9122159
	⁵⁷ Fe	0.0214543
	⁵⁸ Fe	0.0028833
	¹⁴ N	0.0000100
	⁷⁵ As	0.0000500
Boron carbide density: 1.38 g/cm ³	¹⁰ B	0.1442400
	¹¹ B	0.6385400
	C	0.2172200
UO ₂ +MgO for Core (10% enrichment) density: 5.042 g/cm ³	²³⁵ U	0.0796910
	²³⁸ U	0.7285570
	¹⁶ O	0.1420220
	Mg	0.0497300
Aluminum alloy (CAB1) density: 2.7 g/cm ³	Mg	0.00004000
	²⁸ Si	0.00011025
	²⁹ Si	0.00000578
	³⁰ Si	0.00000397
	⁵⁴ Fe	0.00002882
	⁵⁶ Fe	0.00046868
	⁵⁷ Fe	0.00001102
	⁵⁸ Fe	0.00000148
	⁶³ Cu	0.00006850

	⁶⁵ Cu	0.00003150
	⁵⁵ Mn	0.00001000
	Zn	0.00009400
	Ti	0.00014100
	⁵⁸ Ni	0.00000269
	⁶⁰ Ni	0.00000107
	⁶¹ Ni	0.00000005
	⁶² Ni	0.00000015
	⁶⁴ Ni	0.00000004
	¹⁰ B	0.00000151
	¹¹ B	0.00000669
	S	0.00312000
	Ba	0.00000220
	Ca	0.0000393
	⁵⁰ Cr	0.00000019
	⁵² Cr	0.00000377
	⁵³ Cr	0.00000044
	⁵⁴ Cr	0.00000011
	²³ Na	0.00038000
	³¹ P	0.00013500
	²⁷ Al	0.99529179
Duraluminum alloy density: 2.7 g/cm ³	Mg	0.00050000
	²⁸ Si	0.00275620
	²⁹ Si	0.00014454
	³⁰ Si	0.00009926
	⁵⁴ Fe	0.00005650
	⁵⁶ Fe	0.00091898
	⁵⁷ Fe	0.00002161
	⁵⁸ Fe	0.00000290
	⁶³ Cu	0.00034250
	⁶⁵ Cu	0.00015750
	⁵⁵ Mn	0.00025000
	Zn	0.00050000
	Ti	0.00100000
	Al	0.99325000
Graphite density: 1.666 g/cm ³	C	1
Concrete density: 2.3 g/cm ³	¹ H	0.0028000
	C	0.0766000
	¹⁶ O	0.4454000
	S	0.0004000
	Mg	0.0006000
	Ti	0.0005000
	²⁷ Al	0.0032000
	²⁸ Si	0.3477000
	Ca	0.0470000
	¹⁴ N	0.0723000
	⁵⁶ Fe	0.0029000
	K	0.0006000
Borated polyethylene	C	0.8051000

density: 0.983 g/cm ³	¹ H ¹⁰ B ¹¹ B ¹⁶ O Ca ⁵⁶ Fe Pb	0.1364000 0.0015000 0.0064000 0.0351000 0.0128000 0.0026000 0.0001000
Water density: 1 g/cm ³	¹ H ¹⁶ O	0.1111110 0.8888890
Copper density: 8.96 g/cm ³	⁶³ Cu ⁶⁵ Cu	0.6850000 0.3150000
Vacuum density: 1.29E-9 g/cm ³	¹⁴ N ¹⁶ O	0.7885000 0.2115000
Organic glass density: 1.19 g/cm ³	C ¹ H ¹⁶ O	0.5998500 0.0805400 0.3196100
Cadmium sheet density: 8.65 g/cm ³	Cd	1.00
Cellular polystyrene (sintered) density: 0.05 g/cm ³	C ¹ H ¹⁴ N ¹⁶ O	0.04984600 0.00415400 0.44146700 0.50453300

Table D.5: Main parameters of fission chambers KHT-5 and KHT-31

Fission chamber type	Diameter, mm	Detector length, mm	Sensitive detector length, mm	Isotope	Sensitive area, cm ²	Sensitive layer, (mg/cm ²)	Filling gas
KHT-5	7	70	5	²³⁵ U	1	1	98% Ar + 2% N ₂
KHT-8	7	70	10	²³⁵ U	2	5	98% Ar + 2% N ₂

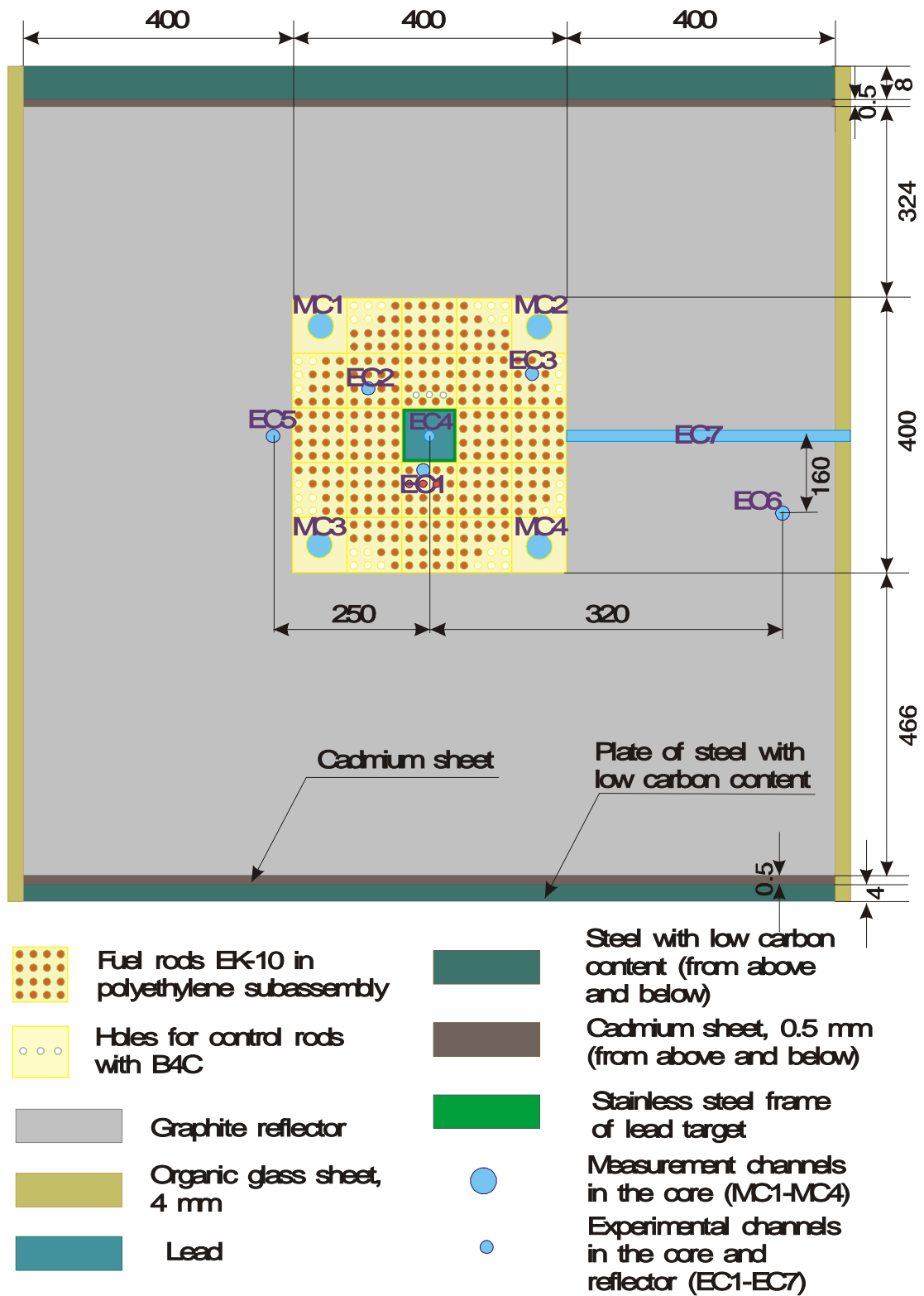


Figure D.1 : X-Y cross-section of the YALINA-T assembly, dimensions in mm ($65 \text{ mm} < Z < 280 \text{ mm}$).

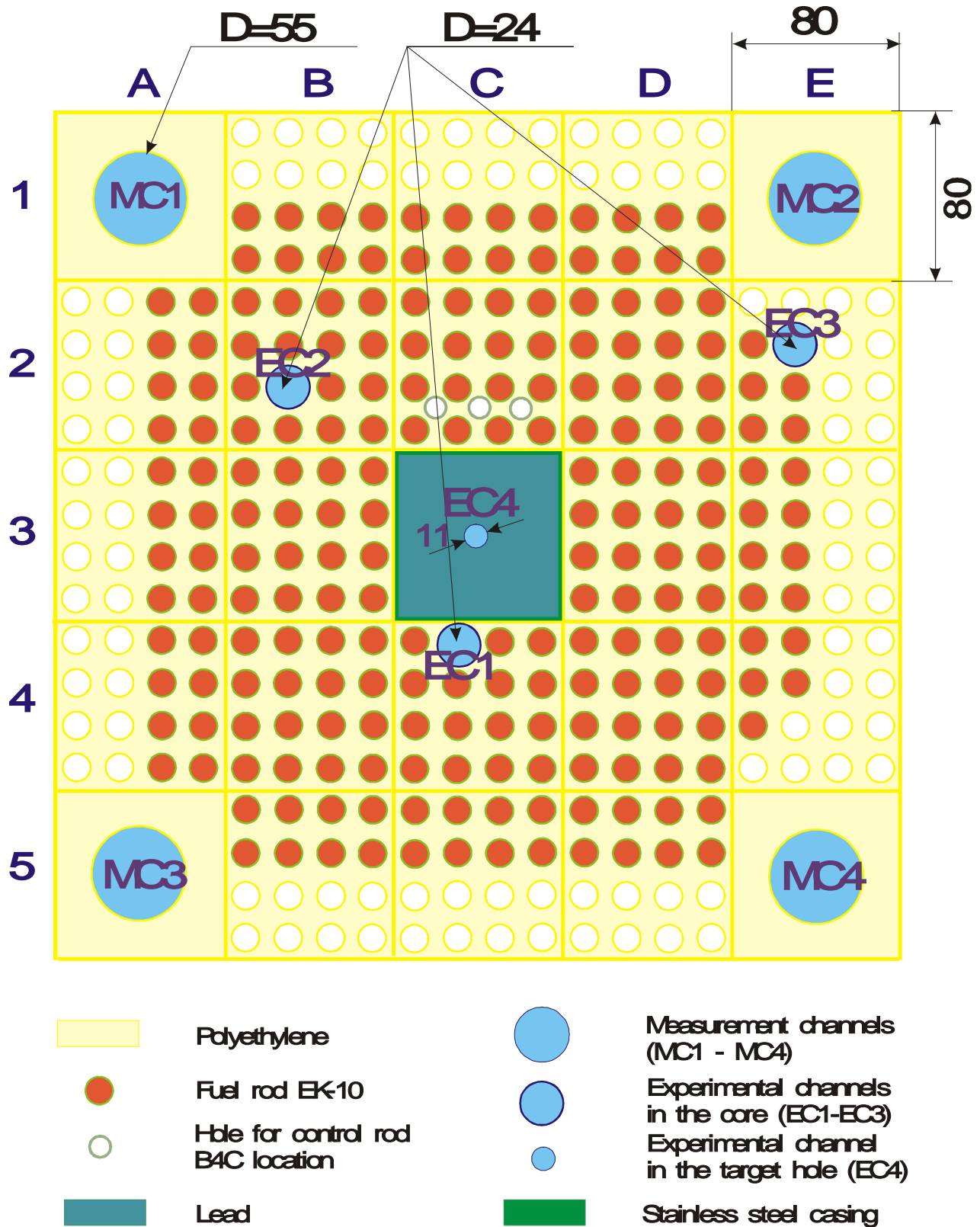


Figure D.2: X-Y cross-section of YALINA-Thermal core with 216 EK-10 fuel rods (65 mm < Z < 280 mm).

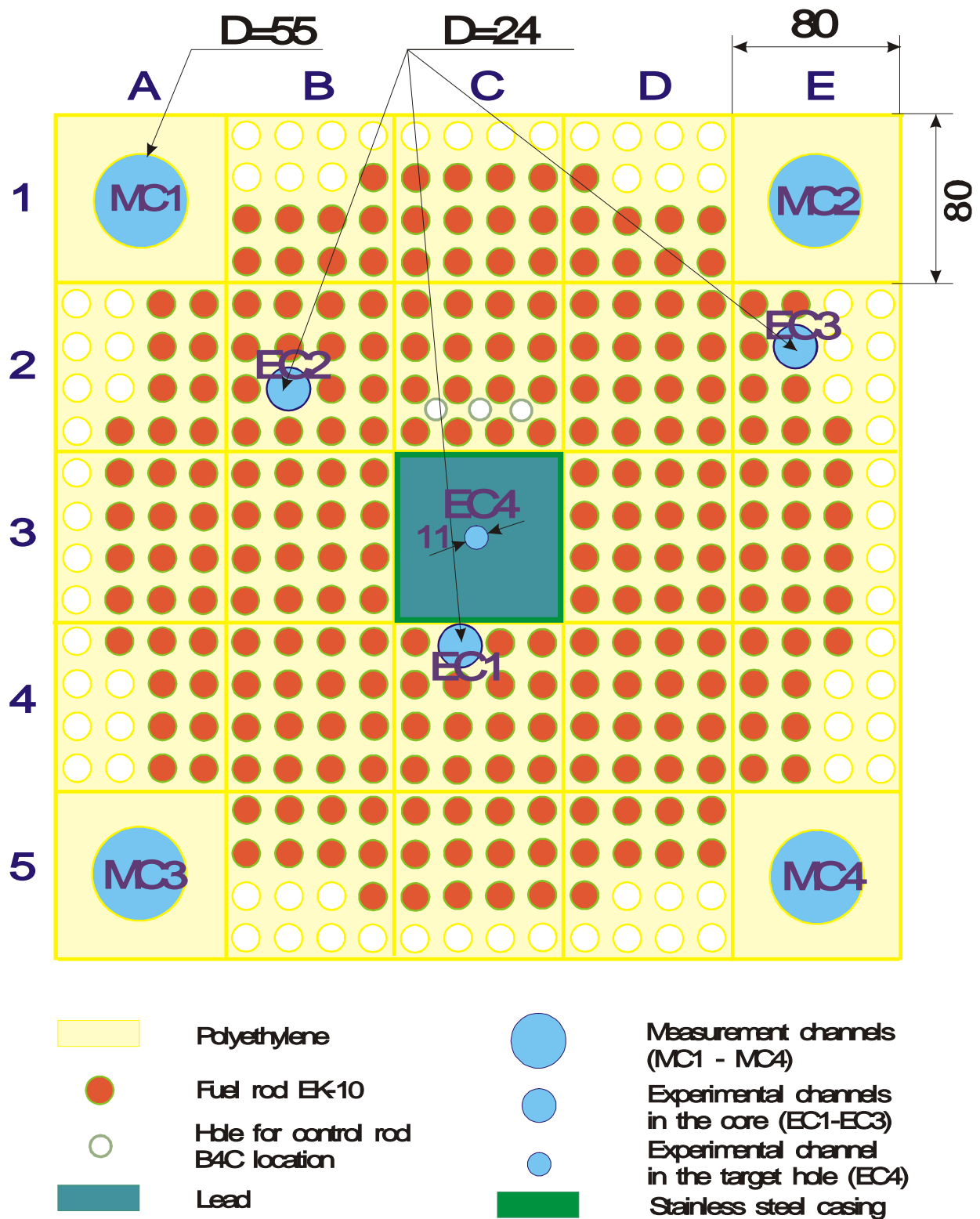


Figure D.3: X-Y cross-section of YALINA-Thermal core with 245 EK-10 fuel rods (65 mm <Z<280 mm).

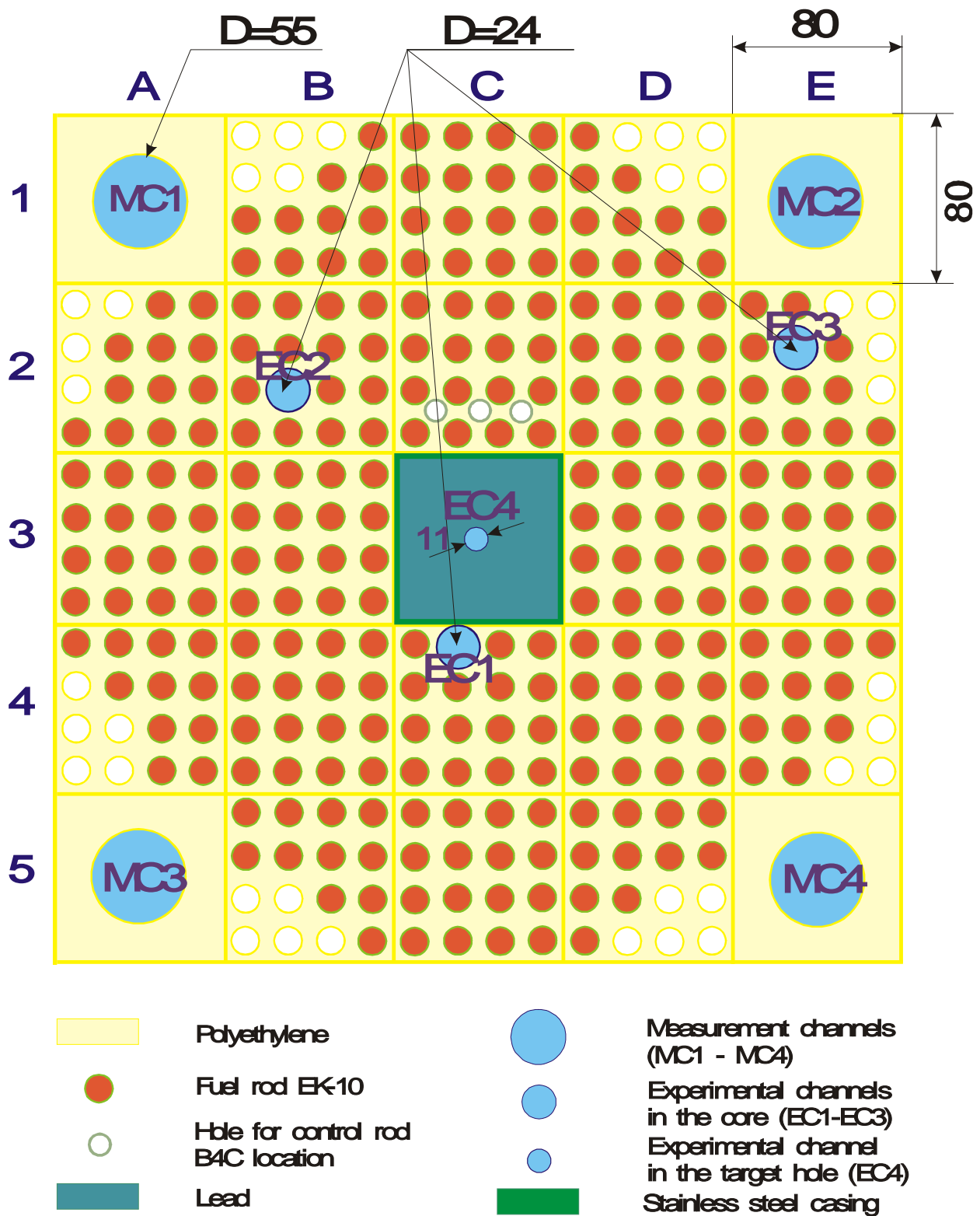
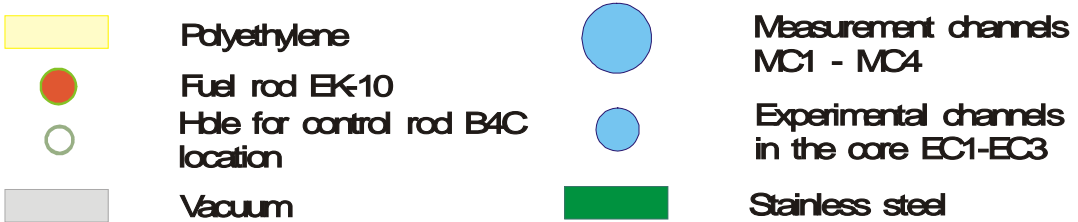


Figure D.4: X-Y cross-section of YALINA-Thermal core with 280 EK-10 fuel rods (65 mm < Z < 280 mm).



127

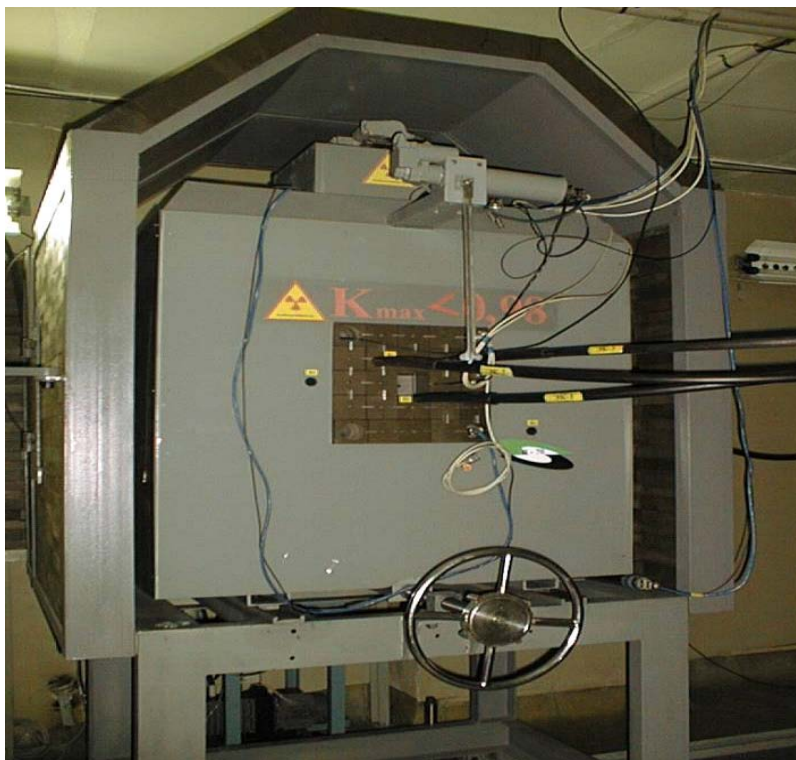


Figure D.6: General view of YALINA -Thermal assembly.

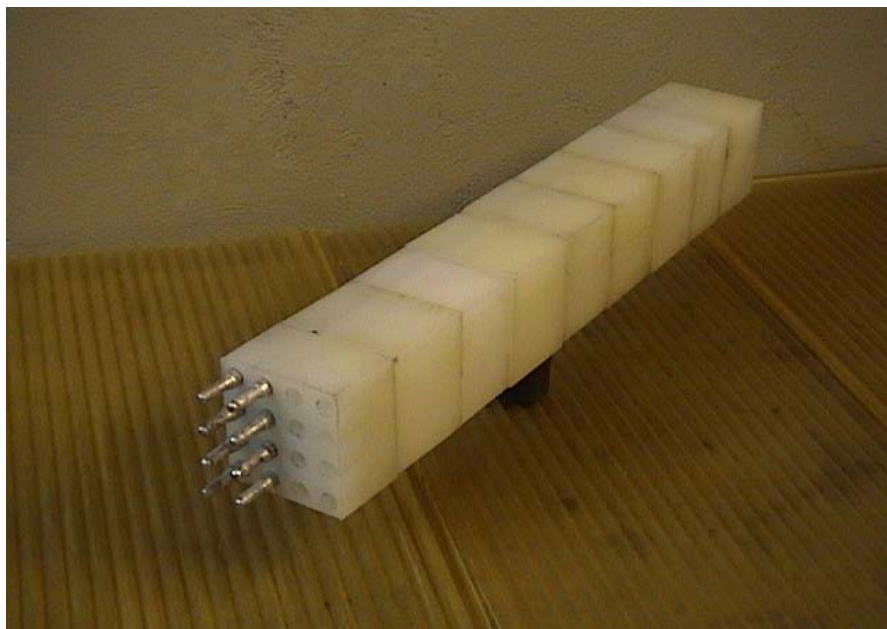


Figure D.7: Fuel sub-assembly

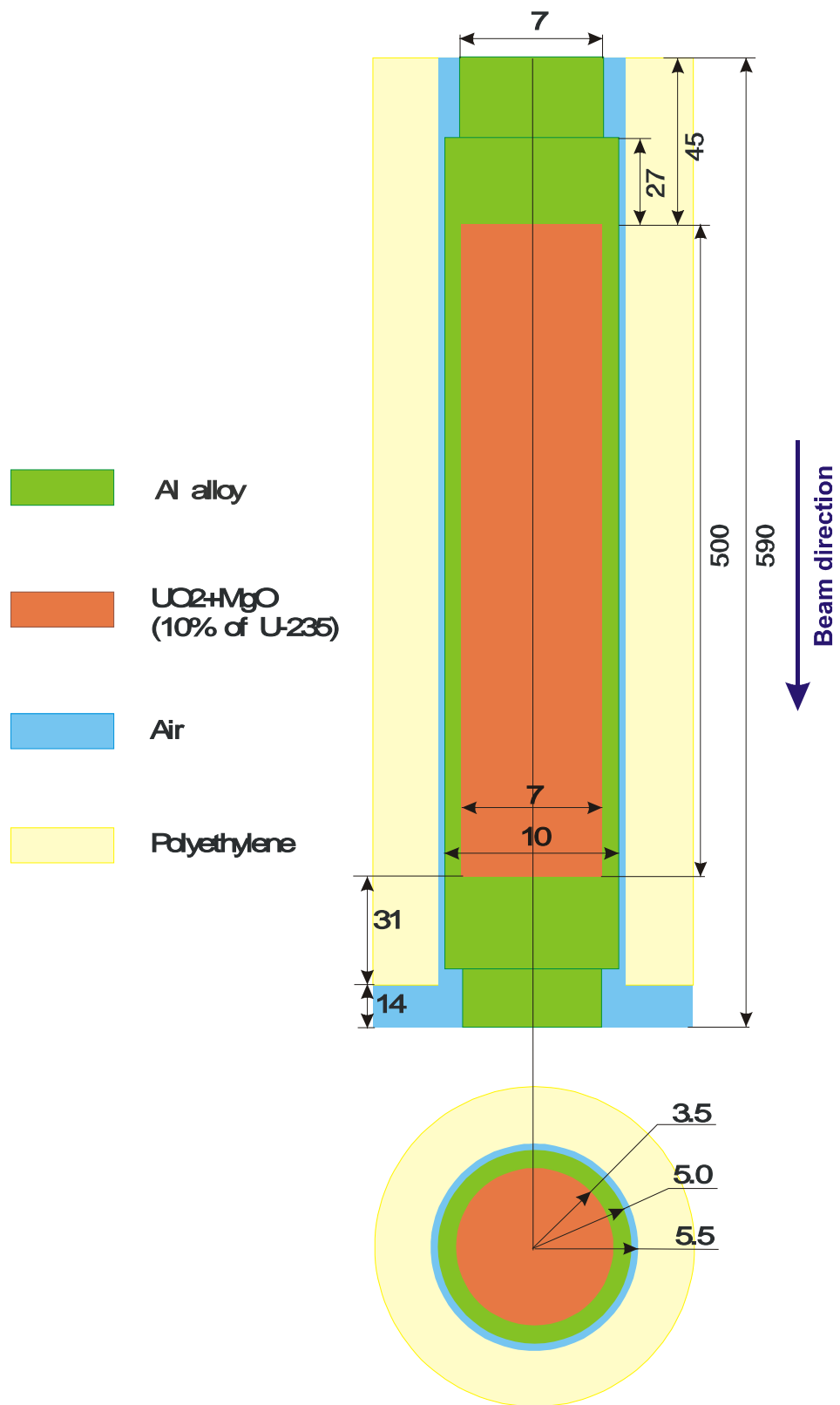


Figure D.8: X-Z and Z-Y cross-sections of the EK-10 fuel rod, dimensions in mm.

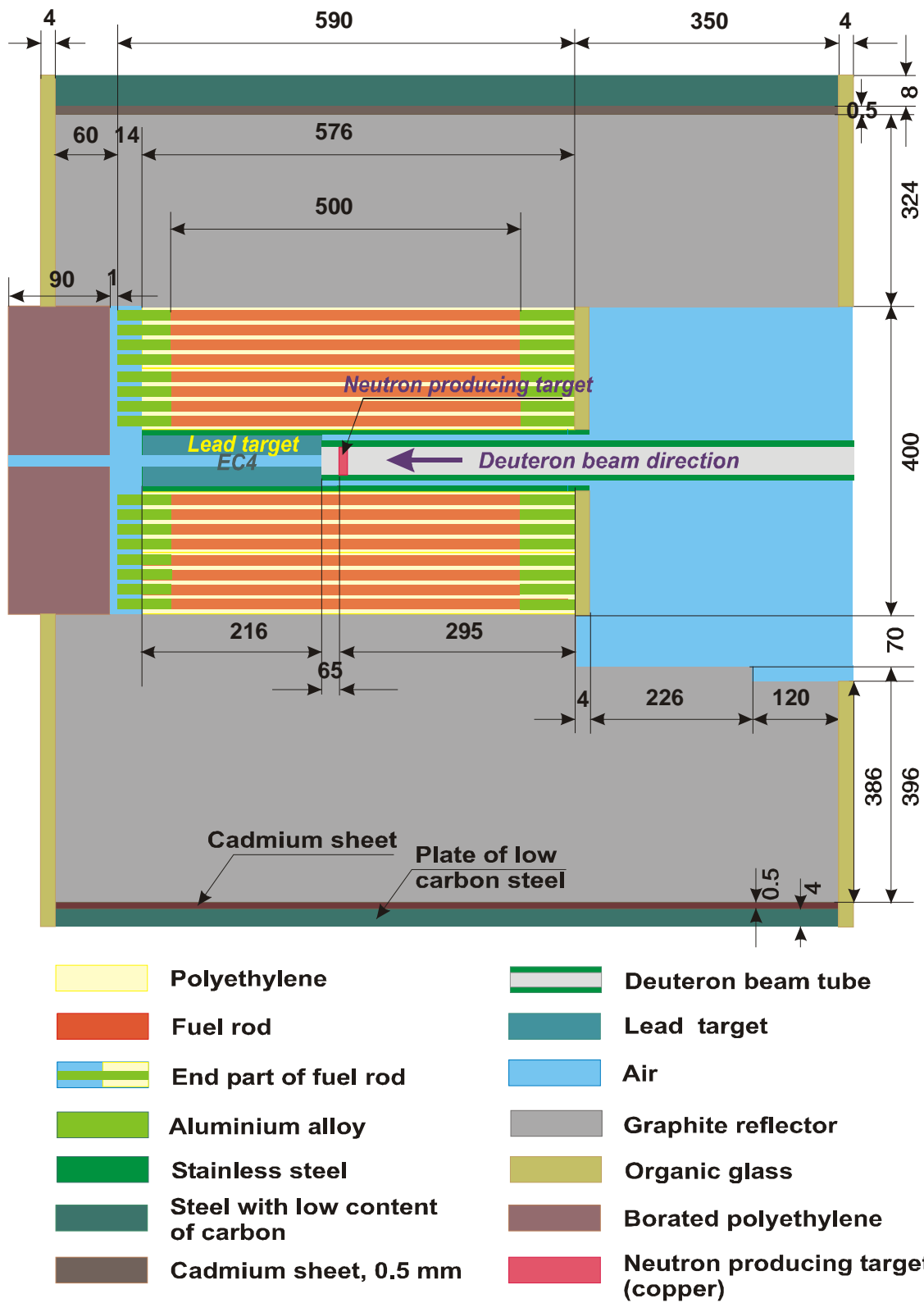


Figure D.9: X-Z cross-section of the YALINA Thermal assembly (Y=0), dimensions in mm.

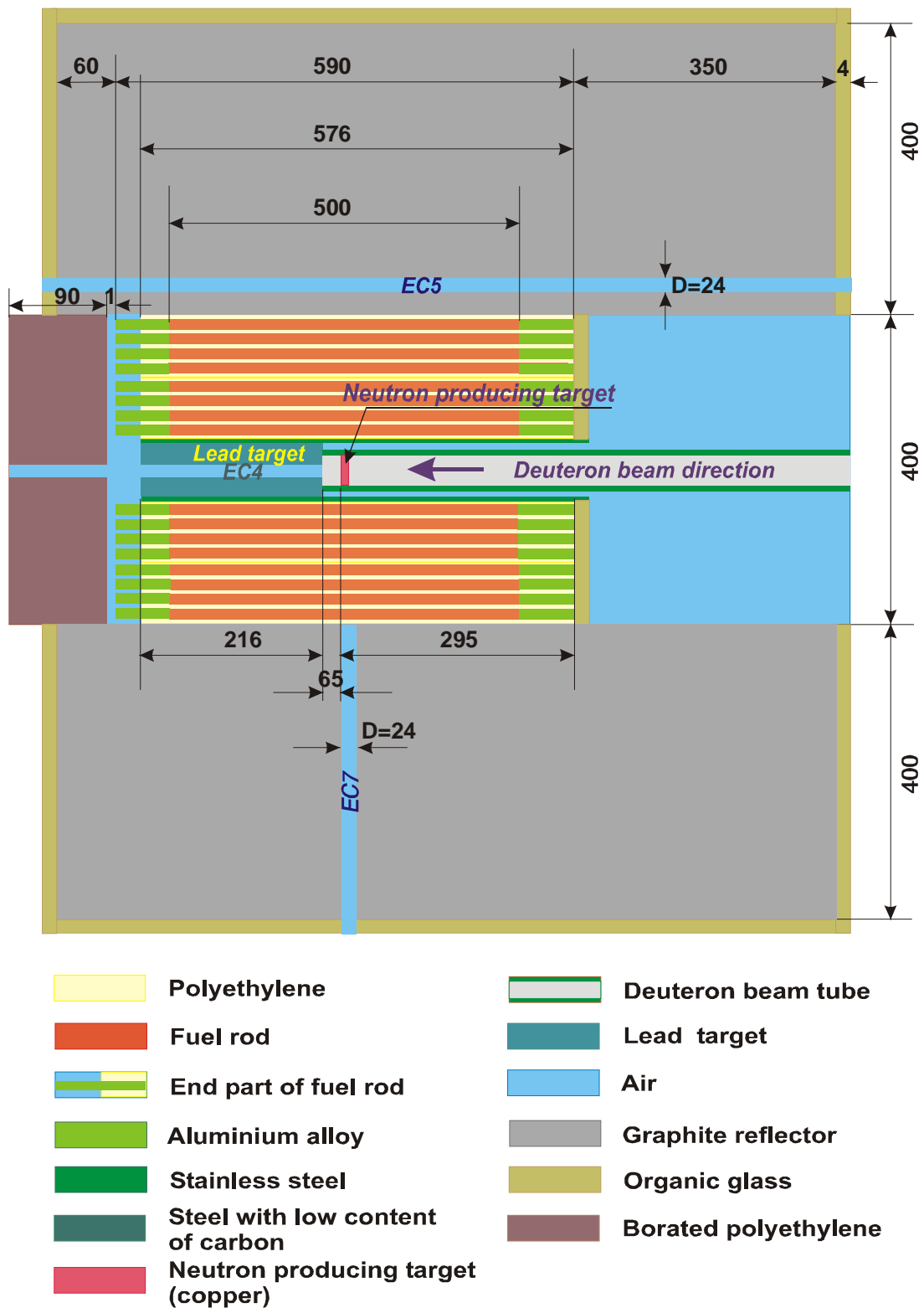


Figure D.10: Y-Z cross-section of the YALINA Thermal assembly (X=0), dimensions in mm.

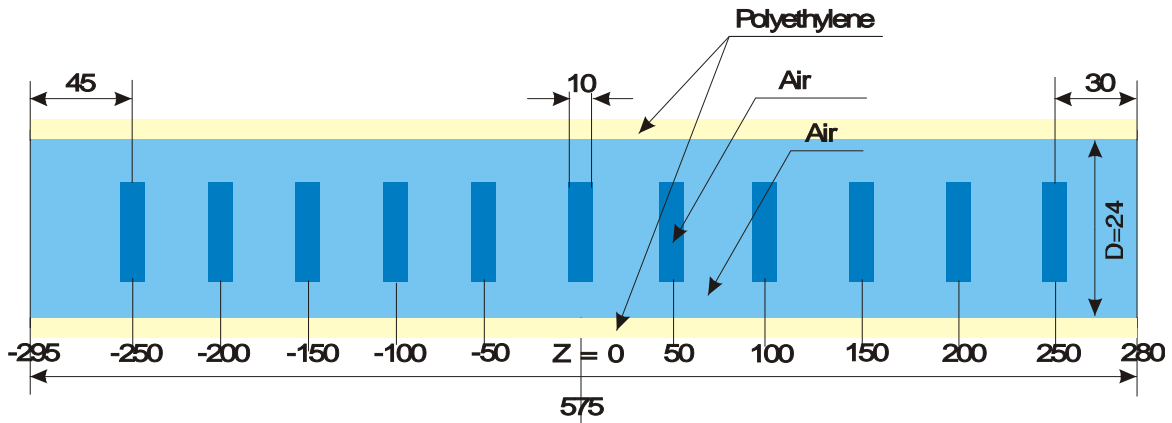


Figure D.11: Cylindrical air cells specified inside the experimental channels (EC1, EC2, and EC3) of the fuel zone and experimental channel (EC5) of the reflector zone for calculating the reaction rates of tasks 1a and 1b, dimensions in mm.

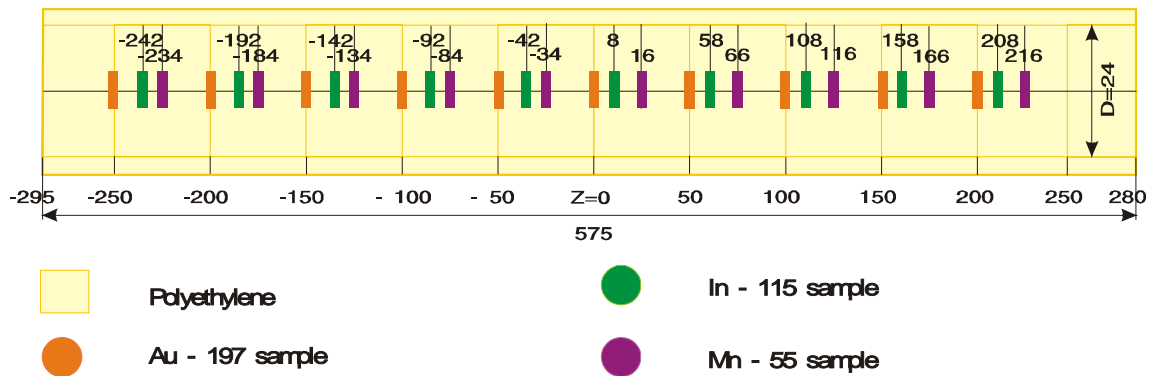


Figure D.12: Position of the ^{197}Au (thin sample, 10 mm diameter, mass 0.05 g), ^{115}In (10 mm diameter, 0.35 mm height, 0.202 g mass) and ^{55}Mn (10 mm diameter, g mass 0.1) samples in experimental channels EC1, EC2, and EC3, dimensions in mm.

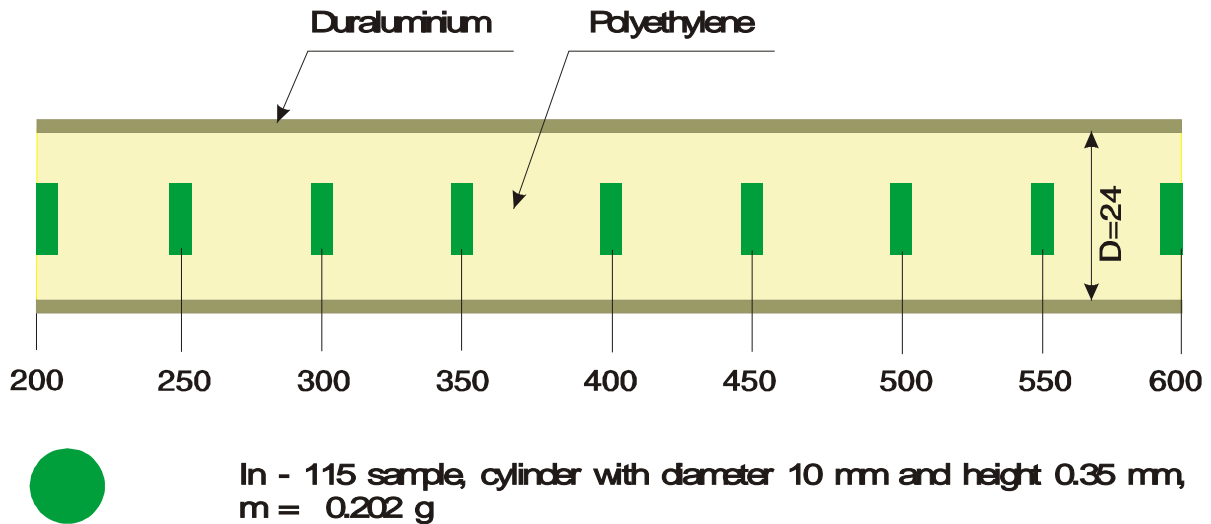


Figure D.13: Position of the ^{115}In samples in the EC7 experimental channel, dimensions in mm.

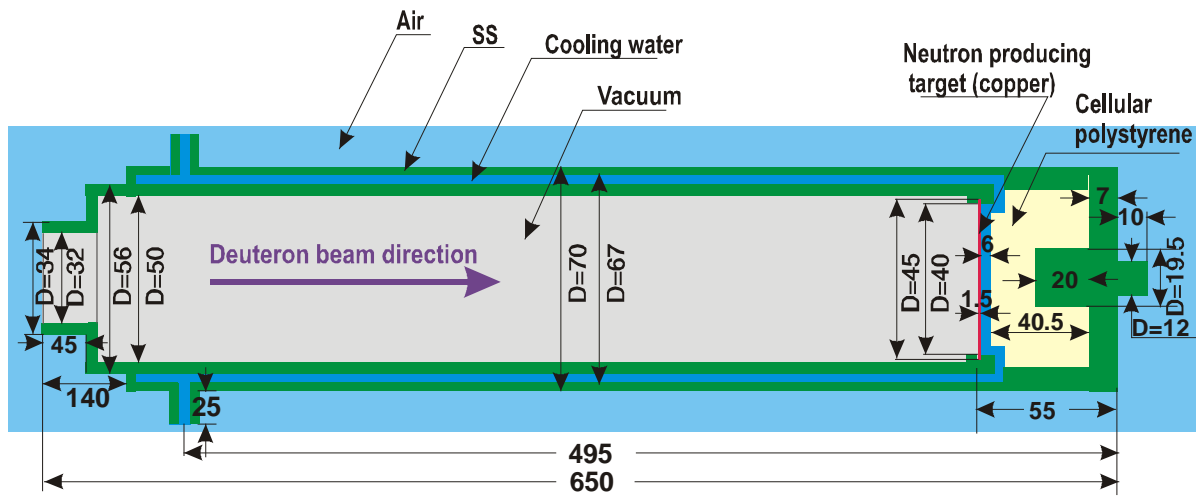


Figure D.14: Deuteron beam tube design, dimensions in mm.

Appendix E

YALINA Booster Benchmark Specifications

The basic design concept and operating procedures of the YALINA Booster (YALINA-B) sub-critical assembly are discussed in general terms in Chapter IX and won't be repeated here. This appendix is devoted to document the essential information needed to provide input for Monte Carlo and deterministic codes used to simulate the performance of this facility, and to establish an orderly procedure for inter-comparing results from various laboratories participating in the IAEA CRP, including Argonne National Laboratory (see Chapter V). This is clearly very important, otherwise meaningful comparisons cannot be made between the results that are produced using different computational methods and nuclear databases, and that are produced by various institutes. It is also a requirement in order to be able to perform meaningful comparisons of these calculations with experimental data. The material presented here includes the exact layout of two booster core configurations commonly considered in these calculations, including precise dimensions, material compositions, and suggested analytical tasks. The content of this appendix consists of a major portion of a 2007 report listed in the References and Publications section of the present report. The material presented in this appendix is edited from the original document to conform to the format and style of the present report. Also, some of the introductory information in the earlier report has been omitted to avoid redundancy with the main body of the present report.

The sub-critical assembly is surrounded radially by a graphite reflector and axially by borated polyethylene. The radial reflector and the backside of the thermal zone are covered by organic glass sheet. There are four axial experimental channels (EC1B, EC2B, EC3B, and EC4B) in the fast zone, three axial experimental channels in the thermal zone (EC5T, EC6T, and EC7T), two axial experimental channels in the reflector (EC8R, with the channel center 32 mm below the assembly mid-plane and 520 mm left of the assembly center line of Fig. E.1, and EC9R, with the channel center 356 mm below the assembly mid-plane and 600 mm right of the assembly center line of Fig. E.1), and one radial experimental channel in the reflector zone (EC10R). The experimental channels are shown in Fig. E.1 and a complete list is given in Table E.1.

Two sub-critical configurations are considered for the YALINA Booster benchmark. These configurations have different loadings in the thermal zone, 902 and 1141 EK-10 fuel rods, as shown in Figs. E.2 and E.3, respectively. In both configurations, the booster zone is fully loaded. The deuterons are assumed to impinge on the target located at the sub-critical assembly center. The recommended benchmark calculations chosen for inter-comparisons between various participating institutes in the IAEA CRP for each configuration were specified as follows (taken directly from the original report, except that the indicated table and figure numbers refer to the present report):

Recommended Benchmark Calculations

1. Axial distribution of the following reaction rates:
 - a. $^3\text{He}(n,p)$ in EC6T experimental channel, normalized to one external source neutron and one ^3He atom. The reaction values are calculated using the average neutron flux, $\phi(E)$, in the cylindrical cells specified in Fig. E.13 from $z = -250$ mm to $z = 250$ mm in steps of 50 mm. The detector is not modeled in the calculation.
 - b. $^{235}\text{U}(n,f)$ in the EC2B and EC6T experimental channels, normalized to one external source neutron and one ^{235}U atom. In both channels, the reaction values are calculated using the average neutron flux, $\phi(E)$, in the cylindrical cells specified in Figures E.13 and E.14,

respectively, from $z=-250$ mm to $z=250$ mm in steps of 50 mm. The ^{235}U material is not modeled in the calculation.

- c. $^{115}\text{In}(n,\gamma)$ in the EC2B, EC5T, EC6T, and EC7T experimental channels, normalized to one external source neutron and one ^{115}In atom. Values are to be calculated in the ^{115}In samples located from $z=-242$ mm to $z=208$ mm in steps of 50 mm. The ^{115}In samples are to be simulated together with their polyethylene holder, as shown in Figs. E.15 and E.16, without loading the any other isotopes in the holder.
2. Radial distribution of the $^{115}\text{In}(n,\gamma)$ reaction rate in the EC10R radial experimental channel for the radial distances of 480, 530, 580, 630, 680 and 730 mm. All reaction-rate values are normalized to one source neutron and one ^{115}In atom. The samples are simulated together with their polyethylene holder, as described in Fig. E.17.
3. $^{197}\text{Au}(n,\gamma)$ and $^{55}\text{Mn}(n,\gamma)$ reaction rates in the EC2B and EC6T experimental channels, normalized to one external source neutron and one isotope atom. The samples are to be simulated together with its sample holder, as done in the task 1-C. The isotope loading distribution is shown in Figs. E.15 and E.16. The calculation has to be performed with the holder containing only ^{197}Au or ^{55}Mn .
4. The neutron energy spectra in the EC2B, EC6T and EC8R experimental channels are calculated at $z=0$ in 172-energy-groups structure given in Table E.2. The integral of the neutron spectrum should equal unity:

$$\int \phi(E)dE = 1.$$

5. The neutron flux is calculated as function of time after a neutron pulse insertion. The pulse duration is 5 μs of D-D or D-T neutrons at $z=0$. The neutron flux calculations are performed for a period of 20 ms with two different detectors:
 - a. $^3\text{He}(n,p)$ detector in the EC6T and EC8R experimental channels without modeling the detector in the calculation. The results should be normalized to the maximum value in EC6T experimental channel.
 - b. $^{235}\text{U}(n,f)$ detector in the EC1B, EC2B, and EC3B experimental channels without modeling the detector in the calculation, The results should be normalized to the maximum value in EC1B experimental channel.

The calculations are to be done with 10 μs time bin from 0 to 1 ms and with 100 μs time bin from 1 ms to 20 ms.
6. Kinetic parameters for both configurations:
 - a. Effective multiplication factor, k_{eff} .
 - b. Source multiplication factor, k_s .
 - c. Mean neutron generation time, Λ .
 - d. Prompt neutron lifetime, l_p , and mean neutron lifetime, l .
 - e. Effective delayed neutron fraction, β_{eff} .

The participants are requested to define the used computer code(s), nuclear data libraries, etc. The following information is requested:

1. Author(s) of the solutions with affiliation.
2. Name and version of the code used with bibliographic references.
3. Name of the nuclear data library(ies) that have been used with a description of preprocessing or changes made.

4. Description of any geometrical model approximations.
5. Description of the computational methods used for calculating the kinetic parameters k_s , Λ , l_p , l and β_{eff} .
6. Statistical error bars for the Monte Carlo results.

The participants were also requested to use a standardized Excel spreadsheet for reporting their results to facilitate the compilation and comparison of the results.

YALINA Booster Assembly Design

The sub-critical assembly of the YALINA Booster facility is made of rectangular parallelepiped sections, as can be seen in Fig. E.4. The central axis of the assembly is aligned horizontally. The neutron producing deuteron target can be situated along the central axis at different distances from the core center. The fast booster zone consists of 36 lead sub-assemblies. An empty lead sub-assembly is shown in Fig. E.5. The thermal zone consists of 108 polyethylene sub-assemblies. A polyethylene sub-assembly with eight EK-10 fuel rods is shown in Fig. E.6. For structural reasons, the sub-assemblies are encased into a stainless steel frame. Nine sub-assemblies are arranged in each frame. The frame thickness is 4 mm and the total length along the Z-axis is 771 mm in the thermal zone and 804 mm in the fast zone. The central part of the fast zone has the highly enriched (90%) metallic uranium fuel and a lead block, as shown in Fig. E.4. In the axial direction, the frame exceeds the boundaries of the fuel rods. The extension is 64 mm at the neutron generator side and 95 mm at the opposite side, as shown in Fig. E.11.

The Lead Target

An X-Y cross section of the fast zone is shown in Fig. E.7. There is a hole with side dimensions of 80×80 mm in the center of the fast zone that is formed by cutting out the inner corners of the four central lead blocks. A lead zone consisting of 12 blocks in the axial direction, each with X-Y dimensions of 78×78 mm and total target length of 645 mm, can be located in this hole. When the deuteron beam is used for generating neutrons, a part of the hole is occupied by the beam tube as shown in Fig. E.11.

The Inner Part of the Fast Zone

The innermost part of the fast zone surrounding the lead target contains 132 fuel rods in a lead block, which are marked by red color in Fig. E.7. The fuel material is metallic uranium with 90% ^{235}U enrichment arranged in a square lattice. The fuel-rod pitch is 11.143 mm and the lead block dimension is 78×78 mm. The total length of the lead sub-assembly is 645 mm. A detailed description of the fuel rod design is depicted in Fig. E.8.

The Outer Part of the Fast Zone

The fast fuel zone surrounding the 90%-enriched zone consists of 32 lead sub-assemblies with 563 fuel rods. The fuel material is UO_2 ceramic with 36% ^{235}U enrichment. Each lead sub-assembly has 25 fuel rods. The fuel rod details are given in Fig. E.8. The UO_2 density is 9.694 g/cm³. The cladding material is stainless steel alloy 12X18H10T. The fuel is arranged in a square lattice with 16-mm pitch. All fuel rods in the booster zone are inserted into stainless steel tubes with 9-mm outer diameter and 0.7-mm wall thickness. Four experimental channels, EC1B, EC2B, EC3B, and EC4B, are located in this zone. The first three experimental channels have a stainless-steel alloy 12X18H10T liner

with 36-mm outer diameter and wall thickness 1 mm. The experimental channel EC4B has the same liner material, but the outer diameter and the wall thickness are 12 and 1.5 mm, respectively.

The Absorber Zone

The absorber zone surrounds the fast zone. It consists of an inner layer of natural metallic uranium rods with stainless steel cladding. The cladding outer diameter is 9 mm and its thickness is 0.7 mm. The outer layer of the absorber zone consists of boron carbide (B_4C) rods. The rod details are shown in Fig. E.9. The number of metallic natural uranium rods is 108 and the number of B_4C rods is 116. The B_4C rods are located in the same lattice as the uranium fuel rods in the fast zone with 16 mm pitch. The density of the boron carbide is 1.38 g/cm^3 . This absorber zone permits fast neutrons to penetrate into the thermal zone from the fast zones, and prevents thermal neutrons from entering the fast zone from the thermal zone. The result is a fast-neutron coupling of the fast and the thermal zones. The B_4C rods are constrained inside the assembly and cannot be taken out accidentally; this prevents undesired reactivity insertion.

The Thermal Zone

The thermal zone surrounds the absorber zone. It consists of 108 polyethylene sub-assemblies. Each polyethylene sub-assembly has 16 holes for loading EK-10 fuel rods. The holes are arranged in a square lattice with 20-mm pitch. The outer cladding diameter of the EK-10 rod is 10 mm. The active fuel length is 500 mm and the average amount of ^{235}U is 7.73 g per rod. The total rod length is 590 mm. The EK-10 fuel rods are inserted into the polyethylene blocks. Each sub-assembly has a total length of 576 mm, obtained by arranging twelve blocks in the axial direction. The block dimensions are $80 \times 80 \times 48 \text{ mm}$. The polyethylene density is 0.859 g/cm^3 . For the polyethylene moderator and the EK-10 fuel rods, the 20-mm pitch is the optimal configuration for neutron multiplication. The detail description of the EK-10 fuel rod is shown in Fig. E.10. Three experimental channels, EC5T, EC6T and EC7T, are inserted into the thermal zone. Finally, the thermal zone is surrounded in the radial direction by a 250-mm graphite reflector. The graphite reflector has three experimental channels, EC8R, EC9R, and EC10R. In the axial directions, borated-polyethylene reflectors are used, as shown in Figs. E.11 and E.12. In the thermal zone, and close to the fast zone, it is possible to insert three small B_4C rods as shown in Figs E.2, E.3, and E.4. During operation these rods are not inserted and, consequently, the holes are filled with air. The diameter of each hole is 11 mm with a duraluminum liner. The liner thickness is 0.5 mm. The main parameters of the YALINA-Booster sub-critical assembly are given in Table E.3.

YALINA Booster Geometrical Cross Sections

Simplified geometrical cross sections are shown in Figs. E.11 and E.12; they help in understanding and generating the computational models. The detailed material compositions are given in Table E.4.

The Deuteron Beam Tube

The design details of the deuteron-beam tube are shown in Fig. E.18. The material composition is given Table E.4.

Detectors

The experimental measurements used three detectors, a ^3He -detector and two different ^{235}U fission chambers. The detectors are described briefly here, although modeling them in the calculations is not required in order to avoid unnecessary difficulties.

The ^3He detector

The ^3He detector is made by CANBERRA and its model number is 05NHI/IK. The filling gas consists of 8 bar ^3He and 2 bar Kr. The gas chamber length and diameter are 10 and 9 mm, respectively. The wall thickness of the gas chamber is 0.5 mm and it is made of Ni (73%) and Cu (27%) alloy.

The ^{235}U fission chamber

Two types of ^{235}U fission chambers are used for the experimental measurements. They have different sizes and sensitivity; their main parameters are given in Table E.5.

..... Tables and figures for Appendix E begin on the following page

Table E.1: List of experimental channels in YALINA Booster.

Experimental Channels in YALINA-B		
Name	Location	Orientation
EC1B	Booster zone	Axial
EC2B	Booster zone	Axial
EC3B	Booster zone	Axial
EC4B	Booster zone	Axial
EC5T	Thermal zone	Axial
EC6T	Thermal zone	Axial
EC7T	Thermal zone	Axial
EC8R	Reflector	Axial
EC9R	Reflector	Axial
EC10R	Reflector	Radial
MC1	Reflector	Axial
MC2	Reflector	Axial
MC3	Reflector	Axial
MC4	Reflector	Axial
MC5	Thermal zone	Axial
MC6	Thermal zone	Axial

Table E.2: Upper boundaries for the 172-neutron-energy groups.

Gr.	En. [MeV]	Gr.	En. [MeV]	Gr.	En. [MeV]	Gr.	En. [MeV]
1	1.96403E+01	44	1.50344E-02	87	8.31529E-06	130	9.10000E-07
2	1.73325E+01	45	1.11378E-02	88	7.52398E-06	131	8.60000E-07
3	1.49182E+01	46	9.11882E-03	89	6.16012E-06	132	8.50000E-07
4	1.38403E+01	47	7.46586E-03	90	5.34643E-06	133	7.90000E-07
5	1.16183E+01	48	5.53084E-03	91	5.04348E-06	134	7.80000E-07
6	1.00000E+01	49	5.00451E-03	92	4.12925E-06	135	7.05000E-07
7	8.18731E+00	50	3.52662E-03	93	4.00000E-06	136	6.25000E-07
8	6.70320E+00	51	3.35463E-03	94	3.38075E-06	137	5.40000E-07
9	6.06531E+00	52	2.24867E-03	95	3.30000E-06	138	5.00000E-07
10	5.48812E+00	53	2.03468E-03	96	2.76792E-06	139	4.85000E-07
11	4.49329E+00	54	1.50733E-03	97	2.72000E-06	140	4.33000E-07
12	3.67879E+00	55	1.43382E-03	98	2.60000E-06	141	4.00000E-07
13	3.01194E+00	56	1.23410E-03	99	2.55000E-06	142	3.91000E-07
14	2.46597E+00	57	1.01039E-03	100	2.36000E-06	143	3.50000E-07
15	2.23130E+00	58	9.14242E-04	101	2.13000E-06	144	3.20000E-07
16	2.01897E+00	59	7.48518E-04	102	2.10000E-06	145	3.14500E-07
17	1.65299E+00	60	6.77287E-04	103	2.02000E-06	146	3.00000E-07
18	1.35335E+00	61	4.53999E-04	104	1.93000E-06	147	2.80000E-07
19	1.22456E+00	62	3.71703E-04	105	1.84000E-06	148	2.48000E-07
20	1.10803E+00	63	3.04325E-04	106	1.75500E-06	149	2.20000E-07
21	1.00259E+00	64	2.03995E-04	107	1.67000E-06	150	1.89000E-07
22	9.07180E-01	65	1.48625E-04	108	1.59000E-06	151	1.80000E-07
23	8.20850E-01	66	1.36742E-04	109	1.50000E-06	152	1.60000E-07
24	6.08101E-01	67	9.16609E-05	110	1.47500E-06	153	1.40000E-07
25	5.50232E-01	68	7.56736E-05	111	1.44000E-06	154	1.34000E-07
26	4.97871E-01	69	6.79041E-05	112	1.37000E-06	155	1.15000E-07
27	4.50492E-01	70	5.55951E-05	113	1.33750E-06	156	1.00000E-07
28	4.07622E-01	71	5.15780E-05	114	1.30000E-06	157	9.50000E-08
29	3.01974E-01	72	4.82516E-05	115	1.23500E-06	158	8.00000E-08
30	2.73237E-01	73	4.55174E-05	116	1.17000E-06	159	7.70000E-08
31	2.47235E-01	74	4.01690E-05	117	1.15000E-06	160	6.70000E-08
32	1.83156E-01	75	3.72665E-05	118	1.12300E-06	161	5.80000E-08
33	1.22773E-01	76	3.37202E-05	119	1.11000E-06	162	5.00000E-08
34	1.11090E-01	77	3.05113E-05	120	1.09700E-06	163	4.20000E-08
35	8.22975E-02	78	2.76077E-05	121	1.07100E-06	164	3.50000E-08
36	6.73795E-02	79	2.49805E-05	122	1.04500E-06	165	3.00000E-08
37	5.51656E-02	80	2.26033E-05	123	1.03500E-06	166	2.50000E-08
38	4.08677E-02	81	1.94548E-05	124	1.02000E-06	167	2.00000E-08
39	3.69786E-02	82	1.59283E-05	125	9.96000E-07	168	1.50000E-08
40	2.92830E-02	83	1.37096E-05	126	9.86000E-07	169	1.00000E-08
41	2.73945E-02	84	1.12245E-05	127	9.72000E-07	170	6.90000E-09
42	2.47875E-02	85	9.90556E-06	128	9.50000E-07	171	5.00000E-09
43	1.66156E-02	86	9.18981E-06	129	9.30000E-07	172	3.00000E-09

Table E.3: Main parameters of the YALINA Booster assembly.

Target Zone	
Material	Pb
Dimensions [mm]	78×78×645
Density [g/cm ³]	11.34
Fast Zone with 90% Enrichment Fuel	
Lead block dimensions [mm]	78×78×645
Number of fuel rods	132
Fuel rod pitch [mm]	11.143
Fuel material	metallic uranium
Fuel density [g/cm ³]	17.95
Fuel enrichment	90%
Clad outer diameter [mm]	7
Clad thickness [mm]	0.2
Clad material	Stainless steel alloy 12X18H10T
Clad density [g/cm ³]	7.9
Fast Zone with 36% Enrichment Fuel	
Lead block dimensions [mm]	80×80×645
Number of fuel rods	563
Fuel rod pitch [mm]	16
Fuel material	UO ₂
Fuel density [g/cm ³]	9.694
Average fuel enrichment	35.73%
Clad outer diameter [mm]	7
Clad thickness [mm]	0.2
Clad material	Stainless steel alloy 12X18H10T
Clad density [g/cm ³]	7.9
Number of experimental channels	4 (EC1B, EC2B, EC3B, and EC4B)
Experimental channel liner	Stainless steel alloy (12X18H10T)
Liner outer diameter for EC1B, EC2B, EC3B [mm]	36
Liner inner diameter for EC1B, EC2B, EC3B [mm]	34
Liner outer diameter for EC4B [mm]	12
Liner inner diameter for EC4B [mm]	9
Absorber Zone - First Layer Next to the Fast Zone	
Lead block side dimension [mm]	80×80×645
Number of absorbing rods	108
Material	Natural metallic uranium
Natural uranium density [g/cm ³]	18.41
Clad outer diameter [mm]	7
Uranium isotopic content:	
²³⁴ U	0.0057%
²³⁵ U	0.7202%
²³⁸ U	99.2741%
Clad thickness [mm]	0.2
Clad material	Stainless steel alloy 12X18H10T

Absorber Zone - Second Layer Next to the Thermal Zone	
Number of absorbing rods	116
Absorber material	B ₄ C (powder)
Boron carbide density [g/cm ³]	1.38
Boron isotopic content:	
- ¹⁰ B	20%
- ¹¹ B	80%
Clad outer diameter [mm]	7
Clad thickness [mm]	0.2
Clad material	Stainless steel alloy 12X18H10T
Thermal Zone	
Moderator block dimensions [mm]	80×80×576
Maximum number of fuel rods per block	16
Fuel rod pitch [mm]	20
Fuel material	UO ₂ + MgO
Fuel material density [g/cm ³]	5.042
Fuel enrichment	10%
Fuel material isotopic content, weight fractions:	
- ²³⁵ U	0.079691
- ²³⁸ U	0.728557
- ¹⁶ O	0.142022
- Mg	0.049730
Clad outer diameter [mm]	10
Cladding thickness [mm]	1.5
Cladding material	Aluminum alloy
Moderator	Polyethylene
Moderator density [g/cm ³]	0.859
Hole diameter [mm]	11
Number of experimental channels	3 (EC5T, EC6T, and EC7T)
Experimental channel diameter [mm]	24
Graphite Radial Reflector	
Density [g/cm ³]	1.67
Thickness [mm]	240-250
Organic glass density [g/cm ³]	1.19
Organic glass thickness [mm]	4
Number of experimental channels:	3
- Axial channels	EC8R, EC9R
- axial channel diameter [mm]	24
- Radial channel	EC10R
- radial channel diameter [mm]	24
Axial Reflector	
Material	Borated polyethylene
Density [g/cm ³]	0.983

Table E.4: YALINA Booster material compositions.

Material	Composition	Weight fraction
Polyethylene density: 0.859 g/cm ³	C	0.85714000
	¹ H	0.14286000
Air density: 0.00129 g/cm ³	¹⁴ N	0.78850000
	¹⁶ O	0.21150000
Stainless steel alloy 12X18H10T density: 7.9 g/cm ³	C	0.00082000
	⁵⁰ Cr	0.00783052
	⁵² Cr	0.15685511
	⁵³ Cr	0.01812647
	⁵⁴ Cr	0.00458790
	⁵⁸ Ni	0.07842230
	⁶⁰ Ni	0.03124467
	⁶¹ Ni	0.00138111
	⁶² Ni	0.00446982
	⁶⁴ Ni	0.00118210
	Ti	0.00512500
	²⁸ Si	0.00029860
	²⁹ Si	0.00001570
	³⁰ Si	0.00001080
	⁵⁵ Mn	0.00800000
	S	0.00066300
	³¹ P	0.00086300
	⁶³ Cu	0.00132890
	⁶⁵ Cu	0.00061110
	⁵⁴ Fe	0.03763000
	⁵⁶ Fe	0.61196000
	⁵⁷ Fe	0.01439000
	⁵⁸ Fe	0.00193000
	²⁷ Al	0.00038800
	⁷⁵ As	0.00045400
	Ca	0.00012500
	Mg	0.00001300
	Mo	0.00157500
	²⁰⁴ Pb	0.00007063
	²⁰⁶ Pb	0.00121582
	²⁰⁷ Pb	0.00112093
	²⁰⁸ Pb	0.00267062
	Sb	0.00367500
	Zn	0.00094100
Lead (target) density: 11.34 g/cm ³	²⁰⁴ Pb	0.01390573
	²⁰⁶ Pb	0.23937727
	²⁰⁷ Pb	0.22069516
	²⁰⁸ Pb	0.52580513
	⁵⁴ Fe	0.00000035
	⁵⁶ Fe	0.00000570
	⁵⁷ Fe	0.00000013

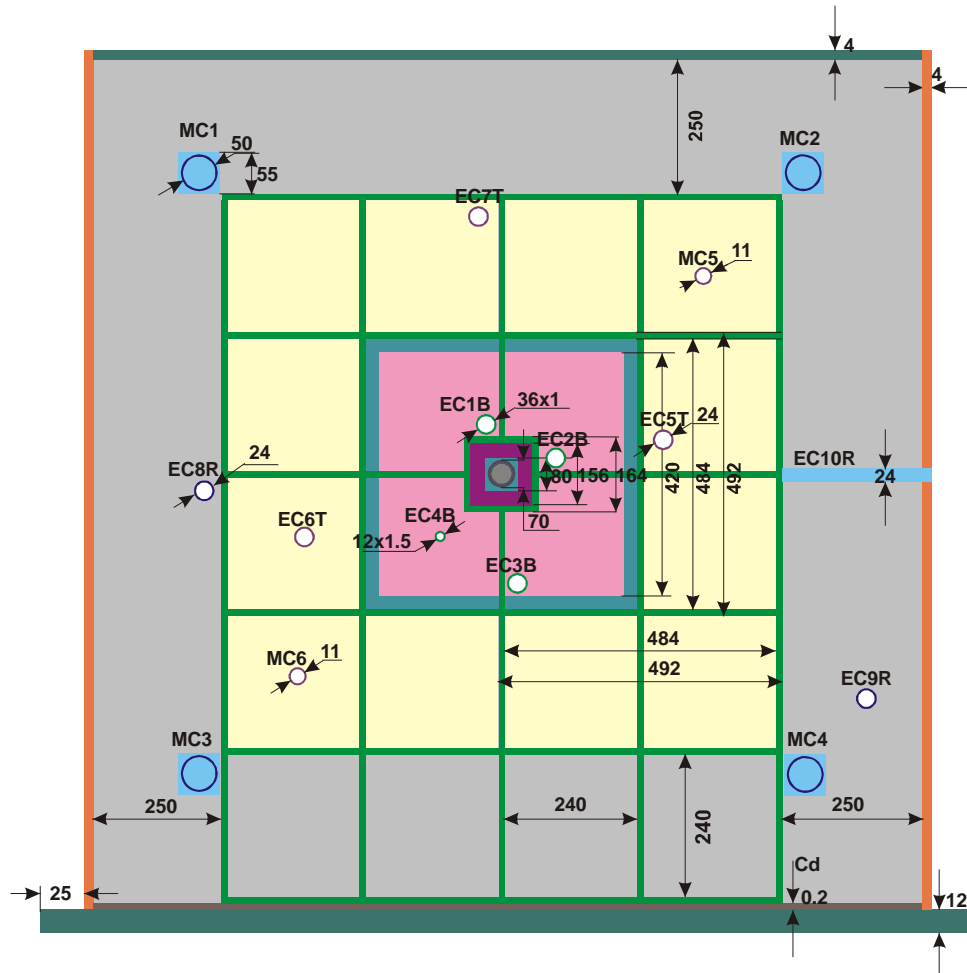
	⁵⁸ Fe	0.00000002
	¹⁰⁷ Ag	0.00000337
	¹⁰⁹ Ag	0.00000313
	²⁰⁹ Bi	0.00010640
	Ca	0.00000410
	⁶³ Cu	0.00000432
	⁶⁵ Cu	0.00000198
	Mg	0.00000290
	²³ Na	0.00001740
	Sb	0.00006440
	Zn	0.00000250
Lead (booster zone) density: 11.34 g/cm ³	²⁰⁴ Pb	0.01390559
	²⁰⁶ Pb	0.23937483
	²⁰⁷ Pb	0.22069291
	²⁰⁸ Pb	0.52579977
	¹⁰⁷ Ag	0.00000358
	¹⁰⁹ Ag	0.00000332
	²⁰⁹ Bi	0.00011100
	Ca	0.00000280
	⁶³ Cu	0.00000466
	⁶⁵ Cu	0.00000214
	⁵⁴ Fe	0.00000055
	⁵⁶ Fe	0.00000901
	⁵⁷ Fe	0.00000021
	⁵⁸ Fe	0.00000003
	Mg	0.00000330
	²³ Na	0.00001570
	Sb	0.00006910
	Zn	0.00000150
Low carbon steel (alloy Fe360-B) density: 7.8 g/cm ³	C	0.00140000
	⁵⁰ Cr	0.0000418
	⁵² Cr	0.0008380
	⁵³ Cr	0.0000968
	⁵⁴ Cr	0.0000245
	⁵⁸ Ni	0.0000672
	⁶⁰ Ni	0.0000268
	⁶¹ Ni	0.0000012
	⁶² Ni	0.0000038
	⁶⁴ Ni	0.0000010
	²⁸ Si	0.0004594
	²⁹ Si	0.0000241
	³⁰ Si	0.0000165
	⁵⁵ Mn	0.0040000
	S	0.0001000
	³¹ P	0.0001000
	⁶³ Cu	0.0000685
	⁶⁵ Cu	0.0000315
	⁵⁴ Fe	0.0560858
	⁵⁶ Fe	0.9122159
	⁵⁷ Fe	0.0214543




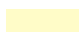






	⁵⁸ Fe	0.0028833
	¹⁴ N	0.0000100
	⁷⁵ As	0.0000500
Metallic uranium (90% enrichment) density: 17.95 g/cm ³	²³⁵ U	0.9
	²³⁸ U	0.1
Metallic natural uranium density: 18.41 g/cm ³	²³⁴ U	0.0000570
	²³⁵ U	0.0072020
	²³⁸ U	0.9927410
UO ₂ for Fast Zone (35.73% enrichment) density: 9.694 g/cm ³	¹⁶ O	0.1189700
	²³⁵ U	0.3147900
	²³⁸ U	0.5662400
Boron carbide density: 1.38 g/cm ³	¹⁰ B	0.1442400
	¹¹ B	0.6385400
	C	0.2172200
UO ₂ for Thermal Zone (10% enrichment) density: 5.042 g/cm ³	²³⁵ U	0.0796910
	²³⁸ U	0.7285570
	¹⁶ O	0.1420220
	Mg	0.0497300
Aluminum alloy (CAB1) density: 2.7 g/cm ³	Mg	0.00004000
	²⁸ Si	0.00011025
	²⁹ Si	0.00000578
	³⁰ Si	0.00000397
	⁵⁴ Fe	0.00002882
	⁵⁶ Fe	0.00046868
	⁵⁷ Fe	0.00001102
	⁵⁸ Fe	0.00000148
	⁶³ Cu	0.00006850
	⁶⁵ Cu	0.00003150
	⁵⁵ Mn	0.00001000
	Zn	0.00009400
	Ti	0.00014100
	⁵⁸ Ni	0.00000269
	⁶⁰ Ni	0.00000107
	⁶¹ Ni	0.00000005
	⁶² Ni	0.00000015
	⁶⁴ Ni	0.00000004
	¹⁰ B	0.00000151
	¹¹ B	0.00000669
	S	0.00312000
	Ba	0.00000220
	Ca	0.0000393
	⁵⁰ Cr	0.00000019
	⁵² Cr	0.00000377
	⁵³ Cr	0.00000044
	⁵⁴ Cr	0.00000011
	²³ Na	0.00038000
	³¹ P	0.00013500
	²⁷ Al	0.99529179
Duraluminum alloy	Mg	0.00050000

density: 2.7 g/cm ³	²⁸ Si	0.00275620
	²⁹ Si	0.00014454
	³⁰ Si	0.00009926
	⁵⁴ Fe	0.00005650
	⁵⁶ Fe	0.00091898
	⁵⁷ Fe	0.00002161
	⁵⁸ Fe	0.00000290
	⁶³ Cu	0.00034250
	⁶⁵ Cu	0.00015750
	⁵⁵ Mn	0.00025000
	Zn	0.00050000
Graphite density: 1.666 g/cm ³	Ti	0.00100000
	Al	0.99325000
	C	1
Concrete density: 2.3 g/cm ³	¹ H	0.0028000
	C	0.0766000
	¹⁶ O	0.4454000
	S	0.0004000
	Mg	0.0006000
	Ti	0.0005000
	²⁷ Al	0.0032000
	²⁸ Si	0.3477000
	Ca	0.0470000
	¹⁴ N	0.0723000
	⁵⁶ Fe	0.0029000
Borated polyethylene density: 0.983 g/cm ³	K	0.0006000
	C	0.8051000
	¹ H	0.1364000
	¹⁰ B	0.0015000
	¹¹ B	0.0064000
	¹⁶ O	0.0351000
	Ca	0.0128000
	⁵⁶ Fe	0.0026000
	Pb	0.0001000
Water density: 1 g/cm ³	¹ H	0.1111110
	¹⁶ O	0.8888890
Copper density: 8,96 g/cm ³	⁶³ Cu	0.6850000
	⁶⁵ Cu	0.3150000
Vacuum density: 1.29E-9 g/cm ³	¹⁴ N	0.7885000
	¹⁶ O	0.2115000
Organic glass density: 1.19 g/cm ³	C	0.5998500
	¹ H	0.0805400
	¹⁶ O	0.3196100
Cadmium sheet density: 8.65g/cm ³	Cd	1.00
Cellular polystyrene (sintered) density: 0.05 g/cm ³	C	0.04984600
	¹ H	0.00415400
	¹⁴ N	0.44146700
	¹⁶ O	0.50453300

Table E.5: Main parameters of fission chambers KHT-5 and KHT-31.

Fission chamber type	Diameter, mm	Detector length, mm	Sensitive detector length, mm	Isotope	Sensitive area, cm ²	Sensitive layer, (mg/cm ²)	Filling gas
KHT-5	7	70	5	²³⁵ U	1	1	98% Ar + 2% N ₂
KHT-31	32	235	200	²³⁵ U	500	1	98% Ar + 2% N ₂



	Umet. of 90% enrichment		UO2 of 36% enrichment
	Thermal neutron absorber Umet.(nat)+B4C		Thermal zone
	Air		Organic glass
	Graphite reflector		Cd layer
	Stainless steel frame		Mild (low carbon) steel

EC1B - EC4B - experimental channels in booster zone

EC5T - EC7T - experimental channels in thermal zone

EC8R - EC10R - experimental channels in reflector

MC1 - MC4 - measurement channels in reflector for
neutron flux monitoring

MC5 - MC6 - experimental channels in the thermal zone for neutron flux monitoring.
At the back side of the assembly, the experimental channels do not penetrate the
borated polyethylene or the organic glass.
EC8R (-52, -3.2), EC9R (60, -35.6), EC11RT New (-4.2, Reflector and Poly, diameter 1 cm)

Figure E.1: X-Y cross-section view of the YALINA Booster assembly, dimensions in mm.

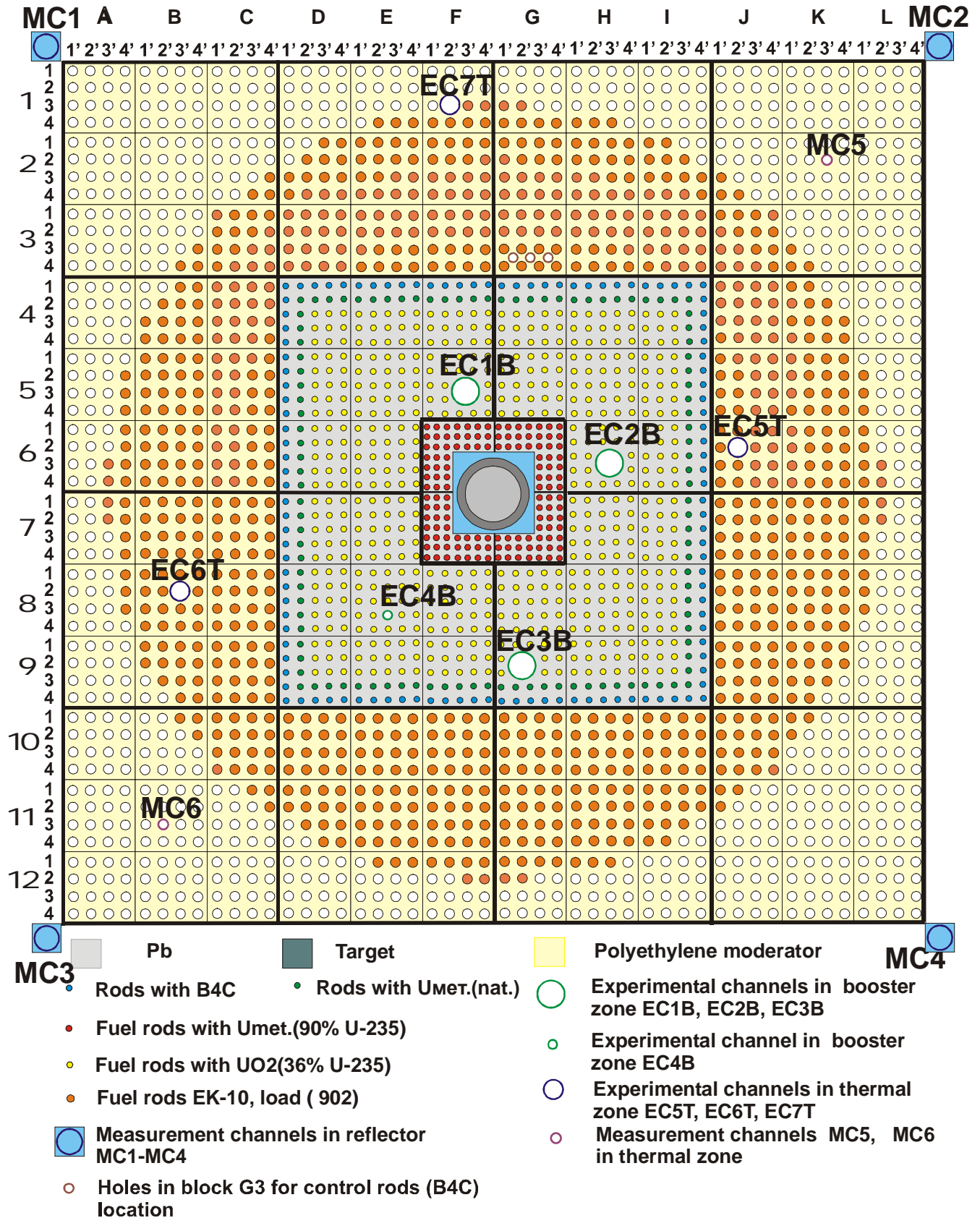


Figure E.2: Fuel loading of YALINA Booster configuration with 902 EK-10 fuel rods.

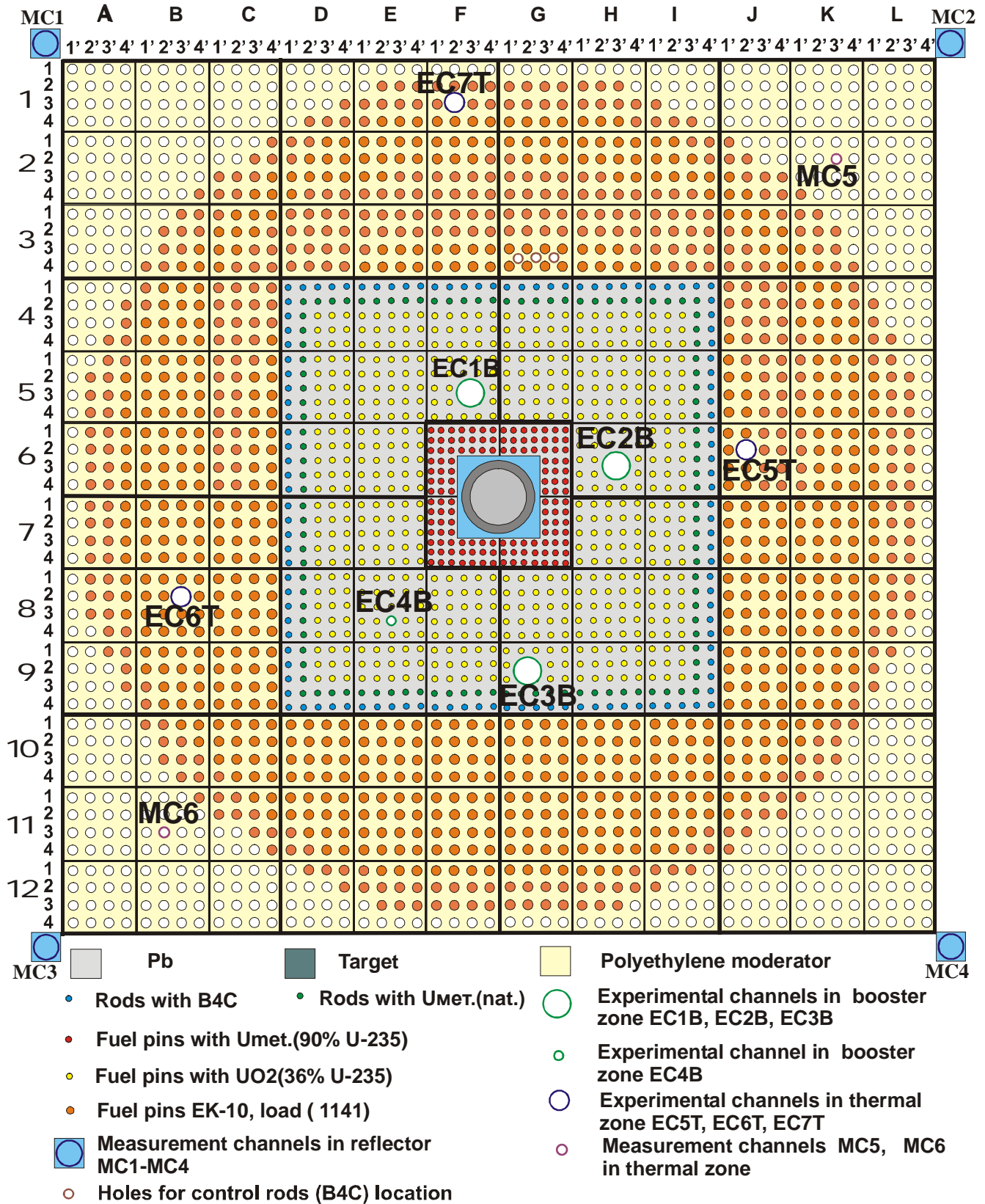


Figure E.3: Fuel loading of YALINA Booster configuration with 1141 EK-10 fuel rods.

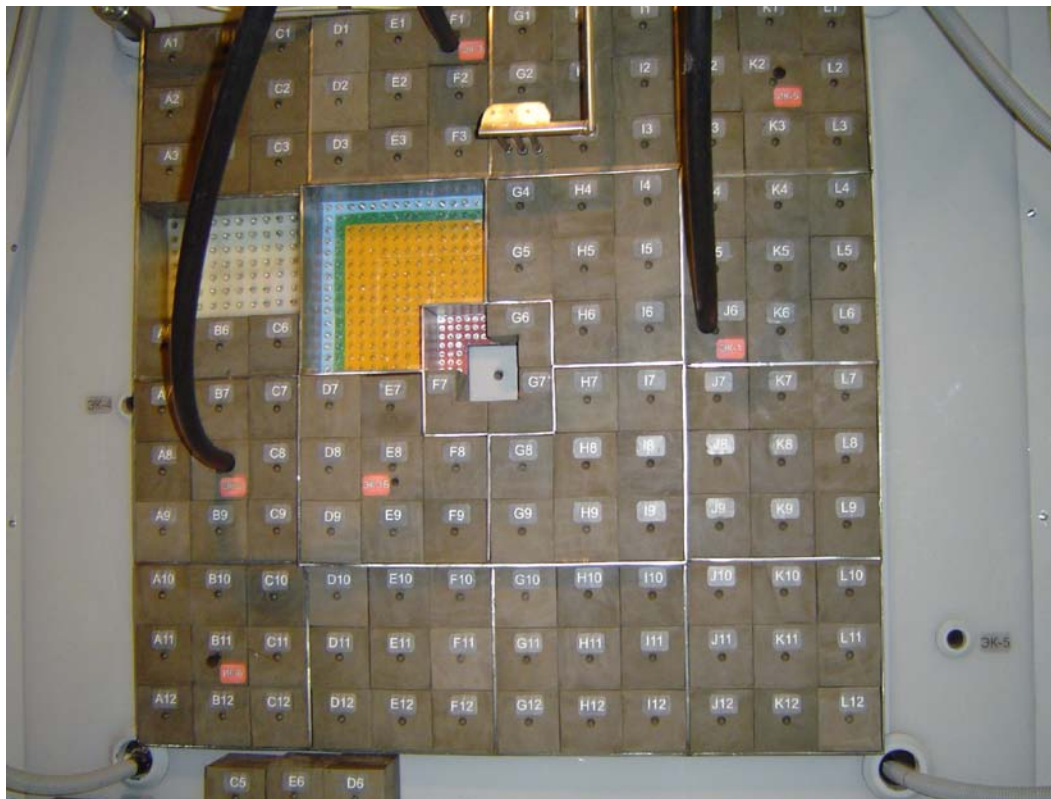


Figure E.4: YALINA Booster assembly showing the different zones.

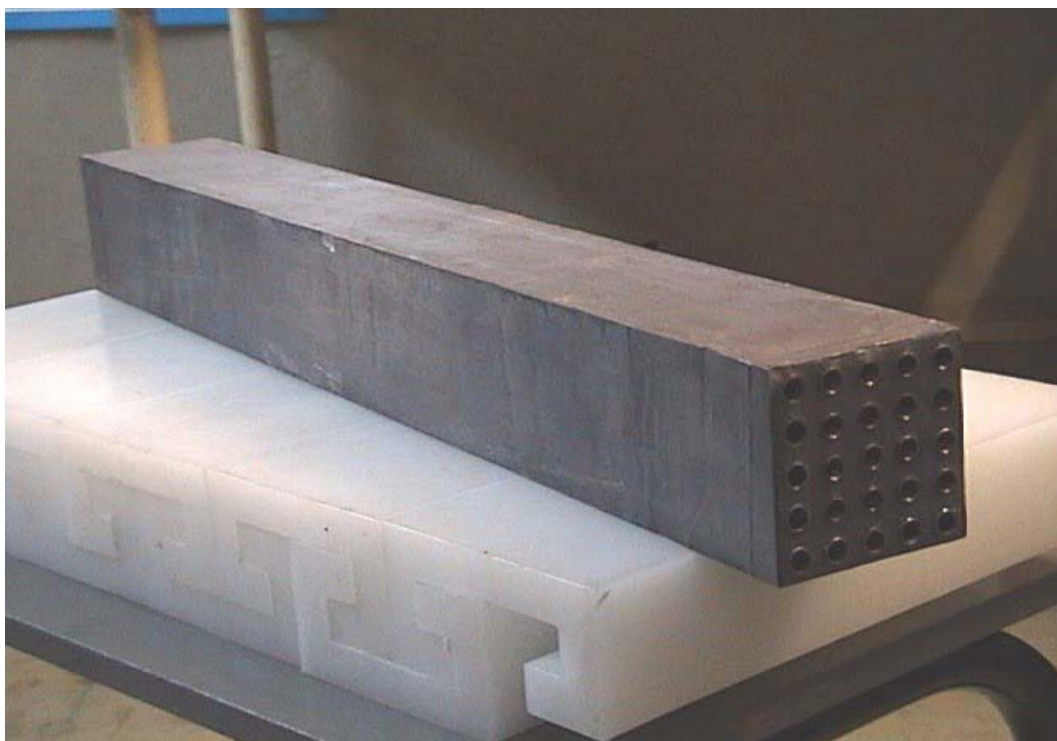


Figure E.5: Lead sub-assembly of the fast zone.

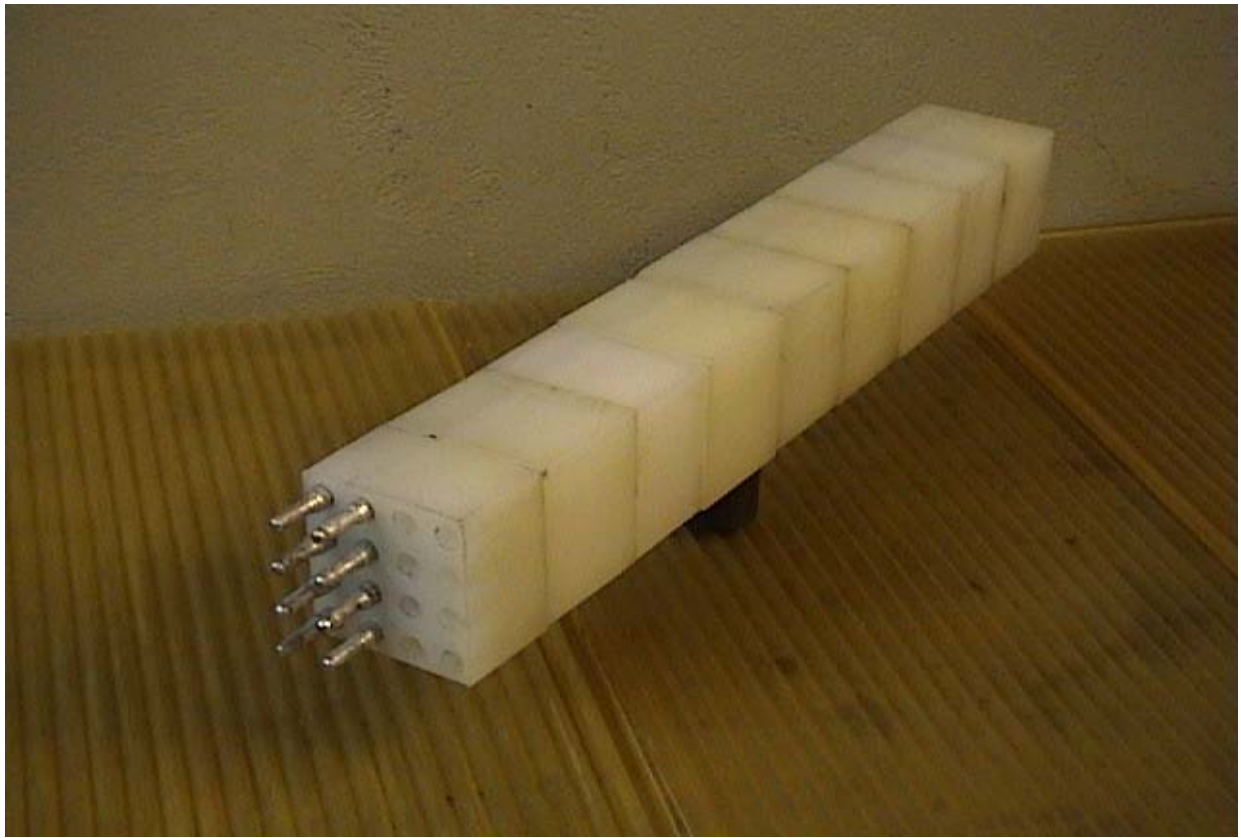


Figure E.6: Polyethylene sub-assembly of the thermal zone.

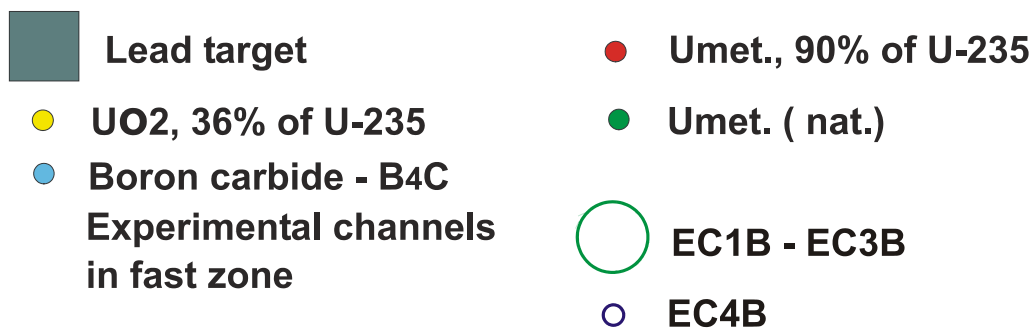
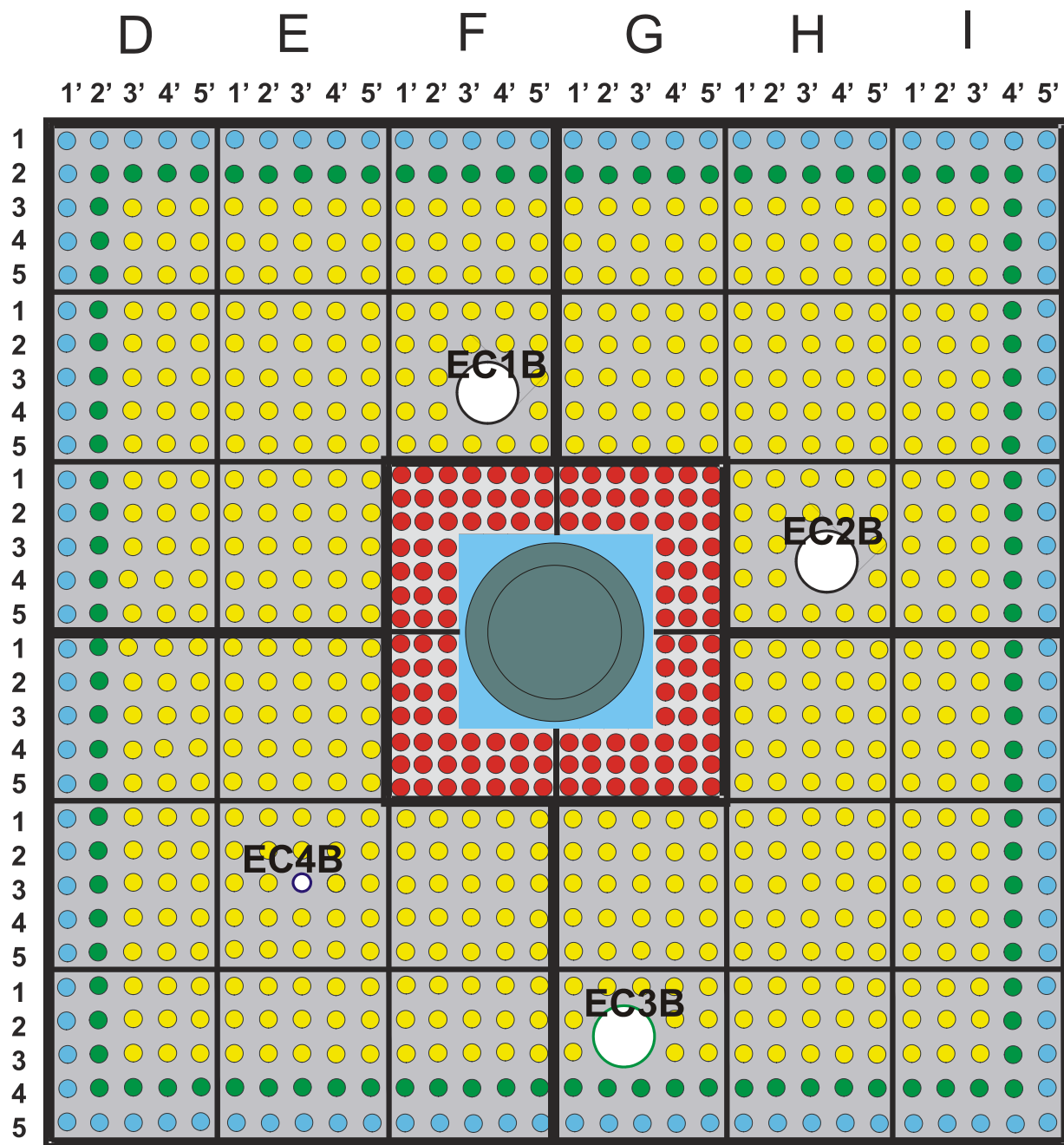


Figure E.7: X-Y cross-section view of the fast zone at the core center (z=0).

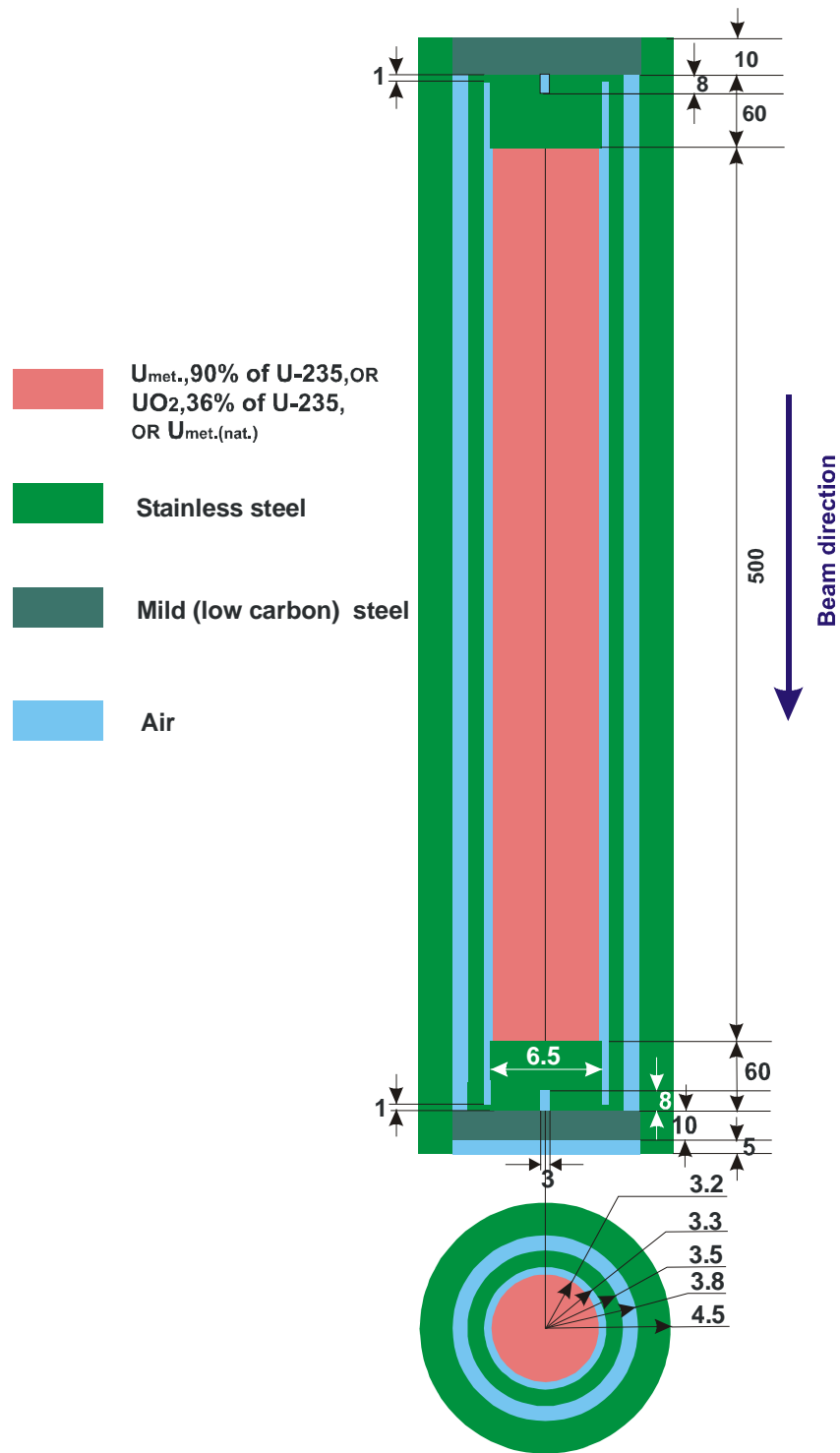


Figure E.8: X-Z and X-Y cross-section views of a fuel rod inside the steel casing, dimensions in mm.

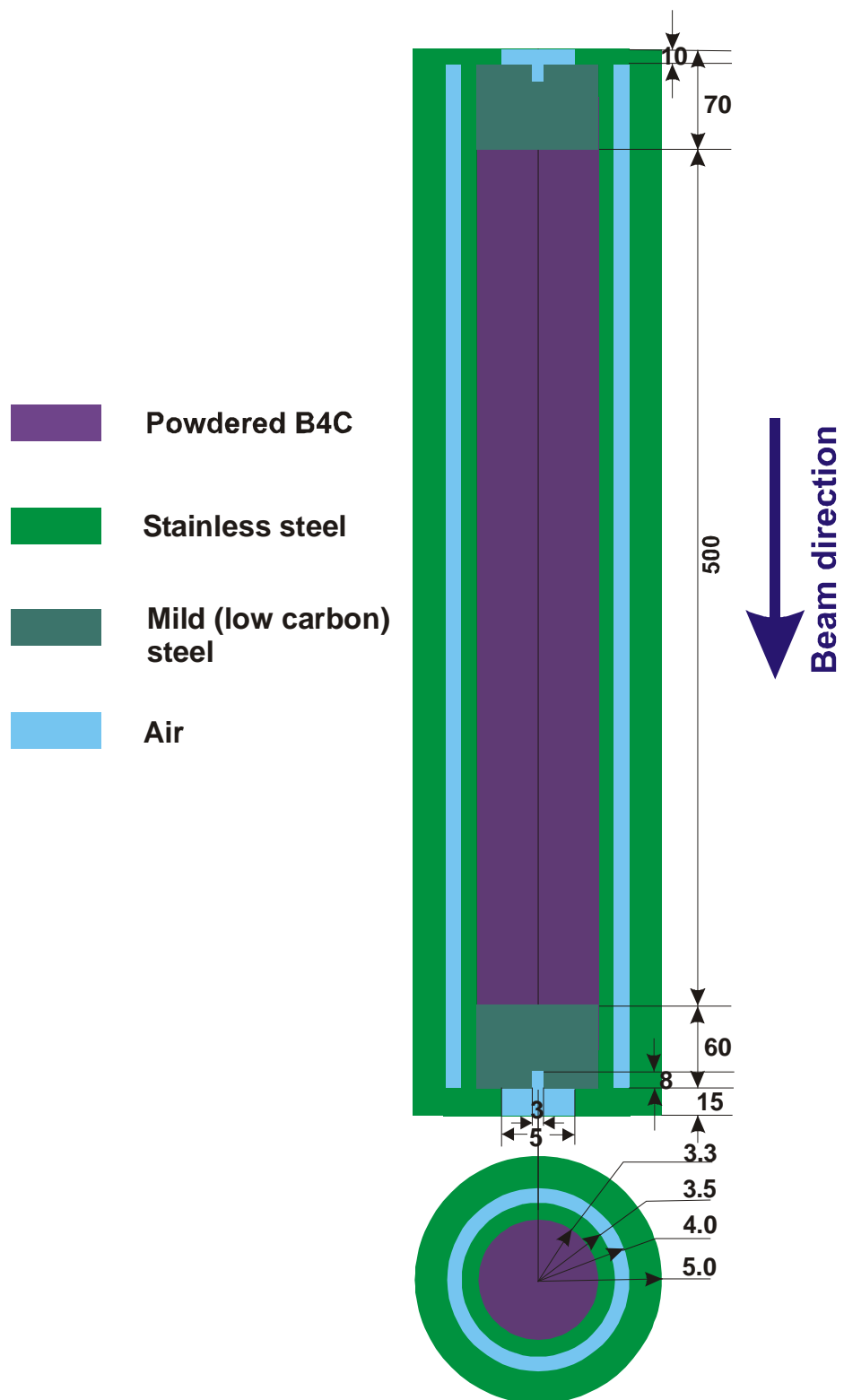


Figure E.9: Cross-section view of the boron-carbide rod, dimensions in mm.

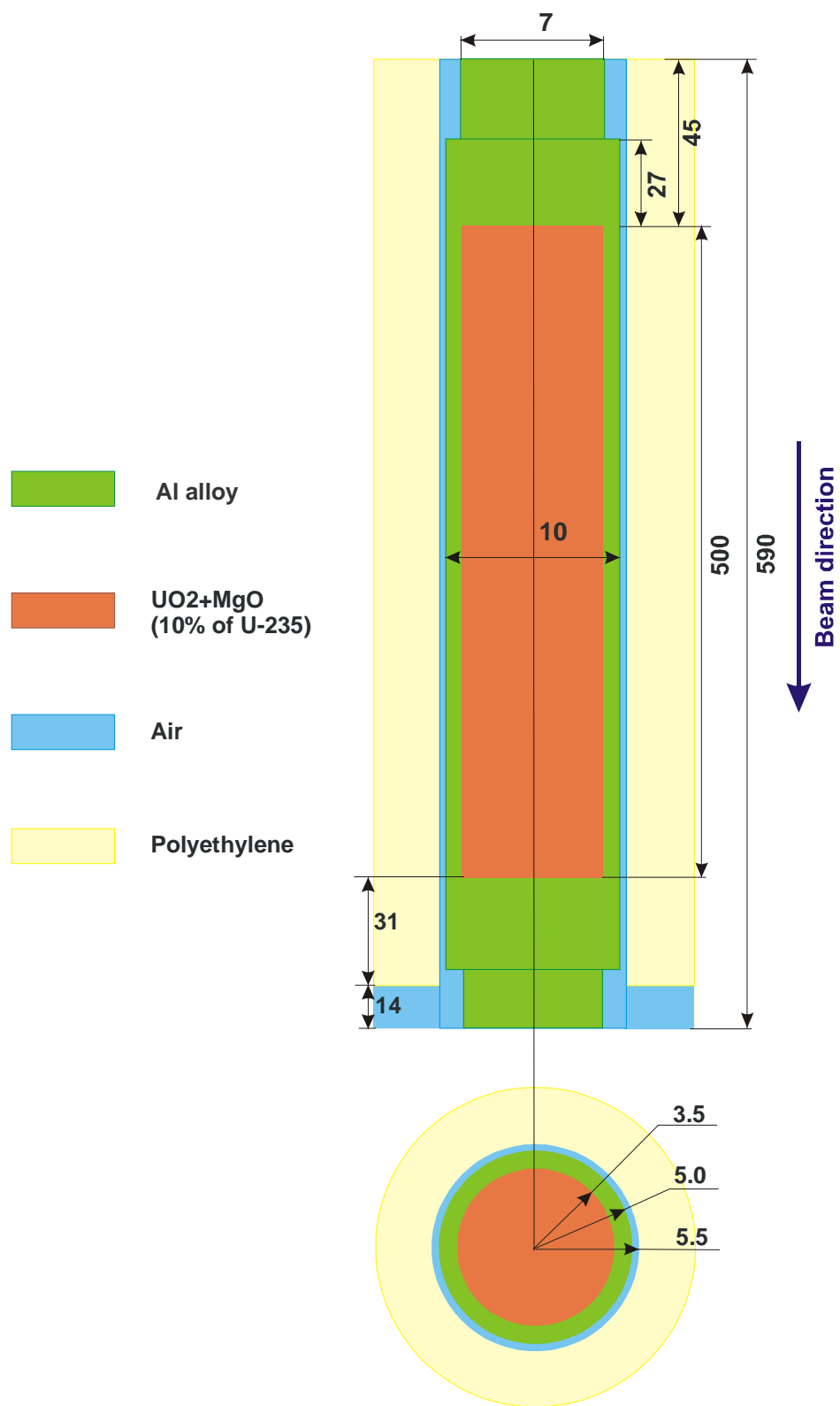


Figure E.10: X-Z and Z-Y cross-section views of the EK-10 fuel rod, dimensions in mm.

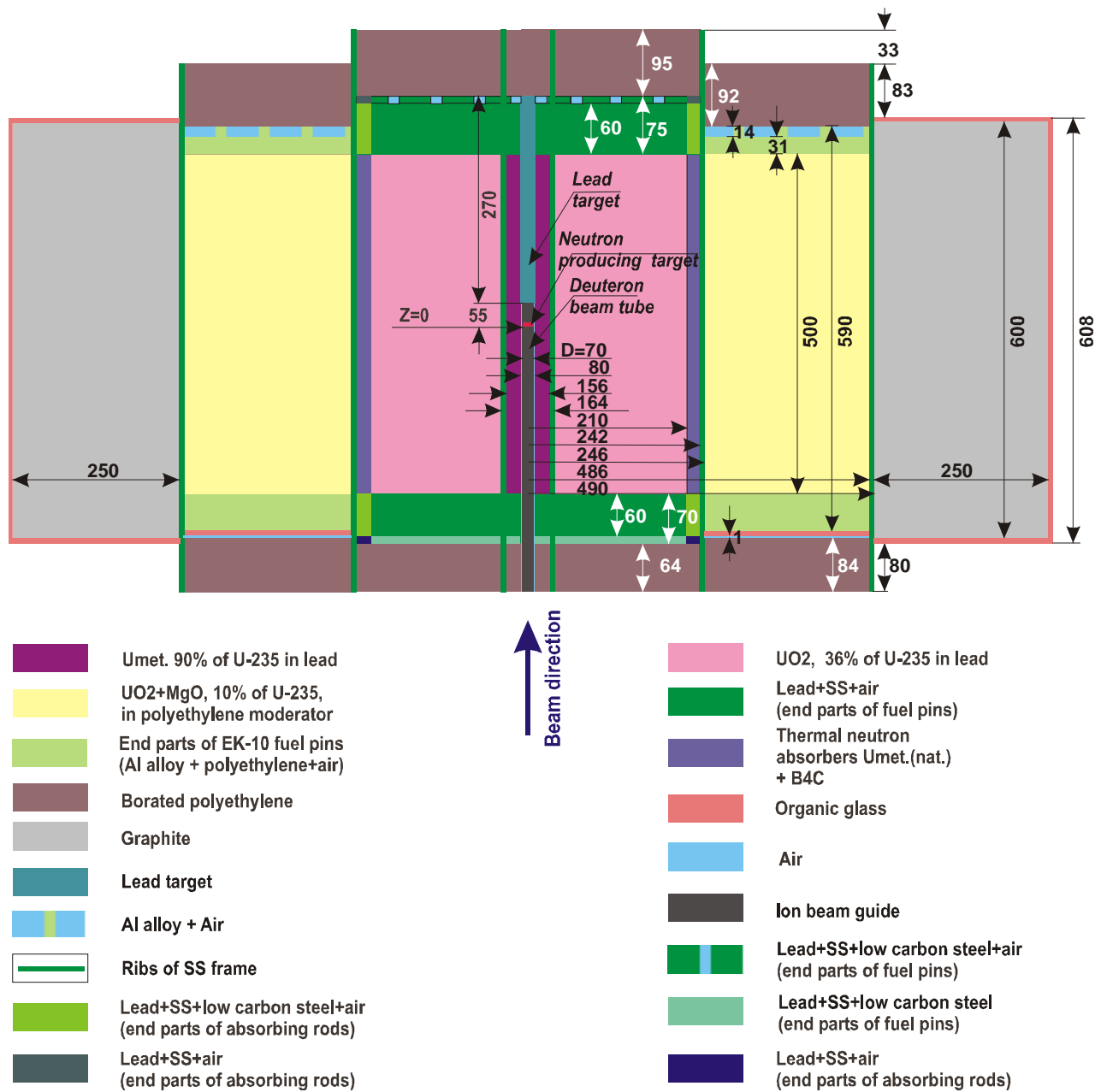


Figure E.11: Y-Z cross-section view of the YALINA Booster assembly (at X=4), dimensions in mm.

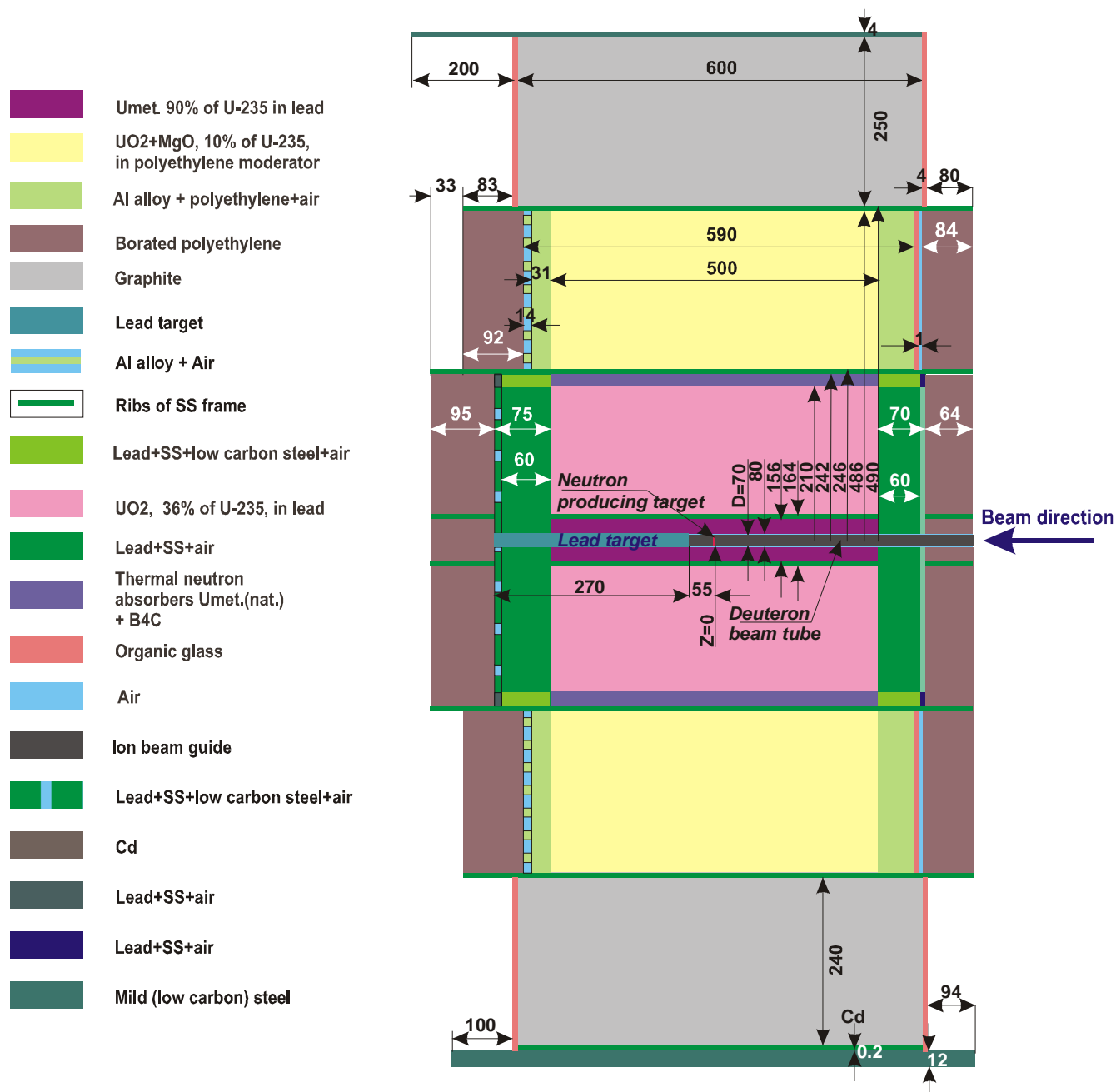


Figure E.12: X-Z cross-section view of the YALINA Booster assembly (at Y=4), dimensions in mm.

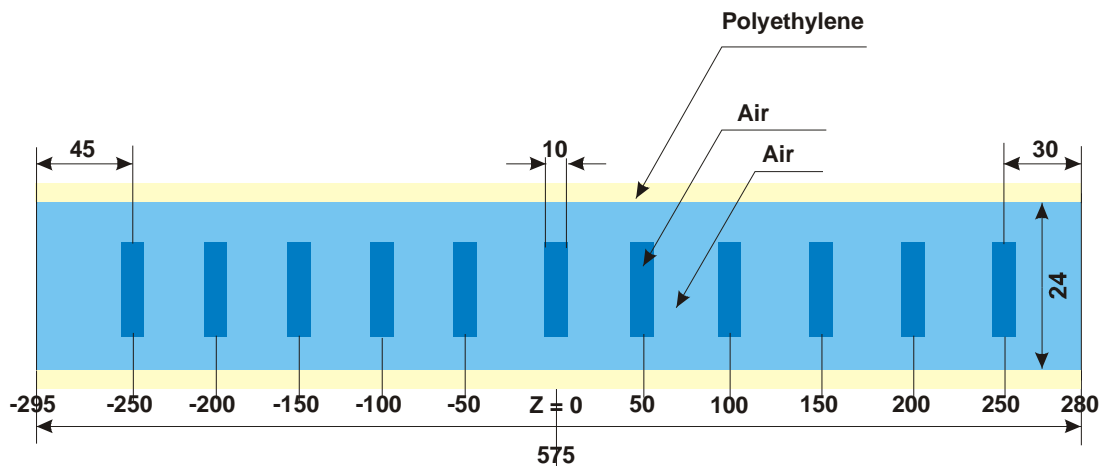


Figure E.13: Cylindrical air cells specified inside the experimental channels of the thermal zone (EC5T-EC7T) and reflector zone (EC8R) for calculating reaction rates of tasks 1a, 1b, 4, and 5a, dimensions in mm.

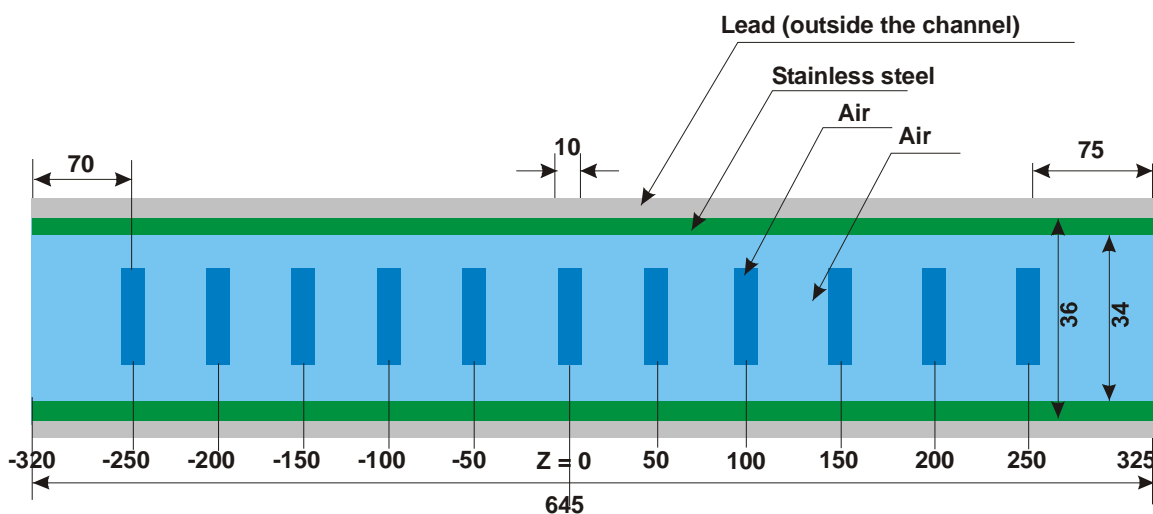


Figure E.14: Cylindrical air cells specified inside the experimental channels of the booster zone (EC1B-EC3B) for calculating the reaction rates of tasks 1b, 4 and 5b, dimensions in mm.

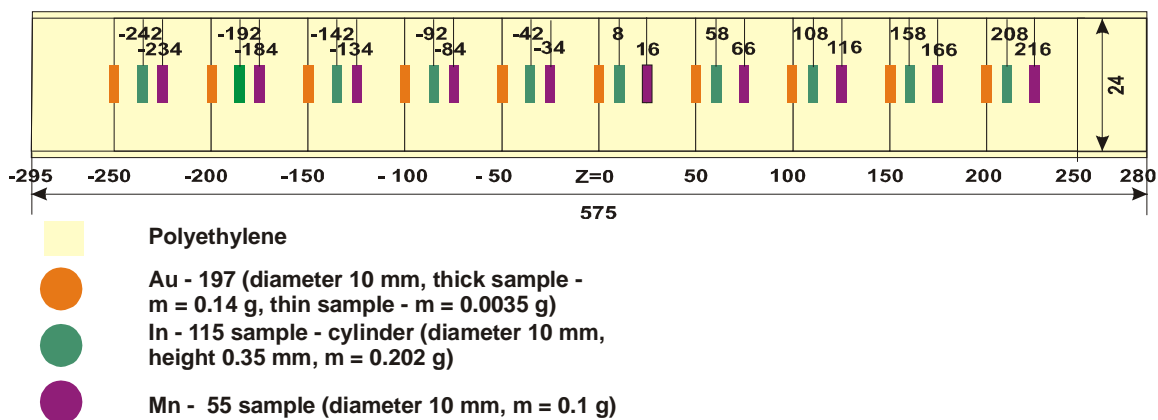


Figure E.15: Position of the ^{197}Au , ^{115}In , and ^{55}Mn samples in the experimental channels of the thermal region, dimensions in mm.

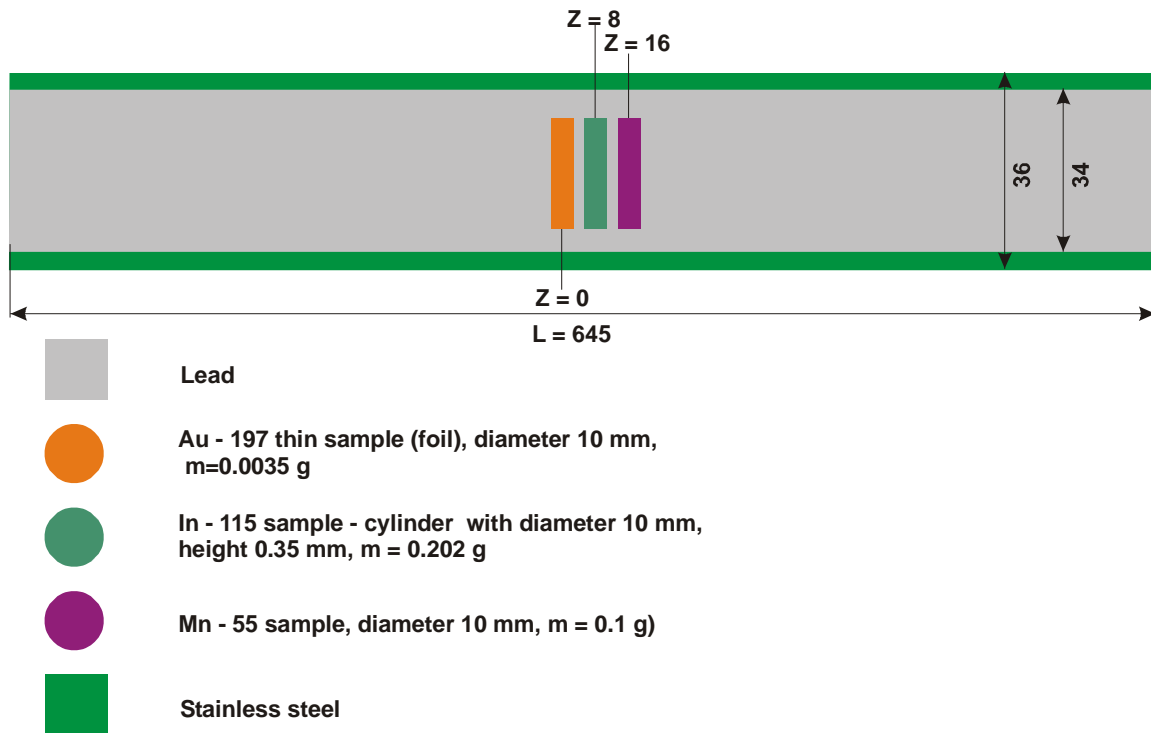


Figure E.16: Position of ^{197}Au , ^{115}In , and ^{55}Mn samples in EC2B experimental channel, dimensions in mm.

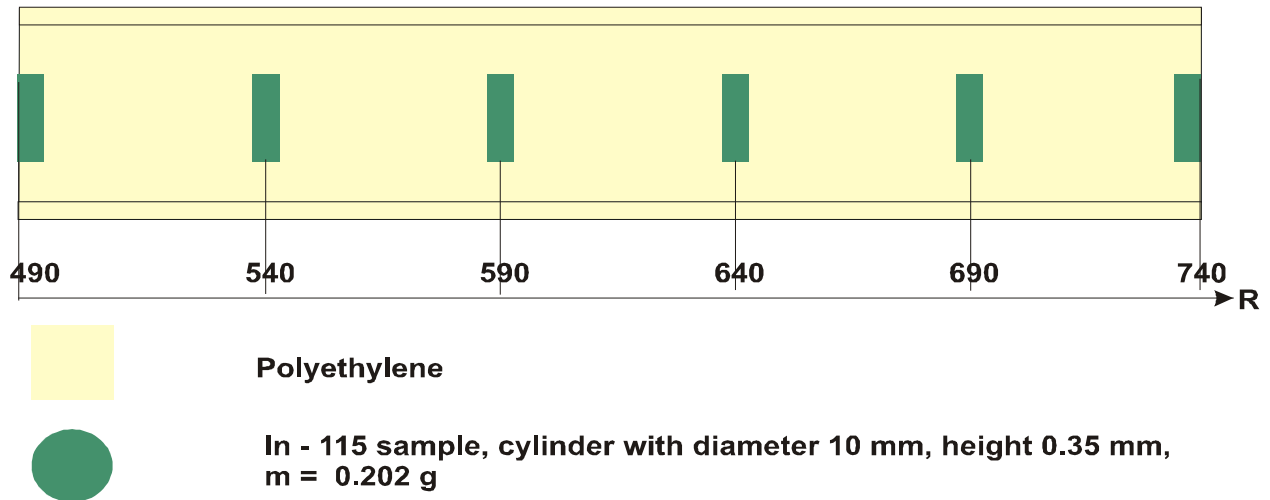


Figure E.17: Position of the ^{115}In samples in the EC10R experimental channel, dimensions in mm.

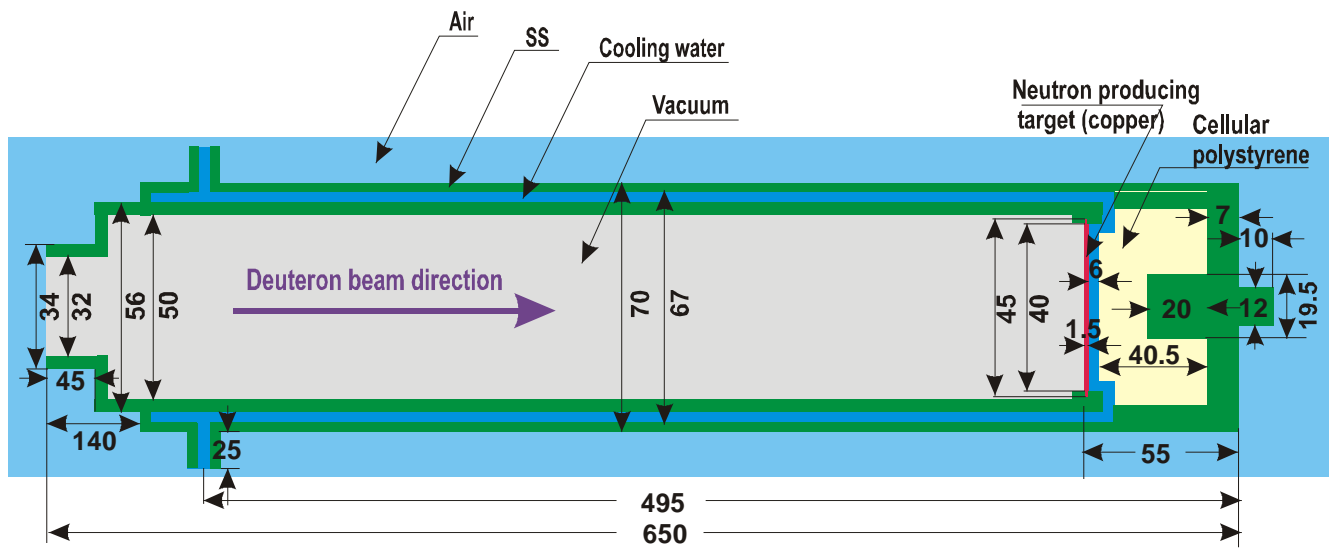


Figure E.18: Deuteron beam-tube design, dimensions in mm.



Nuclear Engineering Division

Argonne National Laboratory
9700 South Cass Avenue
Argonne, IL 60439

www.anl.gov



U.S. DEPARTMENT OF
ENERGY

A U.S. Department of Energy laboratory
managed by UChicago Argonne, LLC